AD-A009 138

DESIGN AND CALIBRATION OF THE ARL MACH 3 HIGH REYNOLDS NUMBER FACILITY

A. W. Fiore, et al

Aerospace Research Laboratories
Wright-Patterson Air Force Base, Ohio

January 1975

DISTRIBUTED BY:

NTIS
National Technical Information Service
U. S. DEPARTMENT OF COMMERCE

UNCLASSIFIED

SECURITY CLASSIFICATION OF THIS PAGE (*When Data Entered*)

REPORT DOCUMENTATION PAGE

READ INSTRUCTIONS
BEFORE COMPLETING FORM

1. REPORT NUMBER ARL 75-0012	2. GOVT ACCESSION NO.	3. RECIPIENT'S CATALOG NUMBER AD-A009 138
4. TITLE (*and Subtitle*) DESIGN AND CALIBRATION OF THE ARL MACH 3 HIGH REYNOLDS NUMBER FACILITY		5. TYPE OF REPORT & PERIOD COVERED Final Technical July 1965 - December 1972
		6. PERFORMING ORG. REPORT NUMBER
7. AUTHOR(s) A. W. Fiore; D. G. Moore; D. H. Murray and J. E. West, Maj, USAF		8. CONTRACT OR GRANT NUMBER(s)
9. PERFORMING ORGANIZATION NAME AND ADDRESS Fluid Mechanics Research Laboratory and Theoretical Aerodynamics Rsch Lab (ARL/LF & LH) Wright-Patterson AFB, OH 45433		10. PROGRAM ELEMENT, PROJECT, TASK AREA & WORK UNIT NUMBERS 61102F; 7065-14-28 61102F; 7064-02-06
11. CONTROLLING OFFICE NAME AND ADDRESS Aerospace Research Laboratories (AFSC) Bldg. 450, Area B Wright-Patterson AFB, OH 45433		12. REPORT DATE January 1975
		13. NUMBER OF PAGES 184
14. MONITORING AGENCY NAME & ADDRESS(*if different from Controlling Office*)		15. SECURITY CLASS. (*of this report*) Unclassified
		15a. DECLASSIFICATION DOWNGRADING SCHEDULE

16. DISTRIBUTION STATEMENT (*of this Report*)

Approved for public release; distribution unlimited.

17. DISTRIBUTION STATEMENT (*of the abstract entered in Block 20, if different from Report*)

18. SUPPLEMENTARY NOTES

19. KEY WORDS (*Continue on reverse side if necessary and identify by block number*)

Wind Tunnel	Design
Mach Number 3	Calibration
High Reynolds Number	

PRICES SUBJECT TO CHANGE

20. ABSTRACT (*Continue on reverse side if necessary and identify by block number*)

The design philosophy and details of the ARL Mach 3 High Reynolds Number Facility are described and the results of extensive calibration tests are presented. The facility is an intermittent cold flow wind tunnel having a constant area test section 8 inches wide and 8.2 inches high, with a test rhombus 23 inches long. It operates in a blowdown mode using dry compressed air which is exhausted to the atmosphere through a silencer. Tunnel stagnation pressures range from 40 psia to 570 psia, with stagnation temperatures in a range from 400 degrees Rankine to 500 degrees Rankine depending upon ambient conditions. The corresponding free

Reproduced by
NATIONAL TECHNICAL
INFORMATION SERVICE
US Department of Commerce
Springfield, VA. 22151

20. (Cont'd)

stream unit Reynolds numbers vary from 7 million per foot to 140 million per foot. The tunnel has been operated with a vacuum exhaust which permitted stagnation pressures as low as 4.2 psia with a corresponding free stream unit Reynolds number of 0.8 million per foot. The aerodynamic calibration measurements were made at nominal stagnation pressures of 100, 300 and 500 psia with an average stagnation temperature of 480 degrees Rankine. Test rhombus determinations included lateral and longitudinal Mach number distributions and flow angularity measurements. A limited number of tunnel blockage tests were performed and some flow visualization tests were made to determine characteristics of the start-stop process.

PREFACE

This report was prepared jointly by the Fluid Mechanics Research Laboratory of ARL under Project 7065, "Aerospace Simulation Techniques," and by the Hypersonic Research Laboratory of ARL under Project 7064, "High Velocity Fluid Mechanics." This report covers the design and calibration of the ARL Mach 3 High Reynolds Number Facility.

The authors wish to acknowledge the significant contributions of Mr. Emil Walk, formerly of the Fluid Mechanics Research Laboratory, as the project monitor, and Ms. Constance M. Woehle and Mrs. Shirley E. McGrath for typing the manuscript.

TABLE OF CONTENTS

TABLE OF CONTENTS (CONT'D)

SECTION PAGE

TABLE OF CONTENTS (CONT'D)

SECTION PAGE

LIST OF ILLUSTRATIONS

LIST OF ILLUSTRATIONS (CONT'D)

LIST OF ILLUSTRATIONS (CONT'D)

LIST OF ILLUSTRATIONS (CONT'D)

LIST OF ILLUSTRATIONS (CONT'D)

APPENDIX

LIST OF TABLES

SECTION I

INTRODUCTION

In July 1965 the Aerospace Research Laboratories at Wright-Patterson Air Force Base began to give serious consideration to the construction of a high Reynolds number aerodynamic test facility, the intention being to study turbulent flow phenomena at supersonic and low hypersonic speeds. The need for aerodynamic test data at high Reynolds numbers, particularly in this speed range, had become increasingly apparent in the course of identifying critical problem areas associated with the fluid mechanics of new and advanced Air Force systems. Increased attention was being given to "low and fast" aircraft and other weapon delivery systems, and there was also a trend toward larger rocket boosters and reusable launch vehicles. Fundamental information, such as heat transfer data, was scant in the appropriate Mach number/Reynolds number range, and extrapolation was virtually impossible. It was clear that there was a need for experimental data pertaining to pure turbulent boundary layers, flow interactions, heat transfer rates, skin friction values, wake characteristics, and aerodynamic stability under turbulent flow conditions. The Mach number range of particular interest appeared to extend from Mach 2 to Mach 6, with Reynolds numbers ranging up to 10^8 or greater. A thorough review of existing supersonic and hypersonic facilities throughout the country(1-6) revealed that very few were designed for operation at free stream unit Reynolds numbers much above 10^7 per foot. The principal exceptions were the shock tunnels which are unsuitable for some types of detailed flow studies due to their extremely short running times. In view of the very limited high Reynolds number testing capability which the country had, there appeared to be little doubt that the establishment of a high Reynolds number simulation capability at ARL would be a sound and timely investment in a research and development tool necessary for servicing current and future needs of Air Force systems.

Convinced of the need, ARL undertook to study the problem of providing the desired simulation capability as quickly and as inexpensively as possible, using existing technology wherever possible. It was apparent early in the study that the Mach number range could not be satisfactorily covered with one flow channel. The logical approach appeared to be to have a facility consisting of an unheated leg for low Mach numbers and a heated leg for higher Mach numbers, with as much common equipment as possible. It was decided that representative Mach numbers for the two legs should be Mach 3 and Mach 6, with no immediate provisions to be made for varying the test section Mach number of each leg.

Based upon the above decisions, a preliminary design study was made in which the requirements for major components were analyzed to establish the overall technical feasibility of the approach, and to ascertain costs, manpower requirements, and the effect of the facility on the existing research complex. Test section sizes and run times were of prime consideration due to their direct impact on facility size and facility service demands. Following this study, which concerned itself with conventional blowdown wind tunnel designs, two intensive reviews and several small studies were made to see if new or emerging technology could be expected to produce significantly superior facilities which would warrant a delay in the construction of a new facility. Since this did not appear to be the case, in February 1967 the decision was made to proceed with the design and construction of the Mach 3 leg of the facility. In-house work on the detailed design started immediately and construction effected by the FluiDyne Engineering Corporation of Minneapolis, Minnesota, was completed approximately two years later. This was followed by an exhaustive series of component check-out tests comprising well over one hundred tunnel runs. These were completed during March 1969. The installation and check-out of research instrumentation occupied the facility until September 1969, when calibration tests were started. These were completed in July 1970 and regular aerodynamic testing began during August 1970. The first aerodynamic test report containing data obtained from the tunnel was published in October 1971.(7)

The purpose of this report is to provide a single published source of information on the facility. It is intended to be useful to those preparing for tests in the facility and to those interpreting data obtained in the facility. For the interest of those engaged in the design and construction of similar facilities, an appendix covering the basic design considerations which led to the detailed design described in Section II of the report has been included.

SECTION II

DETAILED WIND TUNNEL DESIGN

The detailed design of the wind tunnel was based upon the design criteria and calculations discussed in the appendix. A facility design goal was established, namely, the safe production and control of a uniform Mach 3 flow, having a free stream unit Reynolds number (Re_∞) of 10^8 per foot at a stagnation pressure (P_0) of 570 psia and a stagnation temperature (T_0) of 500^0R. The test section size was to be nominally 8 inches square, with allowances for nozzle boundary layer growth. The tunnel was to be designed for direct exhaust to the atmosphere, and for exhaust to an existing 100,000 ft^3 vacuum sphere capable of being evacuated to a pressure of 1 torr. Based upon this design goal, a facility concept was developed, and expanded to the point of specifying design or performance criteria for all significant systems, subsystems and components. The end result of this effort is depicted in the facility perspective presented in Figure 1.

In order to identify the major components in the system, a brief description of the facility is given in terms of the path taken by the air through the facility. Air passes from a high pressure storage area through two parallel four-inch diameter Schedule XXS high pressure pipes into two remotely controlled isolation valves, which are manifolded together on the downstream side. This manifold connects to the common intake of a six-inch diameter pressure control valve and a two-inch diameter pressure control valve, of which both are hydraulically actuated. The two valves are connected in parallel to permit individual selection for operation at either high or low mass flow. Air passes from the active control valve to the settling chamber through a wide angle expansion, which incorporates a flow spreader to promote a uniform velocity profile. The settling chamber experiences the full stagnation pressure of the flow, and is fitted with a rupture disc to protect it from overpressurization in the event of control valve failure. Screens in the settling chamber help to reduce the scale and intensity of the turbulence in the flow prior to acceleration through the aerodynamic nozzle to the test section Mach number of 3. After the air passes over the model in the test section, it undergoes some deceleration in the diffuser, and then enters the downstream ducting and exhaust system. Further details on the facility components are given below with the same flow sequence.

1. HIGH PRESSURE AIR SYSTEM

The ARL high pressure air system includes over 15,000 ft^3 of 3000 psi air storage for the use of many special purpose test rigs and wind tunnels. Three four-stage reciprocating air compressors are able to take atmospheric air and deliver it to the storage vessels at a combined mass flow rate of 1.0 lb_m/sec. In addition to removal of condensed water and oil by separators, oil vapor is removed by a special "oil-sorb" unit. The saturated air is then dried by passage through one of two automatically cycled silica gel drying towers, which permit dew points as low as -100^oF to be achieved. Fine mesh filters assure that the air passing to the storage tanks is essentially particulate free. One 8250 ft^3 section of the storage area is normally available to the facility. The maximum system pressure is 3000 psia, but the pressure available to the Mach 3 facility is often lower due to the operation of other facilities. The air consumption/recovery ratio can be as high as 200 to 1 for this facility, which means that a sequence of three 60 second high pressure runs consumes more air than can be recovered in ten hours of compressor plant operation. Further details of the high pressure air system of interest to this particular facility are given below.

a. Storage Tanks

The 8250 ft^3 of storage volume referred to above is made up of twenty-eight 250 ft^3 tanks and one 1250 ft^3 tank. The tanks contain no heat sink materials and are completely exposed to atmospheric conditions. The small tanks each have a 2 in.-2500# ASA Ring Joint Flange outlet connection. The corresponding internal diameters are 1.503 inches and 2.300 inches, respectively, which are sufficient to keep local outlet velocities below 50 ft/sec for the small tanks and 100 ft/sec for the large tank.

b. Manifolding

The storage tanks are connected to two four-inch diameter Schedule XXS pipe manifolds through individual high pressure gate valves. Each pipe manifold is connected to fourteen 250 ft^3 tanks, but only one is connected to the 1250 ft^3 tank. The manifolds therefore have connected volumes of 3500 ft^3 and 4750 ft^3. Under normal conditions corresponding manifold air velocities should not exceed 150 ft/sec and 200 ft/sec, respectively.

c. Piping

The manifolds are connected to the facility by independent four-inch diameter Schedule XXS pipes, each incorporating a pressure balance four-inch high pressure shut-off gate valve upstream of the corresponding facility isolation valve. With the usual allowances for elbows, valves, tees and reducers, the approximate equivalent lengths of the two supply lines, including manifolds, are 400 ft and 300 ft, the longer length being associated with the manifold connected to the 1250 ft^3 tank. Figure 2 shows how the pressure drop increases with the mass flow rate for the combined supply lines for a range of storage pressures. Losses have been estimated up to, but excluding, the control valves. These curves can be used to establish the minimum storage pressure (P_{ST}) required for a run, providing allowances are made for the pressure drop through the control valve, and for the pressure drop in the storage vessels due to the air consumed and the associated expansion cooling. From an examination of the wide range of operating conditions possible, a good rule-of-thumb would be to have a minimum storage pressure of at least three times the tunnel stagnation pressure.

All of the components of the high pressure air system described above were subjected to a hydrostatic test at 4500 psig prior to use.

2. WIND TUNNEL PROPER

The wind tunnel proper comprises those mechanical elements essential to the conveyance, control, and aerodynamic conditioning of the test air. The design of the most important elements is discussed below, primarily from the standpoint of function and physical characteristics. Control and instrumentation aspects of the wind tunnel are discussed in Section III.

a. Tunnel Foundation

The tunnel foundation has the function of supporting the tunnel components, the upstream piping, and a portion of the downstream ducting. It is designed to resist the horizontal thrust loads that occur at maximum mass flow conditions, and the vertical loads that would occur following the rupture of either of two eight-inch rupture discs. By combining the foundations of the various components into one unit, the opposing horizontal forces are cancelled out in the foundation, and are not transmitted to the ground. The foundation is of reinforced concrete containing sleeved anchor bolts for component mountings. It is vibrationally isolated from the building slab by a 1/2-inch peripheral expansion joint.

b. Pressure Control System

The high pressure air control system comprises two isolation valves, one primary control valve, one secondary control valve, one equalization valve, and a control system. The function of the overall system is to control discretely the stagnation pressure in the settling chamber during a run.

(1) Isolation Valves

The two isolation valves are four-inch Grove Series G gate valves which are provided to assure positive remote isolation of the facility from the high pressure air supply system. In addition, the electro-hydraulic actuators operate fast enough (less than one second) for the valves to be used as shut-off valves under emergency conditions if the pressure control valve malfunctions in the open position. An adjustable differential pressure switch across the isolation valves can be used to time-sequence the operation of the control valves. In the event of power failure, the valves are hydraulically actuated to the closed position to provide a failsafe condition.

(2) Pressure Control Valves

The primary pressure control valve is a six-inch Annin Model 4510 valve, with a C.G.S. Model 361 electro-hydraulic actuator. It has a Cv of 290 and is used to control mass flows over a range of 50 to 200 lb_m/sec. The secondary pressure control valve is a two-inch Annin Model 4510, with a C.G.S. Model 321 actuator. It has a Cv of 35 and is used to control mass flows below 50 lb_m/sec. Both valves have linear characteristics, and can be operated in either an automatic mode or manual mode to achieve a set-point operating pressure in the settling chamber.

(3) Equalization Valve

The equalization valve is a Jamesbury 3/4-inch Type HP ball valve which provides a means of pressurizing the upstream side of the control valves prior to operation of the isolation valves. The equalization valve is fitted with a failsafe spring-loaded air cylinder operator which closes upon air or electrical power failure.

(4) Control Elements

The stagnation pressure control elements consist of a programmer, two controllers, two servo amplifiers, and three pressure sensing transducers which are integrated with the control valves and actuators to form the control loops for establishing and maintaining the desired air flow conditions. These form a process control system which is described later in Section III.

c. Settling Chamber

The settling chamber has the function of conditioning the air before it passes through the nozzle. Conditioning includes promoting a uniform velocity profile at the nozzle entrance, and reducing the scale and intensity of turbulence. In addition, the settling chamber volume must be sufficient to eliminate time variations in the sensed stagnation pressure, so that any control valve perturbations are not amplified in the control loop. Particular features of the settling chamber assembly are discussed below.

(1) Shell Assembly

The settling chamber shell assembly constitutes a pressure vessel, designed for 700 psi air service in accordance with Section VIII of the ASME code for unfired pressure vessels.(8) The upstream end of the welded structure incorporates a flanged manifold for mounting the two control valves, followed by a 90^0 long radius elbow. A conical wide-angle expansion member connects the downstream side of the elbow to the main cylindrical member of the shell. This main member incorporates a downstream connection flange, thrust mount pads, and a rupture disc assembly mounting flange. The eight-inch diameter rupture disc is sandwiched between flanges, and is sufficient to prevent overpressurization of the vessel in the event of control valve failure (wide open) at the maximum system pressure of 3000 psi. Thrust forces are transmitted by the brackets to the tunnel foundation through a steel thrust support member. Welded to the top of vessel are three mounting pads for the tunnel side-wall swing-arm assembly. The settling chamber diameter was chosen to provide a mass-averaged velocity of approximately 30 ft/sec. One of the primary concerns in the design was that air temperatures would on occasion be considerably below -20^0F, where many carbon and low alloy steels begin to suffer serious decreases in impact resistance. Instead of using a stainless steel, or of complying with the special material impact tests requirements, the code option of designing to a pressure equal to 2 1/2 times the maximum working pressure was chosen. The cylindrical section of the vessel did not require special low temperature consideration due to the use of an inner steel liner not subject to pressure loads. Since run times are short, on an absolute time scale, the pressure vessel itself does not reach the low air flow temperature.

(2) Flow Spreader

The limited building space available to the facility made it necessary to have a 90^0 long radius elbow, immediately followed by a wide-angle diffuser section, in order to make the transition from the high pressure piping to the full settling chamber diameter. Because of the high mass flow rates there was considerable concern that turbulence and asymmetry at the control valve, and centrifuging in the elbow, would lead to significant flow nonuniformities in the settling chamber. To counter this possibility it was decided to incorporate a perforated cone with the wide-angle diffuser. The idea of using such a device was not new, having been mentioned by Ferri and Bogdonoff as early as 1954,(9) but no experimental performance data were available. In fact, there was considerable room for debate on whether such a device might be more effective pointing downstream, rather than upstream as depicted in the few literature references discovered.(9-11) In view of this, some small scale studies were made by ARL to determine the influence of orientation on effectiveness. These studies are discussed further in connection with flow angularity measurements in Section IV. Pending the outcome of the small scale tests, the flow spreader was designed to be reversible. The cone has a semi-vertex angle of 45° (the semi-expansion angle of the wide-angle diffuser is 30°) and is fabricated from 3/4-inch thick perforated steel plate having .707 in. diameter holes and a porosity of 36%. The base is reinforced with a steel ring to support and align the cone inside the shell. Movement of the spreader is prevented by four steel stops welded to the shell upstream and by steel spacer rings downstream.

(3) Screens

Three turbulence screens are used downstream of the flow spreader to reduce the scale and intensity of turbulence and to improve further the velocity profile across the chamber. The screens can be variously located within the shell, depending on the cone orientation and ring spacer positions, but can never be placed closer than approximately one shell diameter to the cone apex, in order to avoid possible adverse wake effects. They are fabricated from stainless steel wire cloth silver soldered to a steel ring. Fairly high stresses can be experienced in taut mesh screens, so that the effects of low temperature brittleness, cloth to ring bonding, uniformity of screen tautness, and shock loading must be considered in estimating allowable stresses and arriving at acceptable mesh sizes. The effect of a screen failure can be remarkably detrimental to the finish of a precision machined nozzle and model. The Mach 3 facility uses one screen having a mesh size of 16 x 16 x .015 in. and two screens having mesh sizes of 22 x 22 x .010 inches. Original screens having mesh sizes of 20 x 20 x .010 in. and 32 x 32 x .0068 in. failed during check-out testing and were replaced by the heavier gauge ones. Screen spacings are 167 and 250, expressed in terms of the usual ratio of screen separation distance to screen wire diameter.

d. Entrance Bellmouth

The entrance bellmouth makes the transition from the circular cross-section of the settling chamber to the rectangular cross-section of the nozzle blocks. It consists of top and bottom flat aluminum plates, and circular aluminum side blocks. The side blocks attach flush to the straight nozzle sidewalls and extend upstream at a 14-inch radius to the settling chamber inner diameter. The flat plates are tangent to the upstream ends of the nozzle blocks (41° 38 ft from horizontal), and also extend to the settling chamber diameter. The bellmouth blocks are a precision fit with the nozzle block assembly, and with the bellmouth plates which they carry.

e. Nozzle

The nozzle is the single most important component of the facility, and as such received considerable attention in the design, fabrication, and installation processes. The nozzle assembly was designed to permit the use of different nozzle blocks producing Mach numbers up to 4.5, but to date the facility has been operated exclusively at Mach 3.0 with the original blocks.

(1) Aerodynamic Design

The inviscid contour of the nozzle is based upon a completely analytical design method due to Friedrichs(13) as modified by Nilson.(14) It was successfully used by Baron(15) for the design of a number of supersonic nozzles at the Naval Supersonic Laboratory of the Massachusetts Institute of Technology in 1954. The mathematical method of characteristics is not directly employed; rather a truncated series solution of the nonlinear wave equation is used to express the pertinent flow properties adjacent to the nozzle axis. The solution is valid in both the subsonic and supersonic portions of the field, and no assumptions need to be made with respect to the disposition of the sonic line. The method computes characteristic lines of the field by a numerical integration process, and downstream from one of these the flow may be made uniform by a simple mass-flow criterion for the simple-wave region streamlines. By examining the series it is possible to estimate the magnitude of the errors introduced by the discarded terms, whereas a comparative check using the method of characteristics requires recomputation with a finer mesh size. Reference 15 contains conveniently tabulated coordinates for the design characteristics, and corresponding potential-flow nozzle coordinates, for a Mach number range from 1.5 to 3.5. Direct use was made of the Mach 3.0 potential-flow data in arriving at that portion of the contour downstream of the nozzle inflection point. A circular arc profile was used for the contour upstream of this point. The circular arc was fitted to the fixed ordinates of the throat and inflection point, and was made tangent to the slope at the inflection point. It should be noted that the arc was fitted after correcting the inviscid contour for boundary layer effects. The boundary layer displacement thickness was calculated from Burke's equation (16) which relates the local turbulent boundary layer displacement thickness to the local Mach number and Reynolds number in the following way:

$$\frac{\delta^*_X}{X} = 0.0463 \frac{M_X^{1.311}}{Re_X^{0.276}}$$

The displacement thickness on the nozzle at the exit plane was calculated to be 0.0231 in. and 0.0482 in. for free-stream unit Reynolds number of 10^8 per foot and 7 x 10^6 per foot, respectively, corresponding to stagnation pressures of 570 psia and 40 psia at a stagnation temperature of 500°R. To avoid the possibility of recompression in the nozzle at low Reynolds numbers, the largest viscous correction in the operating range must be used. The value of 0.0482 in. was rounded off to 0.0500 in., and was used for both the sidewall correction and the contoured wall correction. Rather than calculate δ^* as a function of x down the nozzle, the displacement thickness was assumed to be a linear function of x, starting from zero at the nozzle throat. The magnitude of the correction is such that any inaccuracy so introduced is negligible. In order to preserve the benefits of plane parallel sidewalls, the total viscous correction was applied to the contoured walls. The nominal test section size of 8.0 in. high by 8.0 in. wide therefore became an actual size of 8.2 in. high by 8.0 in. wide. Figure 3 summarizes the nozzle configuration, and Table I gives the nozzle coordinates.

(2) Mechanical Design

The nozzle assembly is made up of top and bottom contoured aluminum nozzle blocks, two steel nozzle block supports, and two steel

Table I

MACH 3 NOZZLE COORDINATES

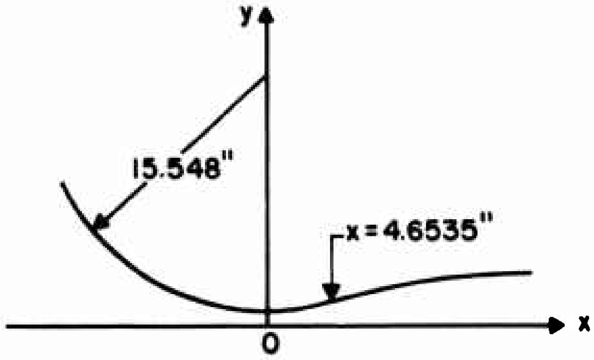

The contour of the Mach number 3 nozzle is based on Friedrich's method and is corrected for boundary layer growth. The subsonic intake and the supersonic starting portion to x = 4.6535 (the inflection point in the contour) are formed by a radius of 15.548 inches with the center located on the ordinate through x = 0, the nozzle throat. Since the coordinates are given upstream of the inflection point by this radius, the coordinates given below are for the contour from the inflection point to the nozzle exit.

x	y	x	y
0.	0.9445	6.5000	2.1905
4.6535	1.6572	6.5158	2.1948
4.6830	1.6662	6.6479	2.2306
4.7971	1.7006	6.7810	2.2661
4.9123	1.7352	6.9157	2.3019
5.0000	1.7614	7.0000	2.3240
5.0285	1.7699	7.0513	2.3374
5.1459	1.8046	7.1884	2.3729
5.2644	1.8397	7.3267	2.4084
5.3841	1.8748	7.4663	2.4437
5.5000	1.9087	7.5000	2.4521
5.5049	1.9101	7.6072	2.4789
5.6268	1.9454	7.7493	2.5140
5.7503	1.9810	7.8924	2.5495
5.8748	2.0165	8.0000	2.5749
6.0000	2.0519	8.0372	2.5837
6.0006	2.0521	8.1838	2.6184
6.1275	2.0878	8.3313	2.6530
6.2558	2.1235	8.4800	2.6872
6.3852	2.1592	8.5000	2.6918

Table I (continued)

x	y	x	y
8.6301	2.7214	14.9968	3.7389
8.7817	2.7553	15.0000	3.7421
8.9345	2.7891	15.2028	3.7593
9.0000	2.8033	15.4106	3.7795
9.0887	2.8225	15.5000	3.7877
9.2443	2.8557	15.6200	3.7987
9.4012	2.8887	15.8316	3.8178
9.5000	2.9092	16.0000	3.8323
9.5595	2.9215	16.0477	3.8362
9.7193	2.9545	16.2598	3.8539
9.8804	2.9861	16.4768	3.8711
10.0000	3.0094	16.5000	3.8729
10.0430	3.0178	16.6956	3.8880
10.2070	3.0497	16.9165	3.9041
10.3723	3.0809	17.0000	3.9100
10.5000	3.1047	17.1393	3.9198
10.5391	3.1120	17.3642	3.9348
10.7073	3.1426	17.5000	3.9431
10.8771	3.1729	17.5909	3.9486
11.0000	3.1945	17.8196	3.9631
11.0481	3.2030	18.0000	3.9734
11.2207	3.2326	18.0506	3.9763
11.3948	3.2617	18.2833	3.9889
11.5000	3.2790	18.5000	4.0002
11.5704	3.2906	18.5181	4.0011
11.7474	3.3192	18.7555	4.0124
11.9259	3.3473	18.9949	4.0232
12.0000	3.3587	19.0000	4.0234
12.1059	3.3750	19.2366	4.0333
12.2876	3.4024	19.4804	4.0427
12.4706	3.4293	19.5000	4.0434
12.5000	3.4335	19.7265	4.0517
12.6553	3.4558	19.9479	4.0595
12.8414	3.4819	20.0000	4.0603
13.0000	3.5038	20.2257	4.0672
13.0291	3.5078	20.4789	4.0737
13.2186	3.5328	20.5000	4.0742
13.4095	3.5575	20.7346	4.0797
13.5000	3.5690	20.9926	4.0850
13.6021	3.5819	21.0000	4.0851
13.7964	3.6057	21.2530	4.0898
13.9921	3.6291	21.5000	4.0933
14.0000	3.6300	21.5162	4.0935
14.1897	3.6521	21.7819	4.0966
14.3889	3.6745	22.0000	4.0984
14.5000	3.6866	22.0503	4.0988
14.5896	3.6963	22.2801	4.1000
14.7925	3.7179		

sidewalls. These components are bolted to each other and to the nozzle flange which mates with the downstream flange on the settling chamber. In this manner, and with the aid of linear "O"-ring type seals, a pressure tight box was designed to withstand 700 psig upstream of the throat, 200 psig downstream of the throat, and a pressure of 1 torr throughout. The nozzle blocks are aluminum plates eight inches wide by 32-3/8 inches long, and are bolted and keyed to the steel support members which transmit axial and vertical loads from the blocks into the nozzle flange. The sidewalls of the box are steel flat plates which are flanged at the upstream ends to provide a means of attachment to the nozzle flange. The design pressure of 200 psig downstream of the nozzle throat relates to the stagnation pressure attainable behind a normal shock at a Mach number of 3 and a stagnation pressure of 600 psi. Higher pressures due to emergency conditions are not reached due to the rupture disc located further downstream.

f. Test Section

(1) Aerodynamic Design

A closed test section was chosen in contrast to an open jet, since it was felt that at the high operating densities the strong shear layer at the jet boundary might induce significant secondary flow disturbances, and might also lead to a significant noise problem. A nominally square test section was chosen in preference to any other cross-sectional shape due to a wide variation in anticipated test model configurations. Geometrically then, the test section is a parallel wall continuation of the nozzle exit cross-section. No further corrections for boundary layer growth were made initially, for reasons of simplicity in fabrication and the ever present uncertainty of computed boundary layer displacement thicknesses. It is therefore to be expected that a slight negative Mach number gradient will exist in the test section due to the uncompensated boundary layer growth.

(2) Mechanical Design

The test section comprises a top wall, a bottom wall, and two sidewalls. The top and bottom walls are bolted to the nozzle flange upstream and to the diffuser plates downstream. In addition to the end support, this framework is supported from below by a movable nozzle-test section cart which can be adjusted to achieve vertical and lateral alignment during assembly. The sidewalls attach to the top and bottom walls with quick-release latches, and are supported during assembly and removal by a swing arm support permanently mounted to the settling chamber. Sealing of the various rectangular components comprising the nozzle-test section assembly is accomplished with linear O-ring type seals, which include several "tee" intersections requiring careful handling during assembly. Once assembled, the components form a pressure-tight box which is designed for 200 psig. The sidewalls extend from the diffuser inlet to a point ten inches upstream of the nozzle exit, in order to provide maximum window coverage. Three sets of sidewalls were fabricated, one set being furnished with eight-inch diameter window assemblies centered on the nozzle exit plane, the others being blank for future window locations as desired. All the sidewalls are symmetrical, and can be turned end for end to double the window location possibilities. The window assemblies themselves comprise two-inch thick schlieren quality glass discs, permanently mounted in steel frames to insure a flush fit with the sidewalls at all times. The top wall of the test section accommodates a four-inch diameter steel blank which can be replaced by similarly sized instrumentation plugs as desired. The plan bottom wall originally installed in the test section can be replaced by either of two other walls which are associated with the two model support assemblies described later.

g. Model Support Systems

The tunnel is equipped with two model support assemblies, one providing a pitch capability of $\pm 10^{0}$, and one giving a fixed zero pitch angle. Both assemblies have their own test section bottom wall to permit complete bench setup of models and instrumentation. The sting socket on each strut is identical in design to permit the interchange of stings. The maximum design loads were ±2000 lbs. normal force, acting at a point on the sting centerline three inches upstream of the plane of intersection of the model base with the sting, and ±1000 lbs. axial force, acting along the sting centerline. Maximum moments were taken as those resulting from the application of the maximum normal and axial forces acting either together or independently. Since the maximum loads indicated result from an abrupt nonsteady flow condition, the model support systems were designed for an impact factor of two. If required, the tunnel can be operated in a "clean" condition by employing a plain test section bottom wall furnished with the tunnel.

(1) Fixed Strut

The fixed strut model support system comprises a straight strut support mounted on a plate which is attached to the test section bottom wall. The strut and mounting plate can be removed from the test section as an assembly without removing the test section bottom wall if desired. The upper end of the strut contains a tapered socket for mounting the sting. The back of the socket contains a sting nut which is used for both seating and unseating the sting plug in the socket. The main length of the strut has a wedge-shaped leading edge, and an instrumentation cavity machined into the trailing edge to route leads from the model to the outside through openings machined in the mounting plate. The machined cavity is slotted to accommodate an insert cover plate, and a screwed cover plate behind the sting socket completes the mechanical assembly.

(2) Movable Strut

The movable strut model support system comprises a strut, strut support assembly, actuator, potentiometer, and enclosure. The movable strut is similar to the fixed strut except that it is a circular arc segment supported and guided by a support assembly bolted to the test section bottom wall. A hydraulic cylinder actuator is trunnion-mounted to the strut support casting, and is attached to the strut with a clevis bracket. The full piston stroke provides exactly the required $\pm 10^0$ pitch angle range, and a linear potentiometer provides remote readout of the strut pitch angle. Provision has been made for centering the pitch angle about the tunnel centerline. The entire lower portion of the assembly, including the actuating cylinder and potentiometer, is enclosed in a pressure-tight enclosure which is sealed and bolted to the test section bottom wall. The lower half of the enclosure is removable to provide access to the inner assembly without disturbing electrical and hydraulic feedthroughs.

h. Diffuser

The diffuser was designed as a constant area duct, having the same cross section as the test section, followed by a diverging section. A diffuser throat configuration was considered, but not employed for the following reasons. At Mach 3 the theoretical ratio of the diffuser throat area to the test section area is 0.7192 for a clean tunnel. This value is based upon the diffuser throat being just sufficient to swallow the test section normal shock during starting. However, the presence of a model in the test section during the starting process creates a shock system with greater losses, resulting in a lower total head downstream. On the basis of mass flow continuity the diffuser throat must therefore be larger than the theoretical clean tunnel value, and in practice a 30% increase in throat area ratio is usually employed. Applying this factor to the calculated value at Mach 3 raises the diffuser throat area to 0.9350 of the test section area. In view of the closeness of this ratio to unity, and in view of the thickening boundary layers on the diffuser walls, there appeared to be little point in providing a diffuser convergence. However, the requirement was established that the constant area duct be designed to accommodate top and bottom throat plates at a later date, if desired. The resulting diffuser subassembly consists of a constant area duct section, a diverging transition section, a slip joint, and a safety tee.

(1) Constant Area Section

The constant area section is made up of four separate machined plates, bolted and keyed together to form a rectangular duct 8.0 in. wide x 8.2 in. high x 80.0 in. long. The plates are sealed with linear O-ring type seals, and can be individually replaced or provided with inner blocks or plates to provide a different aerodynamic configuration. The duct assembly is entirely supported by the adjacent components to which it is bolted.

(2) Transition Section

A transition from rectangular to circular flow cross section is accomplished by a machined weldment which changes from an upstream internal cross section of 8.0 in. x 8.2 in. to a downstream internal diameter of 13.25 inches. This allows the flow to diverge to more than twice the area over a length of 38.0 inches. The downstream end of the transition piece is continued as a straight pipe section for 6.5 in. to form part of the slip joint which follows. The weldment is supported by a movable cart, which allows alignment of the diffuser in the same manner as that of the test section cart, and in turn supports the downstream end of the constant area duct.

(3) Slip Joint and Safety Tee

This is a dual purpose component designed to provide a slip joint for removing upstream equipment, and to provide a mounting flange for a rupture disc assembly. A 14 x 14 x 8 in. weld tee is used to accomplish this. The upstream end is flanged, and has a machined socket to accept the downstream end of the transition section to form the slip joint. A movement of 2.5 in. is possible, which is sufficient to allow removal of the nozzle, test section, or diffuser duct. An eight-inch diameter rupture disc is mounted on the top outlet flange of the tee. The disc has a rating of 200 psig and prevents overpressurization of all components upstream as far as the nozzle throat. The rupture disc assembly is sandwiched between the tee flange and the lower flange of a vent stack which penetrates the building roof. Replacement of the disc requires only that the flanges be slightly separated by jack screws. The downstream flange of the tee connects with the exhaust ducting, and the tee itself is supported by a thrust mount tied to the tunnel foundation.

3. EXHAUST SYSTEM

As discussed later in the appendix, the tunnel was initially designed to exhaust into a 100,000 ft^3 vacuum sphere, due to uncertainties about the availability and effectiveness of low pressure drop silencers, and this system is described in paragraph a. below. Operational experience with this system pointed up a significant low frequency sphere vibration problem which gave rise to concern for the continued structural integrity of the sphere. Due to ambient and localized temperature effects, appendages, and widely differing ways in which the sphere was used to serve several facilities, a meaningful determination of vessel fatigue life was considered unreliable. It was therefore decided to disconnect the Mach 3 wind tunnel from the vacuum sphere, and to utilize a common exhaust silencer for it and the Mach 6 wind tunnel, which was subsequently completed in 1972. This atmospheric exhaust system is now in use and is described in paragraph b. below.

a. Vacuum

The vacuum exhaust system configuration was as depicted in Figure 4. The entire system, including the vacuum sphere, was designed for service between 60 psig pressure and 1 torr pressure. The wind tunnel was isolated from the vacuum sphere by the 36 in. diameter sphere valve. The only purpose of the 14 inch diameter tunnel valve was to provide personnel safety in the event of sphere valve failure with an open test section. The vent valve permitted depressurization of the system to atmospheric pressure if required. The 90^{0} turn was designed as a tee to provide a full 36 in. access hatch to the model catcher, which was installed at 45^{0} to the incident flow. Apart from the sphere vibration noted above, the system performed entirely satisfactorily. The system performance of sphere pressure versus run time is given for the full range of tunnel stagnation pressures in Figure 5. Assumptions made include an initial sphere pump-down to 1 torr, and no vacuum pumps on-line during tunnel operation. In practice the vent valve was automatically operated when the sphere pressure reached 45 psig to insure against inadvertent rupture of the sphere safety disc, which was designed to fail at 60 psig.

b. Atmospheric

The currently used atmospheric exhaust system is depicted in Figure 6. Much of the vacuum exhaust system was used to construct the new one, particularly the ducting, sphere valve, and model catcher tee. The tunnel valve was eliminated and replaced by ring spacers, and the vent valve was replaced by a rupture disc designed to fail at 20 psig. The silencer assembly consists of two identical commercial units mounted on a concrete plenum which contains a guide vane assembly. The commerical units are rectangular panel insert types which employ a glass fiber acoustic fill material between perforated steel plates. The units have good dynamic insertion loss ratings at frequencies between 850 and 3400 cycles per second, but measurements to date indicate that much of the acoustic energy is at low frequencies outside of this range. The units are operated with a maximum face velocity of 4500 fpm, compared to a rated maximum of 5000 fpm. Certified performance data on this type of unit indicates that, even when the face velocity approaches zero, the overall attenuation does not improve significantly. It is possible that acoustical lagging of the ducting and silencer will be necessary, since the total radiated noise at a distance of 50 ft from the silencer exhaust was reduced only from 126 dB with one silencer unit to 113 dB with a second unit stacked immediately on top of the first. Efforts to positively identify the major noise sources and frequencies are continuing.

SECTION III

WIND TUNNEL CONTROLS AND INSTRUMENTATION

The instrumentation required to monitor the condition or status of the tunnel at all times, the interlocks which insure safe operation, the stagnation pressure controller, and the model support control system will be described in this section. A prime consideration throughout is to provide a maximum of safety to personnel and equipment while employing the simplest and most trouble free control hardware. The controls and interlocks originally used for the "exhaust to sphere" configuration have been modified, or removed as required, for the "exhaust to atmosphere" configuration. Consideration will be limited to the latter configuration and the safety interlock with the parallel Mach 6 facility.

Figure 7 is a simplified process diagram illustrating all of the necessary monitoring and control stations. With all valves initially closed, a typical run sequence would be as follows:

1) Preset the desired P_o on Controller
2) Open "Supply" valves
3) Open "Exhaust" valve
4) Open "Isolation" valves
5) Initiate "Run" utilizing proper "Control" valve for mass flow desired
6) Close "Control" valve
7) Close "Isolation" valves
8) Close all remaining valves.

1. SYSTEM STATUS MONITORS

The flow variables are monitored and indicated to the operator by the following devices (see Figure 7):

1) P_1, P_2--Supply Pressure

   Ashcroft pneumatic transmitter (C4080TA)

   Ashcroft pneumatic receiver (1224C)

   0-3000 psia calibration

2) P_0--Settling Chamber Pressure

   Ashcroft pneumatic transmitter (C4480S)

   Ashcroft pneumatic receiver (1228)

   0-600 psia calibration

3) T_0--Settling Chamber Temperature

   Conax copper constantan thermocouple probe (T-SS12-B-PJFC-PG2-125AT-18)

   Assembly Products panel meter (355)

   -200 to 100^oF calibration

4) P_c--Test Section Static Pressure--dual range

   Range 1: Taylor pneumatic transmitter (215TA11112-1507)

   Ashcroft pneumatic receiver (1223)

   0-1000 mm Hg calibration

   Range 2: Ashcroft pneumatic transmitter (C4030S)

   Ashcroft pneumatic receiver (1223)

   30 inch vacuum to 300 psig calibration

5) T_c--Test Section Static Temperature (Wall)

   Copper constantan thermocouple

   Assembly Products panel meter (355)

   -200 to 100^oF calibration

6) P_e--Exhaust Pressure

Ashcroft pneumatic transmitter (C4080S)

Ashcroft pneumatic receiver (1223)

30 inch vacuum to 60 psig

In addition, certain flow parameters are sensed by pressure switches and used by the interlock system. They are as follows (see Figure 7):

1) ΔP--Differential pressure across isolation valves

Deltadyne ME101-B-A-R-11

Set to 15 psid

2) P_o--Settling Chamber Pressure

Mercoid Type DA-21-2

Set to 600 psia

3) ΔP_{SRD} --Settling Chamber Rupture Disk Limit

Deltadyne ME102-E-A-R-21

Set to 1/2 psid

4) ΔP_{DRD}--Diffuser Rupture Disk Limit

Deltadyne ME102-E-A-R-21

Set to 1/2 psid

5) P_e--Exhaust Pressure--Dual Range

Barksdale D2T-A80

Set at 20 psia

To complete the interlock system inputs, each valve is fitted with a limit switch at each end of its stroke, thereby giving four logical states to each valve motion:

1) closed

2) not closed

3) not open

4) open

States 2 and 3 are used to indicate a valve in some position between fully closed and fully open.

2. INTERLOCK SYSTEM

The interlock system utilizes 24 volt DC relay and limit-switch logic elements throughout to insure reliable service and easy maintainability. All final control elements are 24 volt solenoid valves which control either air or hydraulic actuators as described in Section II of this report. Figures 9 through 13 illustrate the detailed logic involved in each of the valve operations. Figure 8 illustrates the "and," "or" logic convention. Figure 9 illustrates the "and" logic circuit which gives the combined status of the Control valves. Figure 10 illustrates the complete logic diagram for the Equalization and Isolation valves. The normal operating sequence is first to preselect either Isolation valve #1 or #2 or both and then to initiate an "OPEN" cycle which opens the Equalization valve until the ΔP across the Isolation valves drops below 15 psid, and then the preselected Isolation valve(s) are opened. From the logic diagram it can be seen that, in order to actuate the Equalization valve, eight inputs are required to be "true" simultaneously:

1) the "OPEN" pushbutton must be actuated,

2) the hydraulic pressure must exceed the high limit set point,

3) the Mach 6 air supply valve must be closed,

4) the cabin doors must be closed,

5) the control valves must be closed,

6) the "CLOSE" pushbutton must not be actuated,

7) the exhaust valve must be open, and

8) the isolation valves must not be open.

As soon as the Equalization valve signal is output, the "OPEN" pushbutton may be released and the signal will be maintained. Similarly, the Isolation valve signal will be output when:

1) the "CLOSE" pushbutton is not actuated,

2) the exhaust valve is open,

3) the settling chamber pressure is less than 600 psia,

4) the hydraulic pressure is greater than the low limit set point,

5) the equalization valve signal is "true,"

6) the control valves are closed,

7) the delta pressure across the isolation valve is less than 15 psid,

8) the calibration valve is closed, and

9) one or both of the isolation valves have been selected.

Once the Isolation valve signal has been output it will remain as long as:

1) the isolation valve remains open,

2) the "CLOSE" pushbutton has not been actuated,

3) the exhaust valve remains open,

4) the settling chamber pressure does not exceed 600 psia, and

5) the hydraulic pressure does not drop below the low limit set point.

As soon as the Isolation valve(s) open, the Equalization valve will close, since the "Isolation Valves Not Open" signal will be lost.

Each of the remaining logic diagrams, Figures 11 through 13, similarly indicate the interlock conditions required for each of the other valves and the "ALARM" circuit.

3. STAGNATION PRESSURE CONTROL SYSTEM

The stagnation pressure control is a closed loop electro-hydraulic servo system with major components connected as illustrated in Figure 14. The control system will increase the settling chamber pressure from the initial starting value to any preselected set-point pressure between 20 and 570 psia within three seconds and maintain this pressure to within ±0.5% or ±0.5 psia, whichever is larger, for a maximum run time of 60 seconds. It may be operated in either manual or automatic mode and in automatic mode is interlocked and initiated as outlined in the preceding discussion of interlocks. It is normally operated in the automatic mode with manual control being used for maintenance checkout purposes only.

a. Process

The process is assumed to be influenced only by the settling chamber and nozzle, and it can be shown that the transfer function is of the form:

$$G_T(s) = \frac{P_0}{\dot{m}}(s) \;/\; K(s) = \frac{\tau}{s+1}$$

where P_0 is the settling chamber pressure in psia,

$\dot{m}$ is the pressure control valve mass flow in lb_m/sec,

K is the process gain in psi/lb_m/sec,

τ is the process time constant in sec, and

s is the Laplace operator.

Also, K and τ are given by

$$K = \frac{\bar{P}_0}{\bar{\dot{m}}}$$

$$\tau = \frac{V}{28.4\, A^* \sqrt{T_0}}$$

where $\overline{P}_0$ is the quasi-steady settling chamber pressure in psia,

$\overline{\dot{m}}$ is the quasi-steady nozzle mass flow in lb_m/sec,

V is the settling chamber volume (15 cu ft),

A* is the throat area (0.105 sq ft), and

T_0 is the settling chamber temperature ($\approx 500^oR$).

For this process the gain is 2.78 psi/lb_m/sec and the time constant is 0.225 sec.

b. Pressure Sensor

The pressure sensor consists of three pressure transducers of 0 to 150, 0 to 300, and 0 to 600 psia, switch selectable in accordance with the range desired. To the control loop the three transducers appear to have the same characteristic 120 psia/volt; however, the linearity is improved by switching to a lower range transducer when operating in a lower range. The transducers are Robinson-Halpern P45 Series, with a rated total error band of ±0.15% of full scale, including hysteresis, linearity and repeatability.

c. Programmer

The programmer is a CGS Model 806. A linear 0 to 10 volt ramp is generated when a "RUN" command is received. The ramp time is adjustable from 1.3 to 4.3 seconds and is normally set at 3.0 seconds. The control point is set by adjusting a potentiometer which voltage divides the ramp output; therefore, regardless of the set-point the output always reaches full scale in the preselected time.

d. Controller

The first or "outer loop" controller is a CGS Model 671. The first controller compares the ramp from the programmer to the output of the pressure sensor and then acts upon the difference between these signals with proportional and reset (integral) action.

The second or "inner loop" controller is a CGS Model 672. The second controller compares the output from the first controller to the output of the pressure sensor and then acts upon the difference between these signals with proportional and reset action. The pressure sensor (P_0) signal is input to the second controller to improve the damping characteristics.

An automatic gain control (AGC) is inserted between the two controllers to increase the loop gain and compensate for the decreasing process gain as supply air pressure (Ps) decreases.

e. Servo Amplifiers

The output of the second controller may be manually switched to either of two CGS Model 661 servo amplifiers, one (SA2) matched to the two inch control valve and actuator and the other (SA6) matched to the six inch control valve and actuator. The servo amplifier compares the output of the second controller to the output of the valve position feedback signal and then acts upon the difference between these signals to position the valve correctly. A 60 Hz dither may be added in the servo amplifiers to overcome the static friction of the valve actuators.

f. Process Control Loop

The complete process control loop is illustrated in Figure 15. The principal nonlinear element in the loop is the servo valve. The actuator response is assumed to be a velocity limited capacitance, and the process response is as previously discussed. The pressure transducer has a linear response and acts as the feedback element. The "Inner Loop" controller is adjusted to cancel the denominator of the actuator response term, and the "Outer Loop" controller is adjusted to cancel the denominator of the process response term.

4. VALVE RESPONSE TESTS

A series of valve response tests were run on each of the control valves to determine the response time of the actuator and to verify the process time constant. Figures 16 and 17 show the results of one such test on each of the valves. The tests were run with the control loop open and by applying a step command voltage to the input of the servo amplifier, thus causing the valve to open to a predetermined position in the minimum possible time. The command voltage was then removed to close the valve in the minimum possible time. Valve Position (VP) is the output of the valve position indicating unit in volts and is used only to determine the response time of the control valves. P_S and T_S are the supply pressure and temperature as measured just upstream of the control valves. The valve response is well within the specified one second. The process time constant as determined from each of these tests is 0.23 second, which is in near agreement with the calculated value.

5. WATER HAMMER

From Figures 16 and 17 one can observe the commonly referred to "water hammer," which is due to momentum exchange of the rapidly accelerating or decelerating fluid in the pipeline. This can become a serious problem as mass flows increase in high Reynolds number facilities.

The pressure rise,(17) with the neglect of frictional losses, due to the rapid closing or opening of a valve and the subsequent change in velocity of a fluid in a pipe is

$$\Delta p = \frac{\rho a \Delta V}{g}$$

provided the valve closure time is less than the time required for the acoustic wave to travel the length of the pipeline to the supply reservoir and back. The time of travel in sec. is

$$t = 2 \frac{Lp}{a}$$

where Lp is the length of pipe from valve to reservoir in ft, a is the speed of sound in air in the pipe in ft/sec, and ρ is the density of air in the pipe in lb_m/ft^3. The frequency of oscillation in Hz in the pipe is

$$f = 1/t$$

For a given mass flow the pressure rise in psi becomes

$$\Delta P = \frac{a \Delta \dot{m}}{Apg} = \frac{1.444 \sqrt{TST} \Delta \dot{m}}{Ap}$$

where

Ap is the pipe cross sectional area in sq in.,

$\dot{m}$ is the mass flow in lb_m/sec, and

T_{ST} is the initial air storage temperature in ^oR.

For the Mach 3 facility operating at maximum mass flow of 200 lb_m/sec, a supply reservoir temperature of 530^{o}R and a pipe area of 15.52 sq in., the maximum pressure rise, with no frictional losses, is 428 psi. From Figures 16 and 17 the time for the acoustic wave to travel the length of the pipe and back is 0.41 sec, which corresponds well with the average length of pipe between the control valve and the reservoir (250 ft). The distributive nature of the air storage bottle connections to the pipeline and the number of valves and elbows between the bottles and the control valve tend rapidly to dampen the oscillation, and stabilization of the settling chamber pressure occurs in less than 1.5 sec.

For design considerations, note that the maximum pressure rise occurs at the minimum cross sectional area through which the mass must flow; therefore, cross sectional areas should be designed large to minimize pressure rise. The pressure rise may be eliminated completely by designing the valve closure time to exceed the time of travel of the acoustic wave through the pipeline from the valve to the reservoir and back.

6. CONTROLLER RESPONSE

The effect of the "water hammer" on stabilization of the settling chamber pressure during a normal controlled run is shown in Figures 18 and 19. The oscillation affects the pressure ramp; however, it dampens out rapidly, and stabilization of the settling chamber pressure occurs within the required four seconds.

The optimum gain and reset rate values were experimentally verified during initial controller test runs. Satisfactory response is obtained by maintaining the "outer loop" controller gain at 0.05 volt/volt and reset rate at 600 repeats per minute. The "inner loop" controller gain must be set according to the valve size in use, 25 volts/volt for the six-inch valve and 100 volts/volt for the two-inch valve. The "inner loop" reset rate may be maintained at two repeats per minute for either valve.

7. MODEL SUPPORT SYSTEM CONTROL

The model support system control consists only of the rudimentary hardware required for a closed loop control system to be added at a later date. The support sector is moved by a linear hydraulic cylinder which is connected at a radius of 18.7 inches from the pitch centerline. The cylinder has a total travel of 6.5 inches, cushions at both ends, and will move the sector exactly 20^{0} or $\pm 10^{0}$ from the tunnel centerline. The hydraulic fluid to the cylinder is controlled by a four-way, center off, solenoid valve which is in turn controlled by a panel mounted switch. The pitch angle is indicated by a panel meter which is calibrated in degrees and is driven by the output of a linear potentiometer operated by the hydraulic cylinder. The error in indicated angle due to the linear actuation is approximately 0.1%, and to the panel meter and potentiometer combination approximately ±1.5%. The pitch rate is controlled by a manually adjusted throttling valve in the hydraulic actuating cylinder return line. It is intended to close the loop between the feedback potentiometer and the actuator by adding a pitch programmer, a servo controller, and replacing the solenoid valve and needle valve with a hydraulic servo valve.

SECTION IV

AERODYNAMIC CALIBRATION OF THE WIND TUNNEL

The aerodynamic calibration of the Mach 3 high Reynolds number facility whose nozzle and test section dimensions are shown in Figure 20, consisted of the following series of tests:

1) measurements to determine the lateral and longitudinal Mach number distributions in the test rhombus
2) measurements to determine the magnitude of flow angularity in the test rhombus
3) a limited number of tunnel blockage tests
4) some flow visualization studies to determine the fluid dynamic problems of the facility's start-stop process.

The measurements were made at an average stagnation temperature of 480^{0}R and three nominal stagnation pressures of 100, 300 and 500 psia. The corresponding free stream unit Reynolds numbers are 18.6 x 10^6; 56 x 10^6 and 93 x 10^6 per foot, respectively.

1. THE LATERAL MACH NUMBER DISTRIBUTIONS

The lateral Mach number distributions in the test rhombus were determined from measurements made with a pitot pressure survey rake, which is shown in Figure 21. It consisted of a diamond airfoil body with a span of 7.562 inches, a chord of 2 inches, and a maximum thickness of 0.5 inch. Attached to the leading edge were seven pitot pressure tubes spaced 1.24 in. apart. These tubes had an outside diameter of 0.125 in, an inside diameter of 0.0635 in. and a 30^{0} internally beveled inlet. The outboard pitot tubes were 1.5 inches long while the centerline tube was a pitot-static probe 2.87 inches long with four orifices located one inch behind the pitot tube inlet. These four static pressure orifices were 90^{0} apart and were manifolded together to give an integrated average of the local static pressure. All the rake tubes were made of stainless steel and were silver soldered inside the diamond shaped airfoil body. The leads were taken through a hollow sting to two separate rotary valve and transducer combinations. One of these units was equipped with a 25 psia variable reluctance transducer and was used to measure the local static pressure, while the second unit was equipped with a 250 psia variable reluctance transducer and was used to measure the seven pitot pressures. The outputs of both of these units were recorded on a 36 channel oscillograph recorder. Other parameters recorded with these units were the stagnation pressure, stagnation temperature, and the wall static pressures along the nozzle and diffuser. The pitot rake was positioned in the facility so that the leading edges of the short pitot tubes were at the following stations: $x_p/x_r = 0$, ±0.345, and ±0.690 (as per nomenclature indicated in Figure 22). At each of these five longitudinal stations the survey rake was rolled to four different angles in order to more fully map the test rhombus Mach number distribution. The roll angle ϕ was measured from the horizontal plane in a clockwise direction while looking upstream. Measurements were made at $\phi = 0^\circ$, 45°, 90° and 135°, respectively.

Under certain conditions portions of the survey rake extended outside the test rhombus. An inspection of the geometry indicates that under the conditions listed below all the pitot tubes were inside the rhombus.

x_p/x_r	ϕ
—	Deg
0	0
±0.345	0
±0.690	45
0	45
0	90
0	135

For the following rake positions the outboard pitot tube on each side of the rake was outside the rhombus,

x_p/x_r	ϕ
—	Deg
± 0.345	45
↓	90
	135

while possibly the two outboard tubes on each side of the rake were outside the rhombus for the following rake positions,

x_p/x_r	ϕ
—	Deg
± 0.690	45
↓	90
	135

No data were taken at station $x_p/x_r = -0.690$ with the rake at $\phi = 90^0$ since the rake was too large for positioning within the tunnel at this station.

The local Mach numbers were computed from Rayleigh's pitot equation in the form

$$\frac{p_o'}{p_o} = \left[\frac{(\gamma+1)M}{(\gamma+1)M^2+2}\right]^{\frac{\gamma}{\gamma-1}} \left[\frac{(\gamma+1)}{2\gamma M^2-(\gamma-1)}\right]^{\frac{\gamma}{\gamma-1}} \qquad (1)$$

where p_o is the tunnel stagnation pressure and p_o' is the measured pitot pressure. The corresponding Mach number was calculated by computer iteration of Eq. (1).

Two other methods were used to check the Mach number calculated from Eq. (1). Since the centerline probe was a pitot-static probe, the centerline Mach number was calculated by another method using Rayleigh's equation in the form

$$\frac{p_o'}{p} = \left[\frac{(\gamma+1)M^2}{2}\right]^{\frac{\gamma}{\gamma-1}} \left[\frac{(\gamma+1)}{2\gamma M^2-(\gamma-1)}\right]^{\frac{-\gamma}{\gamma-1}} \qquad (2)$$

where p_o' is the measured centerline pitot pressure and p is the locally measured static pressure. Here too, the Mach number was calculated by computer iteration of Eq. (2).

The other method for checking the Mach number was carried out through the use of the energy equation in the following form:

$$\frac{p_o}{p_w} = \left(1 + \frac{\gamma-1}{2} M^2\right)^{\frac{\gamma}{\gamma-1}} \qquad (3)$$

where p_o is the tunnel stagnation pressure and p_w is the measured nozzle and/or diffuser wall static pressure. The use of Eq. (3) for such a calculation implies that the flow is isentropic and that dp/dy = 0 through the tunnel wall boundary layer.

The lateral Mach number distributions for a nominal unit Reynolds number of 20.7 x 10^6 per foot are shown in Figures 23a through 23c. Inside the test rhombus the measured Mach numbers are within ±2% of the design Mach number of three. In some cases the measured Mach number near the tunnel side walls was lower than the design value. This decrease in local Mach number is believed to be caused by very weak nozzle disturbances. These free stream disturbances are visible in the shadowgraph and schlieren photos shown in Figures 45 and 46. The corresponding decrease in local Mach number can be observed in Figure 23a for both $\phi = 45^o$ and $\phi = 135^o$, where it is noted that the Mach number near the tunnel side walls were calculated to be approximately 2.8, which is about 6.7% below the design Mach number.

An example where all the pitot tubes were within the test rhombus is shown in Figure 23c for $x_p/x_r = 0$. In this case the data indicate that the Mach number is well within ±2% of the design value. This is true for each of the four roll angles of $\phi = 0^o$, 45^o, 90^o and 135^o.

The root-mean-square Mach number based only on those pitot tubes which were well within the test rhombus for the various planes at $x_p/x_r = 0$ are tabulated below.

ϕ	M_{rms}
Deg	—
0	3.012
45	2.984
90	3.023
135	3.002

The overall root-mean-square Mach number for these specific conditions was 3.005 and was based on a total of approximately 20 measurements.

As was previously mentioned, attempts were made to check these results by two different methods. The centerline Mach number obtained from Eq. (1) was checked by calculation of the Mach number with the centerline pitot-static pressure probe and Eq. (2). The results are shown on most of the curves as a partially shaded point. In almost every case the Mach number calculated from Eq. (2) was either equal to or higher than that calculated by the method dictated by Eq. (1). This difference can be observed in Figures 23a through 23e. Specifically, in Figure 23e for $x_p/x_r = +0.695$ at $\phi = 45^o$, the two Mach numbers were nearly the same; that computed from Eq. (1) was 2.975 while the Mach number computed from Eq. (2) was 2.990. The maximum difference between these two Mach numbers can be observed in Figure 23a where $x_p/x_r = -0.690$. In the plane where $\phi = 0^o$ it is noted that the Mach number calculated from the known tunnel stagnation pressure and the measured centerline pitot pressure is

2.975, while that calculated from measurements with a centerline pitot-static pressure probe is about 3.095, which is about 4% higher than the design Mach number. It is believed that the difference in the Mach numbers calculated by these two methods is due to the fact that the static pressure orifices on the centerline pitot-static probe were not in the optimum location. It should be mentioned that the points obtained with the centerline probe, regardless of whether Eq. (1) or (2) is used for calculation of the centerline Mach number, were measured farther upstream by $\Delta(x_p/x_r) = 0.118$, since the centerline pitot-static probe was longer than the others and did not agree with the indicated x_p/x_r values shown on Figures 23a through 23e. In Figures 26a, 26b, and 26c, where the centerline longitudinal Mach distribution is given, the data have been adjusted by the proper amount.

A second check on the Mach number distribution was made by use of Eq. (3), these points being indicated as solid points on the curves. In general, the comparison in the Mach numbers computed by this method and that dictated by Eq. (1) was excellent. An example of this is shown in Figure 23e, where the two Mach numbers are well within $\pm 1\%$ of each other for each value of ϕ.

Similar results for an intermediate unit Reynolds number are presented in Figures 24a through 24e for nominal test conditions of $p_o = 300$ psia and $T_o = 480^oR$, corresponding to an average unit Reynolds number of 59×10^6 per foot. Here the overall rms Mach number was 2.995. The results for the highest unit Reynolds number of these tests are shown in Figures 25a through 25e. The nominal test conditions for these data were $p_o = 500$ psia at $T_o = 491^oR$, with an average unit Reynolds number of 95×10^6 per foot. Here again the trends and general agreement are as previously described. Under these conditions the overall rms Mach number was determined to be 3.015.

The results indicate that the actual rhombus Mach number corresponds very well with the design Mach number over the unit Reynolds numbers range of the facility. It also indicates that the lateral Mach number gradients are small. These conditions are favorable and necessary for good aerodynamic research.

2. THE LONGITUDINAL MACH NUMBER DISTRIBUTIONS

The longitudinal Mach number distributions were obtained from cross-plotting the lateral Mach number distributions. These data are presented in Figures 26a through 29c and are divided into four groups depending on the value of $r/\Delta s$, the normalized radial distance from the tunnel centerline. The values of $r/\Delta s$ are zero (longitudinal centerline), ±1, ±2, and ±3.

In general, all the data points in the test rhombus fall within ±2.5% of the design Mach number. Figures 26a through 26c show the tunnel centerline longitudinal Mach number distribution for the various free stream unit Reynolds numbers. In each case there is a slight overexpansion in the upstream portion of the test rhombus, which is followed by a slight compression through the downstream part of the rhombus. For example, in Figure 26a, where $Re/\ell = 20.69 \times 10^6$ per foot, at $x_p/x_r = -0.8$ the mean local Mach number is about 2.98. As x_p/x_r is increased, the local Mach number also increases, reaching a value of 3.025 at $x_p/x_r = -0.45$, indicating the presence of a weak expansion wave. As the longitudinal distance x_p/x_r is increased further to $x_p/x_r = 0.60$, the local Mach number decreases monotonically to a value of 2.98, indicating a slight compression in this area of the test rhombus. Once again it should be noted that these local Mach number changes are very small and in this particular case they are well witin ±1% of the design Mach number. Similar trends are noted in Figures 26b and 26c, which are the centerline longitudinal Mach number distributions for $Re/\ell = 59.2 \times 10^6$ and 95×10^6 per foot, respectively.

As we move laterally off the centerline the longitudinal Mach number distribution varies slightly. For the case of $r/\Delta s = \pm 1.0$, the longitudinal Mach number distribution is somewhat similar to that for the tunnel centerline ($r/\Delta s = 0$). As can be seen in Figures 27a through 27c, in the upstream portion of the test rhombus there is a slight overexpansion, ending at a local Mach number slightly larger than the design value. This region is then followed by a weak compression, which indicates the rhombus exit Mach number is about 1% lower than the design value.

At $r/\Delta s = \pm 2.0$ and ± 3.0, the longitudinal Mach number distribution is not defined as well as in the previous two cases. Figures 28a, 28b, and 28c show the longitudinal Mach number distribution at $r/\Delta s = \pm 2.0$ for the free stream unit Reynolds numbers of 20.69×10^6, 59.2×10^6 and 95×10^6 per foot, respectively. In each case the local Mach numbers vary with longitudinal distance through the test rhombus in the same manner; i.e., at the upstream portion of the test rhombus the local Mach number increases monotonically to a value of approximately 2.983 at $x_p/x_r = 0$, and then becomes essentially constant from this point to the end of the test rhombus at $x_p/x_r = \pm 1.0$. In this case the measured mean Mach number is about 0.5% below the design Mach number.

Figures 29a through 29c show similar data for the case where $r/\Delta s = \pm 3.0$ for each of the previously mentioned free stream unit Reynolds numbers, As in the case where $r/\Delta s = \pm 2.0$, there is a slight overexpansion in the upstream portion of the test rhombus, where the local Mach number increases from 2.994 at $x_p/x_r = -0.690$ to 3.090 at $x_p/x_r = -0.340$ and then becomes constant at about 3.01 for the remaining portion of the test rhombus. In the downstream part of the test rhombus this corresponds to a measured Mach number which is about 0.35% higher than the design value.

3. THE TUNNEL EMPTY MACH NUMBER DISTRIBUTION

The tunnel empty Mach number distribution, based on the assumption that $dp/dy = 0$ through the tunnel wall boundary layer, and calculated from the wall static pressure measurements and the known tunnel stagnation pressures, is shown in Figure 30. The data were taken at three different unit Reynolds numbers, namely, 21×10^6, 59×10^6, and 95×10^6 per foot. These data are compared with one-dimensional inviscid isentropic theory in the nozzle only. The results show that the measured Mach numbers are very nearly independent of the unit Reynolds number. The data also indicate that the calculated Mach numbers correspond very well with theory in the subsonic, transonic and supersonic portion of the nozzle up to $x/x_r = -1.15$, at which point the Mach number is approximately 2.65. In the range $-1.15 \leq x/x_r \leq \pm 1.0$ the calculated Mach number is either slightly lower or equal to the design Mach number, depending upon the unit Reynolds number. Finally, as x/x_r is increased beyond the test rhombus, the Mach number shows a continuous decrease with increasing distance. For example, at the end of the test rhombus the Mach number is 2.94; as we move downstream from this point to another point midway in the constant area duct, i.e., $x/x_r = +4.9$, the Mach number decreases to 2.90. In the farthest downstream portion of the constant area duct ($+4.9 \leq x/x_r \leq +9.0$) there is a small difference in the Mach number due to Reynolds number change. This difference is considered to be negligible, so that a linear extrapolation to the end of the constant area duct yields an exit Mach number of 2.82. This decrease in Mach number from 2.95 at $x/x_r = 0$ to 2.82 at $x/x_r = +9.0$ indicates that a very slight longitudinal pressure gradient exists, which can be attributed to the boundary layer growth over this distance. This pressure gradient is considered to be insignificant for purposes of aerodynamic testing in this facility. The longitudinal pressure gradients for the various stagnation pressures are as follows:

p_o	dp/dx
psia	psia/in.
108.47	$+ 1.139 \times 10^{-6}$
315.34	$+ 3.305 \times 10^{-6}$
521.76	$+ 5.460 \times 10^{-6}$

which corresponds to an average Mach number gradient of approximately -1.243×10^{-3} Mach number per inch.

4. THE CENTERLINE RMS MACH NUMBER

All the Mach number calibration data is summarized in Figure 31 in terms of the centerline rms Mach number versus the unit Reynolds number. These data indicate that the Mach number increases monotonically with increasing unit Reynolds number. At a unit Reynolds number of approximately 21×10^6 per foot the average rms Mach is 2.990, while at a unit Reynolds number of 59×10^6 per foot it increases to 2.996. A further increase in unit Reynolds number to 95×10^6 per foot produces an average rms Mach number of 3.00. The reasons for presenting this curve are: (1) to summarize the total results of the calibration in one figure, stressing the fact that all the data are within $\pm 1\%$ of the design Mach number, and (2) to show that the change in the average rms Mach number is essentially invariant with a change in the unit Reynolds number.

5. FLOW ANGULARITY MEASUREMENTS

In the design of wind tunnel nozzles, one attempts to achieve a constant Mach number and uniform parallel flow in the test rhombus. However, this ideal condition is rarely achieved, since other upstream factors such as the settling chamber design and the nozzle inlet design, can have a significant effect upon the flow angularity in the test rhombus. Because of this, tests were conducted as part of the calibration program to determine the presence of flow angularity in this facility.

The primary models used in these tests were two separate 15 degree half-angle cones, one mounted on the tunnel centerline and a second one offset 2 inches with respect to the centerline. A wedge model spanning the test section, having seven pairs of static pressure orifices in the spanwise direction, was used to extend the range of the test. However, the values of flow angularity obtained with the wedge model should be considered as qualitative data for reasons which will become obvious later. The pressure level over the wedge model was made similar to that over the cones by using a smaller half-angle of 10 degrees. The detailed design features of the wedge are shown in Figure 32 while those for the cones are shown in Figure 33.

The basic concept of these tests was to determine the flow angularity from a plot of the difference in upper and lower surface pressure versus angle of attack. Normally this curve passes through the origin; however, if flow angularity is present, the angle corresponding to a surface pressure difference of zero is the angularity present in the flow. Since model orifice irregularities can be a problem, the procedure is to invert the model and repeat the test. Usually this results in another curve of surface pressure difference versus angle of attack which has a slope opposite to that for the model upright case. Because of orifice irregularities, the angle at which the pressure difference is zero for the inverted condition may be different from that for the upright case; therefore, an average flow angularity must be used, and it is taken as the angle corresponding to the point of intersection of these two curves. Examples of some flow angularity curves are shown in Figures 34a through 34e. These curves are plots of the normalized surface pressure differences over a cone versus the angle of attack for both the upright and inverted case. The nominal stagnation pressure was 100 psia at a nominal stagnation temperature of $470^{o}R$; this corresponds to a unit Reynolds number of 20.7×10^{6} per foot. In Figure 34a where $x_p/x_r = -0.690$, when the model was upright, the flow angularity was + 0.125^{o}(by definition the angularity is positive when the model is at a negative angle of attack), and for the inverted case it was + 0.325^{o}. As previously mentioned, this difference in flow angularity was probably due to orifice irregularities; therefore, an average value of + 0.225^{o}, which corresponds to the point of intersection of the two curves, was assumed to be correct. This type of accuracy cannot be obtained in using the multiple pressure orifices on the wedge model, since inverting the model also transposes the position of each pair of pressure orifices, except for the centerline pair. As a result, errors due to model and orifice irregularities cannot be eliminated. The flow angularity data that follows has been generated in this same manner and will be discussed in greater detail in the following paragraphs.

The position and geometry of the settling chamber spreader cone was found to have a signficant influence on flow angularity. In the design of the facility one of the primary concerns was that due to building constraints on the piping design the inlet air to the settling chamber would have a high velocity "spiked" type center core. In order to overcome this undesirable probability, a perforated spreader cone was installed in the settling chamber at the upstream end. The purpose of the spreader cone was to provide a full velocity profile at the downstream end of the settling chamber. As mentioned in the tunnel description, it was designed with a half-angle of 45° and a porosity of 36%. In order to determine the effect of spreader cone orientation on the stagnation section velocity profiles, some small scale tests were conducted. The details of these tests are reported in Ref. 12. In general, the tests were conducted with a spreader cone having the same half-angle as the Mach 3 facility; however, the porosity was 40% rather than 36%. The ratio of air inlet pipe diameter to stagnation section diameter in both cases was about three, while the stagnation section integrated average velocity in the smaller unit was 15 ft/sec, as compared to 30 ft/sec in the full scale facility. There was obviously a Reynolds number or scale effect present between the two facilities; however, these tests were for the purpose of obtaining general trends and nothing more. The purpose of these tests was to determine if the spreader cone would give a more nearly complete velocity profile in the settling chamber when the apex of the spreader cone was oriented upstream or downstream. Some of the results are presented in Figure 35; the three cases investigated are labeled as:

Case A: Turbulence screens without a spreader cone

Case B: The spreader cone apex's pointing upstream plus turbulence screens

Case C: The spreader cone apex's pointing downstream plus turbulence screens.

In each case the velocity downstream of the turbulence screens was measured by hot wire techniques. As expected, Case A, which was without a spreader cone, had a high velocity core in the center which extended over the range $-0.45 \leq r/R \leq +0.45$, with the centerline velocity equal to 23.0 ft/sec. When the spreader cone was introduced with the apex upstream (Case B), the constant velocity region extended from $r/R = -0.70$ to $r/R = +0.70$ and was approximately equal to the centerline velocity, which was 16.9 ft/sec. The spreader cone was then reversed so that the apex was downstream (Case C), and the tests were repeated. These data indicated a high peak velocity in the vicinity of $r/R = \pm 0.80$, which was greater than Case B, and it had a constant velocity region extending from $-0.60 \leq r/R \leq +0.60$, which was somewhat smaller than Case B. The centerline velocity for Case C was 13.9 ft/sec, corresponding to a decrease of 3 ft/sec when compared to Case B. These tests revealed that there was very little practical difference between cases B and C, but due to the more extensive region of uniform flow obtained with Case B, it was decided that the spreader cone in the large facility would be placed with the apex upstream.

Tests were carried out with both a two-dimensional wedge and a cone to determine the lateral flow angularity in the test rhombus at $x_p/x_r = 0$. These tests were conducted at three different unit Reynolds numbers of 20.6×10^6, 58.2×10^6, and 93×10^6 per foot. The data are shown in Figure 36 and indicate a great change in the flow angularity with increasing lateral direction.

It varies from approximately -0.4° at $z/(b/2) = -1.0$, which is the west wall of the test section, to a maximum value of $+ 0.80^{\circ}$ at the centerline. It then decreases until it becomes approximately -0.40° at the east wall. It should be noted that these data were verified by the use of two different models. This same data have been replotted in Figure 38a with the unit Reynolds number as a parameter. In general it can be stated that the flow angularity appears to be essentially independent of the unit Reynolds number for both the wedge and cone model data. The data shown in Figures 36 and 38a imply the possible existence in the nozzle of two large counter rotating vortices with upward flow on the tunnel centerline and downward at each side wall. Reversing the spreader cone so that the apex was downstream yielded the data shown in Figures 37 and 38b. Thus, the configuration change, which was permanently adopted, resulted in considerable reduction in flow angularity distribution to an acceptable limit of approximately + 0.18° and was constant across the test section. Figure 38b confirmed the previous indication that flow angularity was essentially independent of the unit Reynolds number.

In order to determine the variation of flow angularity in the longitudinal direction with the stagnation section spreader cone apex upstream, a shorter series of tests were conducted with the cone model only. The results are shown in Figure 39, where the data was taken at M = 2.99 with a stagnation pressure of 100 psia and a stagnation temperature of 470°R, corresponding to a unit Reynolds number of 20.6×10^6 per foot. In these tests the parameter was the longitudinal distance given in its nondimensionalized form as $x_p/x_r = 0$, $x_p/x_r = \pm 0.345$, and $x_p/x_r = \pm 0.690$. Cross-plots of these data are shown in Figures 40, 41 and 42. Figure 40 is the longitudinal variation of the flow angularity at $z/(b/2) = +0.5$ (the east side of the test section) while Figures 41 and 42 are similar plots for $z/(b/2) = 0$ (the centerline of the test section) and $z/(b/2) = -0.5$ (the west side of the test section), respectively. The results confirm the previous tests and indicate that the flow angularity is constant at approximately + 0.18° in the longitudinal direction as well as the lateral direction.

A final flow angularity check was made at the center of the test rhombus to determine the variation of the flow angularity within the plane containing the point $x_p/x_r = 0$. The test conditions were the same as those given above; the results which indicate a deviation in the flow angularity as a function of the polar coordinate positioning of the cone model, are shown in Figure 43. The cone was mounted off-center at a constant distance given by $z/(b/2) = +0.5$ and was positioned within the plane passing through the point given as $x_p/x_r = 0$ at various angles denoted by ϕ. At $\phi = 0^0$ the flow angularity was measured at $+ 0.24^0$; it decreases to 0.09^0 at $\phi = 45^0$ and continues to decrease until it becomes zero at approximately $\phi = 60^0$. Then the angularity becomes negative at $\phi = 90^0$ and is -0.09^0; from here it increases and becomes zero at $\phi = 135^0$. As ϕ is increased from $\phi = 135^0$ to $\phi = 360^0$, the flow angularity increases until it returns to a value of $+ 0.24^0$ at $\phi = 360^0$. Superimposed on Figure 43 is the mean of all the measured centerline values of the flow angularity, which is $+ 0.12^0$, and it checks reasonably well with those measured in this particular plane. In light of the fact that flow angularity measurements are difficult to make, the difference in these data is not considered to be alarming since it is within the expected inaccuracy of the measuring technique.

6. BLOCKAGE TESTS

Tunnel blockage tests were conducted to determine the criteria on model size limitations. The models chosen were a sharp-nosed cone and a slightly blunted cone, both having a half-angle of 15 degrees. In addition, a 10 degree half-angle wedge was used. The models were placed on the tunnel centerline with the leading edge at $x_p/x_r = 0$, the rhombus vertical centerline. The percent blockage was calculated on the basis of the model maximum frontal area plus the exposed part of the support system referred to the physical cross-sectional area of the test rhombus ($A = 65.6$ in.^{2}). All tests were carried out at an angle of attack of zero degrees. The blockage area of both models was varied by adding or removing bases of different diameters to the cone and constant span bases of various heights to the wedge. The cone percent blockage was changed from 26.11% to 38.19% while the wedge blockage varied from 26.37% to 30.95% of the physical cross-sectional area of the test section. These values are tabulated at the top of Figure 44, and a plot of the percent blockage versus Mach number is shown at the bottom of the same figure. Superimposed are two theoretical curves; one assumes tunnel choking occurs through a normal shock wave positioned at the model location, and the second case, which is not too likely, assumes tunnel choking takes place isentropically. At a Mach number of three, the theory based on tunnel choking by an increase in entropy indicates the tunnel should start up to a maximum model blockage of about 28.7% of the physical cross-sectional area of the test section. In the case of the two-dimensional wedge, tests were performed up to a blockage of 30.95% with no detrimental effects. For the cone, the maximum blockage attained without detrimental effect was 33.58%; however, when the cone blockage was increased to 38.19%, the facility would not start at the lower stagnation pressures but did go into flow at stagnation pressures greater than 300 psia. Based on these tests, it is recommended that all models designed for this facility should not exceed a blockage of approximately 28% of the physical corss-sectional area of the test section. This should include the frontal area due to all effects such as sting support, model angle of attack, flow field probes, etc.

7. REMARKS ON FLOW LIMITATIONS

In order to determine some of the flow limitations encountered during the operation of the Mach 3 high Reynolds number facility some schlieren and shadowgraph photographs were taken of the flow field over a wedge. The wedge had a 10^o half-angle and was capable of being pitched to ± 10 degrees in angle of attack. All the tests were conducted at a stagnation pressure of approximately 100 psia and a stagnation temperature of 470°R, corresponding to a free stream unit Reynolds number of 20.7×10^6 per foot. The resulting schlieren and shadowgraphs, for angles of attack between 0 and + 10 degrees, are shown in Figures 45 and 46. Because of the high density and large density gradients present in the flow at these high Reynolds numbers, the shadowgraphs suffice to show good shock wave details over the model surface, whereas schlieren will show additional minor disturbances very clearly. In Figures 45a and 45c, which are schlieren pictures of the wedge at angles of attack of zero and + 4 degrees, both free stream and minor model disturbances are very noticeable. In Figures 45b and 45d, the shadowgraphs of the same flow fields, it is noted that the free stream disturbances do not appear; however, the model disturbances are evident but are somewhat reduced in intensity. The fact that these disturbances are minor can best be observed in an analysis of the flow field over the wedge as shown in Figures 45a through 45b, where the angle of attack is zero degrees. If we assume a free stream Mach number of three, and a wedge half-angle of 10 degrees, calculations using inviscid theory indicate that the angle of the attached bow shock should be 27.4°, as compared to a measured value of 27.5°. This corresponds to a local Mach number ahead of the surface disturbance over the model of 2.5. From this information and inviscid oblique shock wave theory the angle of the surface disturbance was calculated to be 23.58°, as compared to a measured angle of 23.4°, indicating that this and similar disturbances are very weak Mach waves.

The primary reason for this test was to determine the starting and stopping characteristics of this type of facility, since it is important to both tunnel operation and proper model design techniques. Prior to these tests, it was assumed that the facility could go into and out of flow by one of two methods; namely,

1) symmetrically, i.e., with supersonic and/or subsonic flow over both surfaces

2) nonsymmetrically, i.e., with supersonic flow over one surface and subsonic flow over the support system side.

Needless to say, the aerodynamic loads are very different, with the greatest loads occurring in the latter case. When the model was placed at an angle of attack of either 0° or + 4° and the tunnel put into operation, a normal flow field was established over the wedge, as shown in Figure 45. The tunnel was then shut down and the angle of attack of the wedge was increased to + 10°, after which an attempt was made at starting the faciltiy. As can be seen in Figure 46c the flow was unsteady and the normal supersonic flow field was not established. Specifically, the upper surface of the model was in a supersonic flow field, which was less than the fully established flow at $M = 3$, and the lower surface (which is the model support side) was in a local subsonic flow field, as witnessed by the presence of a normal shock wave near the model's leading edge. The tunnel was shut down, the model angle of attack was decreased to + 7°, and the test was repeated. The results were similar, as indicated in Figures 46a and 46b. A continuous decrease in angle of attack during tunnel operation allowed the flow field to become properly established only after the angle of attack was decreased to $+5.5^{\circ}$. Another series of tests were conducted by first starting the tunnel with the model at zero degrees angle of attack. Once the flow field was established at these conditions, the angle of attack was increased slowly while the facility was in operation, allowing the establishment of the proper flow field at angles of attack as high as + 10 degrees. The following recommendations are made as a result of the above tests:

1) For purposes of establishing the flow at all angles of attack, it is recommended that the facility be started at zero degrees angle of attack, after which the model may be driven to the desired angle of attack within the range $-10^{o} \leq \alpha \leq +10^{o}$. The reverse procedure will be detrimental to flow establishment and the test equipment at the higher angles of attack.

2) All models should be designed to take the loads experienced by the establishment of a flow field as indicated in Figure 46, i.e., supersonic flow at $M = 3$ (even though this is not the case) on the nonsupport side of the model, and a subsonic flow field on the support system side of the model.

SECTION V

CONCLUSIONS

The overall design objectives for the facility were met and the extensive testing carried out demonstrated good aerodynamic performance and reliable mechanical systems. Some of the more significant characteristics of the facility are discussed below together with some recommendations to users of the facilities.

1) The lateral and longitudinal Mach number distribution in the test rhombus is considered to be very good. It varies by approximately ±1% of the design value of 3.0 over the unit Reynolds number range extending from 20×10^6 to 95×10^6 per foot.

2) The lateral and longitudinal flow angularity in the test rhombus was found to be approximately 0.18^o over the entire unit Reynolds number range of the facility.

3) Blockage tests indicate that models with blockage frontal areas (including support system) as high as 38% of the physical cross-sectional area of the test rhombus may be tolerated; however, it is recommended that 28% should be the upper limit for insurance of proper tunnel operation.

4) Based on some basic start-stop flow visualization studies, the following recommendations are made:

a. For the purposes of establishing the flow at all angles of attack the facility should be started with the model at zero degrees angle of attack, after which the model may be driven to the desired angle of attack. Starting the tunnel with the model pitched could be detrimental to flow establishment and to the test equipment, particulary at high angles of attack.

b. All models should be designed to take starting loads based on a nonsymmetrical flow field, i.e., supersonic flow on the support-free side of the model and subsonic flow on the support system side of the model.

5) The possibility exists for the facility to be operated at conditions which could cause condensation of the air in the test section. Such conditions would normally be encountered only on very cold winter days when operating at high stagnation pressures for long periods. It is unlikely that operations would be restricted for more than a few days during the year. More specific details are given in the Appendix.

6) The noise level of the facility is high with the atmospheric exhaust configuration and it is essential that established safety procedures be strictly adhered to. Prior to each series of tunnel runs a positive verification of the proper functioning of the siren and warning lights should be made, and during the run personnel should not approach within 50 feet of the exhaust silencer.

7) The facility vibration level is predictably much higher than that of a normal supersonic wind tunnel. Care must be taken to periodically check bolted connections for tightness, and rupture discs should be replaced at least annually to minimize premature failures due to fatigue.

8) Due to the unheated air supply, the tunnel components are subjected to temperatures far below the dew point temperature of the air in the facility building. Subsequent moisture condensation on components following a series of runs can produce corrosion problems. Whenever facility modifications or additions are contemplated, consideration should be given to the use of corrosion resistant materials.

9) Due to the significant pressure drop between the storage tanks and the control valves, greater utility of the air supply is achieved by conducting the highest stagnation pressure tests at the beginning of a series of runs.

10) For the avoidance of water hammer problems in the air supply lines, the duration of the stagnation pressure programming ramp should be maintained at no less than four seconds, and the isolation valve closure times should never be less than 1 second.

11) Closed circuit television should be used to view the test section windows to insure that no accident occurs as a result of windows cracking due to thermal effects during a run.

For those who may be involved with the design or operation of a similar facility, it may be worth noting that the conveyance and control of high density air at high flow rates and high expansion rates requires a close examination of conventional design assumptions and practices. In the present case it was found that the possibilities for water hammer problems, air condensation problems and low temperature brittle fracture problems were much greater than expected and other more conventional problems such as noise, vibration and mechanical stresses were seriously intensified.

REFERENCES

1. "AFSC Technical Facility Capability Key," AFSCP 80-3, Air Force Systems Command, 1 July 1965.

2. Schaefer, W. T., Jr., "Characteristics of Major Active Wind Tunnels at the Langley Research Center," NASA TM X-1130, July 1965.

3. "A Compilation of Major Hypersonic Wind Tunnels in the United States," The Boeing Company Document No. D2-5785.

4. "National Wind Tunnel Summary," DOD-NASA, July 1961.

5. <u>Test Facilities Handbook, Vol. 1</u>, Arnold Engineering Development Center, July 1961.

6. "STA Wind Tunnel Listing," Supersonic Tunnel Association, 1966.

7. West, J. E. and Korkegi, R. H., "Interaction in the Corner of Intersecting Wedges at a Mach Number of 3 and High Reynolds Numbers," ARL 71-0241, AD734 540, October 1971.

8. "ASME Boiler and Pressure Vessel Code, Section VIII, Unfired Pressure Vessels," American Society of Mechanical Engineers, 1965.

9. Ferri, A. and Bogdonoff, S. M., "Design and Operation of Intermittent Supersonic Wind Tunnels," AGARDograph No. 1, Advisory Group for Aeronautical Research and Development, May 1954.

10. Azzouz, D. and Pratt, N. H., "Supersonic Turbulent Mixing, Part II, Design and Construction of a Mach 3 Blow-down Wind Tunnel and Its Instrumentation," AASU Rept. No. 282, University of Southampton, May 1968.

11. Pope, A. and Goin, K. L., <u>High-Speed Wind Tunnel Testing</u>, John Wiley and Sons, Inc., 1965.

12. Haugen, R. L.; Moore, D. G. and Wennerstrom, A. J., "Velocity Profile Measurements in a Model Settling Chamber," Internal ARL Paper (available upon request), April 1969.

13. Friedrichs, K. O., "Theoretical Studies on the Flow Through Nozzles and Related Problems," Applied Mathematics Group AMG-NYU No. 43, Applied Mathematics Panel 82.1R, New York University, April 1944.

14. Nilson, E., "Analytic Correction of a Two-Dimensional Nozzle for Uniform Exhaust Flow," Meteor Rept UAC-15, United Aircraft Corporation Research Dept., January 1948.

15. Baron, J. R., "Analytic Design of a Family of Supersonic Nozzles by the Friedrichs Method," WADC Technical Rept 54-279, AD 55 902, Naval Supersonic Laboratory, MIT, June 1954.

16. Burke, A. F., "Turbulent Boundary Layers on Highly Cooled Surfaces at High Mach Numbers," AFASD TR 61-645, ASD Symposium on Aerothermoelasticity, Dayton, Ohio, 1961.

17. Giles, Ronald V., "Fluid Mechanics and Hydraulics," Schaum Publishing Co., 1962.

18. Nagamatsu, H. T.; Sheer, R. E. and Graber, B. C., "Hypersonic Laminar Boundary-Layer Transition on 8-Foot-Long, 10° Cone, M_1 = 9.1 - 16," AIAA Journal, Vol. 5, No. 7, pp. 1245-1251, July 1967.

19. Pate, S. R., "Measurements and Correlations of Transition Reynolds Numbers on Sharp Slender Cones at High Speeds," AIAA Journal, Vol. 9, No. 6, pp. 1082-1090, June 1971.

20. Wegener, P., "On the Experimental Investigation of Hypersonic Flow," Naval Ordnance Laboratory Rept. No. 9629, 1948,

21. Schueler, C. J., "An Investigation of Model Blockage for Wind Tunnels at Mach Numbers 1.5 to 19.5," AEDC TN 59-165, 1960.

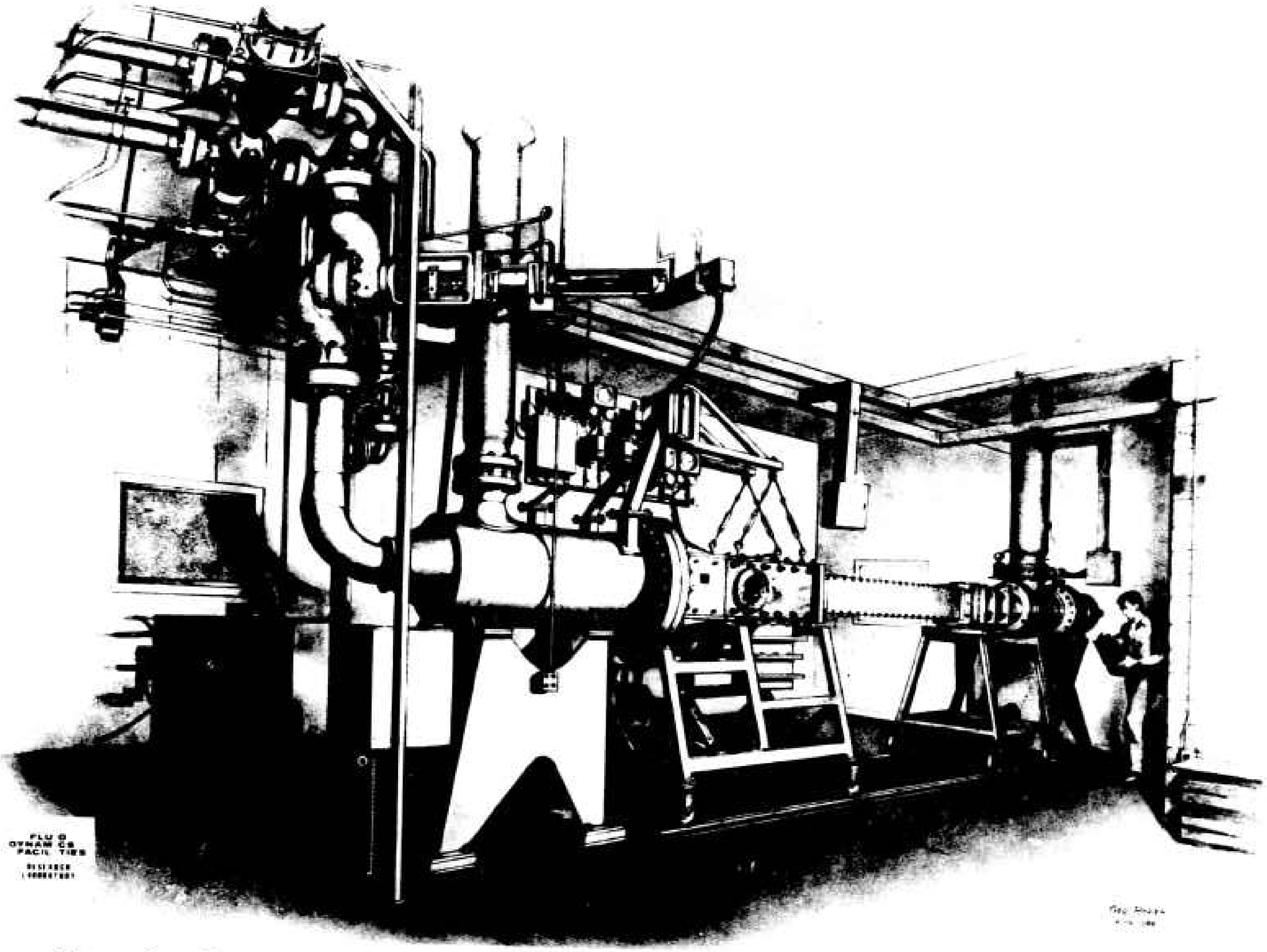

Figure 1. Perspective Drawing of the ARL Mach 3 High Reynolds No. Facility

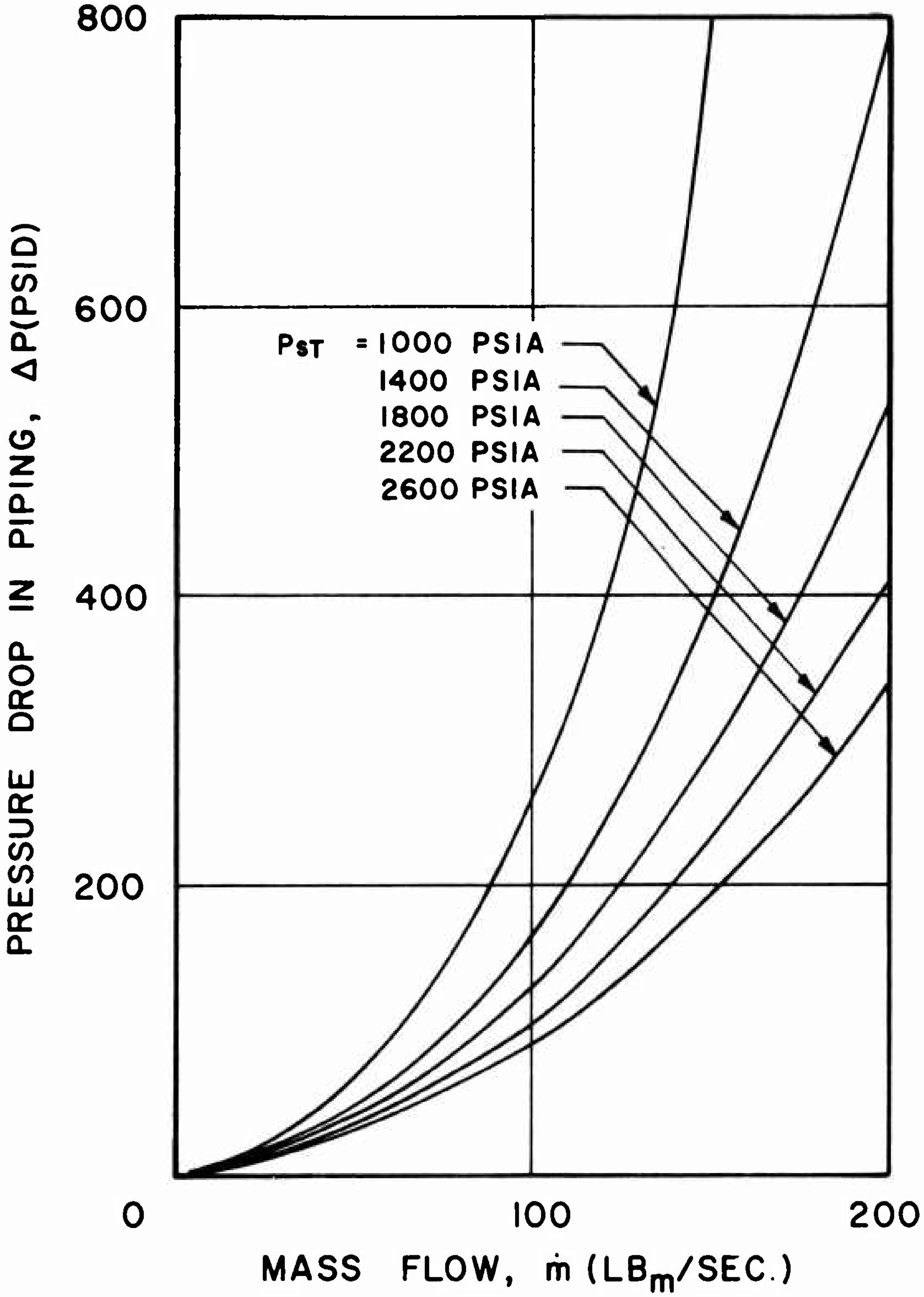

Figure 2. Estimated Pressure Drop in Distribution Piping as a Function of Mass Flow and Storage Pressure

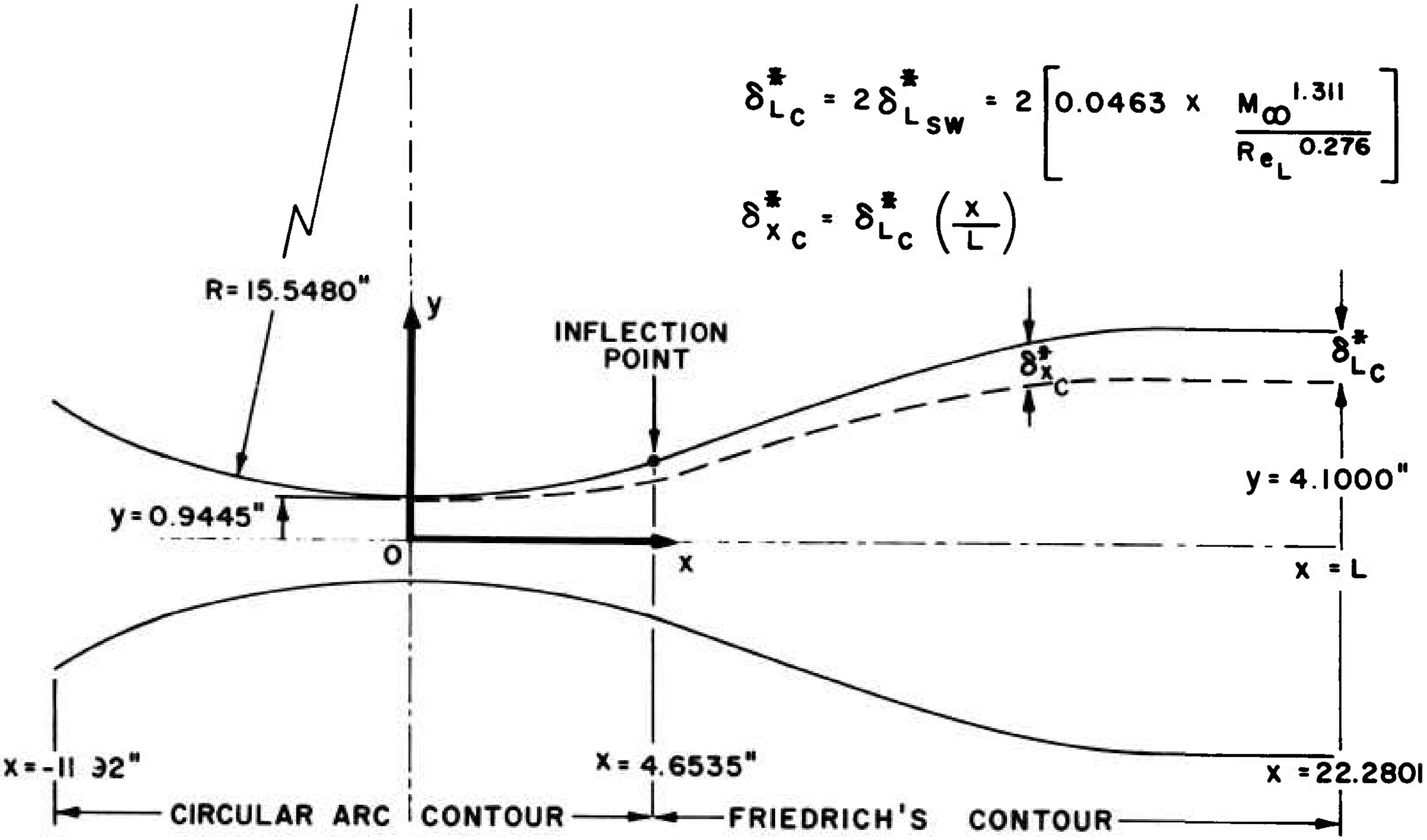

Figure 3. Mach 3 Nozzle Configuration

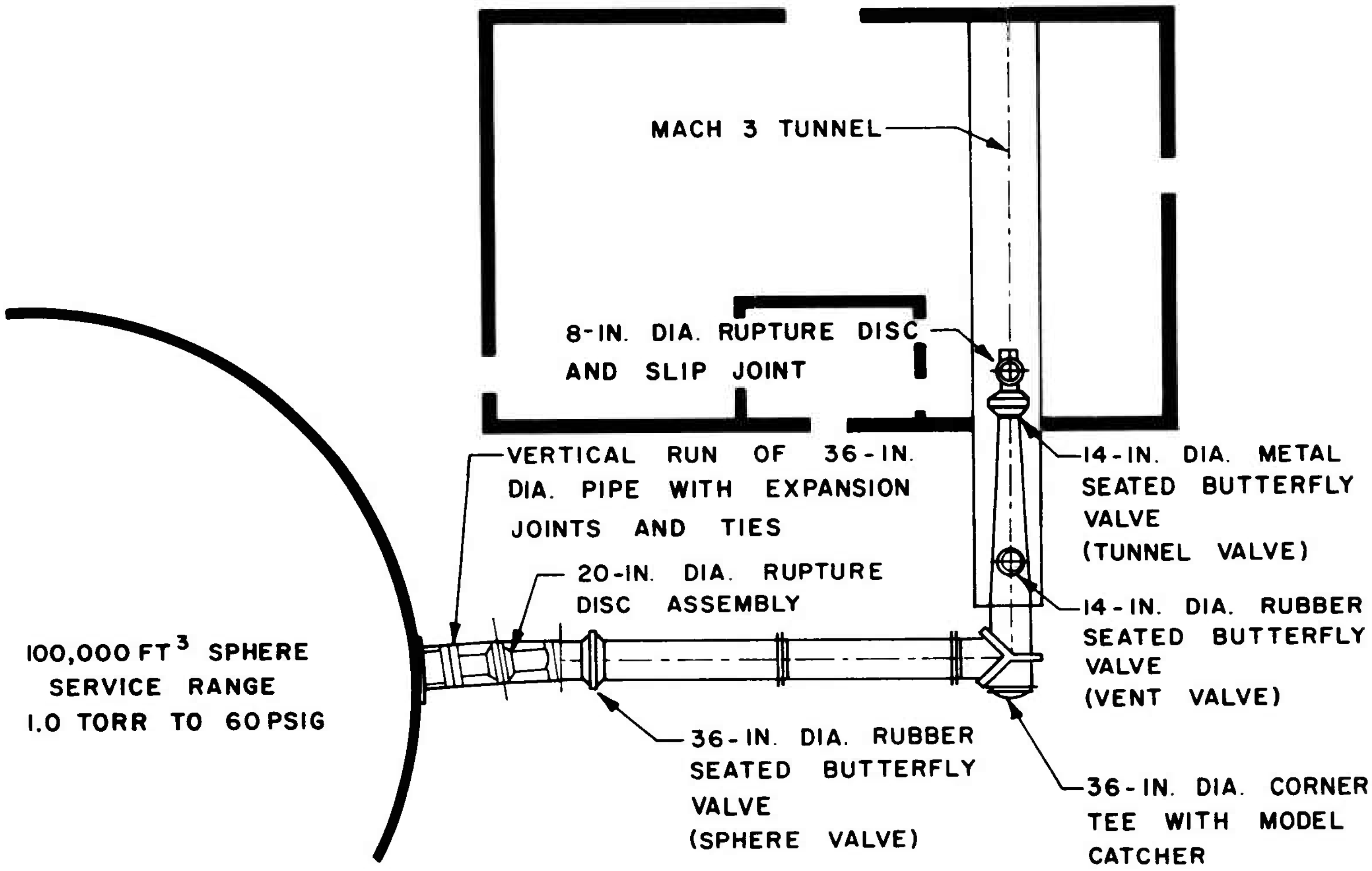

Figure 4. Original Exhaust System Configuration-Vacuum

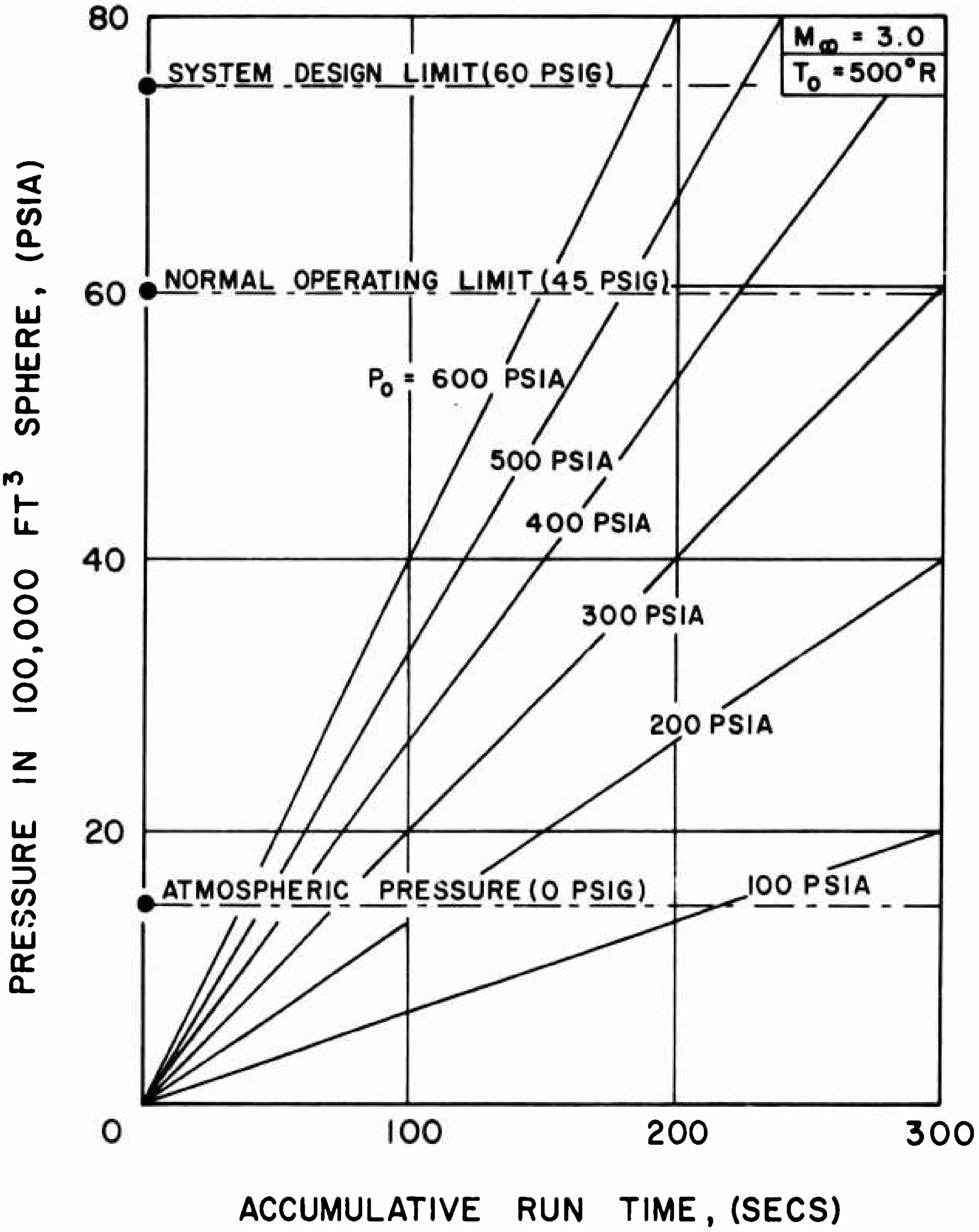

Figure 5. Rise of Sphere Pressure with Run Time for a Range of Stagnation Pressures

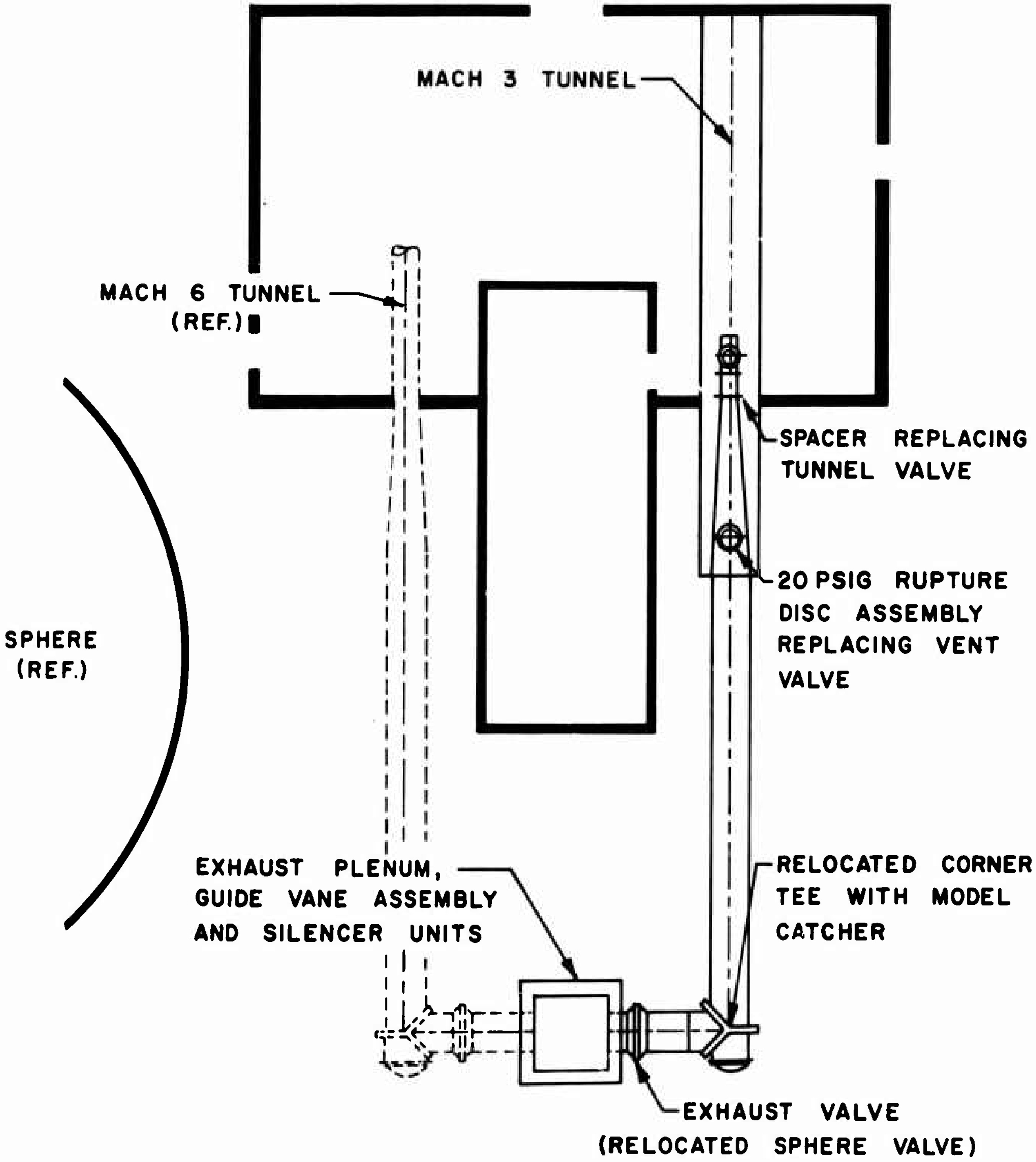

Figure 6. Present Exhaust System Configuration-Atmospheric

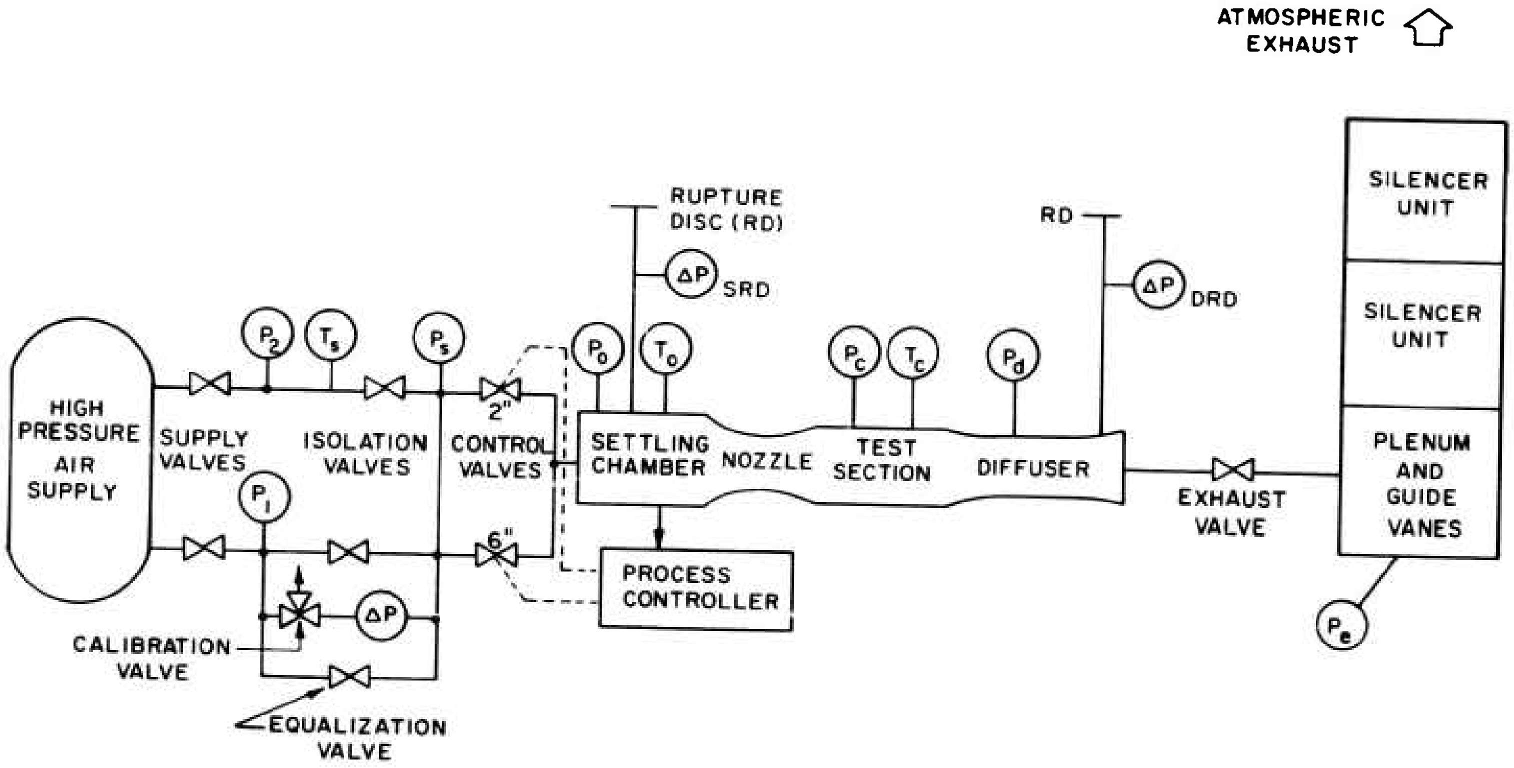

Figure 7. Mach 3 Process Diagram

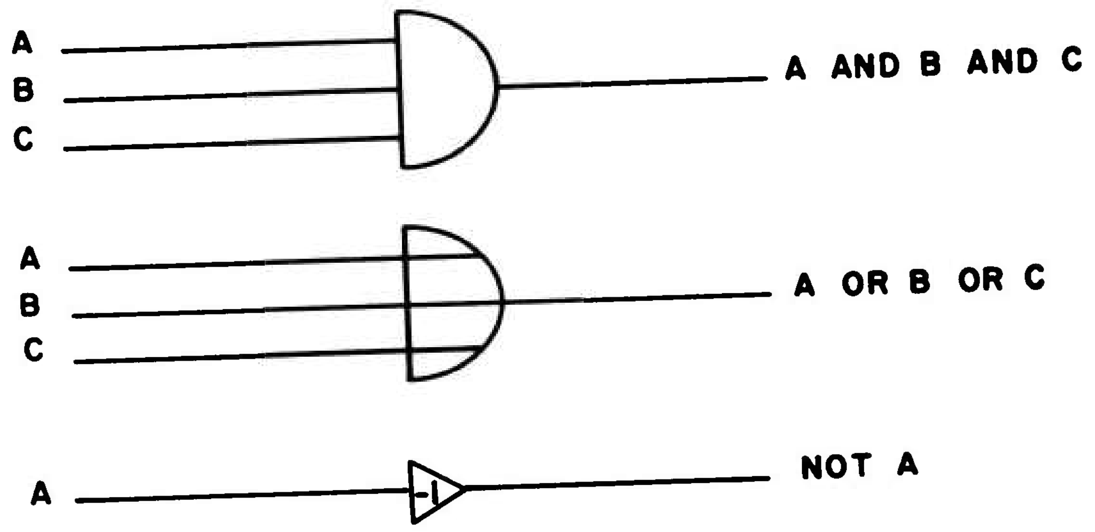

Figure 8. Logic Symbol Convention

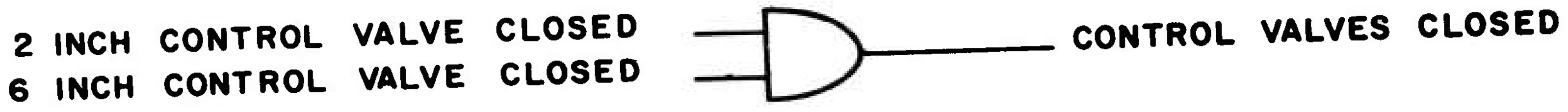

Figure 9. Control Valve Status

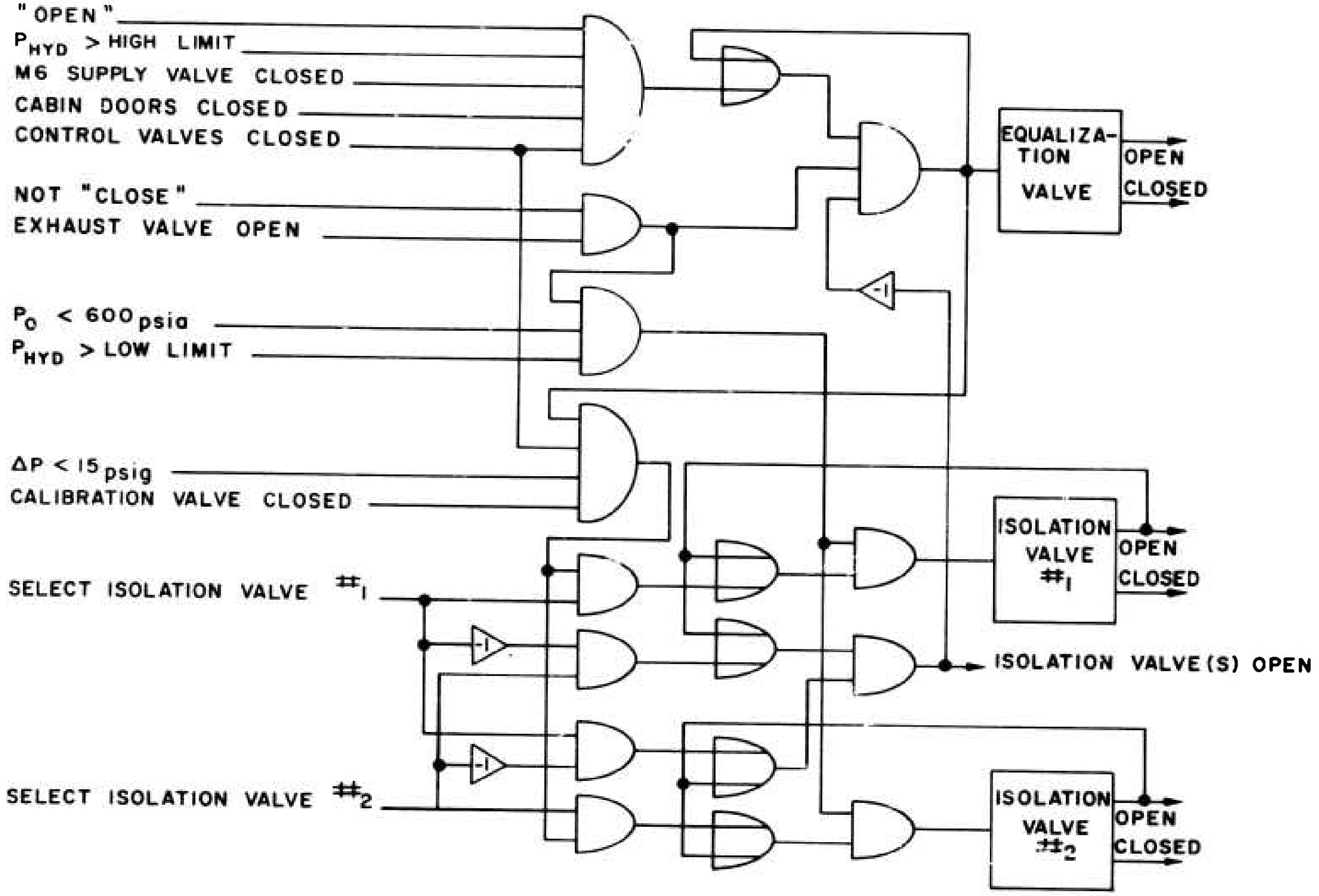

Figure 10. Isolation Valve Control Logic

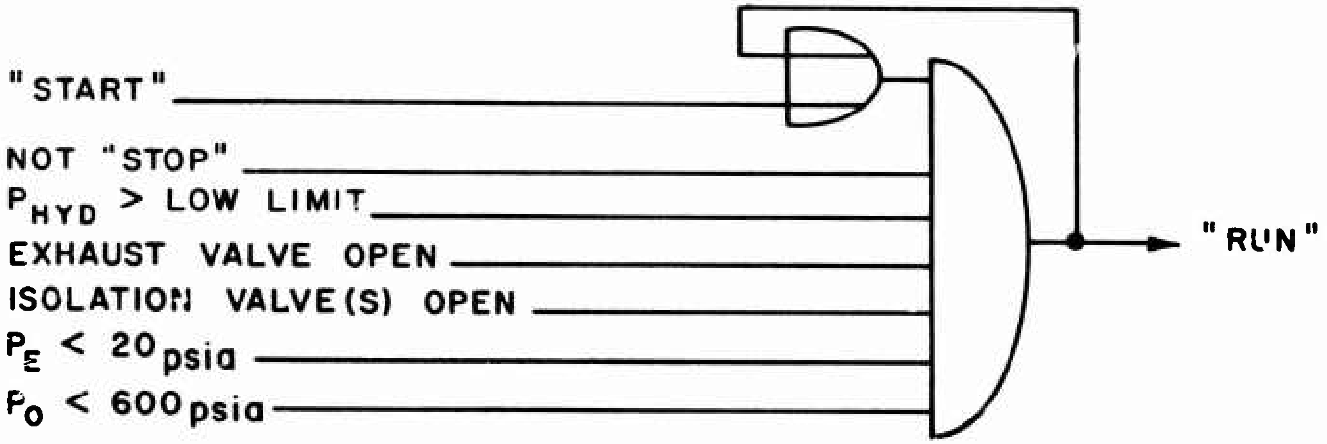

Figure 11. Run Interlock Logic

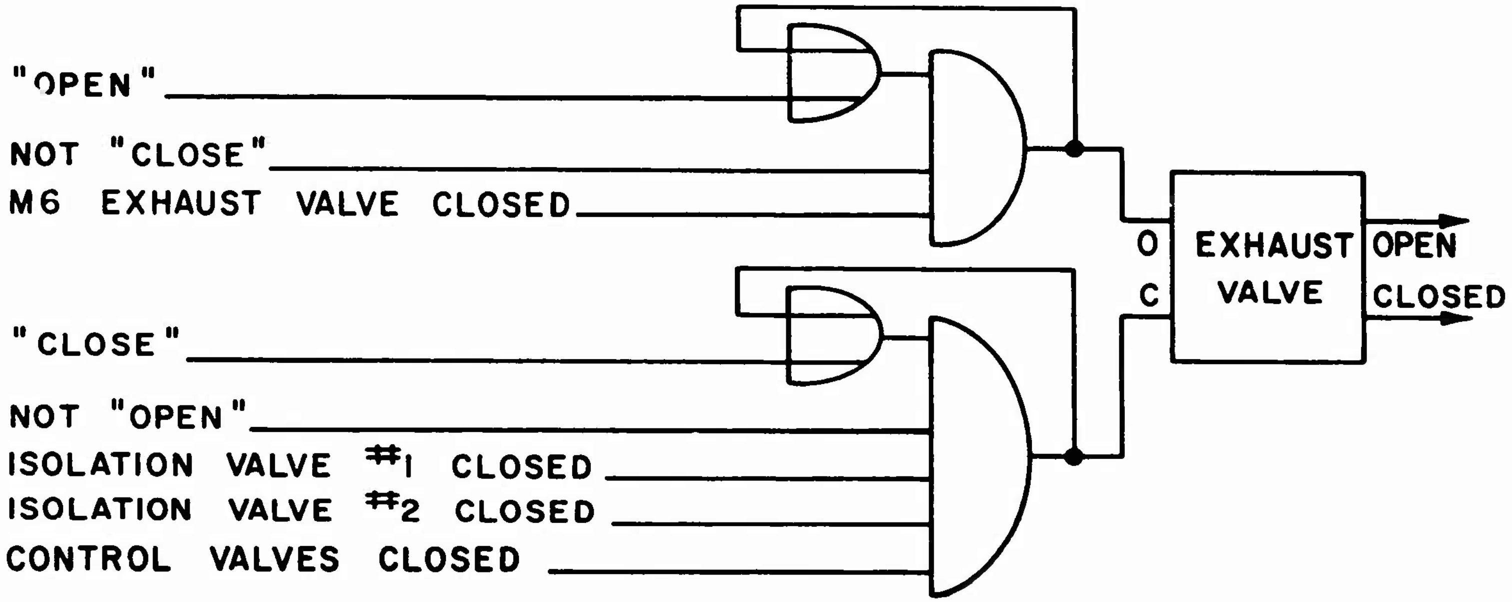

Figure 12. Exhaust Valve Control Logic

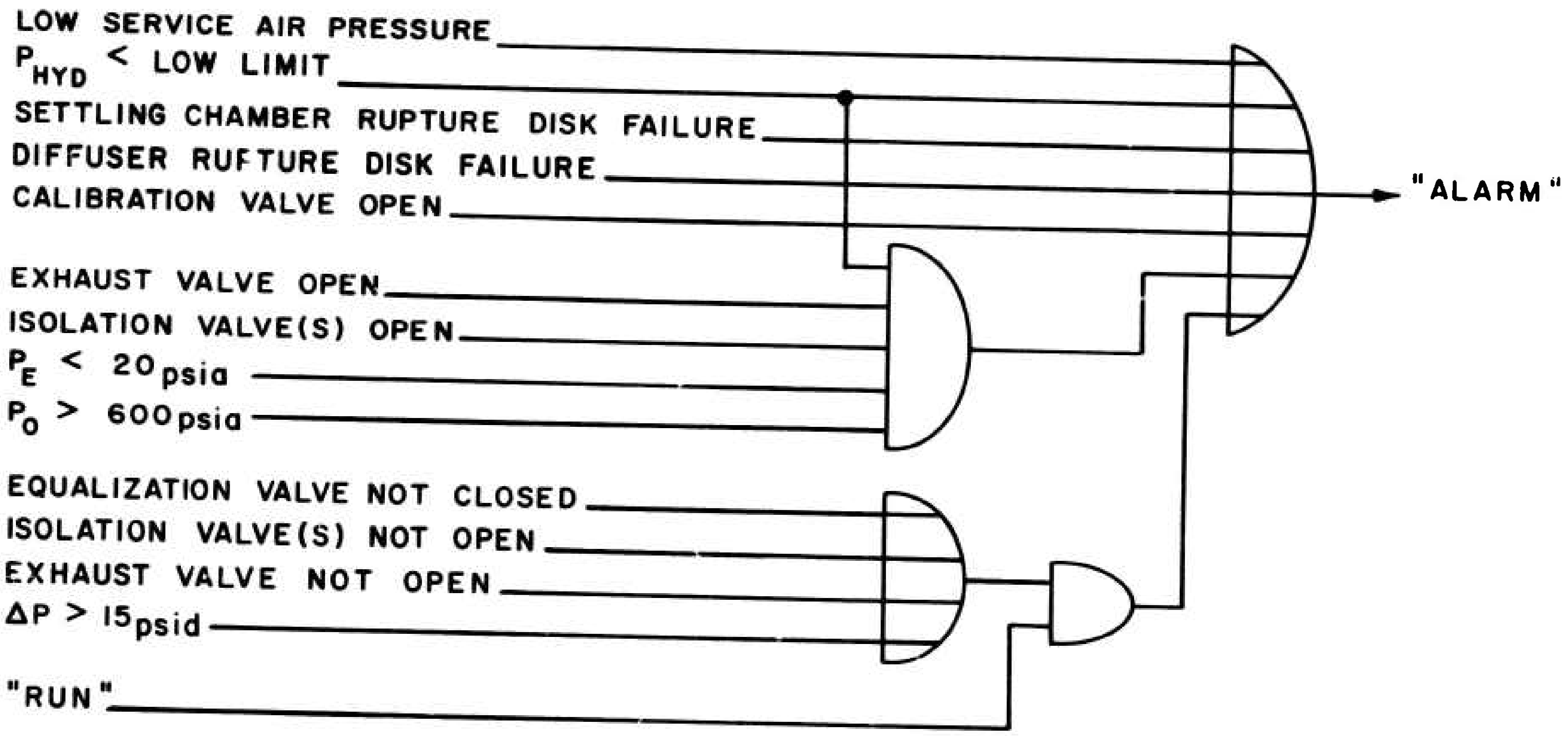

Figure 13. Alarm System Logic

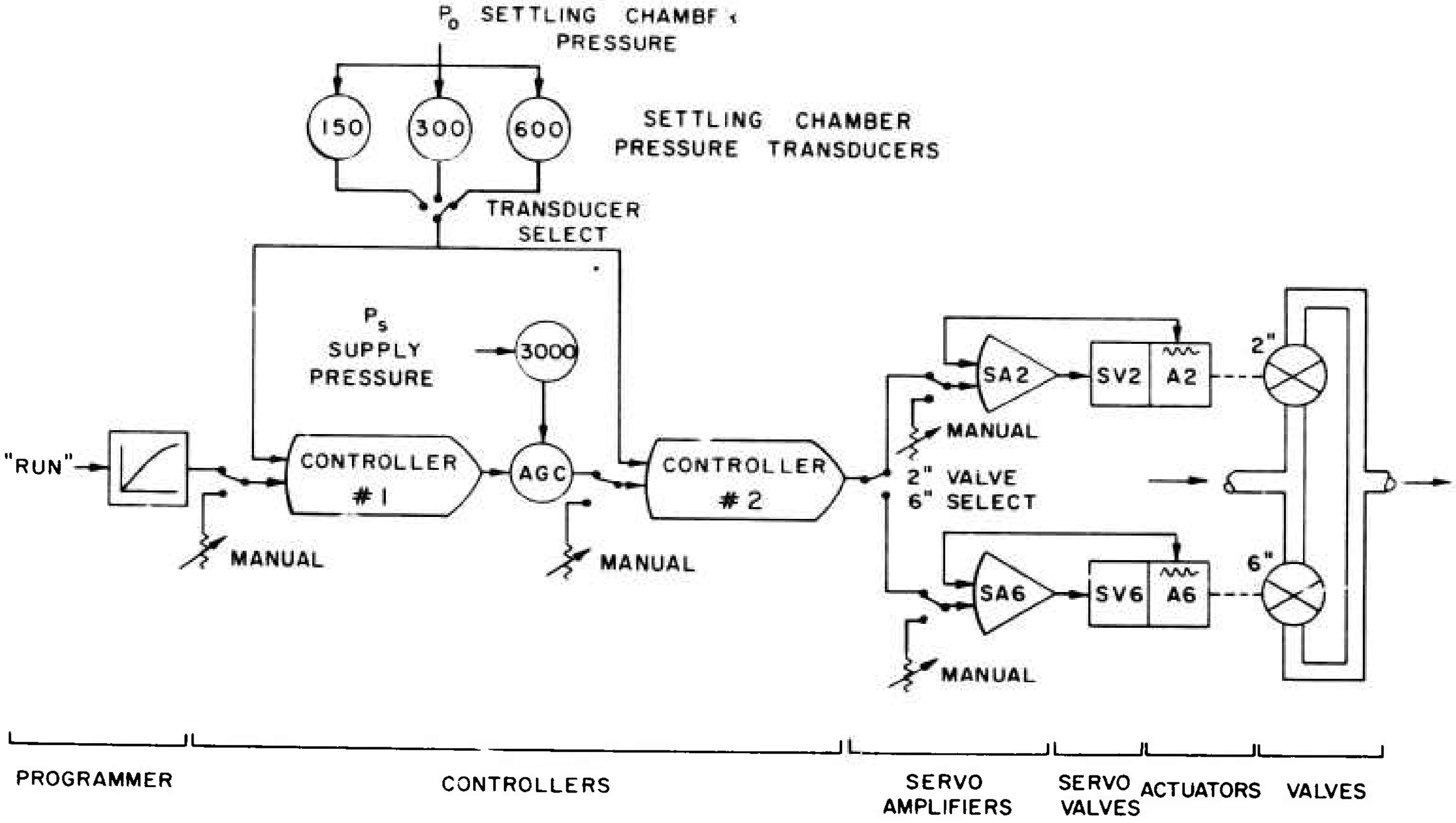

Figure 14. Stagnation Pressure Control System

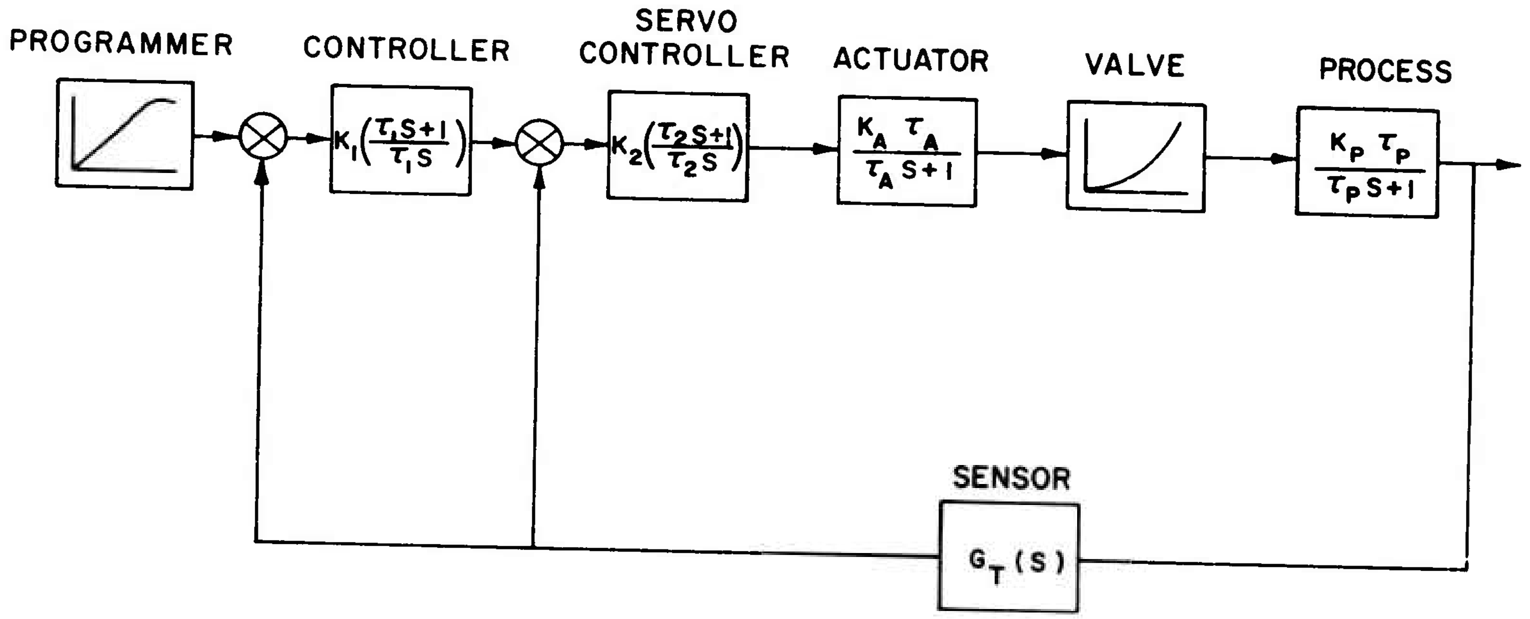

Figure 15. Mach 3 Process Control Loop

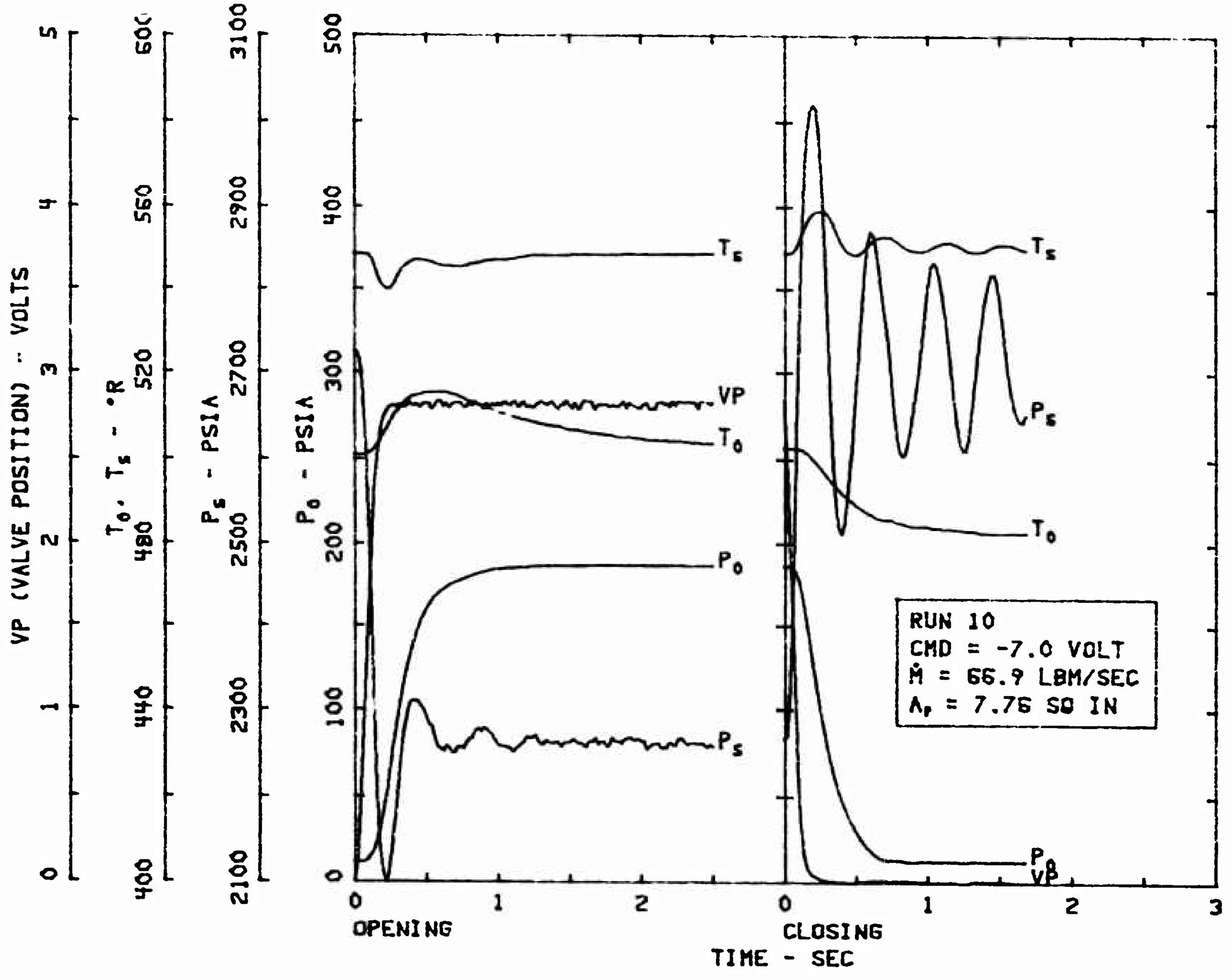

Figure 16. Valve Response Test - 2-inch Valve

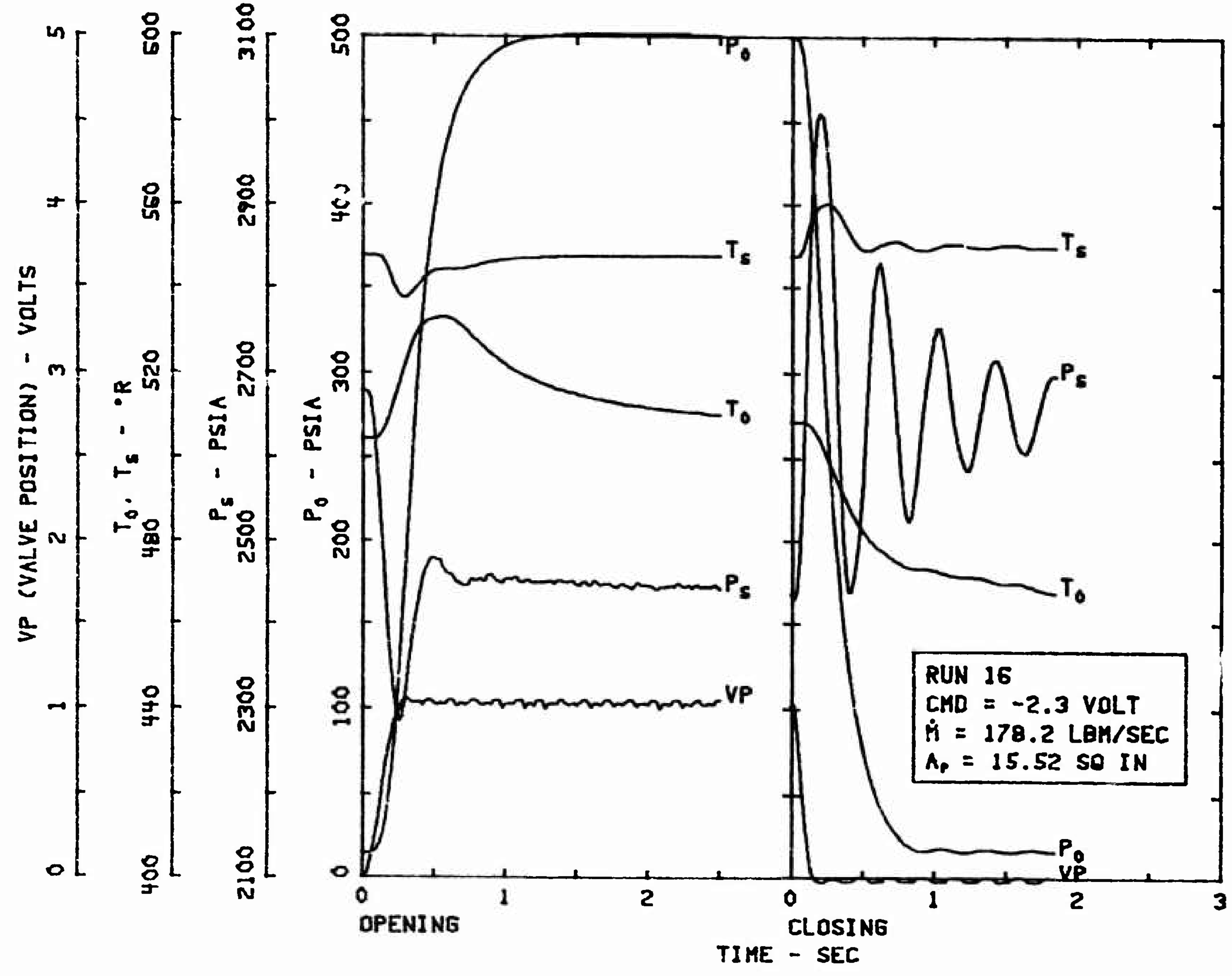

Figure 17. Valve Response Test - 6-inch Valve

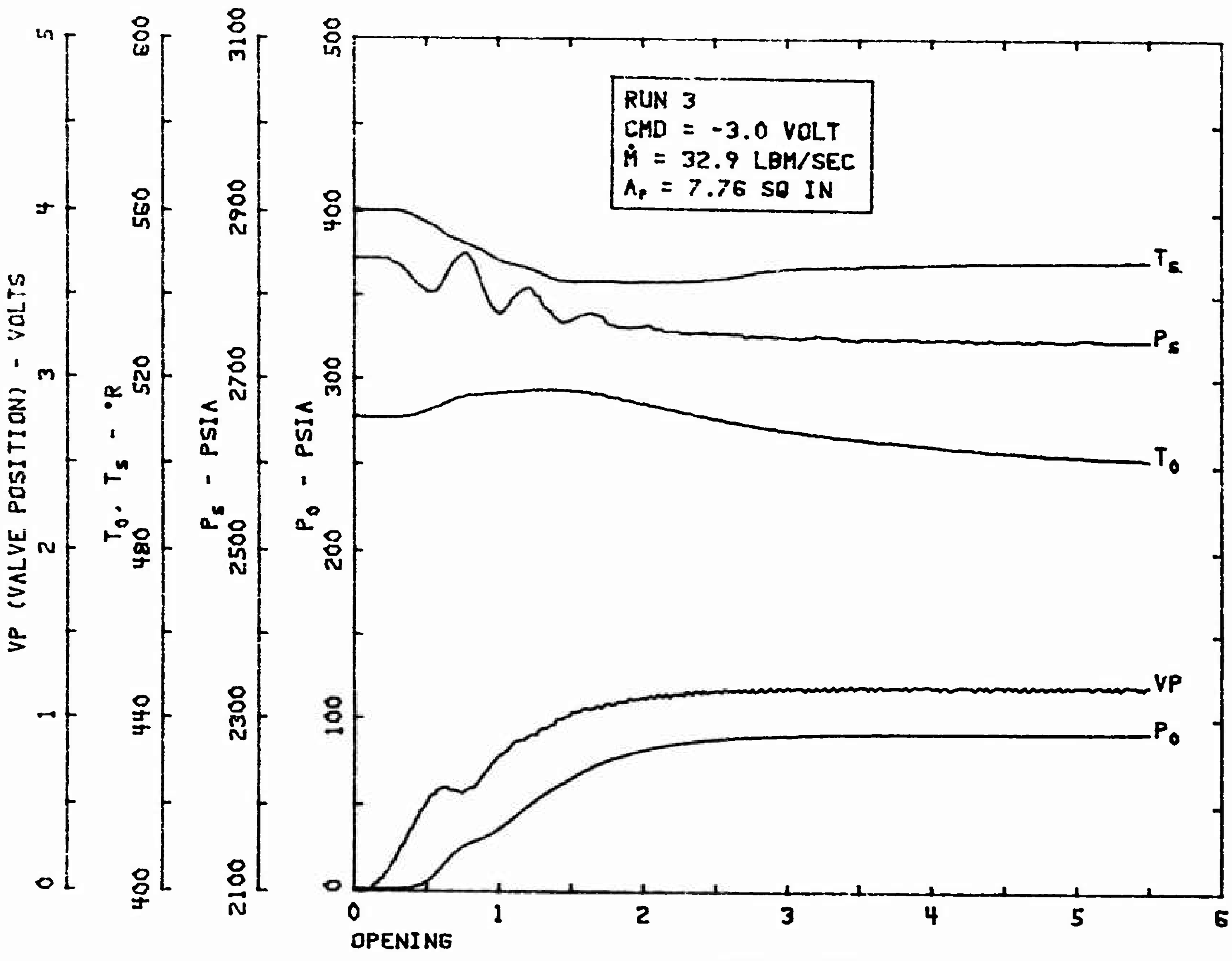

Figure 18. Controller Test - 2-inch Valve

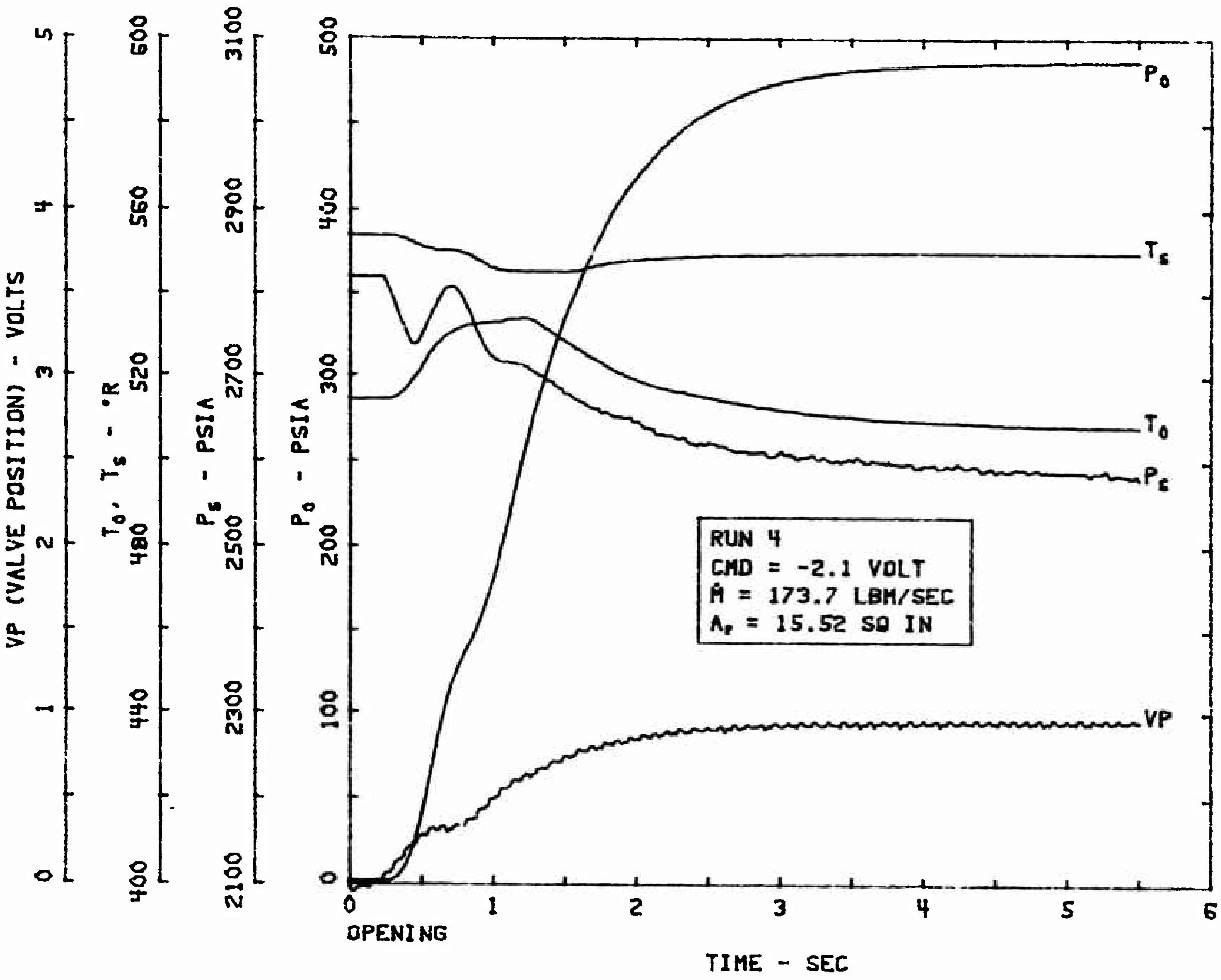

Figure 19. Controller Test - 6-inch Valve

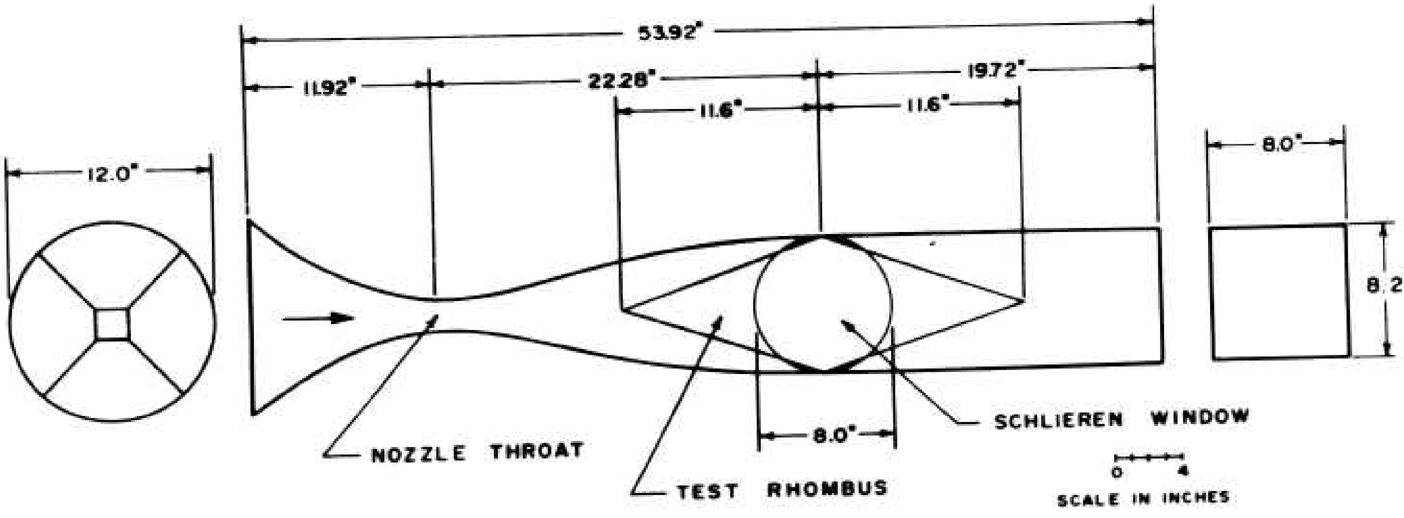

Figure 20. Scale Drawing of the Mach 3 Nozzle and Test Section

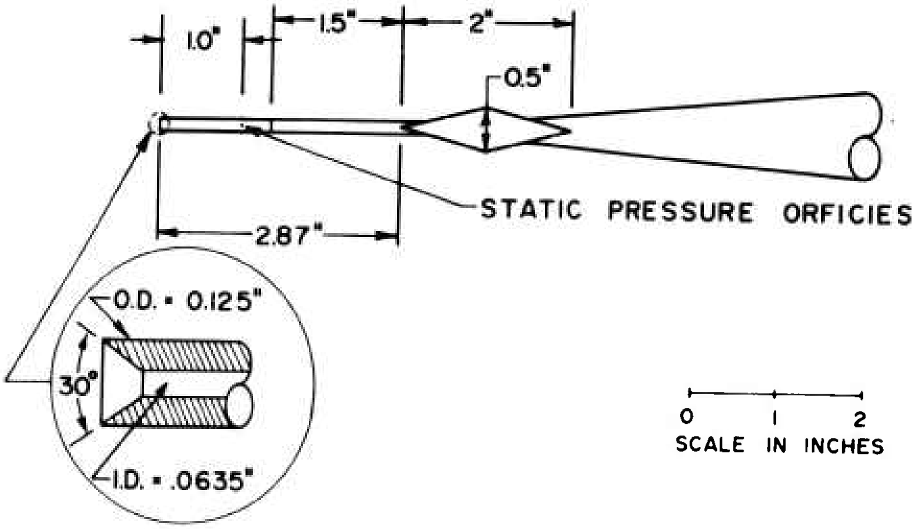

A. RAKE SIDE VIEW

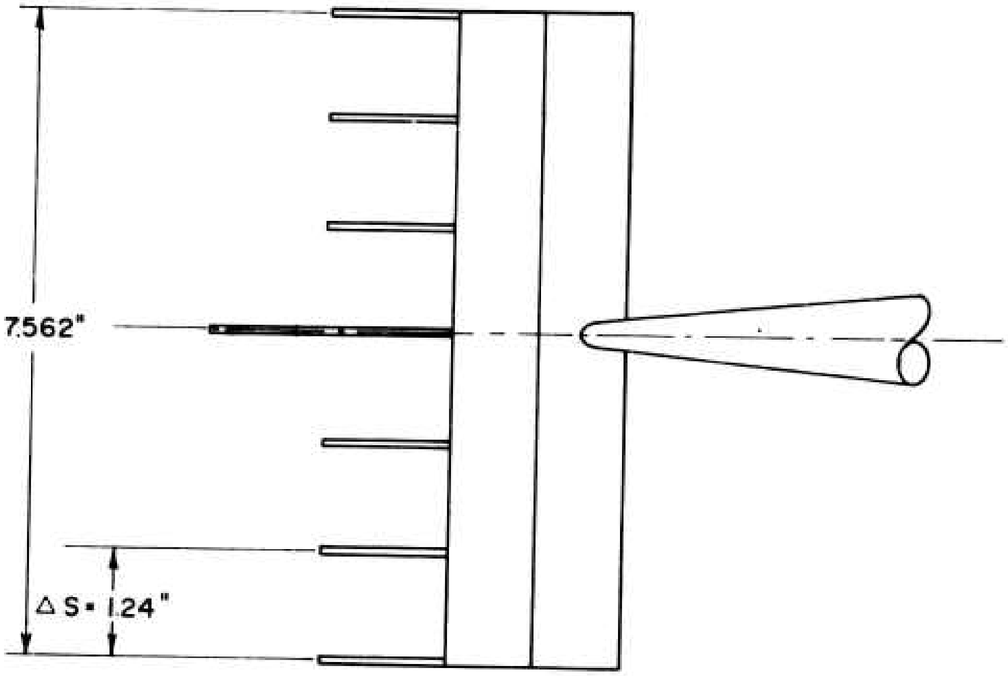

B. RAKE PLAN VIEW

Figure 21. Scale Drawing of Mach Number Survey Rake

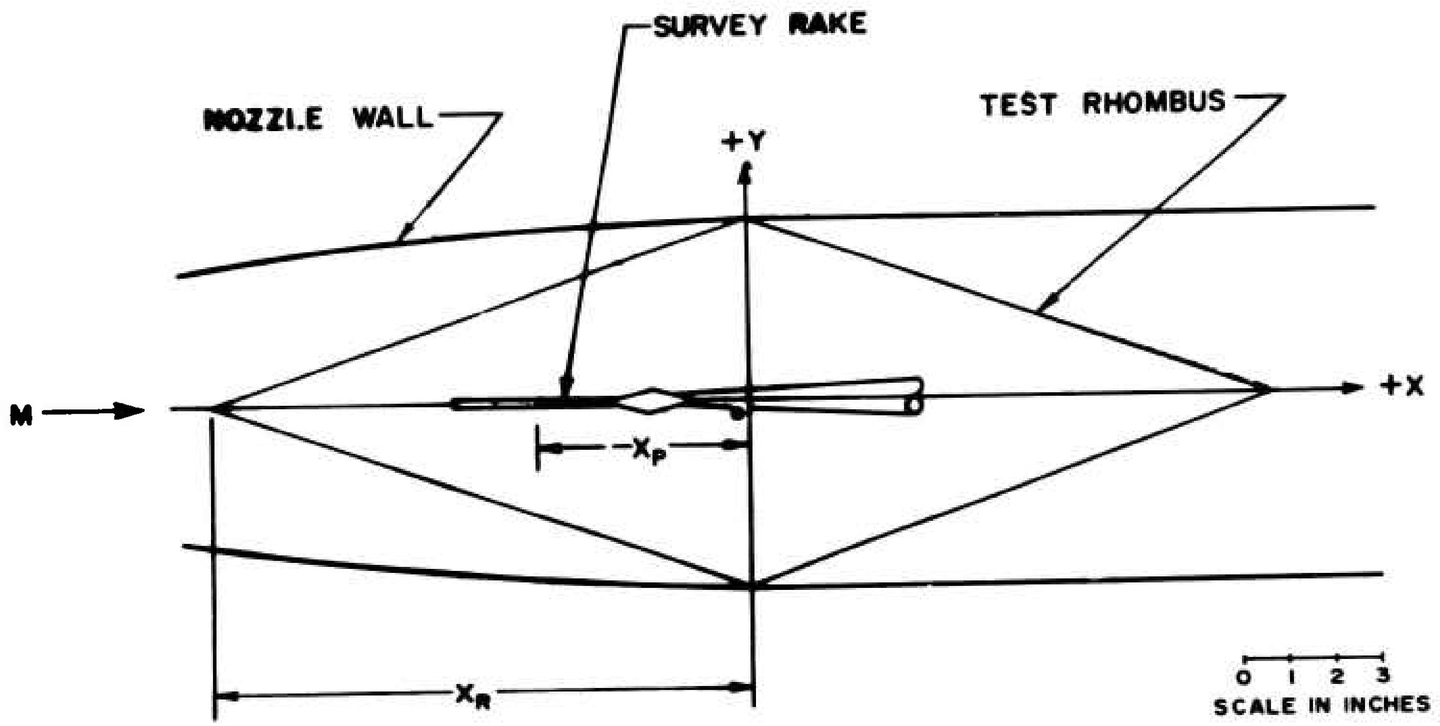

Figure 22. Survey Rake Reference Axis and Nomenclature

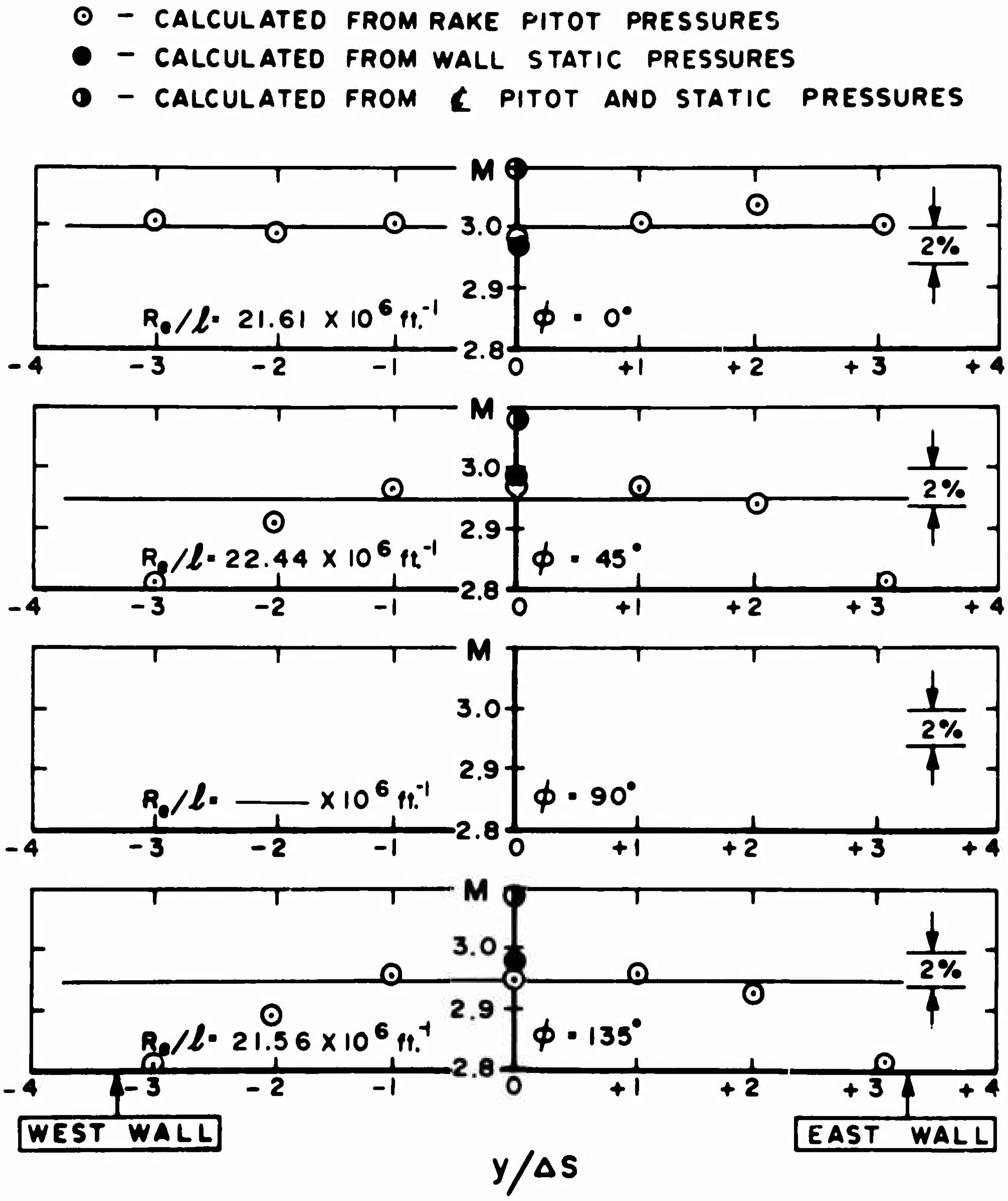

Figure 23a. Impact Mach Number versus y/Δs for xp/xr = - 0.690 at p_0 = 109 psia and T_0 = 430°R

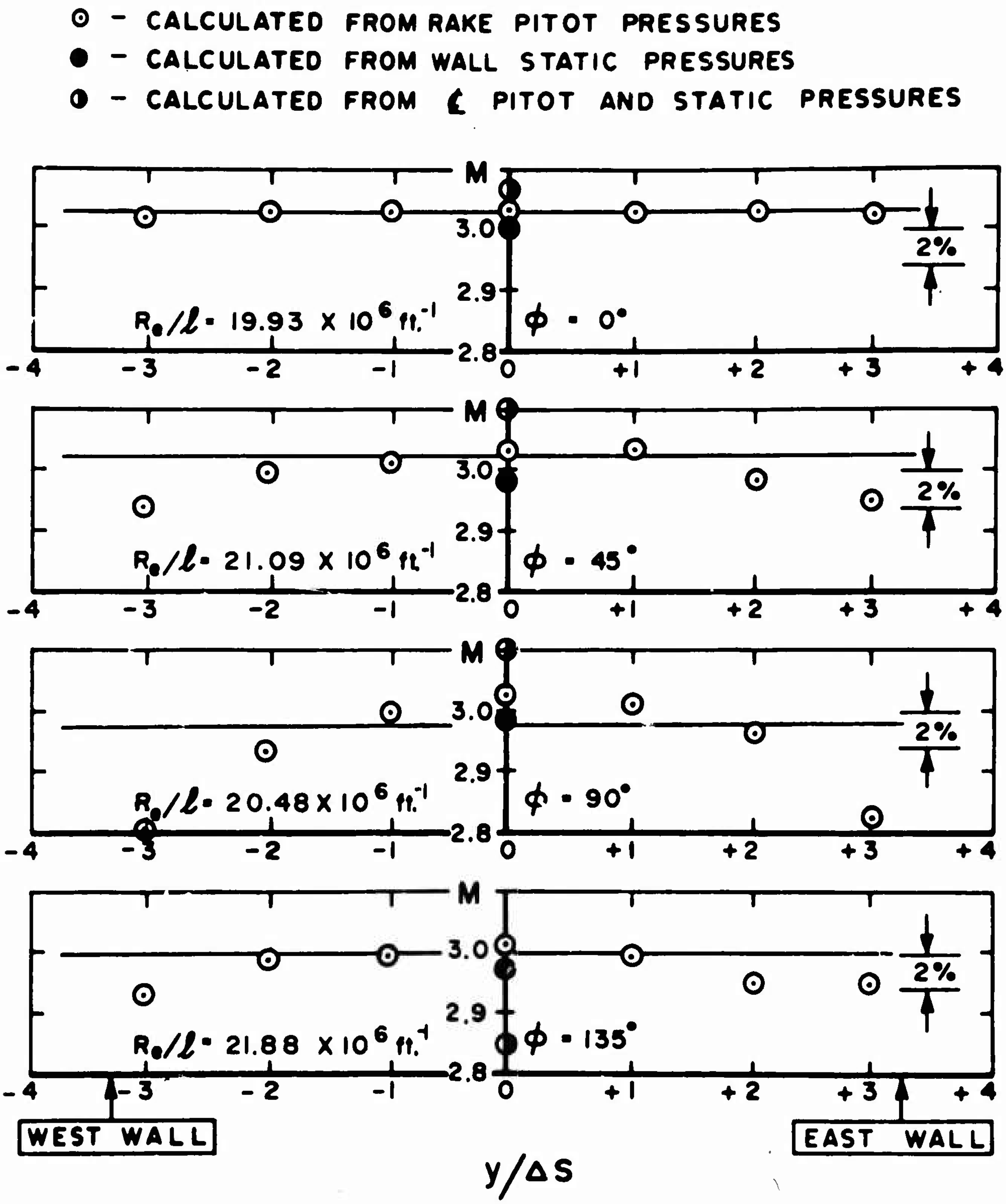

Figure 23b. Impact Mach Number versus y/Δs for xp/xr = - 0.345 at p_0 = 111 psia and T_0 = 477°R

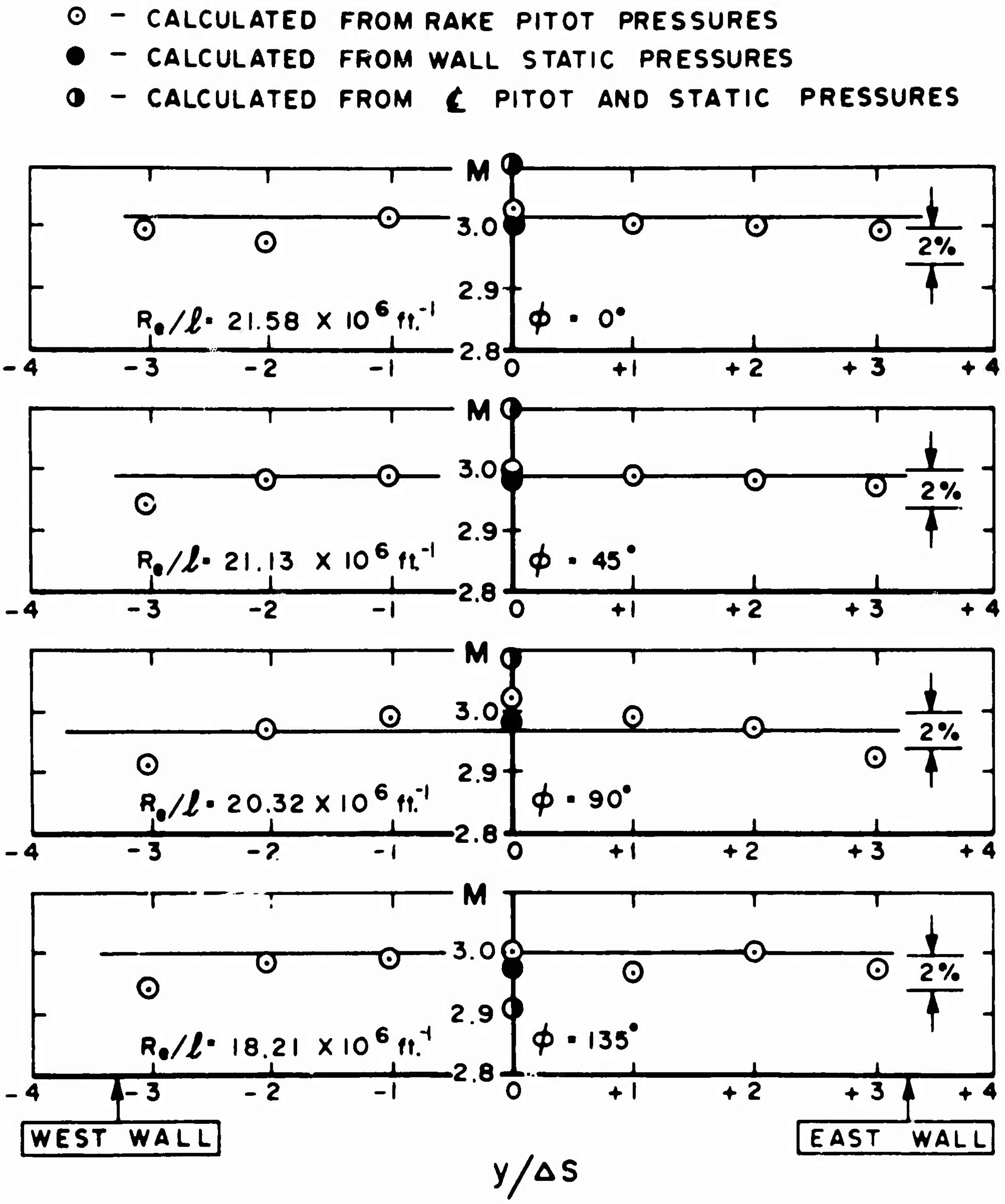

Figure 23c. Impact Mach Number versus y/Δs for xp/xr = 0 at p_0 = 111 psia and T_0 = 484°R

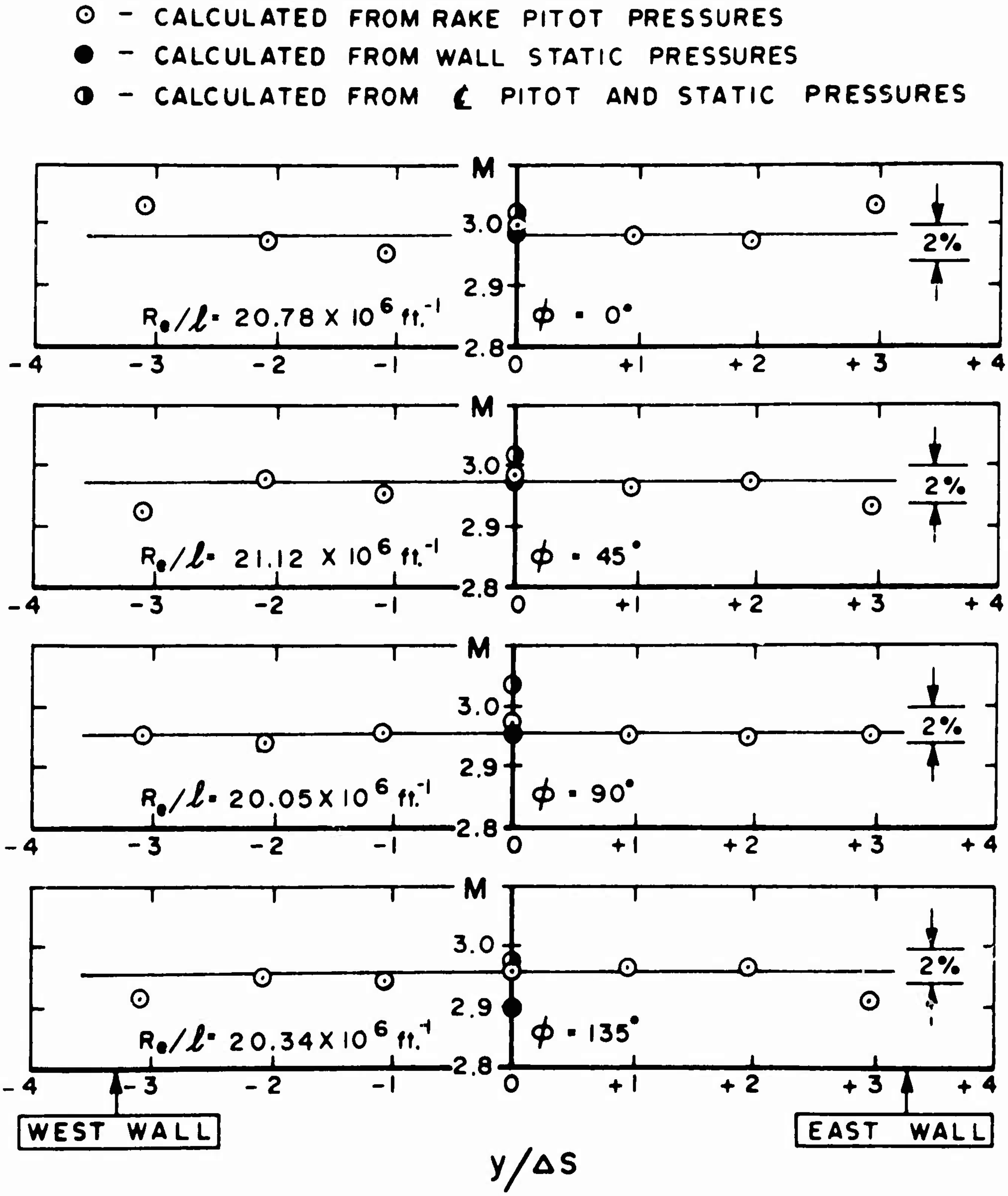

Figure 23d. Impact Mach Number versus y/Δs for xp/xr = + 0.345 at p_0 = 108 psia and T_0 = 477°R

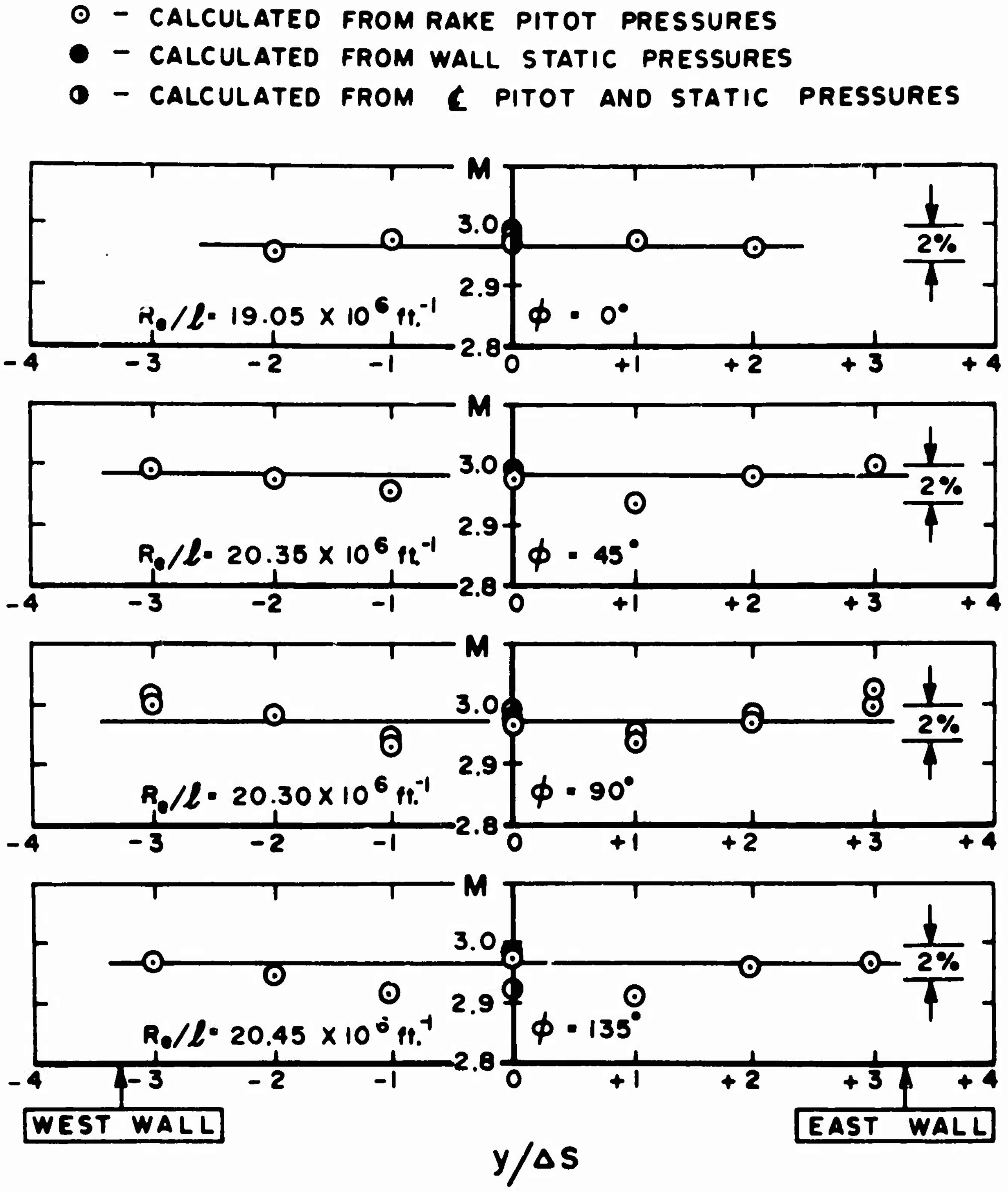

Figure 23e. Impact Mach Number versus y/Δs for xp/xr = + 0.690 at p_0 = 103 psia and T_0 = 472°R

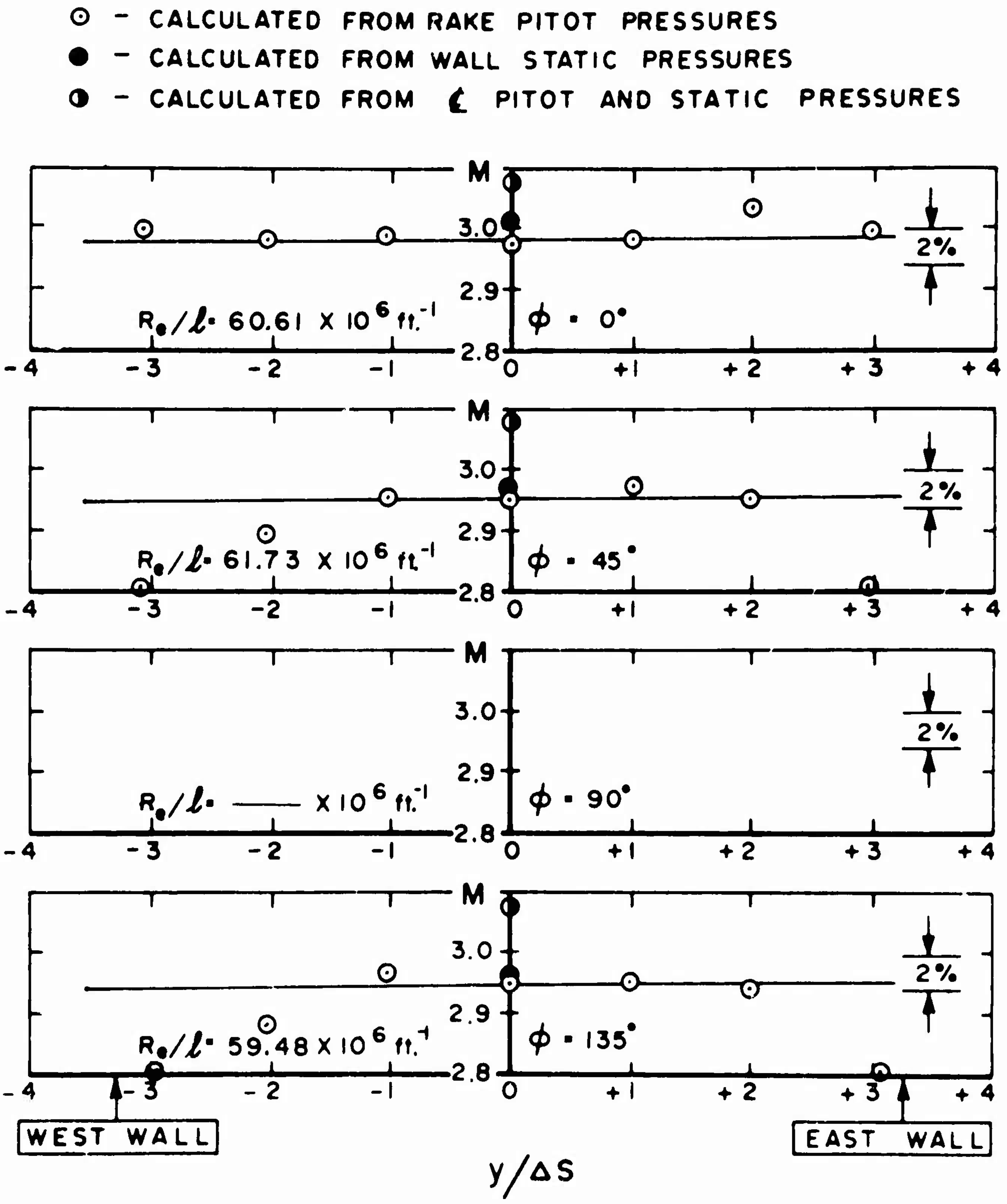

Figure 24a. Impact Mach Number versus y/Δs for xp/xr = - 0.690 at p_0 = 306 psia and T_0 = 468°R

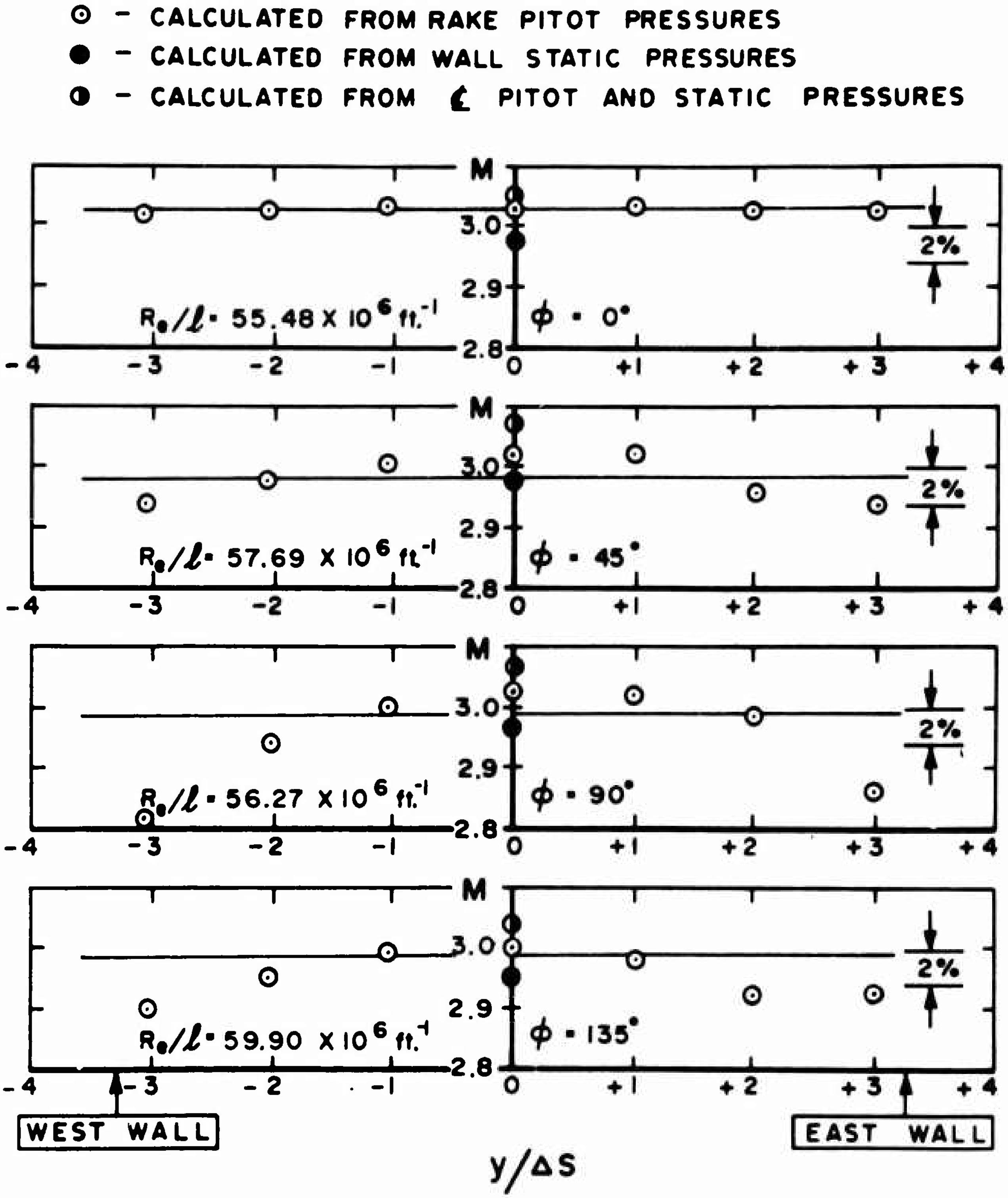

Figure 24b. Impact Mach Number versus y/Δs for xp/xr = - 0.345 at p_0 = 316 psia and T_0 = 482°R

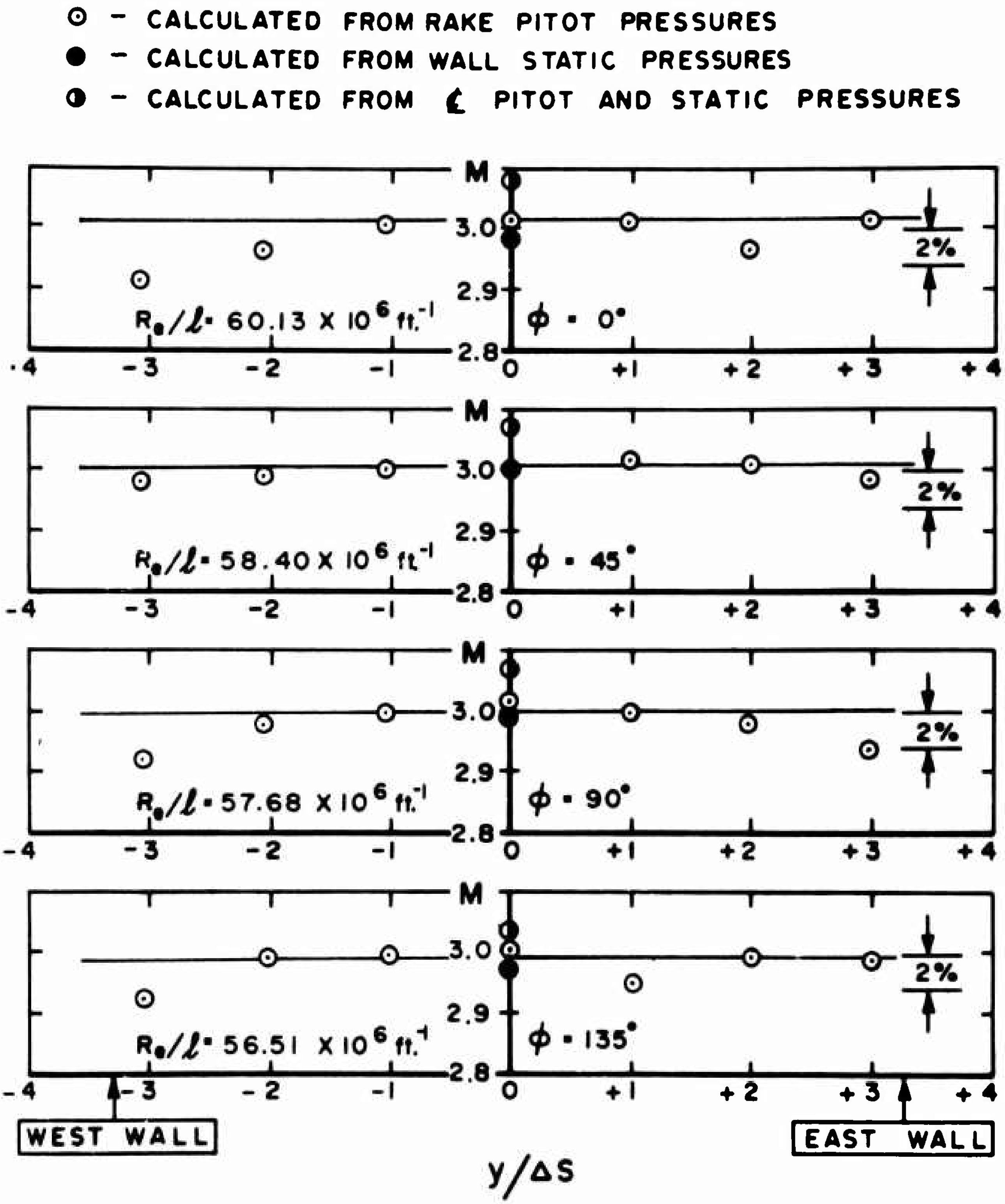

Figure 24c. Impact Mach Number versus y/Δs for xp/xr = 0 at p_0 = 323 psia and T_0 = 491°R

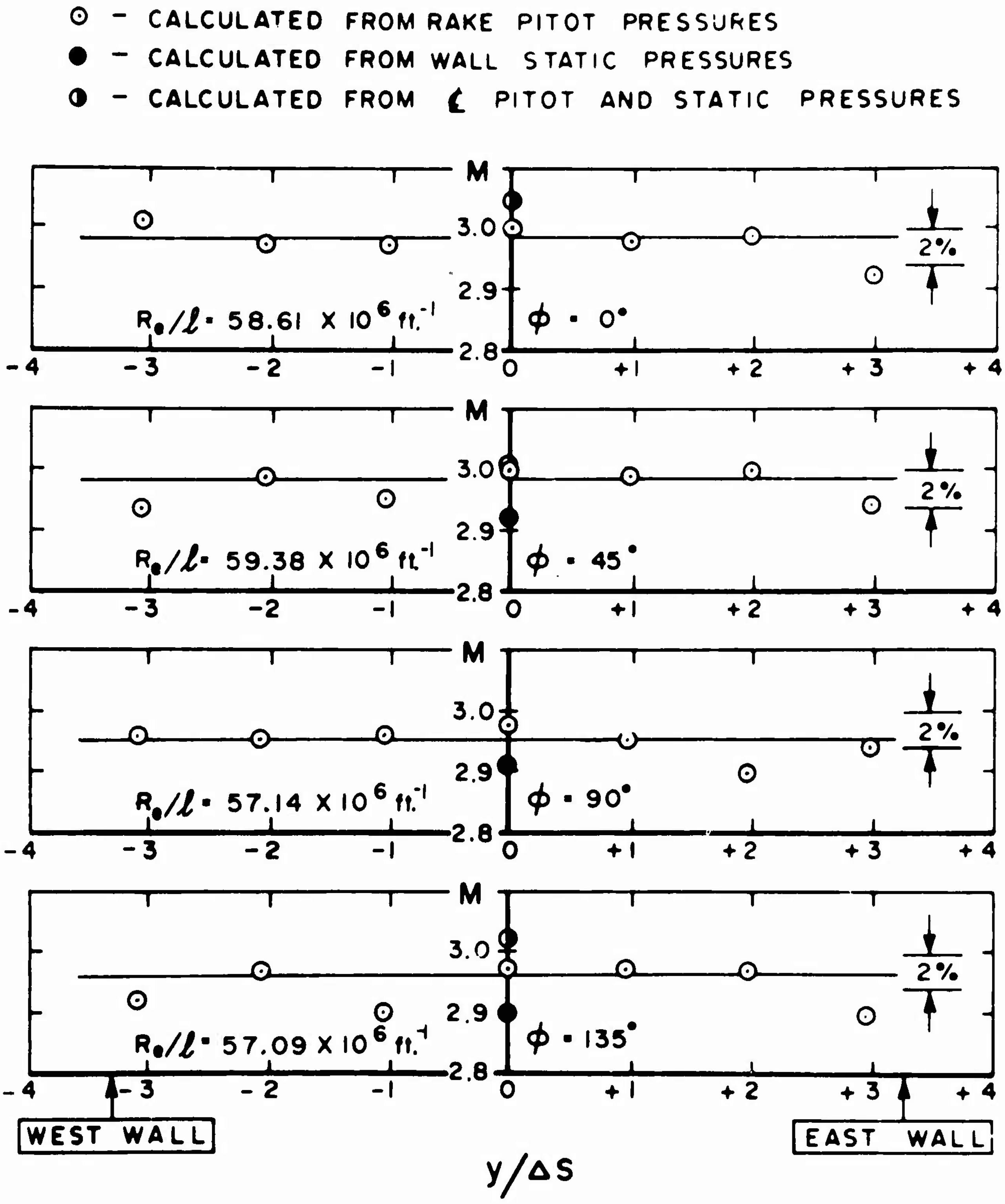

Figure 24d. Impact Mach Number versus y/Δs for xp/xr = + 0.345 at p_0 = 313 psia and T_0 = 483°R

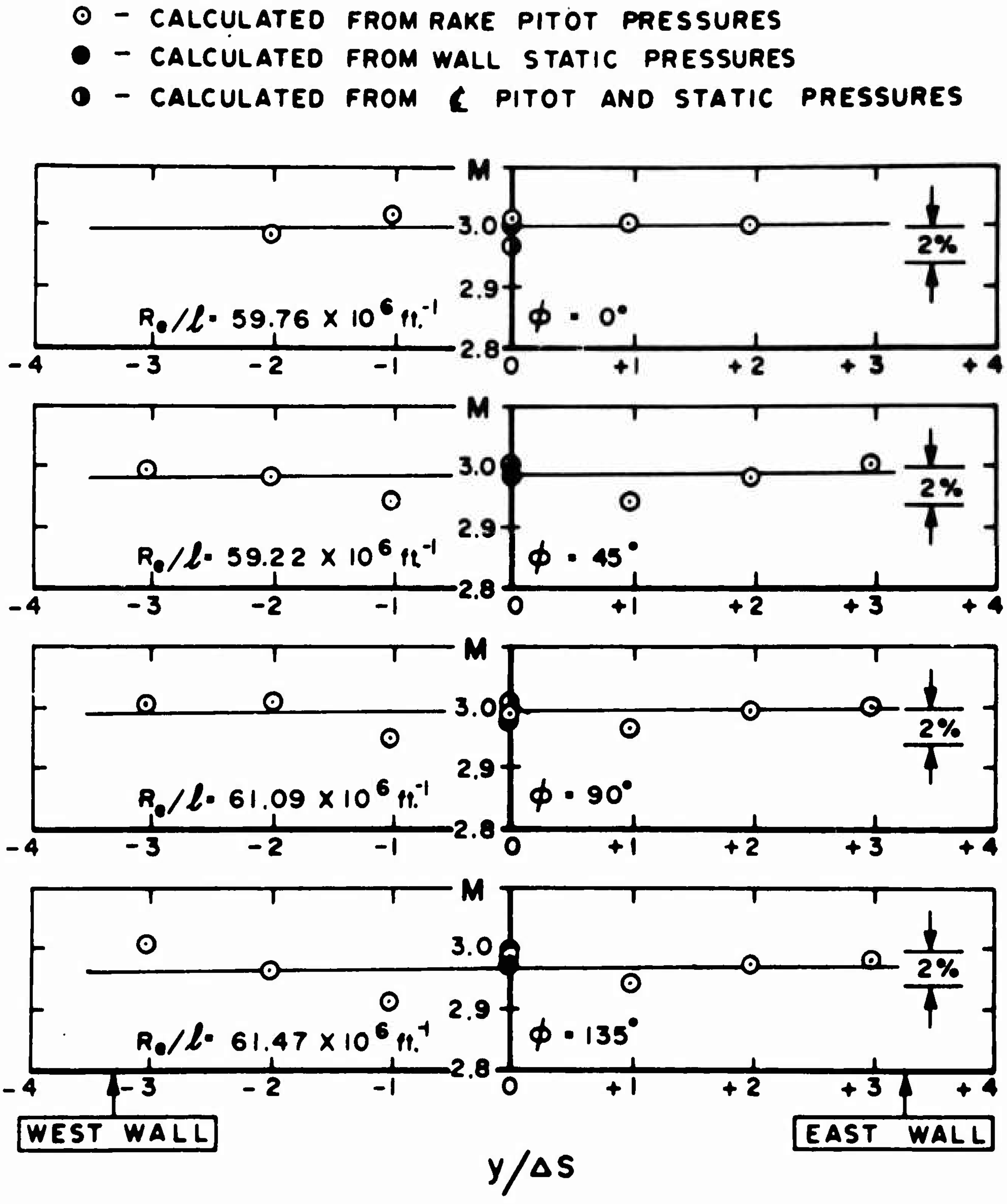

Figure 24e. Impact Mach Number versus y/Δs for xp/xr = + 0.690 at p_0 = 318 psia and T_0 = 476°R

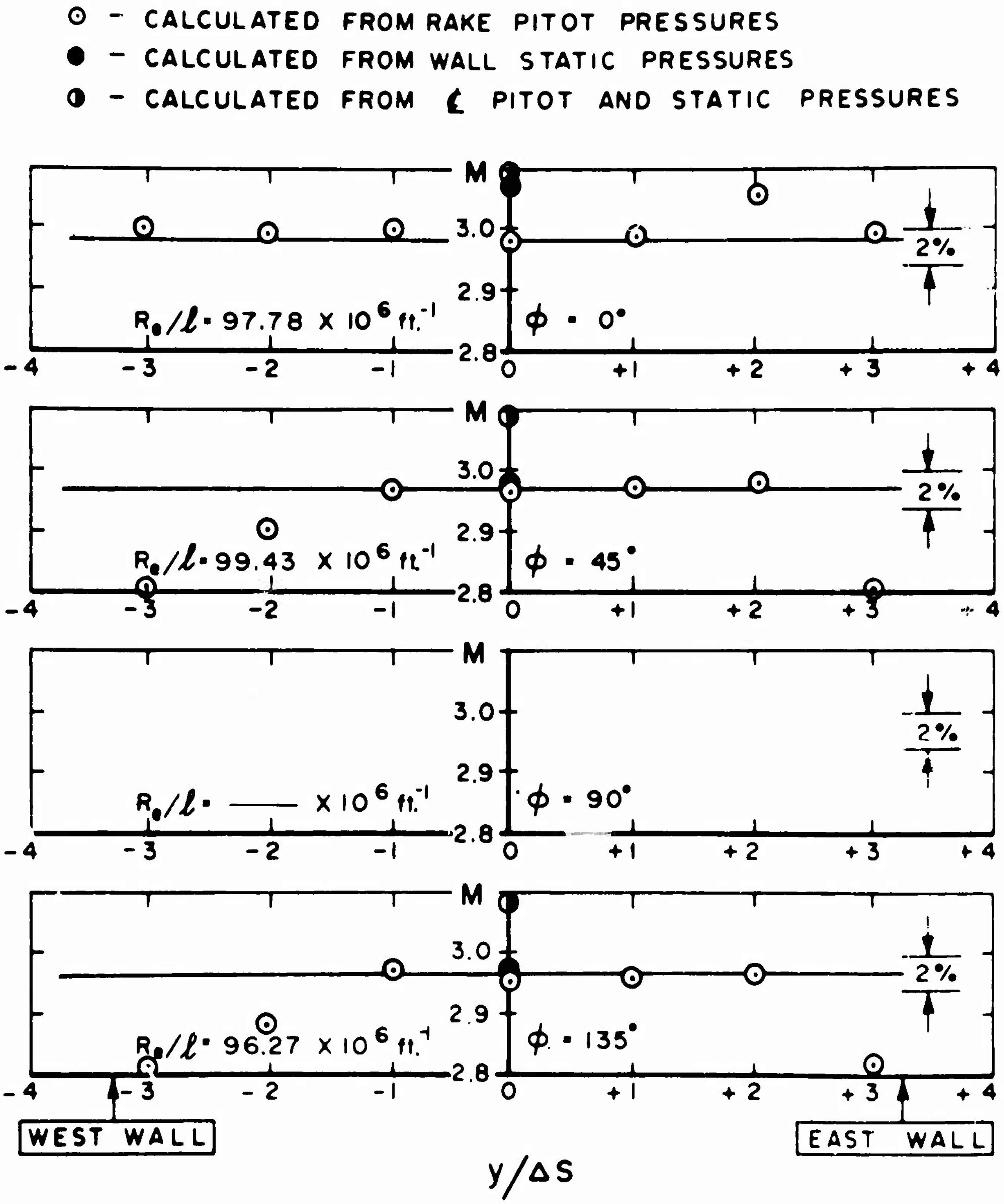

Figure 25a. Impact Mach Number versus y/Δs for xp/xr = - 0.690 at p_0 = 518 psia and T_0 = 478°R

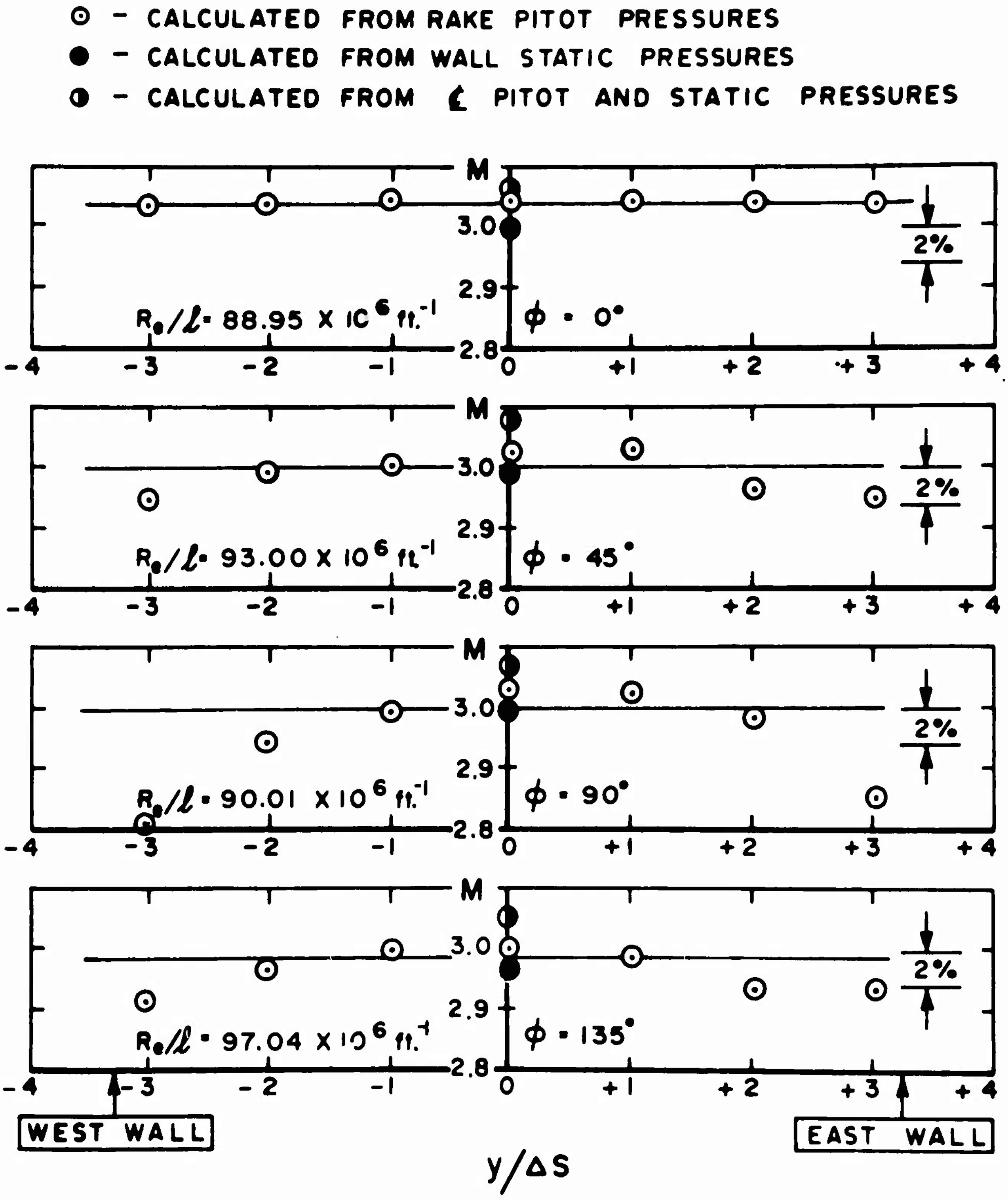

Figure 25b. Impact Mach Number versus y/Δs for xp/xr = - 0.345 at p_0 = 520 psia and T_0 = 491°R

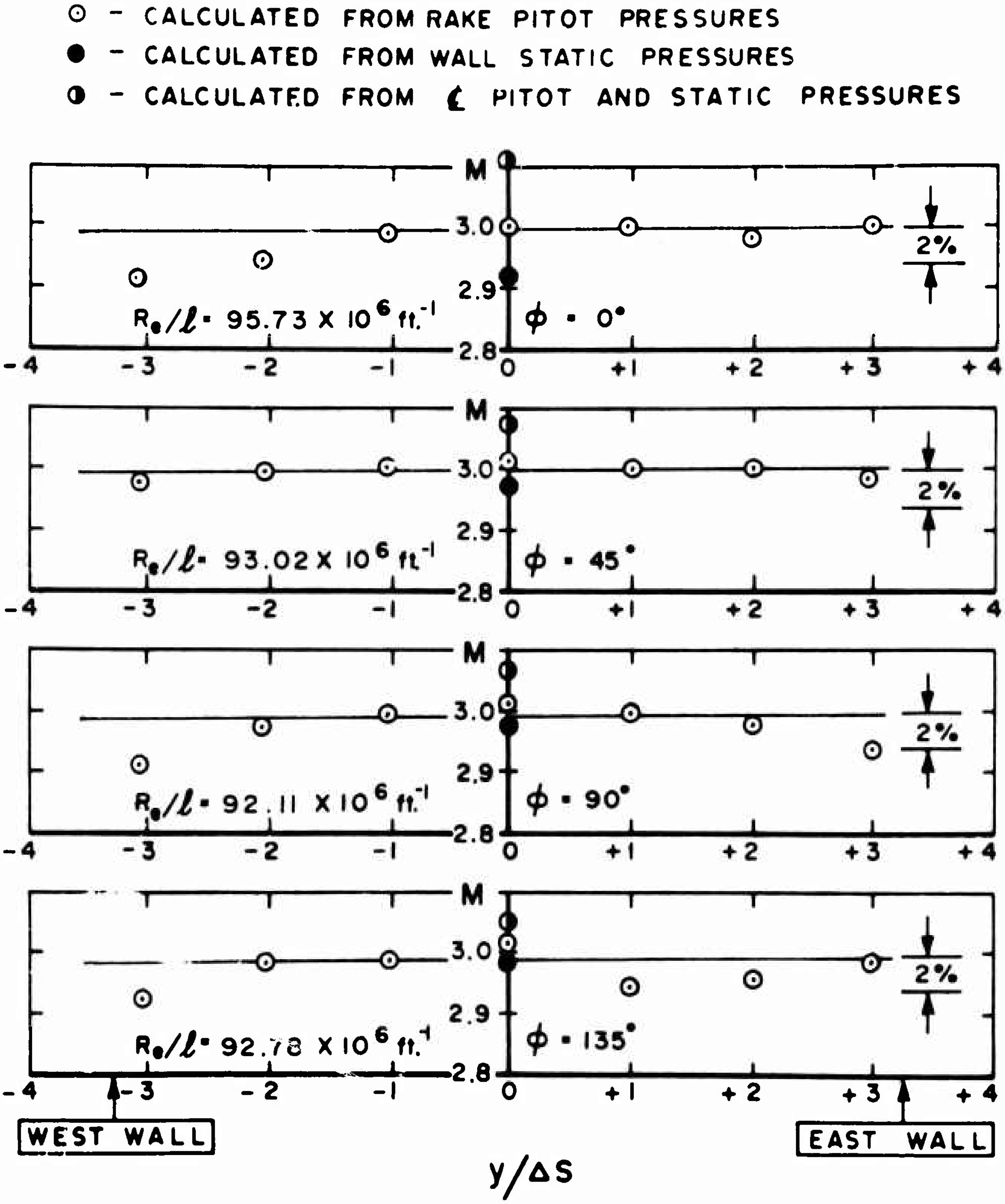

Figure 25c. Impact Mach Number versus y/Δs for xp/xr = 0 at p_0 = 532 psia and T_0 = 499°R

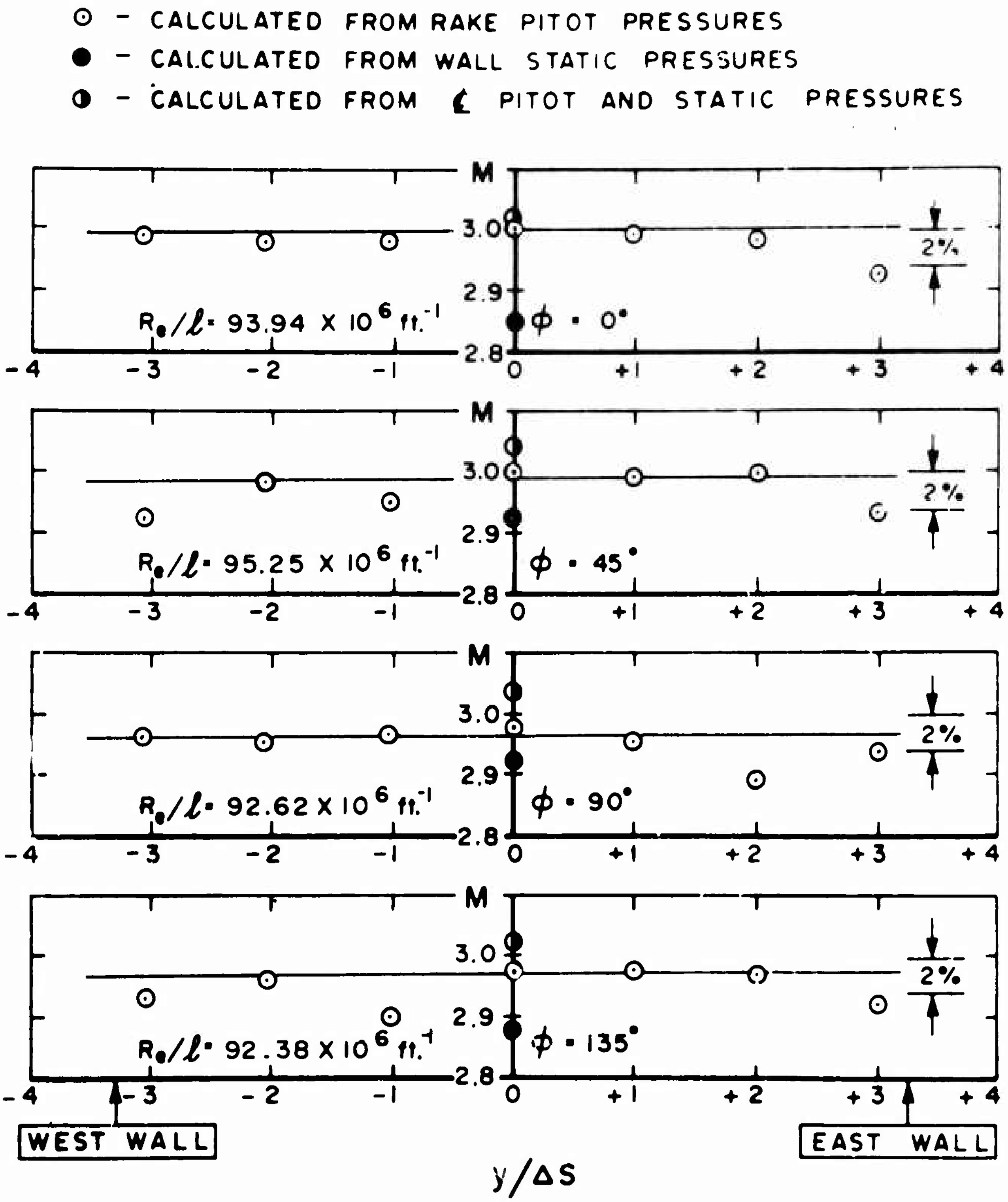

Figure 25d. Impact. Mach Number versus y/Δs for xp/xr = + 0.345 at p_0 = 517 psia and T_0 = 491°R

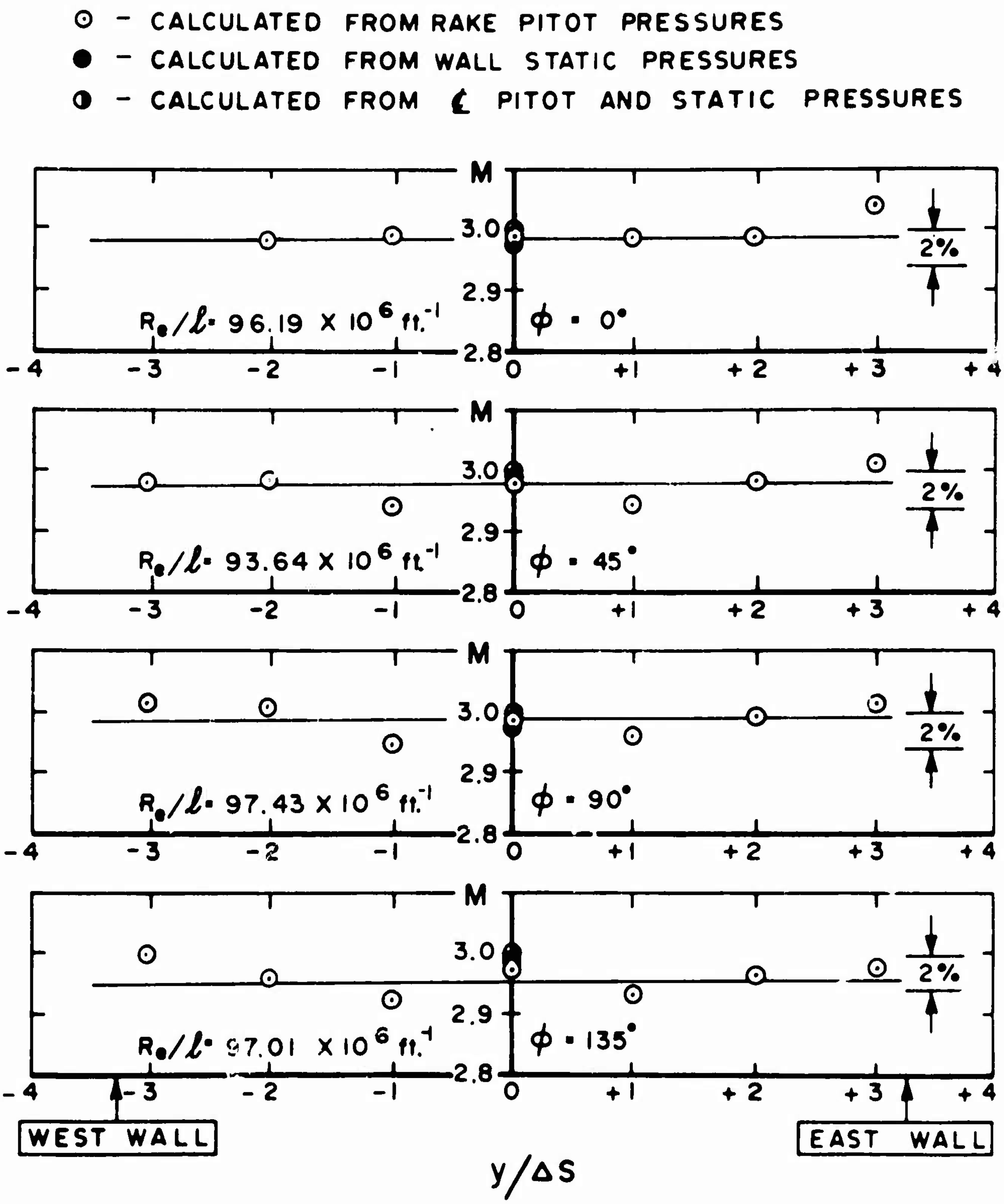

Figure 25e. Impact Mach Number versus y/Δs for xp/xr = + 0.690 at p_0 = 523 psia and T_0 = 486°R

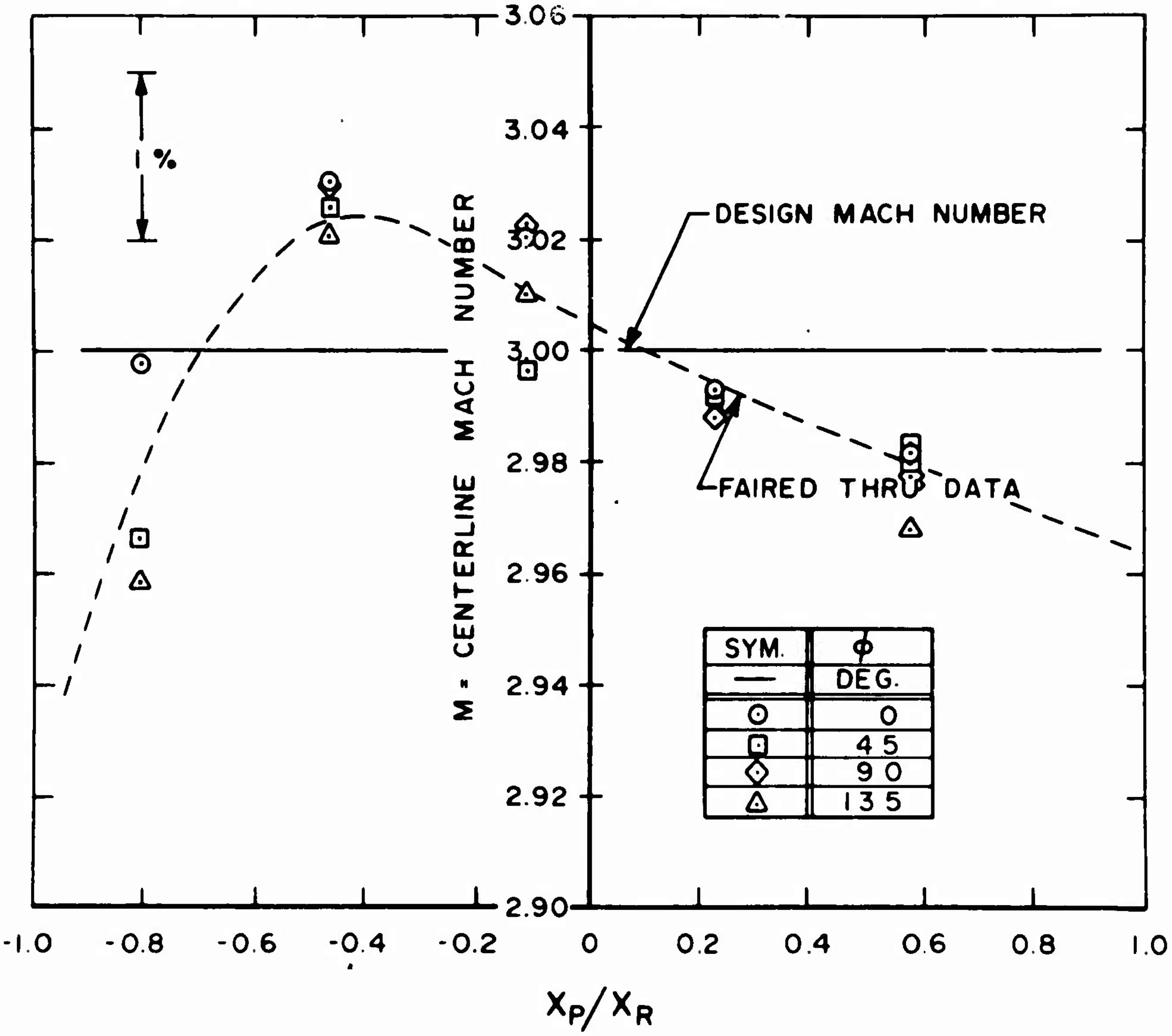

SYM.	φ DEG.
⊙	0
⊡	45
◇	90
△	135

Figure 26a. Centerline Mach Number versus Longitudinal Distance for p_0 = 100 psia, T_0 = 468°R, where $Re/\ell = 20.69 \times 10^6$ per foot

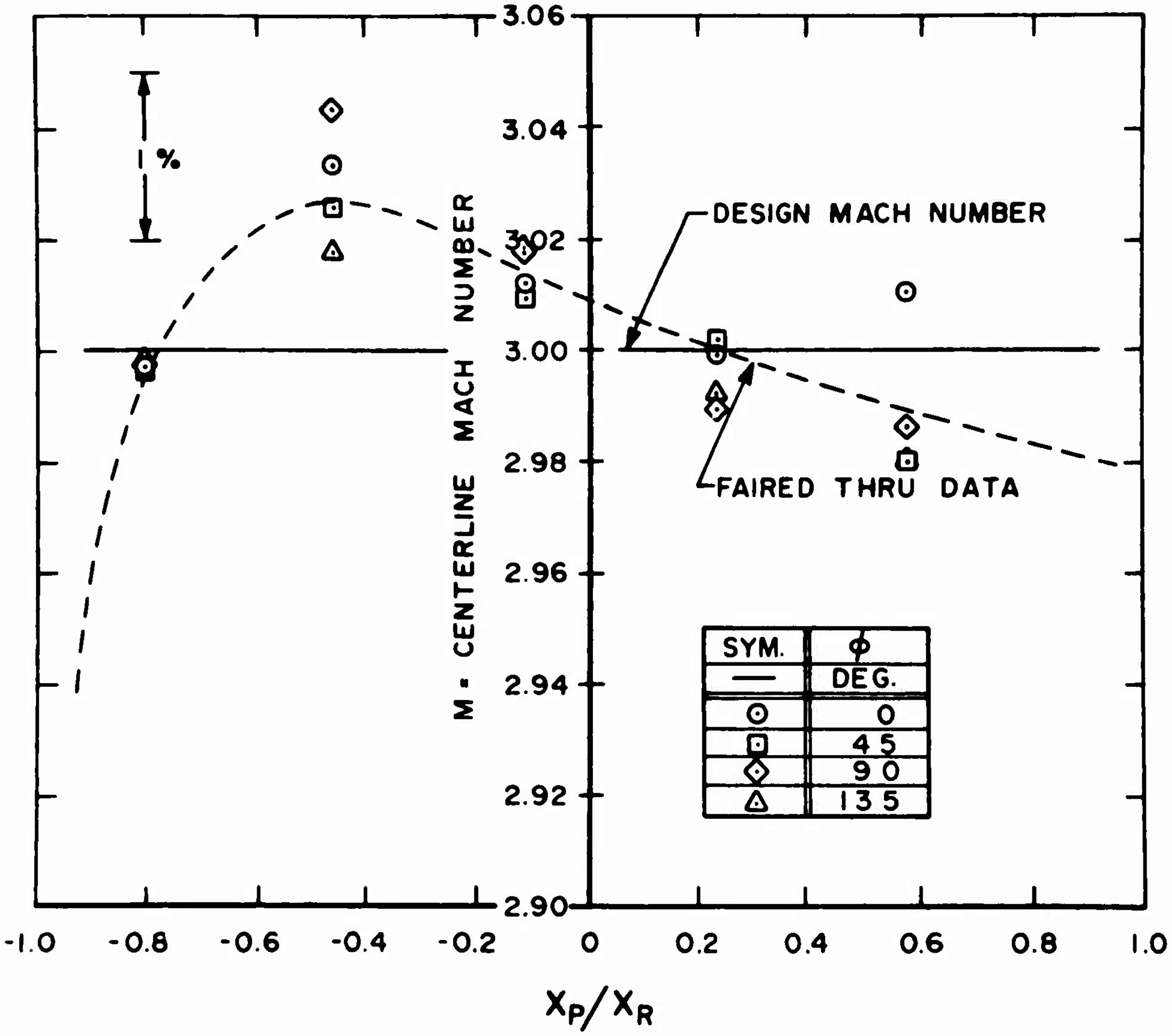

Figure 26b. Centerline Mach Number versus Longitudinal Distance for p_0 = 300 psia, T_0 = 480.06°R, where Re/ℓ = 59.2 x 10^6 per foot

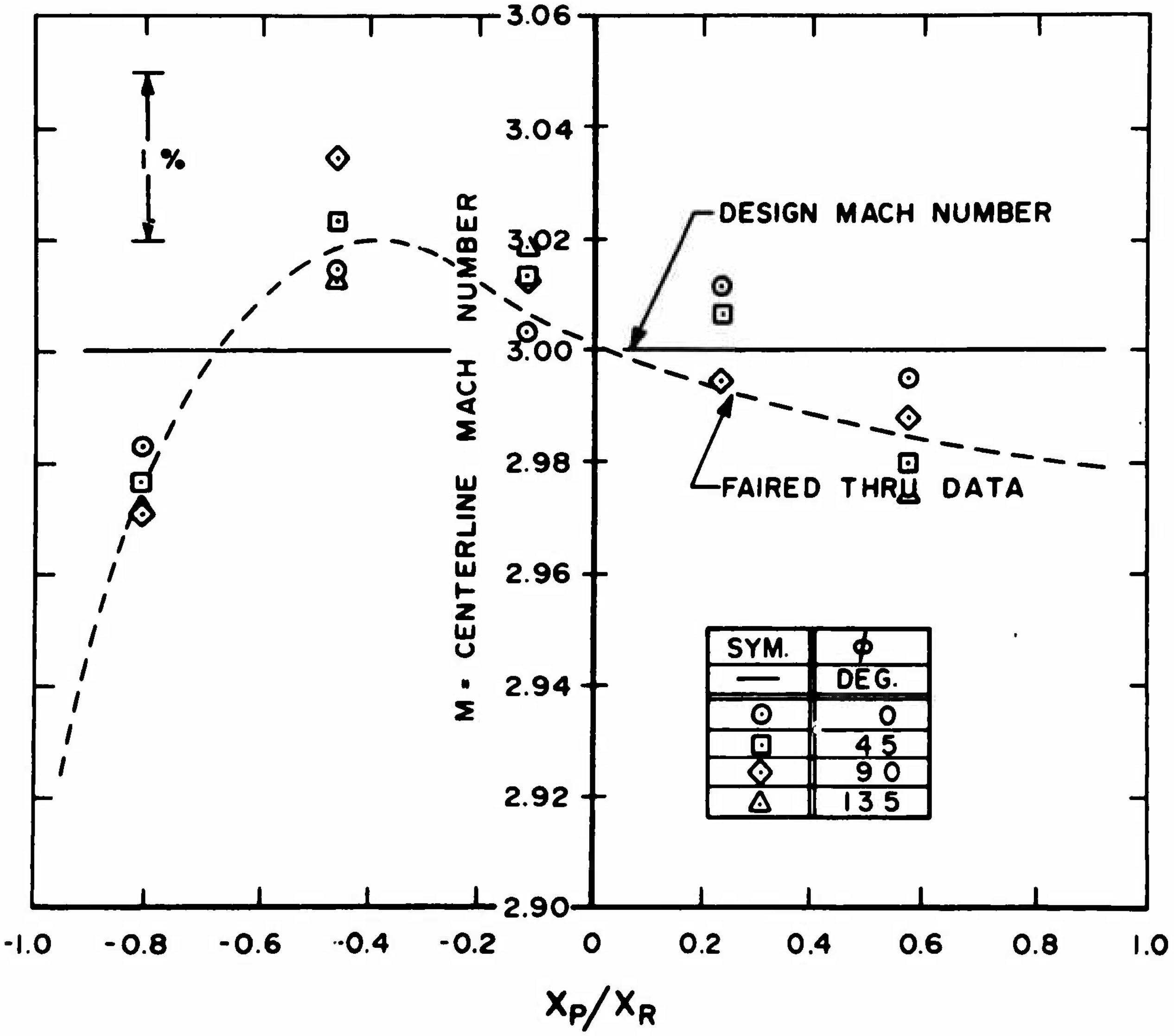

Figure 26c. Centerline Mach Number versus Longitudinal Distance for p_0 = 500 psia, T_0 = 489.05°R where Re/ℓ = 95.0 x 10^6 per foot

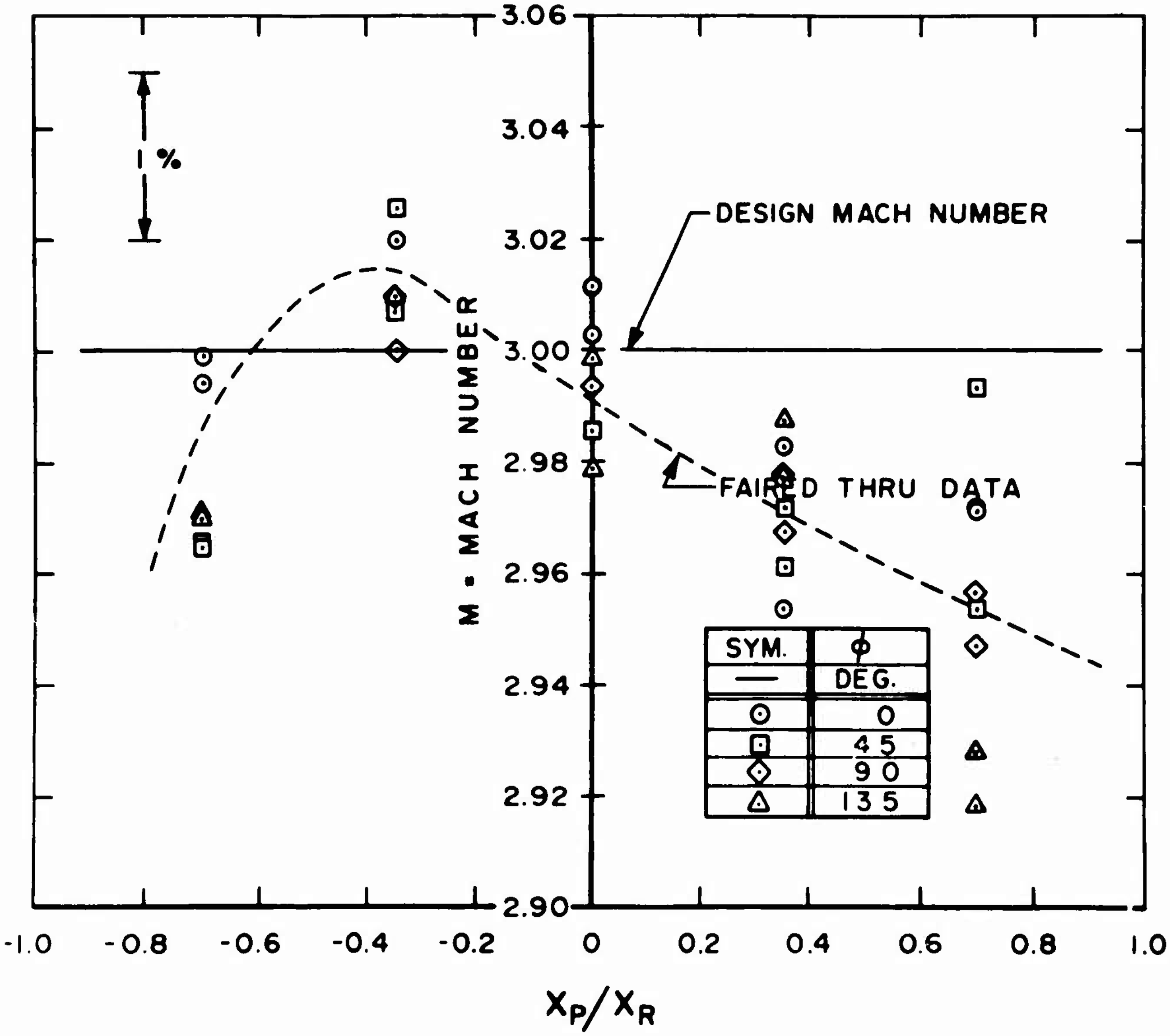

Figure 27a. Mach Number versus Longitudinal Distance for r/Δs = ± 1.0 at P_O = 100 psia, T_O = 468.4°R and Re/ℓ = 20.69 x 10^6 per foot

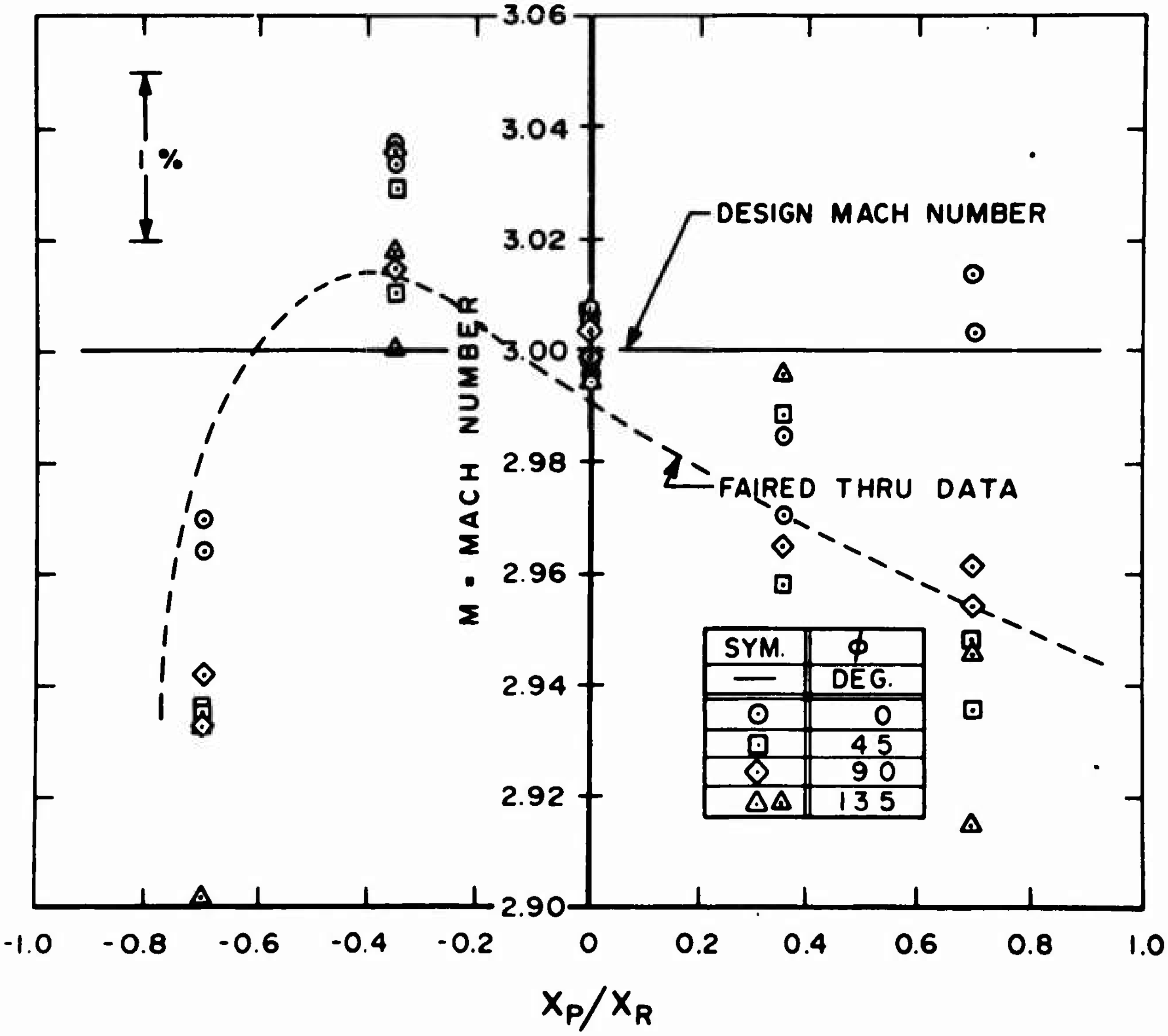

Figure 27b. Mach Number versus Longitudinal Distance for $r/\Delta s = \pm 1.0$ at $p_0 = 300$ psia, $T_0 = 480.06°R$ and $Re/\ell = 59.2 \times 10^6$ per foot

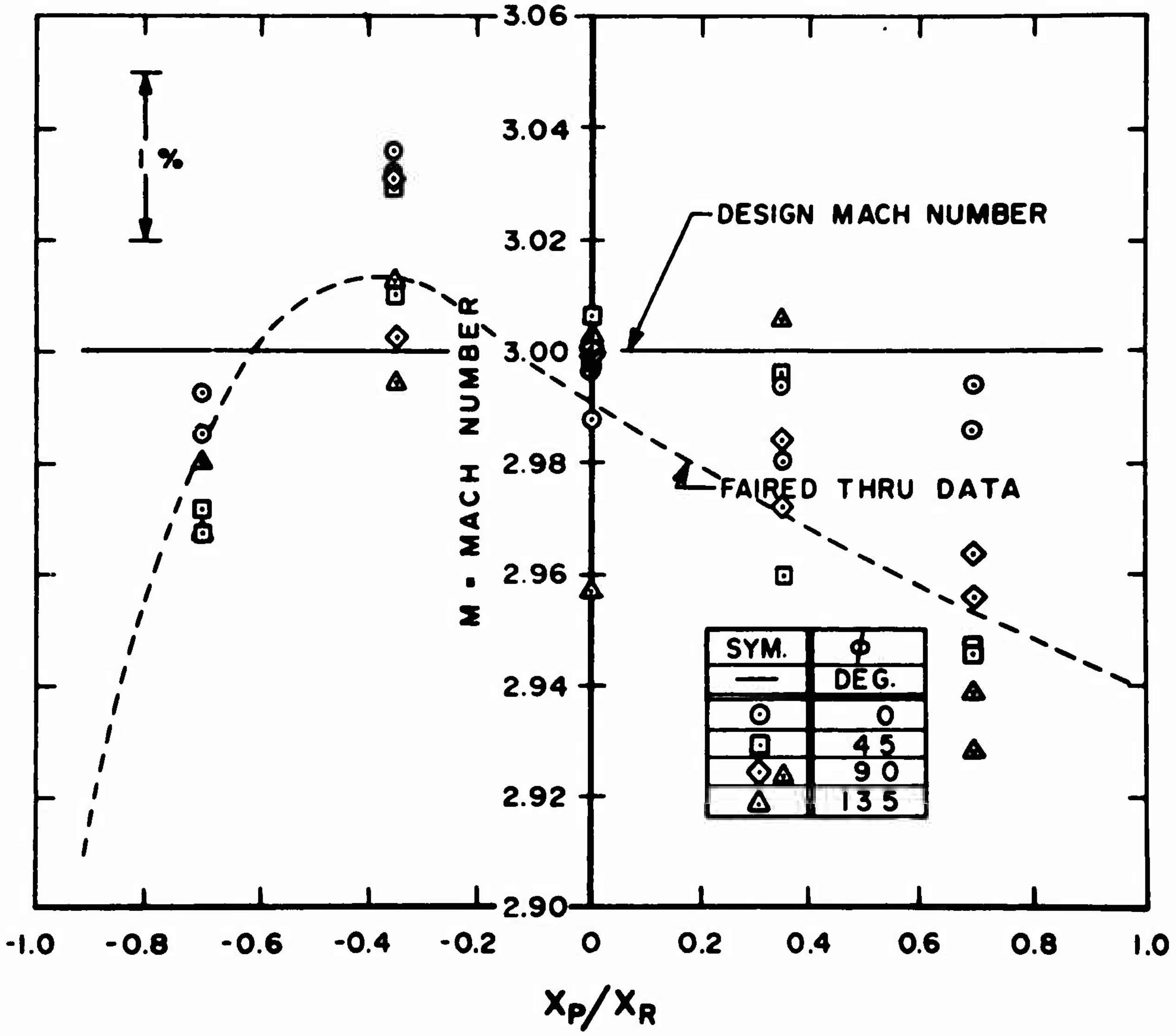

Figure 27c. Mach number versus longitudinal distance for $r/\Delta s = \pm 1.0$ at $P_0 = 500$ psia, $T_0 = 489.05$°R and $Re/\ell = 95.0 \times 10^6$ per foot

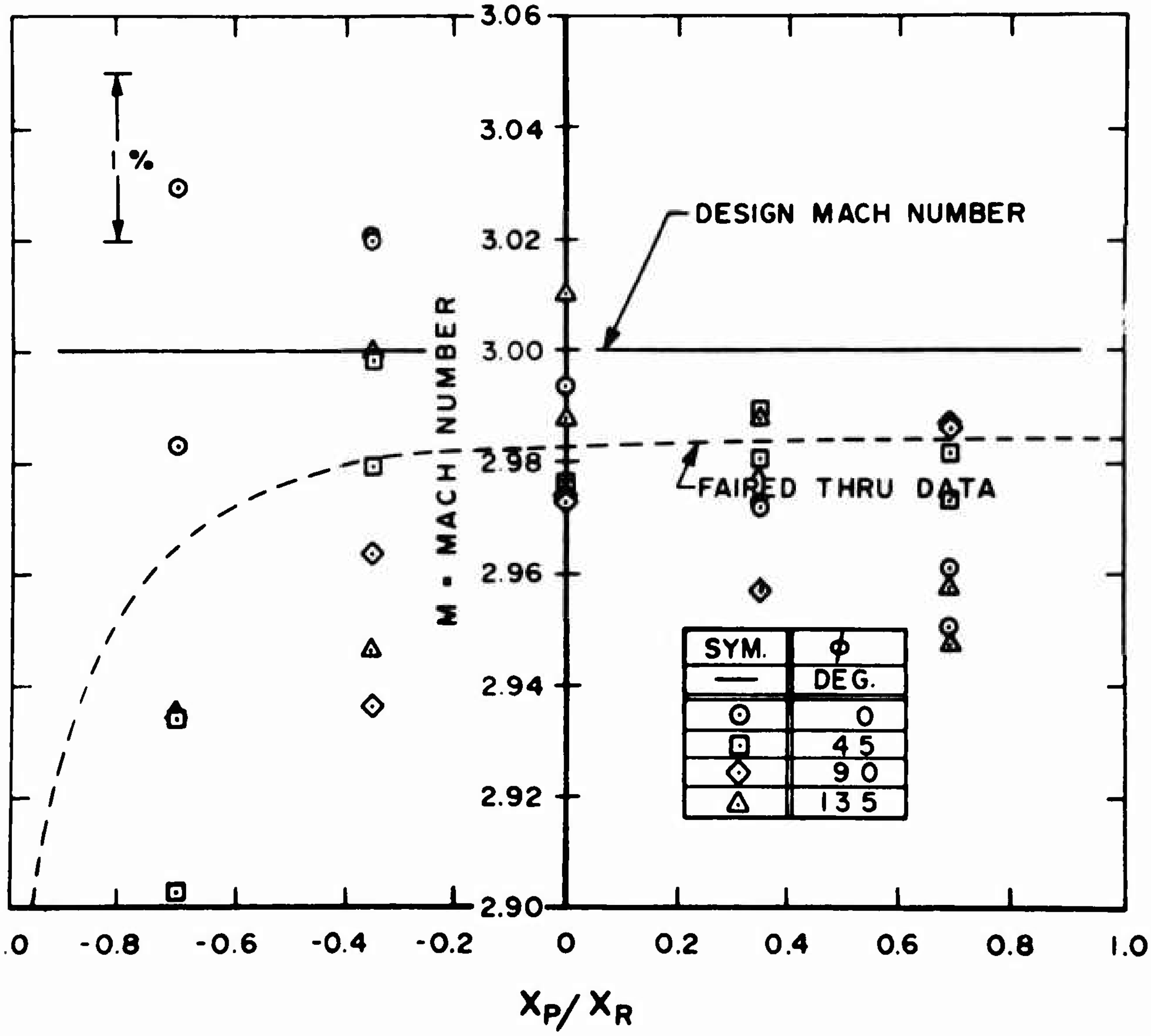

Figure 28a. Mach Number versus Longitudinal Distance for r/Δs = ± 2.0 at p_0 = 100 psia, T_0 = 468.4°R and Re/ℓ = 20.69 x 10^6 per foot

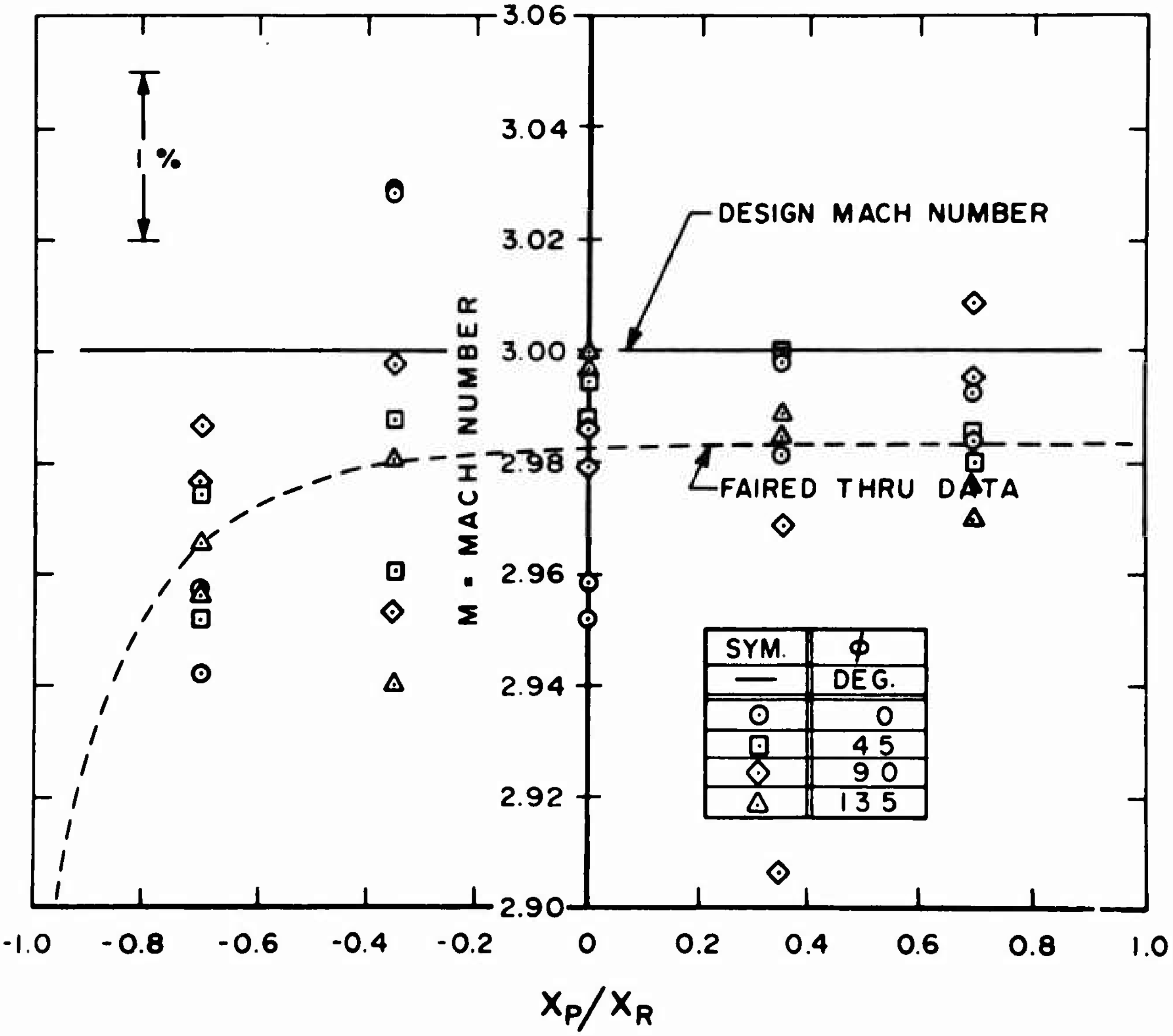

SYM.	φ
—	DEG.
⊙	0
⊡	45
◇	90
△	135

Figure 28b. Mach Number versus Longitudinal Distance for $r/\Delta s = \pm 2.0$ at $p_0 = 300$ psia, $T_0 = 480.06°R$ and $Re/\ell = 59.2 \times 10^6$ per foot

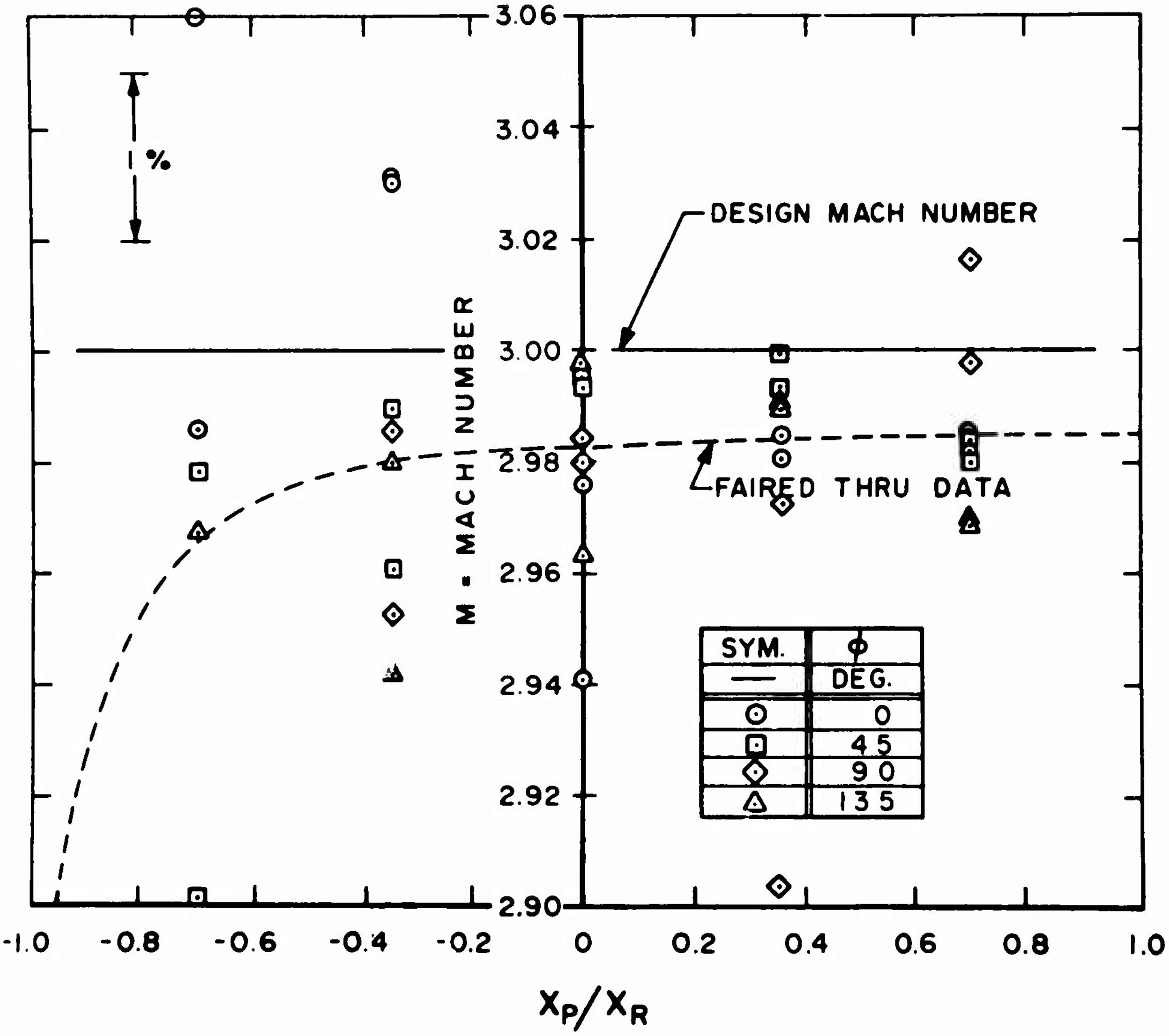

Figure 28c. Mach Number versus Longitudinal Distance for $r/\Delta s = \pm 2.0$ at $p_0 = 500$ psia, $T_0 = 489.05°R$ and $Re/\ell = 95.0 \times 10^6$ per foot

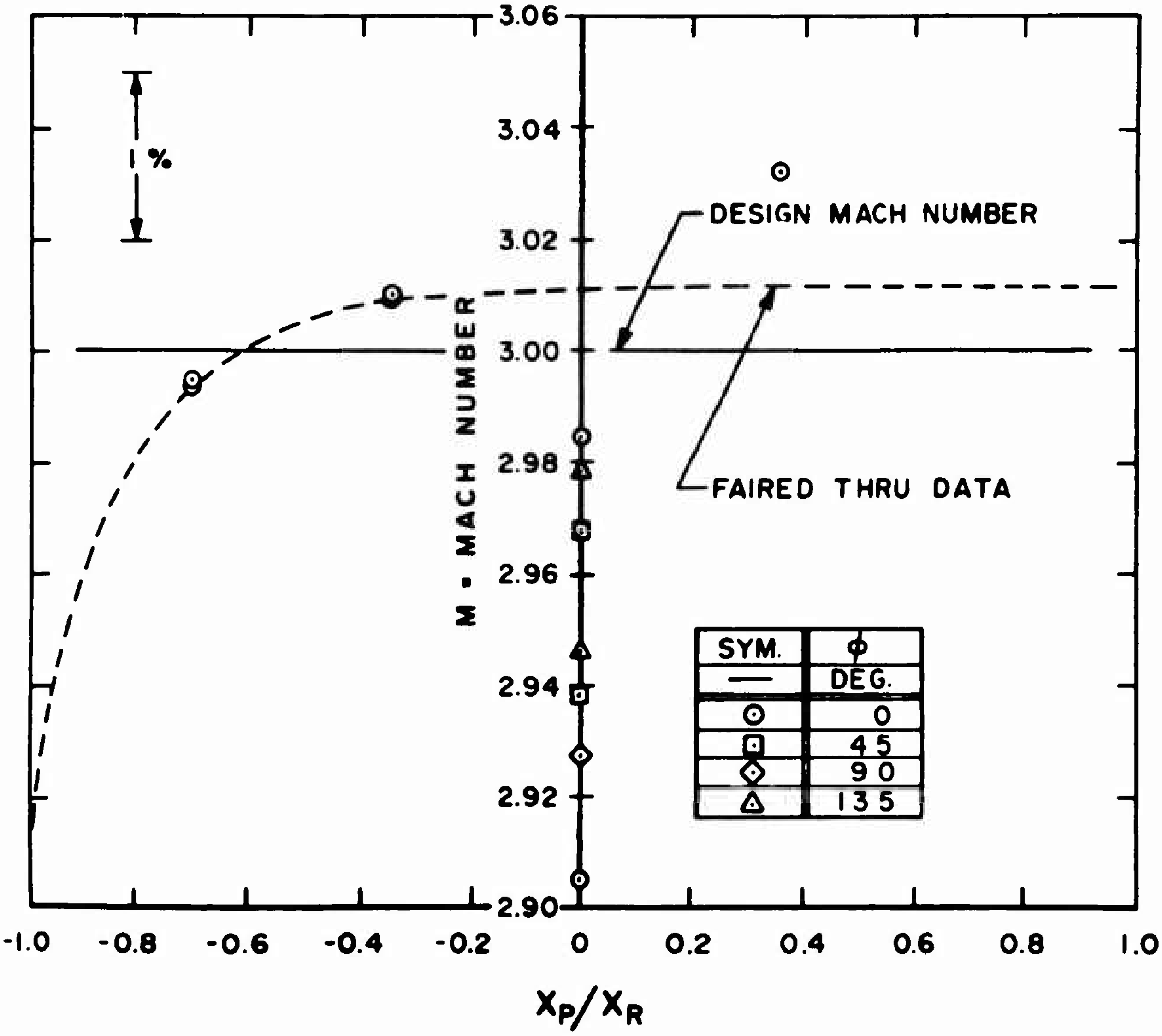

Figure 29a. Mach Number versus Longitudinal Distance for $r/\Delta s = \pm 3.0$ at $p_o = 100$ psia, $T_o = 468.4°R$ and $Re/\ell = 20.69 \times 10^6$ per foot

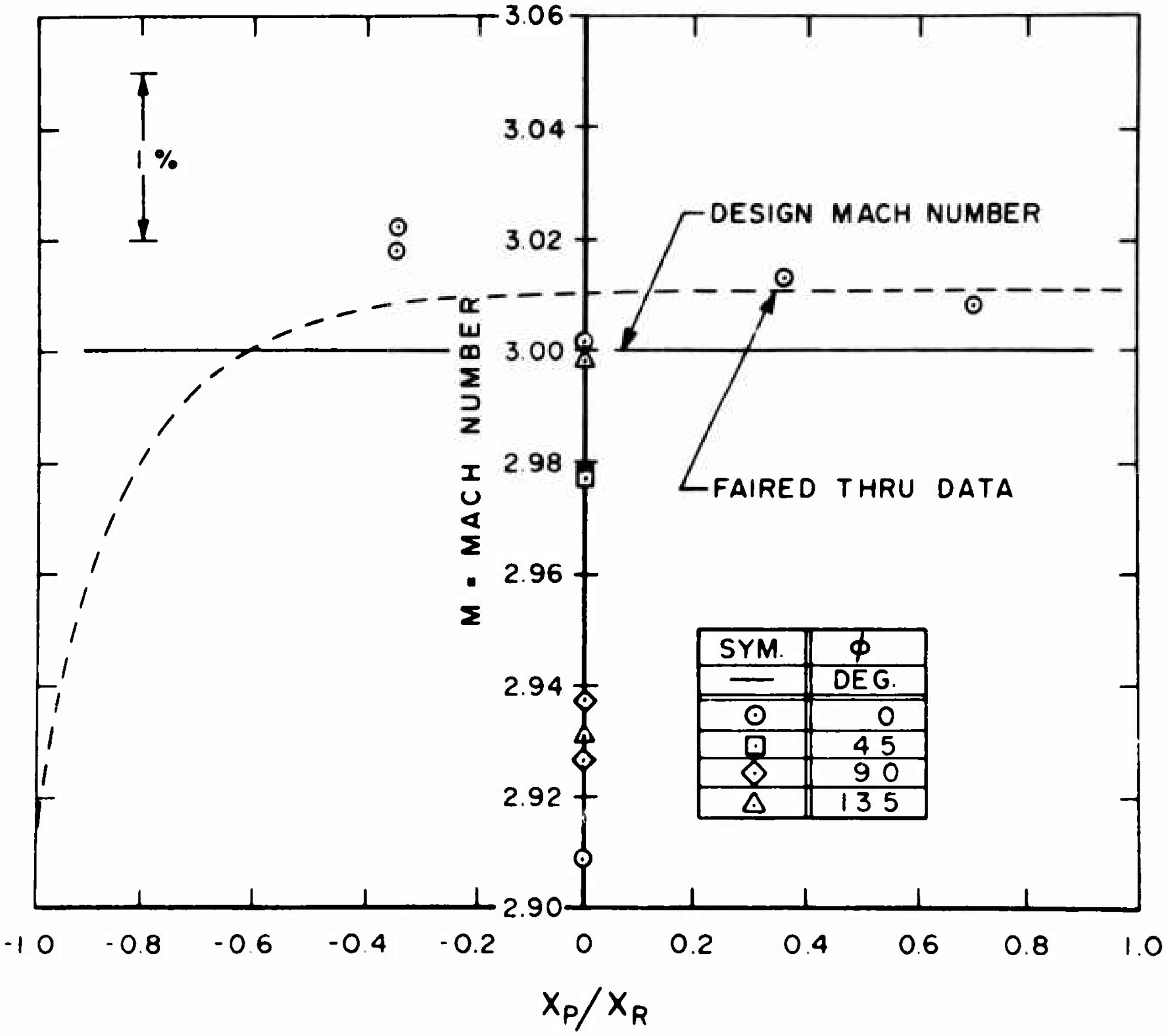

Figure 29b. Mach Number versus Longitudinal Distance for $r/\Delta s = \pm 3.0$ at $p_0 = 300$ psia, $T_0 = 480.06°R$ and $Re/\ell = 59.2 \times 10^6$ per foot

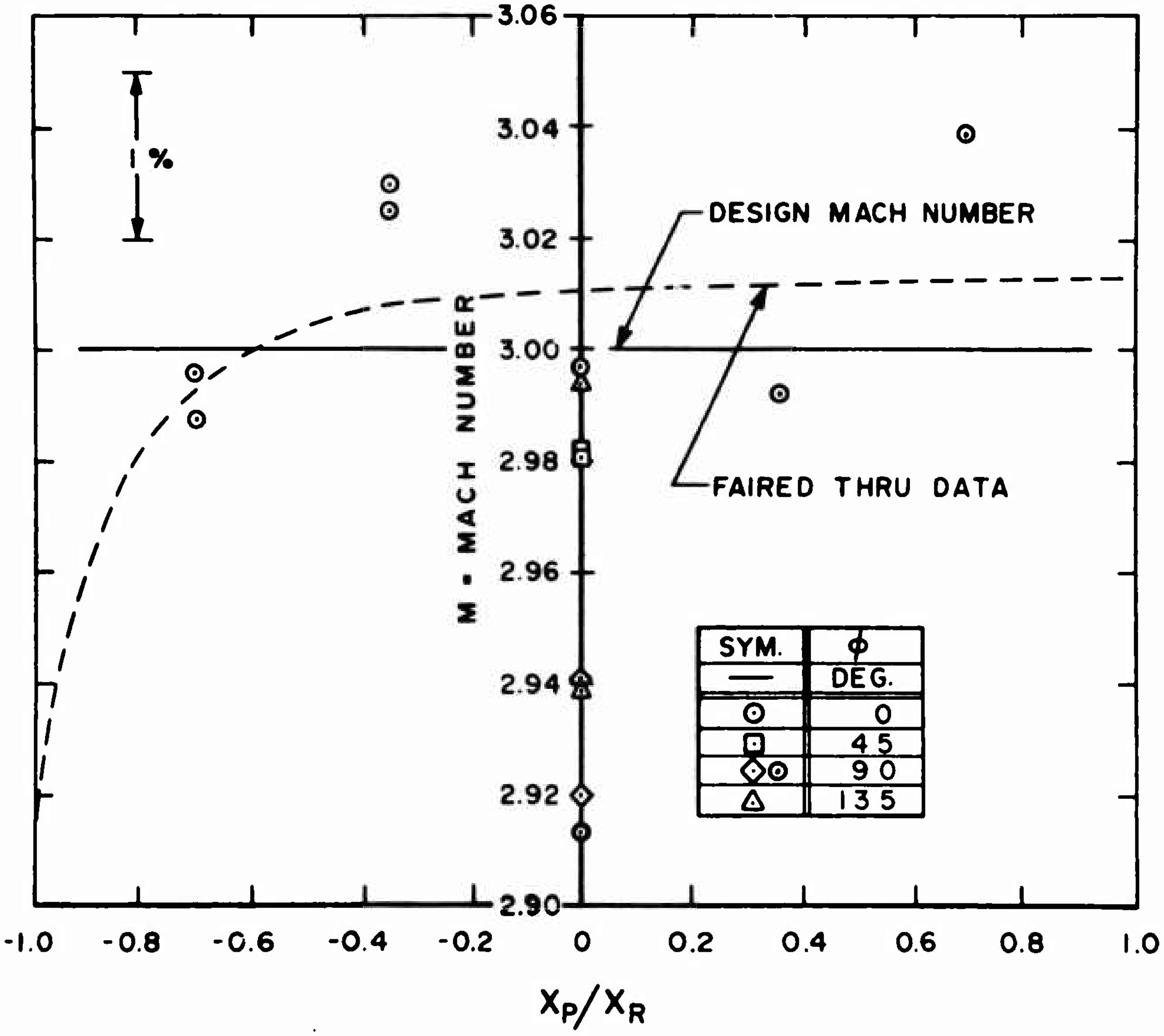

Figure 29c. Mach Number versus Longitudinal Distance for r/Δs = ± 3.0 at p_0 = 500 psia, T_0 = 489.05° and Re/ℓ = 95.0 x 10^6 per foot

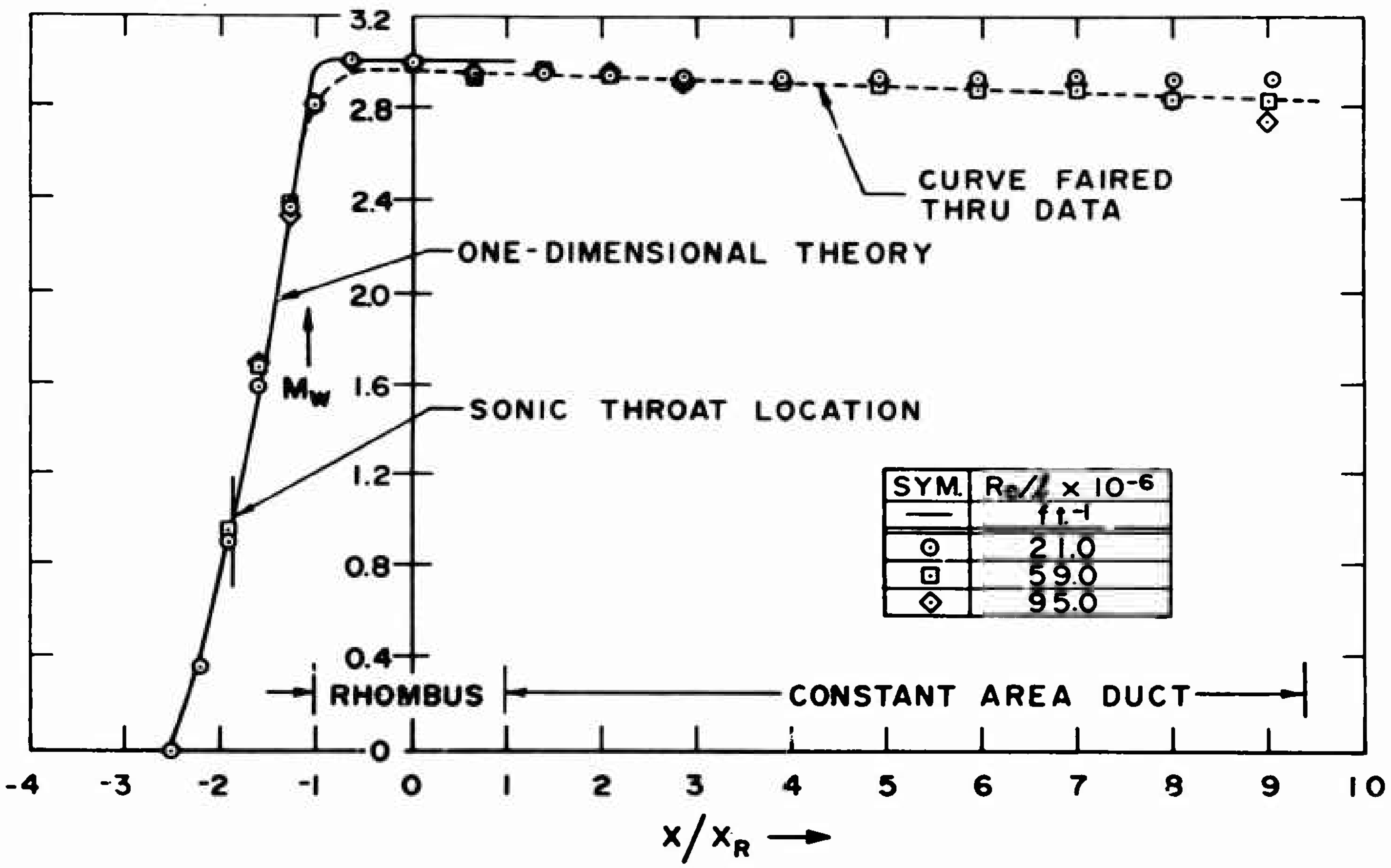

Figure 30. Wall Mach Number versus Longitudinal Distance for Tunnel Empty Condition with Reynolds Number as a Parameter

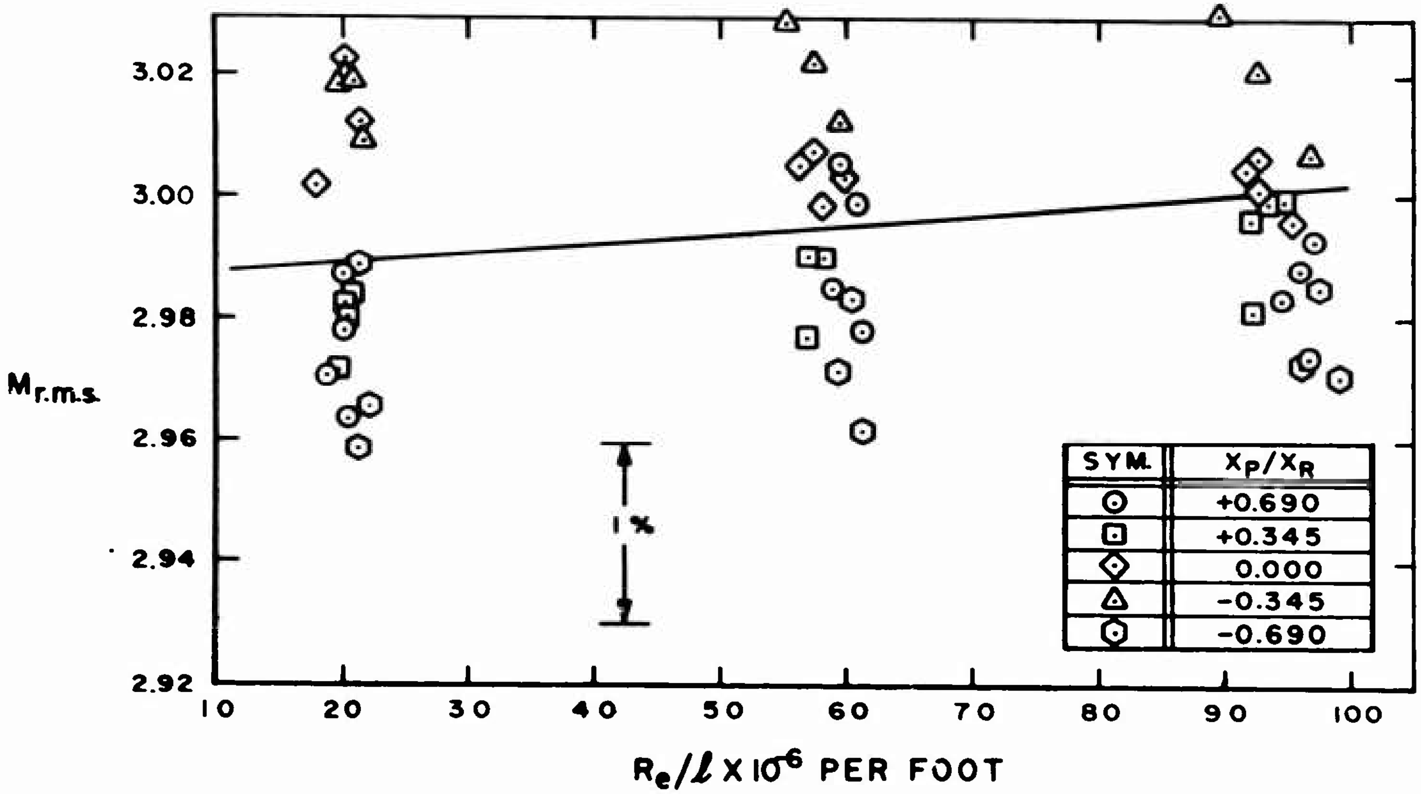

Figure 31. Root-Mean-Square Mach Number versus Unit Reynolds Number Per Foot

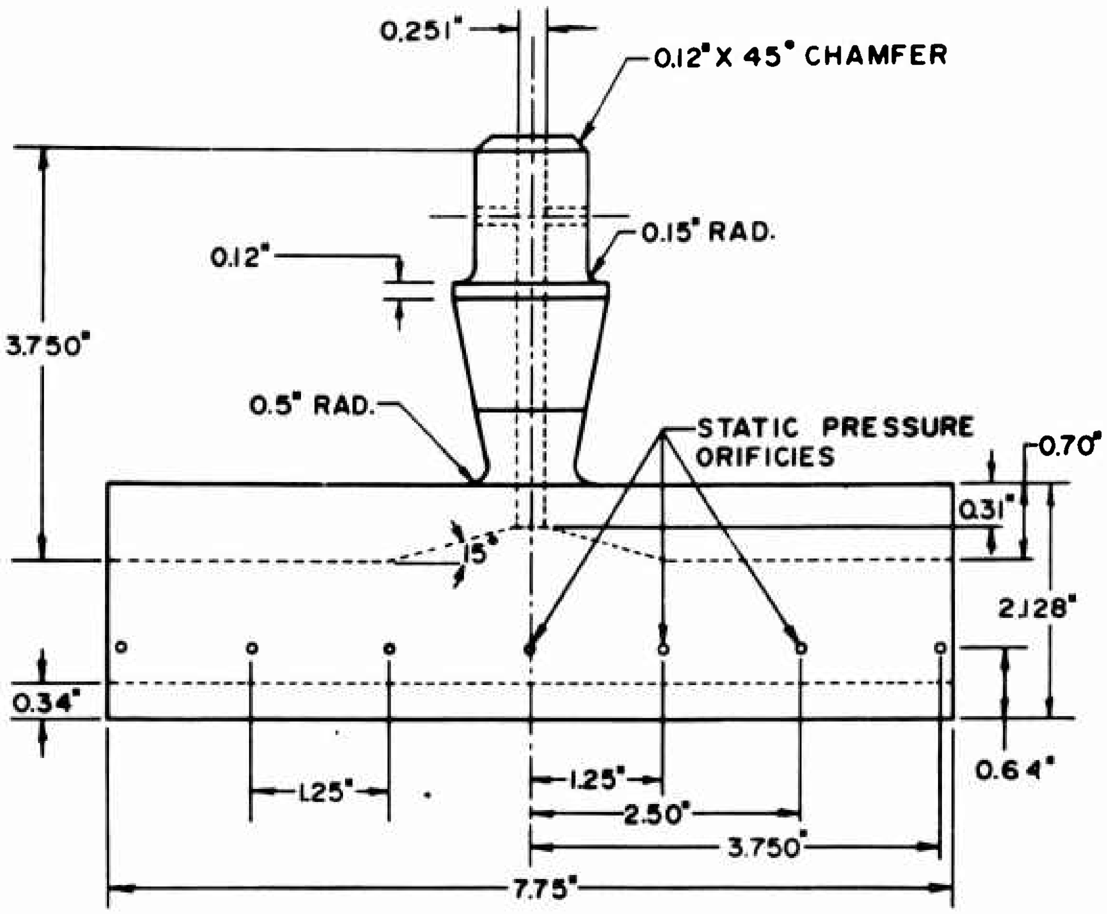

A. WEDGE PLAN VIEW

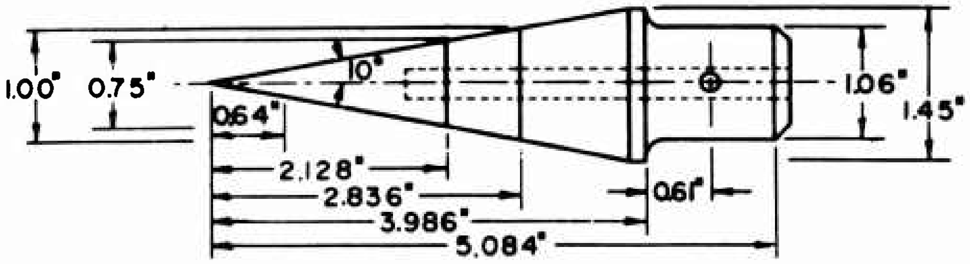

B. WEDGE SIDE VIEW

Figure 32. Scale Drawing of Flow Angularity Wedge

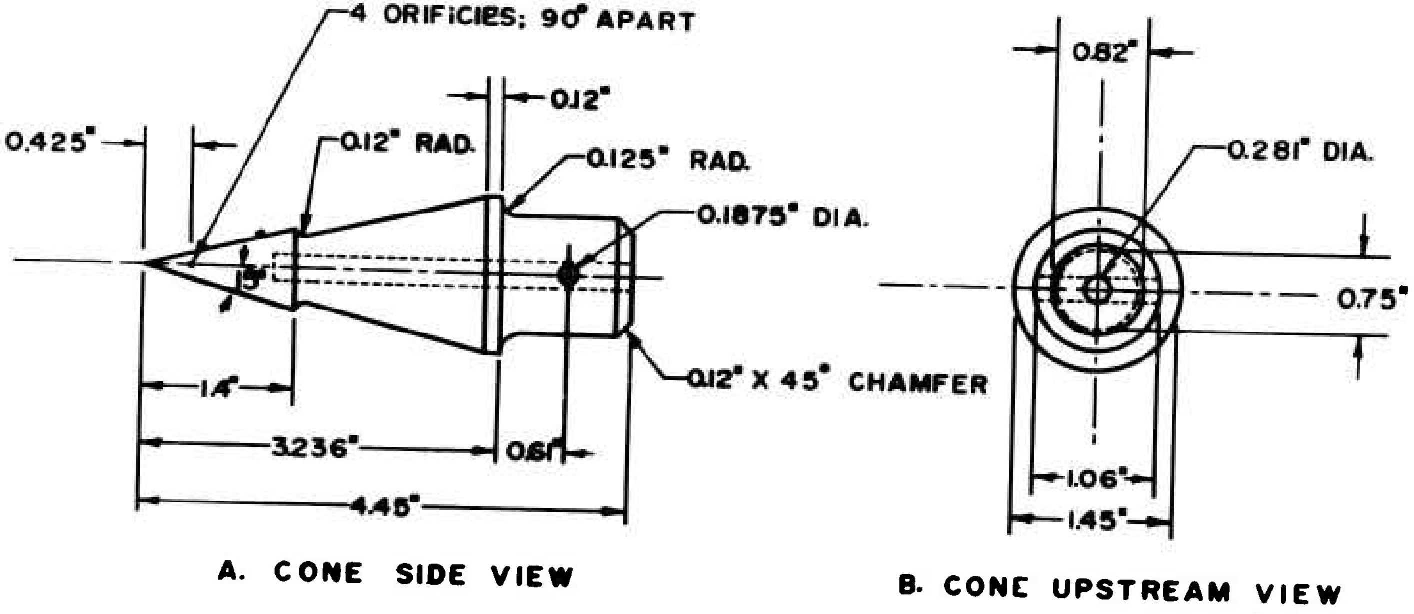

Figure 33. Scale Drawing of Flow Angularity Cone

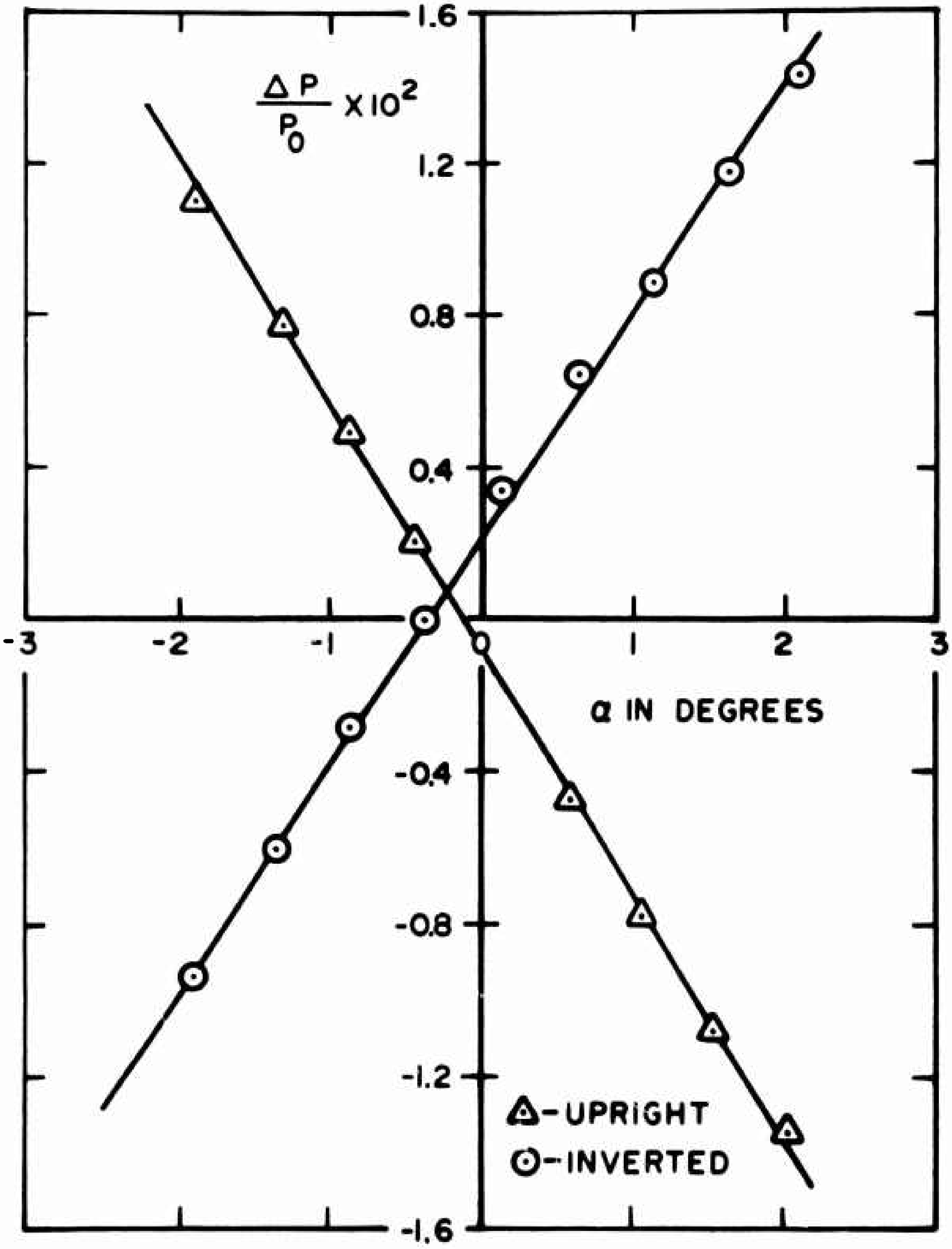

Figure 34a. Normalized Surface Pressure Difference versus Angle of Attack at xp/xr = - 0.690 for p_0 = 103.6 psia with Settling Chamber Spreader Cone Tip Downstream

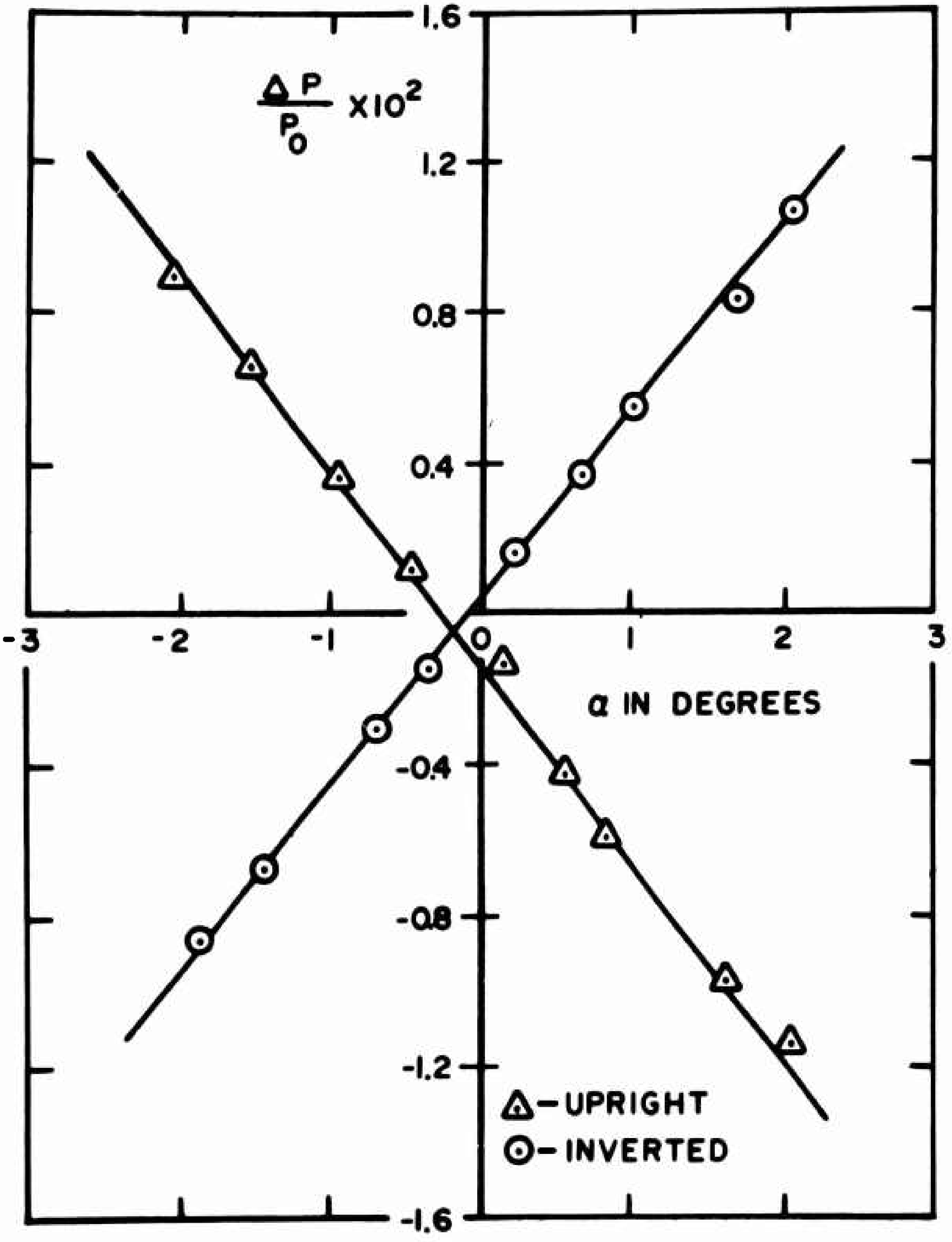

Figure 34b. Normalized Surface Pressure Difference versus Angle of Attack at xp/xr = - 0.345 for p_0 = 100.6 psia with Settling Chamber Spreader Cone Tip Downstream

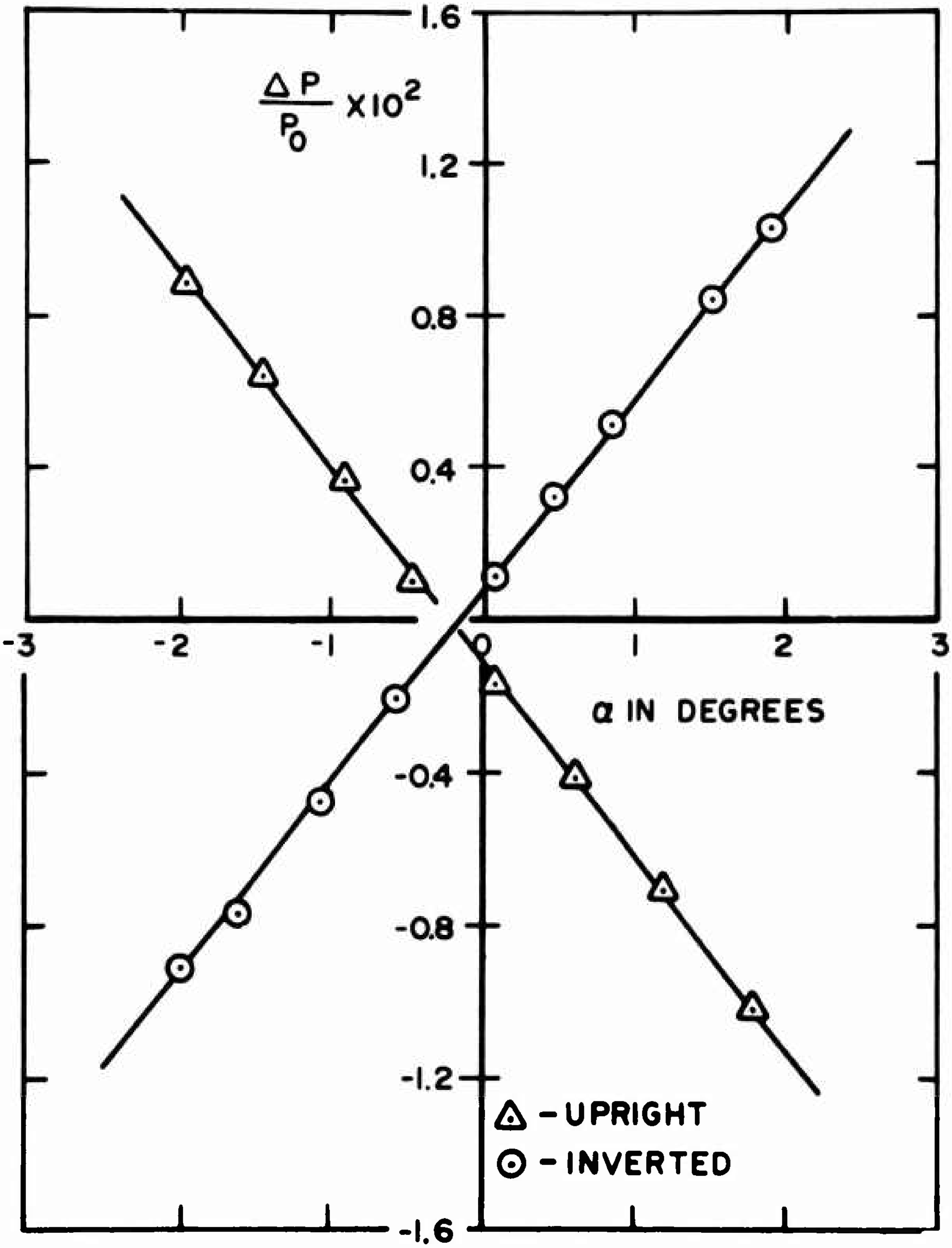

Figure 34c. Normalized Surface Pressure Difference versus Angle of Attack at xp/xr = 0 for p_0 = 100.6 psia with Settling Chamber Spreader Cone Tip Downstream

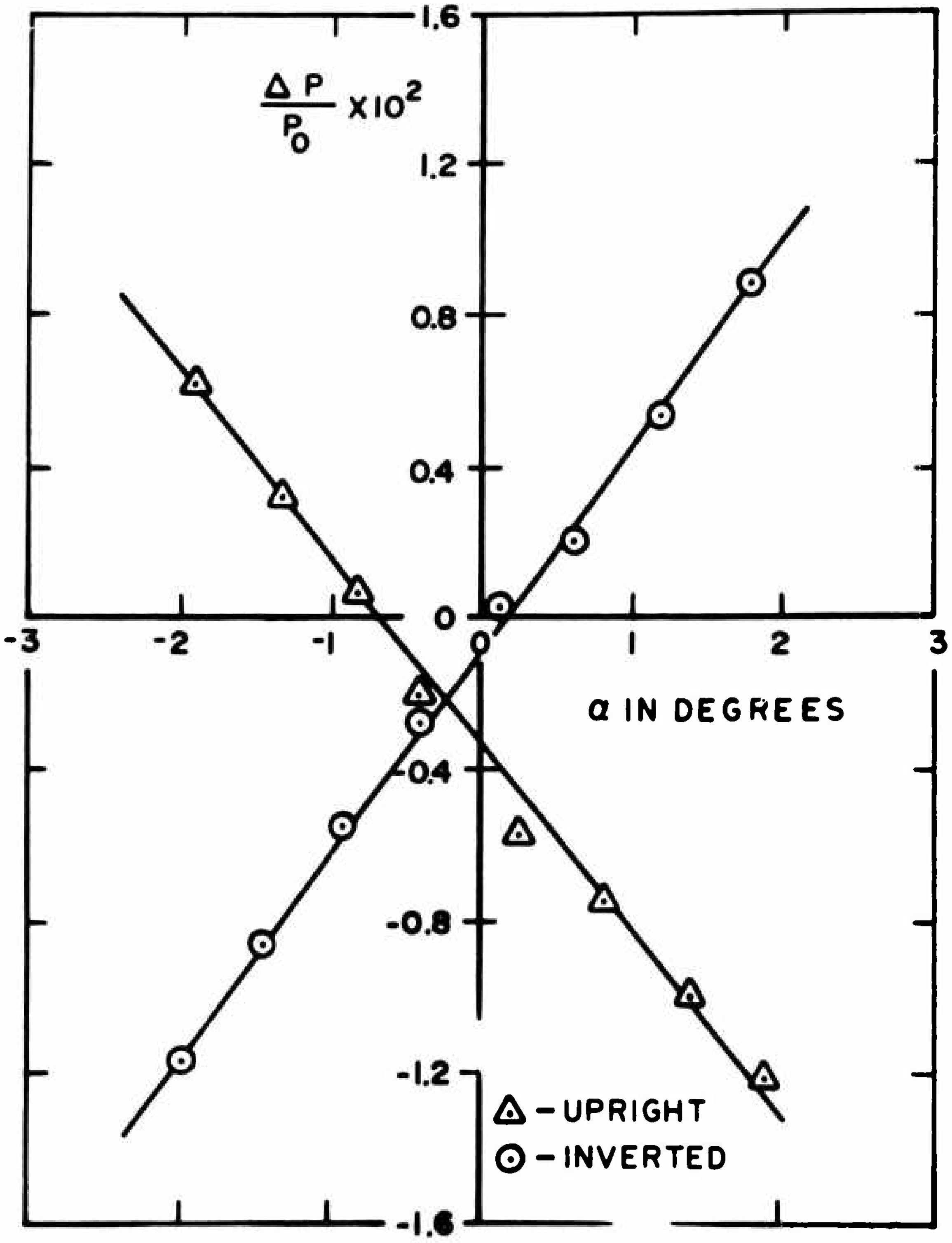

Figure 34d. Normalized Surface Pressure Difference versus Angle of Attack at xp/xr = 0.345 for p_0 = 95.0 psia with Settling Chamber Spreader Cone Tip Downstream

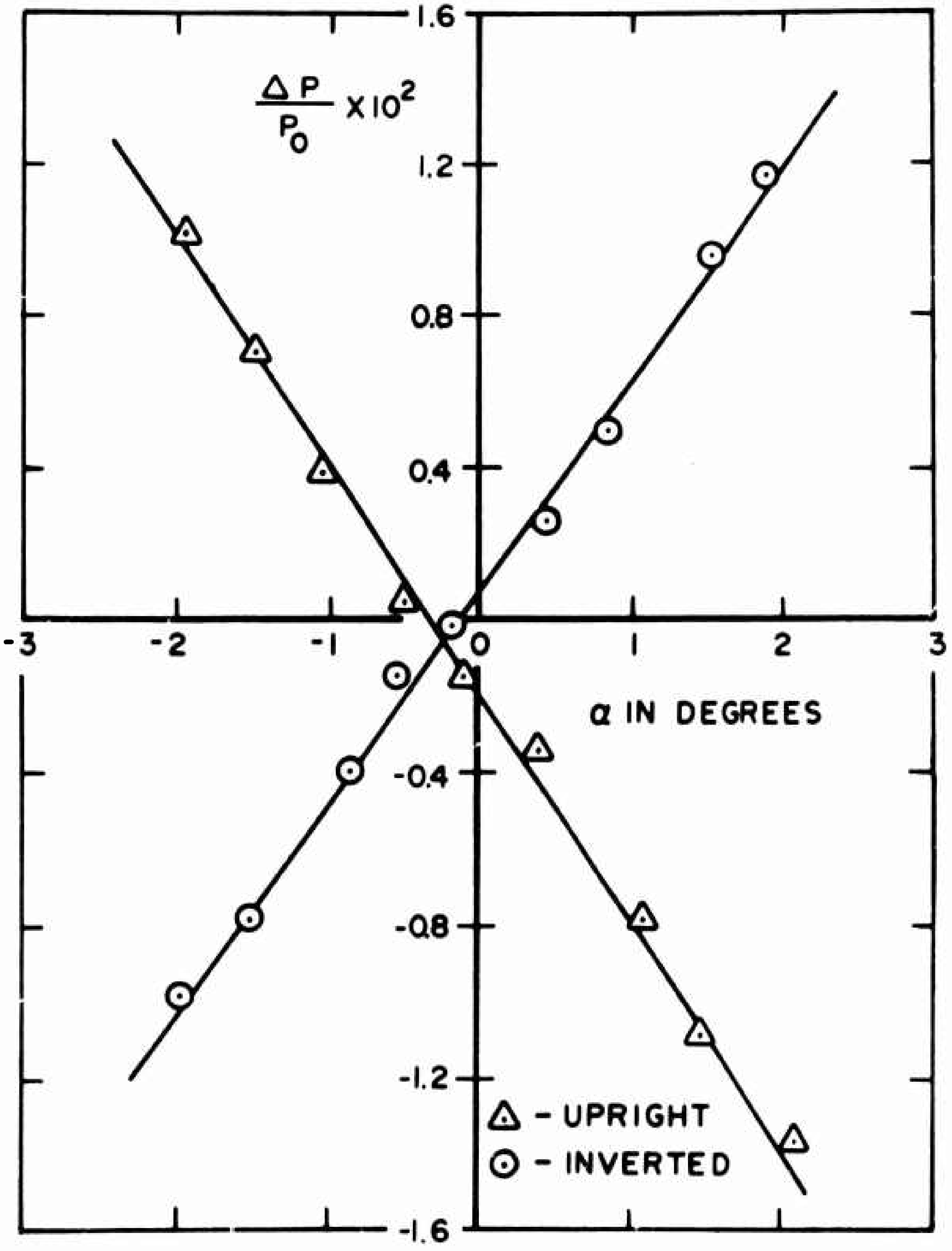

Figure 34e. Normalized Surface Pressure Difference versus Angle of Attack at xp/xr = 0.690 for p_0 = 95.4 psia with Stagnation Section Spreader Cone Tip Downstream

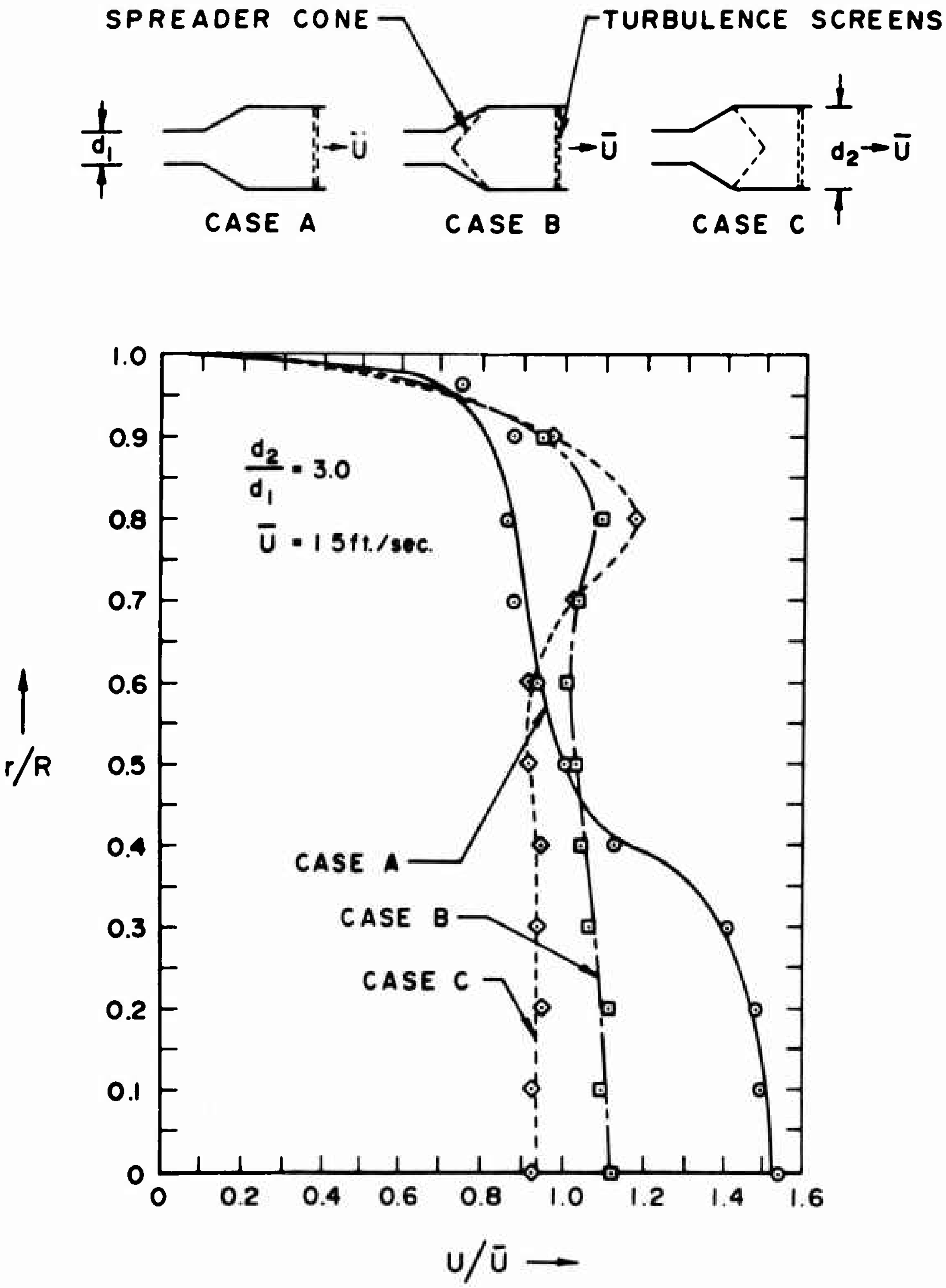

Figure 35. Velocity Profile in a Model Settling Chamber with and without a Spreader Cone

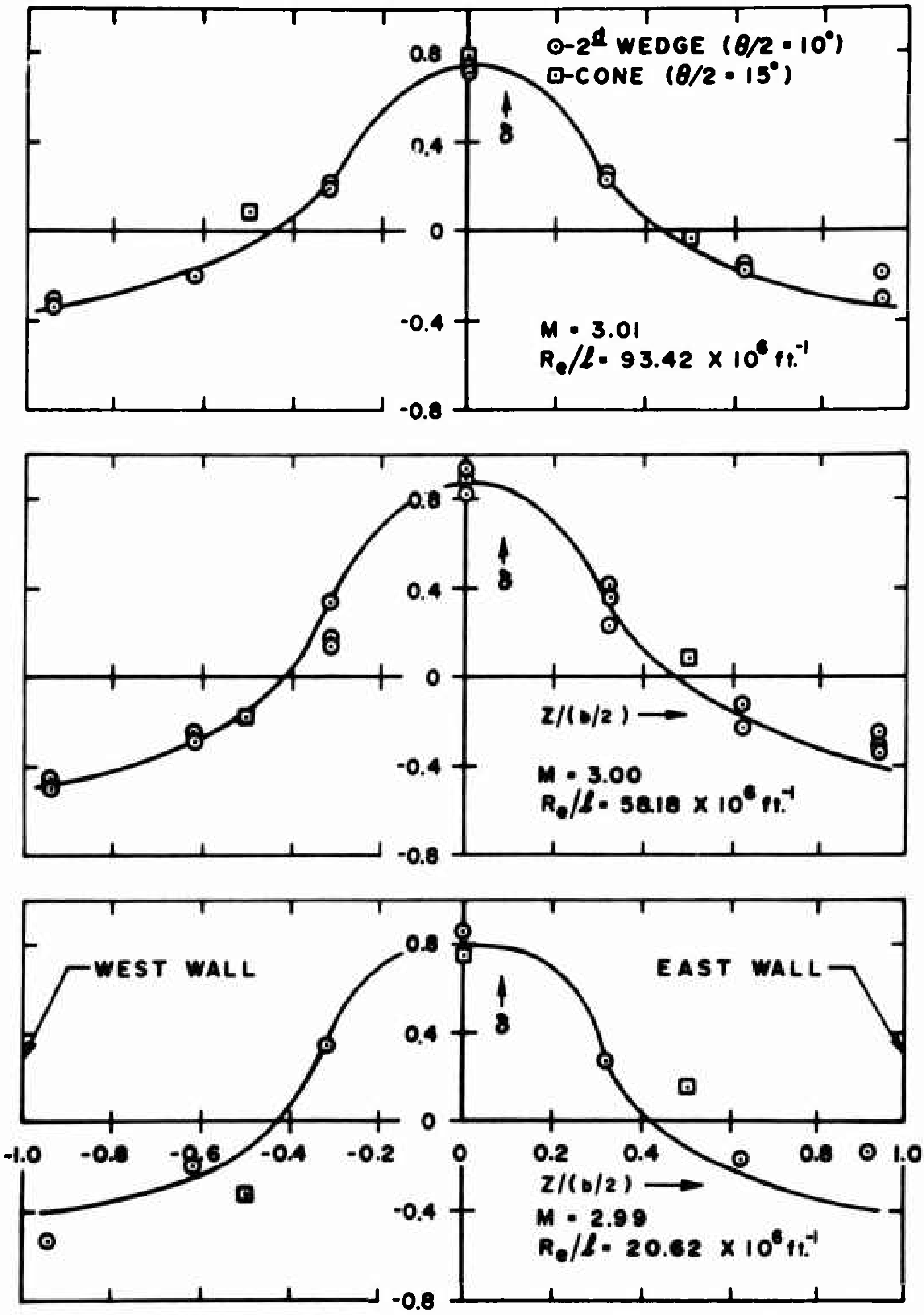

Figure 36. Flow Angularity versus Lateral Distance at xp/xr = 0 (Rhombus Center) with the Spreader Cone Tip Upstream

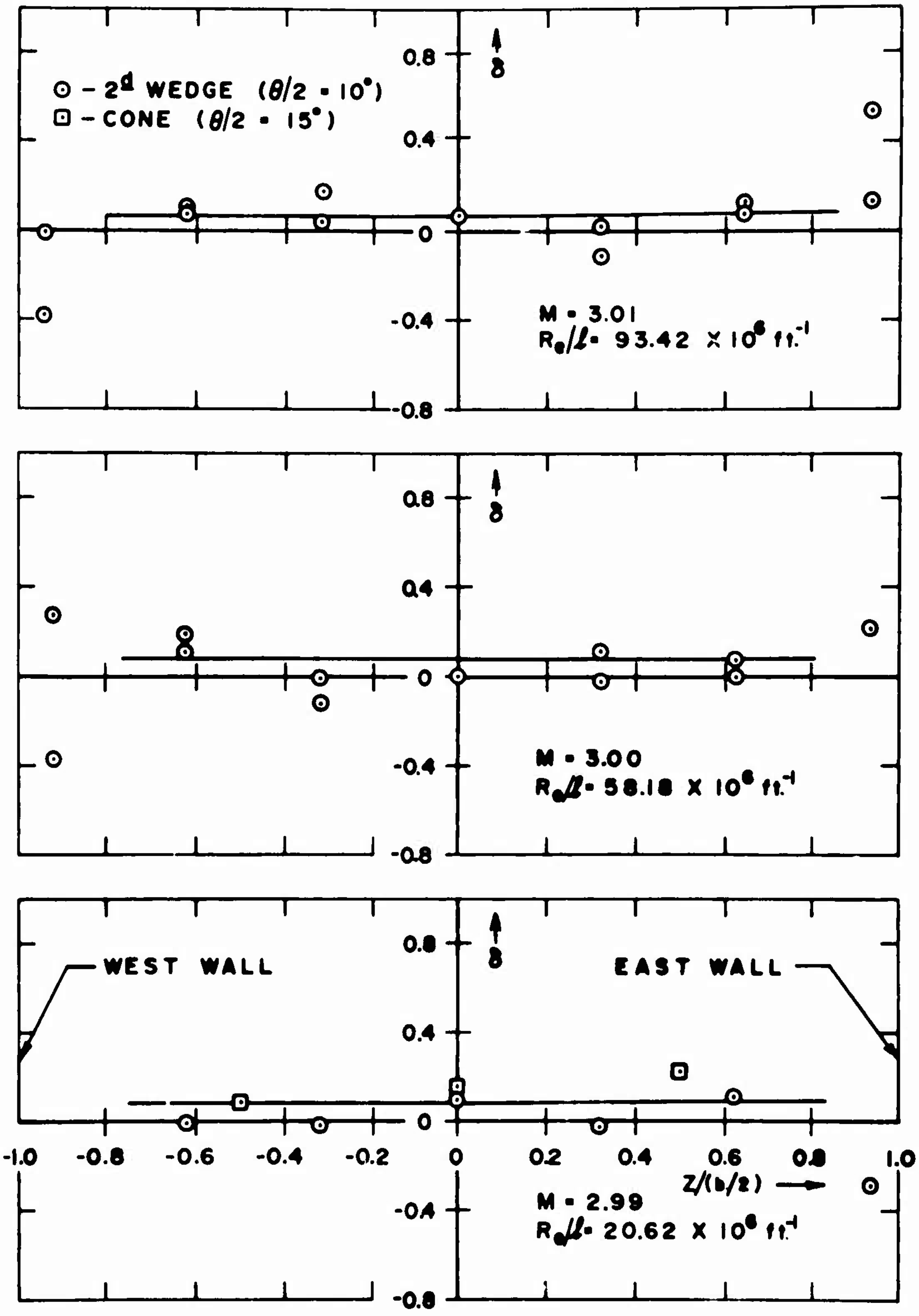

Figure 37. Flow Angularity versus Lateral Distance at xp/xr = 0 (Rhombus Center) with the Spreader Cone Tip Downstream

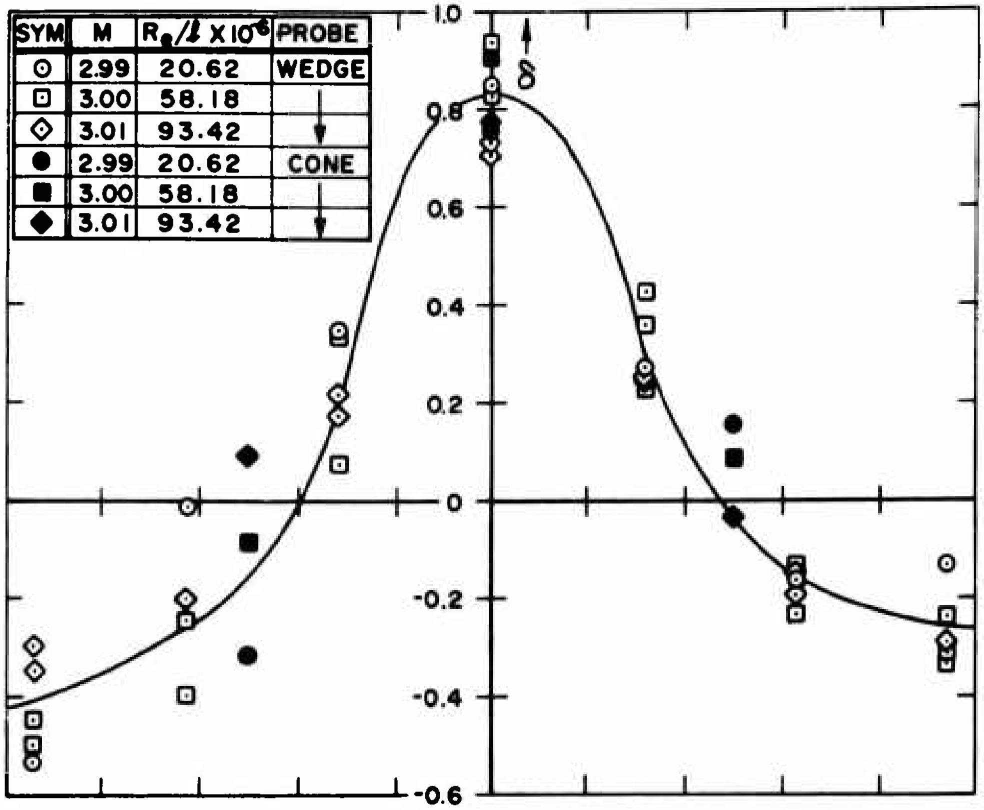

A. SPREADER CONE TIP UPSTREAM

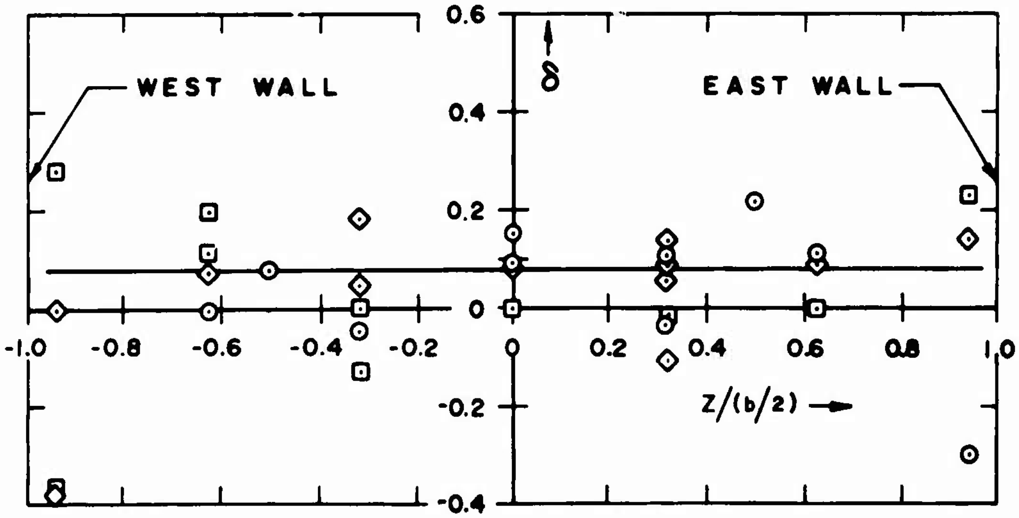

B. SPREADER CONE TIP DOWNSTREAM

Figure 38. Unit Reynolds Number Effect on the Flow Angularity at xp/xr = 0 (Rhombus Center)

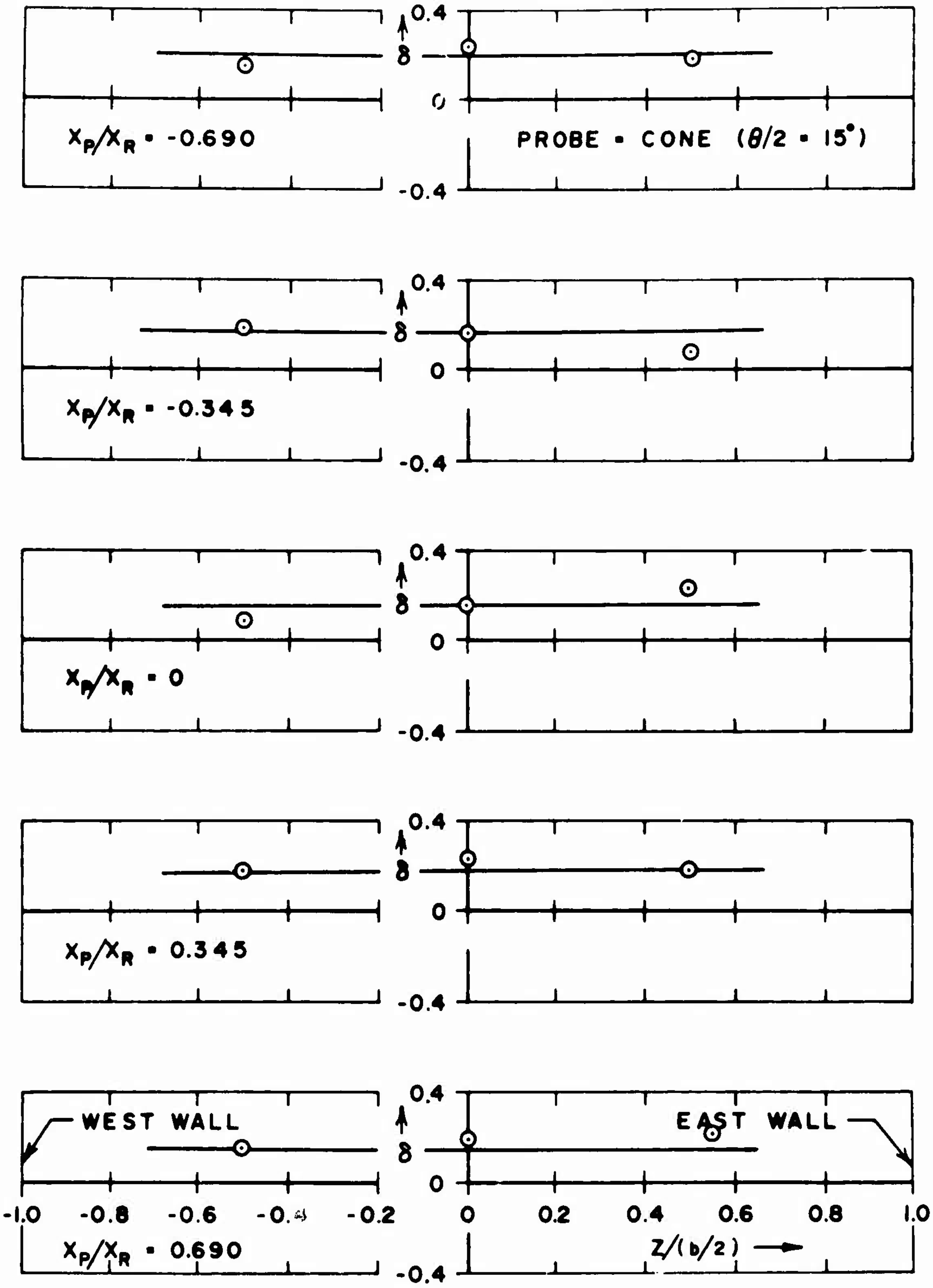

Figure 39. Flow Angularity versus Lateral Distance with Longitudinal Distance as a Parameter for p_0 = 100 psia, T_0 = 470°R, M = 2.99 and Re/ℓ = 20.6 x 10^6 per foot

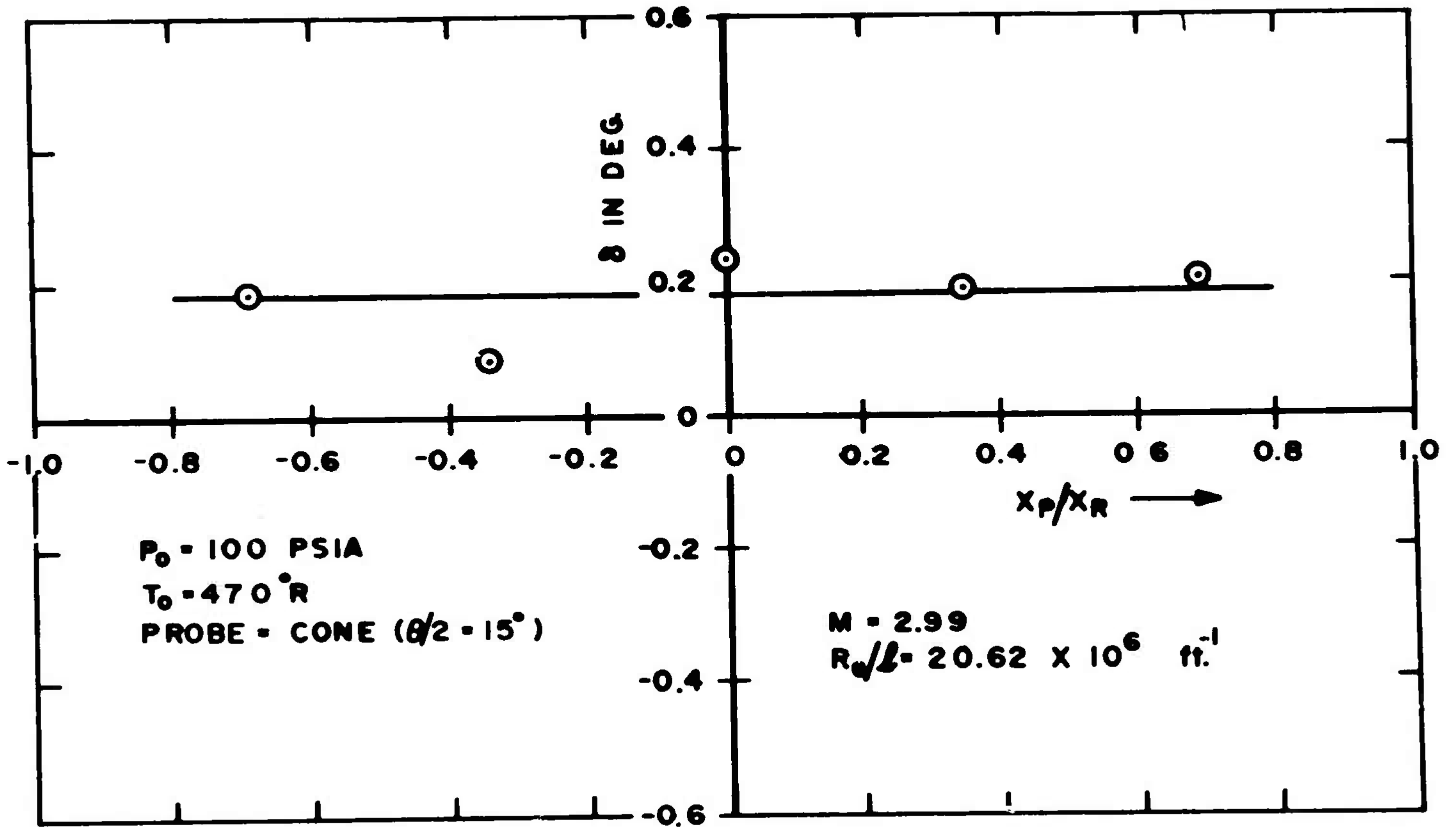

Figure 40. Flow Angularity versus Longitudinal Distance at z/(b/2) = + 0.5 (East Side) with the Spreader Cone Tip Downstream

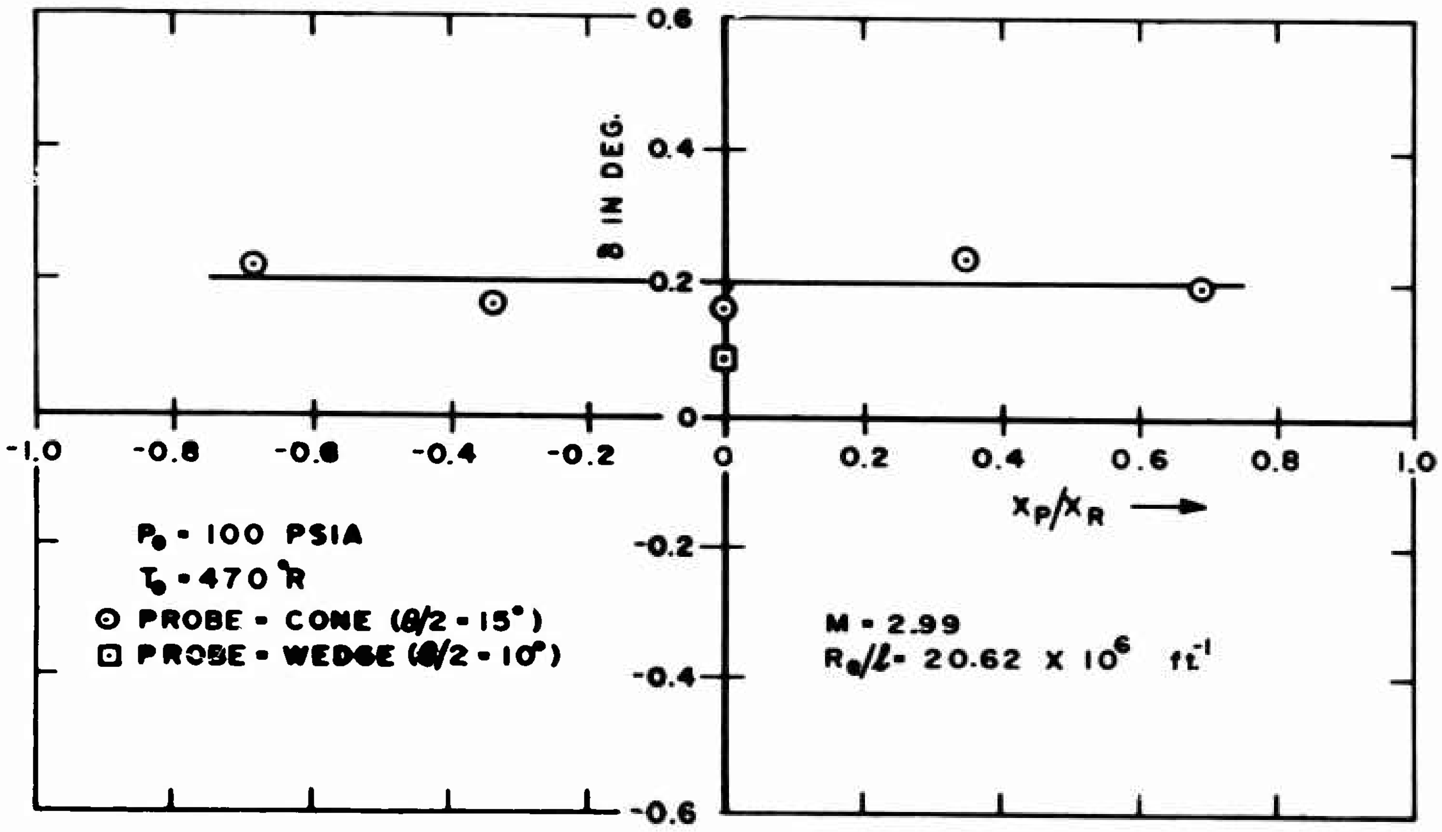

Figure 41. Flow Angularity versus Longitudinal Distance at $z/(b/2) = 0$ (Centerline) with the Spreader Cone Tip Downstream

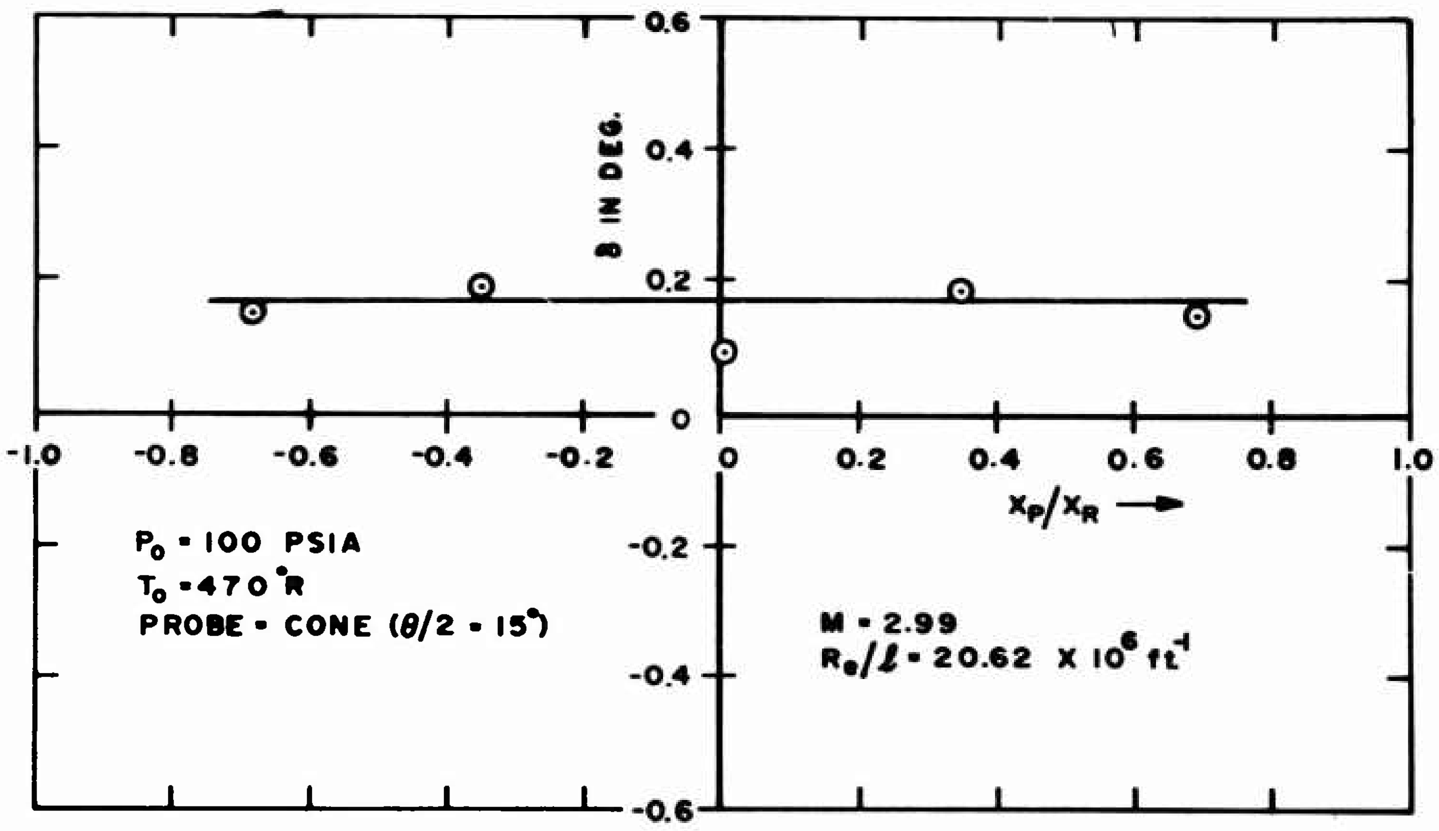

Figure 42. Flow Angularity versus Longitudinal Distance at z/(b/2) = - 0.5 (West Side) with the Spreader Cone Tip Downstream

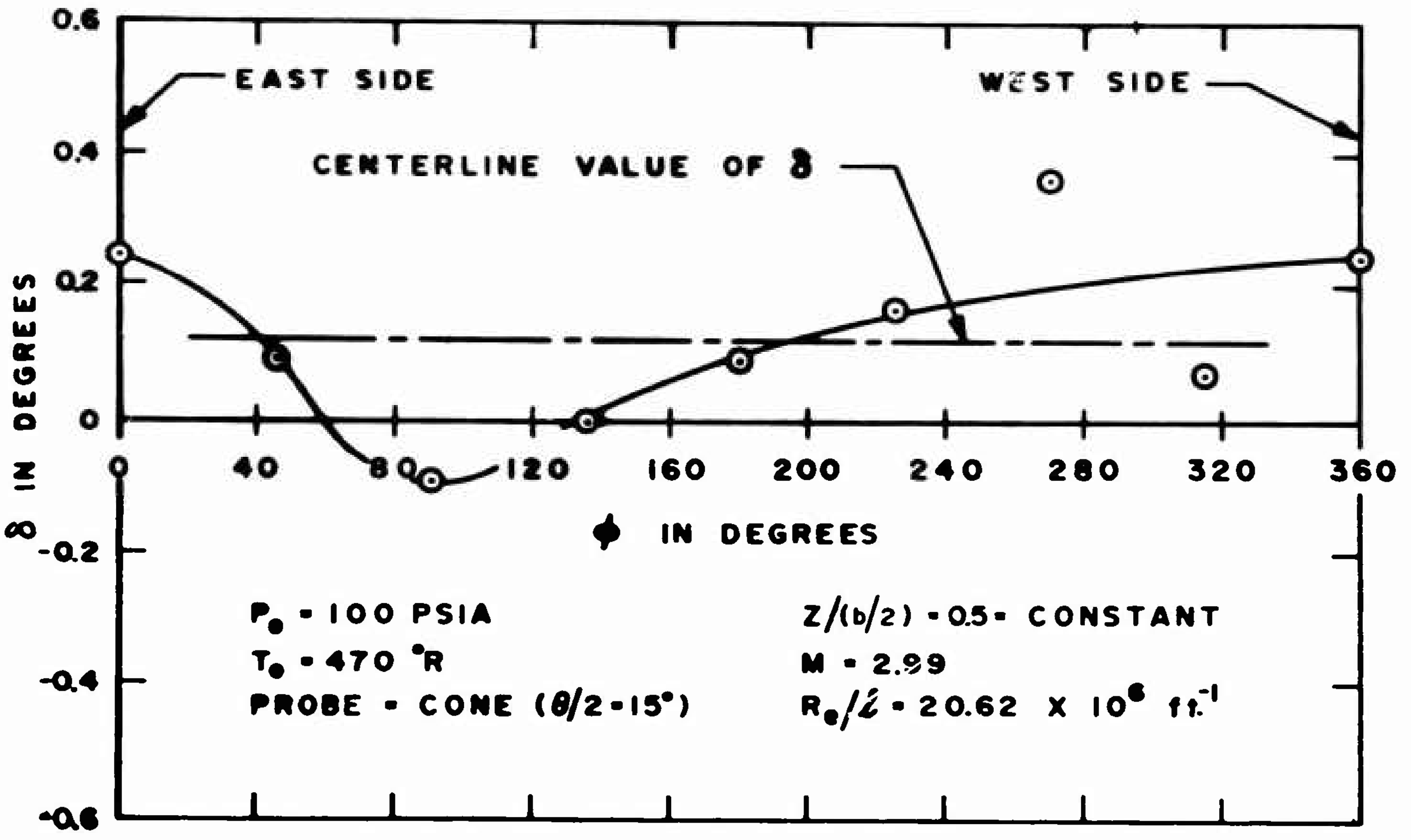

Figure 43. Flow Angularity versus Probe Roll Angle at the Center of the Test Rhombus (xp/xr = 0)

BLOCKAGE TEST RESULTS

MODEL	d	h	$\Delta A_t/A$
——	INCHES	INCHES	——
CONE	4.28	——	.2611
↓	4.53	——	.2866
	4.75	——	.3095
	5.00	——	.3358
	5.41	——	.3819
2^d WEDGE	——	1.492	.2637
↓	——	1.745	.2866
	——	2.000	.3095

$X_p/X_R = 0$ AND $A = 65.6$ IN.^{2}

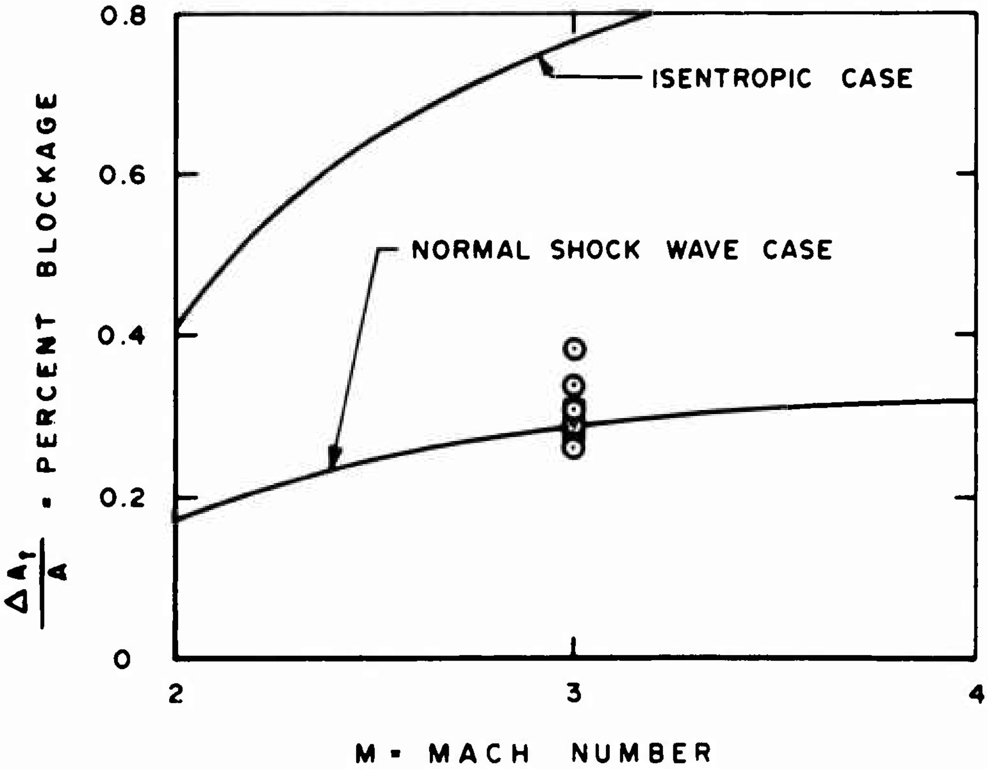

Figure 44. Tunnel Blockage versus Mach Number

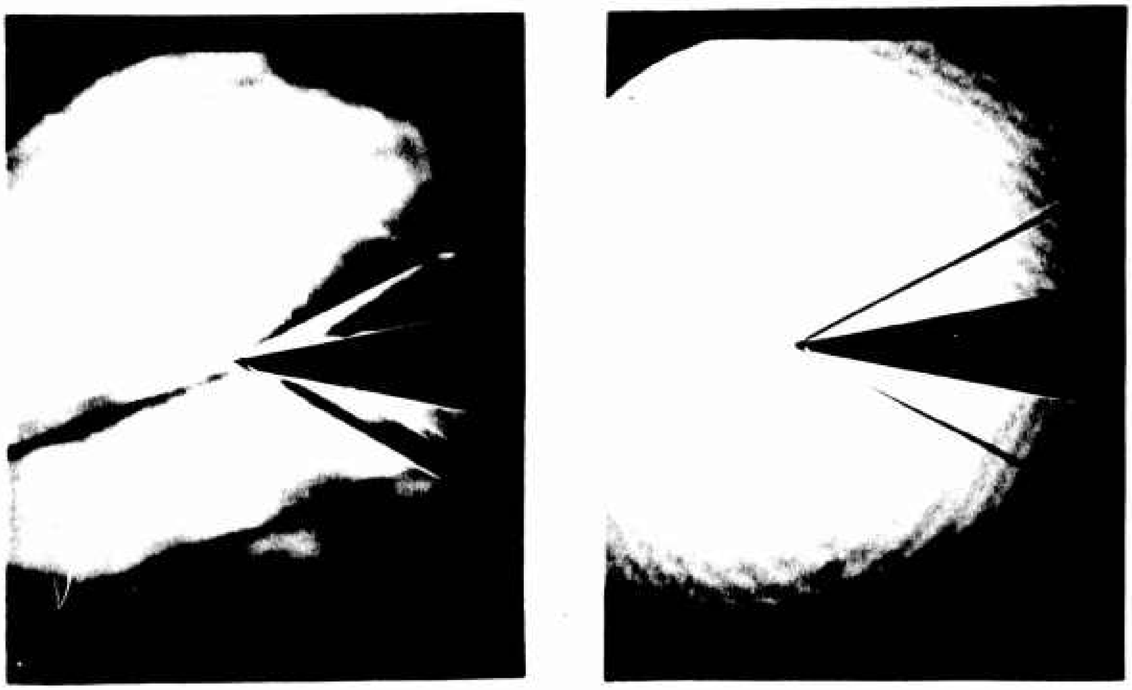

(a) SCHLIEREN AT $\alpha = 0°$ (b) SHADOWGRAPH AT $\alpha = 0°$

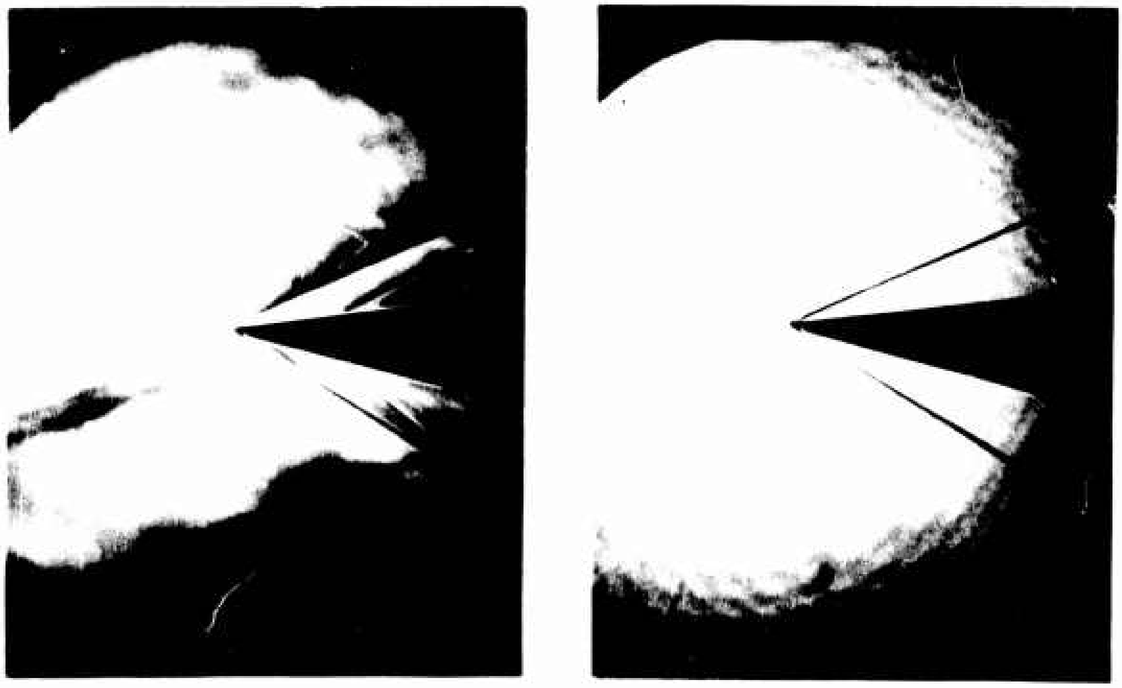

(c) SCHLIEREN AT $\alpha = +4°$ (d) SHADOWGRAPH AT $\alpha = +4°$

Figure 45. Schlieren and Shadowgraphs of Flow Over a Two-Dimensional Wedge at $M = 3.0$ and $Re/\ell = 20.66 \times 10^6$ per foot for $\alpha = 0°$ and $\alpha = 4°$

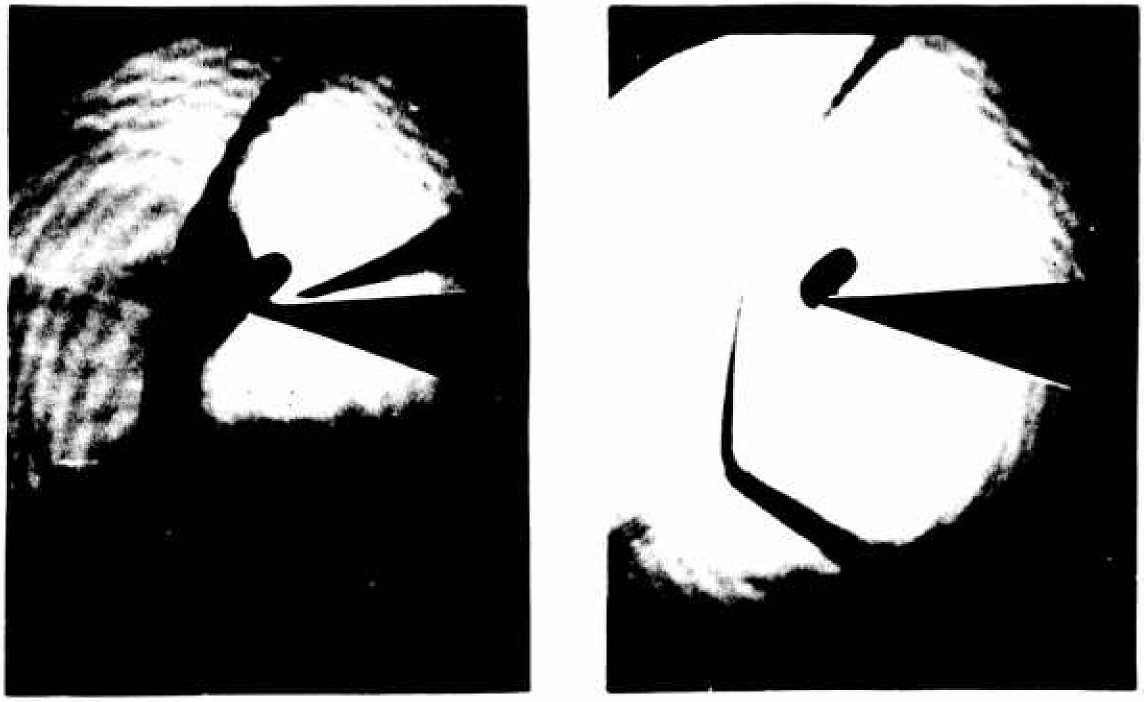

(a) SCHLIEREN AT $\alpha = +7°$ (b) SHADOWGRAPH AT $\alpha = +7°$

(c) SCHLIEREN AT $\alpha = +10°$

Figure 46. Schlieren and Shadowgraphs of Flow Over a Two-Dimensional Wedge at $M = 3.0$ and $Re/\ell =$ 20.66×10^6 per foot for $\alpha = 7°$ and $\alpha + 10°$

APPENDIX

BASIC DESIGN CONSIDERATIONS

The starting point for the design of any wind tunnel is a knowledge of the aerodynamic performance requirements which arise from the particular testing need. These requirements are usually expressed in terms of the desired test section flow conditions, model sizes, and run times. Figure A-1 is a design flow chart which illustrates how this basic input information is used, and modified when necessary, to arrive at firm design parameters which form the basis of the detailed design of the facility. The chart is not complete in the sense that there are always special conditions and constraints which significantly affect the design process. In the present case these included the size and location of the building available to house the facility, and the very common constraint of limited funds. This appendix deals with the basic design process, as distinct from the detailed design process, and discusses some of the key points.

1. INPUT DESIGN PARAMETERS

a. Test Section Mach Number

A test section Mach number of $M_\infty = 3.0$ was required with no provisions for changes in Mach number, other than by replacement of the nozzle blocks at some future time to accommodate nozzles up to Mach numbers of 4.5. There will always be some variation in test section Mach number due to changes in the nozzle wall boundary layer over the facility operating range but for basic design purposes such variations are not usually significant. At the high Reynolds numbers under consideration here this is particularly true, since the boundary layer displacement thickness is very small, and changes in it are proportionately small. The Mach number was therefore held constant at $M_\infty = 3.0$ throughout the design process.

Preceding page blank

b. Desired Model Sizes

Models on the order of one foot long were envisioned as being sufficient to accommodate the necessary instrumentation and to permit external probing with reasonably sized probes without producing severe probe disturbance effects. Probable model geometries included right-circular cones, wedges, flat plates, delta wings and corner flow models.

c. Desired Reynolds Number Range

The Reynolds number range of the tunnel was to be as large as possible, and preferably sufficient to give both laminar and turbulent flow conditions over the models. Based upon Mach 3 transition data available at the time,(18) it appeared that transition took place at Reynolds numbers from 1.5×10^6 to 2.0×10^6 for planar flow fields. Later work by Pate(19) showed that corresponding transition for conical flow fields at Mach 3 would occur at Reynolds numbers higher by a factor of 2.2 to 2.5. Figure A-2 shows how these data translate into freestream unit Reynolds number requirements for transition to occur at a certain point on a model. For example, in order to have transition on a cone completed no further than 0.5 inch from the apex, a freestream unit Reynolds number of at least 1.2×10^8 per foot would be required. It should be noted that Figure A-2 can only serve as a rough guide, such as tunnel size, tunnel freestream turbulence, model surface roughness, and tunnel wall boundary layer noise.

d. Desired Run Times

Run times of at least 60 seconds were sought to allow the possibility of detailed flow field probing of the models, and to permit the use of a pitch-pause model support system. Due to the relatively short response times associated with high Reynolds number testing, it was anticipated that many runs would average only from 20 to 30 seconds.

2. CALCULATED PARAMETERS

a. Tunnel Stagnation Conditions

(1) Stagnation Temperature, T_0

For high Reynolds number testing, where high freestream densities are sought, the test gas is usually unheated unless there is a danger of the gas liquefying upon expansion through the nozzle. At high Mach numbers the accommodation of this aspect often dominates the facility design, but at lower Mach numbers it is not a major problem. This is not to say that it can be ignored, even at a test section Mach number of 3, especially if the tunnel is to operate during winter from a high pressure gas storage system exposed to the elements. This was the case here, and since one of the ground rules for the construction of the facility was that the air supply be unheated, changes in stagnation temperature during and between test runs must be accepted, together with the resulting changes in Reynolds number. The temperature changes are brought about not only by changes in the ambient air temperature but just as significantly by the cooling which takes place in the storage tanks as the air expands polytropically during the depressurization process (a function of mass flow, run time and tank volume), and by the cooling (Joule-Thomson effect) associated with the throttling through the pressure control valve. Since the ARL high pressure air storage tanks do not contain heat storage materials, long run times may cause appreciable temperature changes as a result of the expansion of the air in the tanks, and will be most serious at the higher Reynolds numbers, where the mass flows are largest. Joule-Thomson effects will be more pronounced at the lower Reynolds numbers, due to the greater pressure drop across the pressure control valve. These cooling effects will be partially offset by the transfer of heat from the walls of the storage tanks and piping containing the air, and by the frictional heating associated with the pressure drop through the supply lines to the tunnel. In summary then, factors which influence the temperature of the air delivered to the nozzle include the ambient temperature, the initial storage pressure, the rate of depressurization of the air in the storage tanks, the stagnation pressure required for the run, the run time, and the position of the run within a sequence of runs. While such temperature changes cannot be controlled, and are difficult to estimate with any reasonable precision, they can be easily monitored by continuously recording the tunnel stagnation temperature. Figure A-3 shows the liquefaction limits for air based upon Wegener's equation(20) for static conditions, and assumes an isentropic expansion to Mach 3 from the indicated total conditions. The parameter ΔT represents possible degrees of cooling below the initial air storage temperature (T_{ST}) caused by expansion and throttling effects. The solid line curve corresponds to the case where the tunnel stagnation temperature (T_0) is equal to the initial air storage temperature, i.e., $\Delta T = 0$. The broken line curves show how the static liquefaction limits change with increasing amounts of cooling. The broken line curves are in fact displaced to the right of the solid curve by an amount on the abscissa corresponding to the indicated value of ΔT. Since preliminary estimates showed that values of ΔT up to 100°F were entirely possible, it is clear that the effect of an unheated air supply has to receive consideration before the operating pressure range can be completed. Figure A-4 shows to what extent the unit Reynolds number depends upon the tunnel stagnation temperature, and gives the percentage change in unit Reynolds number per degree Rankine change in temperature for the stagnation temperature range of interest.

(2) Stagnation Pressure, P_o

With a fixed Mach number nozzle and an unheated air supply, the freestream Reynolds number is primarily governed by changes in the tunnel stagnation pressure. From the previous consideration of desired model sizes and boundary layer conditions, freestream unit Reynolds numbers between approximately 1.5×10^6 and 1.2×10^8 per foot appeared to be necessary, with a probable stagnation temperature range of 400°R to 500°R. Figure A-5 gives the variation of freestream unit Reynolds number with stagnation pressure for these two stagnation temperatures. At a stagnation temperature of 500°R, stagnation pressures between 8 psia and 685 psia are necessary to produce the required unit Reynolds number range, whereas at a stagnation temperature of 400°R stagnation pressures between 6 psia and 485 psia are sufficient. However, to avoid condensation of air in the nozzle, operation at stagnation temperatures of 400°R would have to be limited to stagnation pressures of less than 400 psia (see Figure A-3).

b. Tunnel Pressure Ratio, λ

The probable maximum and minimum pressure ratios required to start and run a wind tunnel at various Mach numbers are shown in Figure A-6, which is based upon data given in Reference 11. For a test section Mach number of 3 it appears that a pressure ratio no greater than 5.40 is necessary to start the tunnel, and a pressure ratio as low as 2.75 may be sufficient to keep the tunnel in flow. Based upon achieving a pressure recovery equivalent to that obtained behind a normal shock at the test section Mach number, a value of $\lambda = 3.05$ would be required. In order to exhaust to standard atmospheric pressure, a stagnation pressure of 79.4 psia would be necessary to start the flow, and a stagnation pressure of 40.4 psia would be necessary to maintain the flow once established. This shows that the lower end of the full Reynolds number range previously identified cannot be achieved without a vacuum exhaust or auxiliary pumping capability.

c. Test Section Size

The test section size is primarily governed by the sizes and types of models envisioned for testing which have been previously identified. With the discussion restricted to closed test sections with square cross sections, the most important model parameters are length and thickness (or diameter), which can be conveniently coupled into a parameter called the fineness ratio which is defined as the ratio of model length to maximum model thickness or diameter; i.e., L/t_m or L/d_m. For a particular test section size, the limitations on the model size are those due to the model bow shocks being reflected from the tunnel walls back onto the model, and those due to the inability to start or maintain the flow in the test section because of excessive blockage or restriction of the flow caused by the model and the model support system. In general, models having large fineness ratios are limited by bow shock reflection considerations, whereas models having small fineness ratios are more likely to be limited by blockage considerations. Figure A-7 applies to bow shock reflection limitations and shows how the ratio of maximum model length to test section half-height, L_m/h_{TS}, varies with the fineness ratio for some common model configurations. The figure can be used to find either L_m or h_{TS} when the other is specified. The limiting case of a flat plate of infinitesimal thickness is indicated for reference purposes. Figure A-8 applies to blockage limitations and shows how the ratio of maximum model diameter to inviscid test section area, d_m/A_i, varies with test section Mach number for blunt models. The theoretical curve is based upon an analysis which equates the unblocked area with that necessary to "swallow" a normal shock during the tunnel starting process. In practice, due to the losses in total head associated with the system of model shocks, the actual flow area required is larger than the theoretical value which assumes an isentropic flow downstream of a normal shock at the test section Mach number. The experimental curve shown in Figure A-8 was taken from Reference 21, and indicates that for testing blunt bodies at Mach 3 the allowable blocked area must be reduced from the theoretical value of 28% of the inviscid test section area to 12%, at least during starting. Once the flow is established, blunt body blockage values on the order of 28% can probably be tolerated. For slender models with weaker shock systems higher blockage values should be possible (as evidenced by the calibration tests reported in Section IV). Figure A-9 presents maximum model sizes as functions of test section size for bow shock reflection limited cases, and Figure A-10 presents the same information for blockage limited cases. Vertical lines corresponding to test section sizes of 8 inches x 8 inches and 12 inches x 12 inches are indicated for reference purposes.

d. Mass Flow

The mass flow required to operate a facility at a particular Mach number is proportional to the test section density and area. It is an important parameter since it describes the demands made on the high pressure air supply system and the exhaust system, considerations which usually limit the size of a tunnel. Figure A-11 gives the mass flow rate per unit test section area as a function of the tunnel stagnation conditions. For the tunnel sizes of interest, the maximum mass flow rates are on the order of hundreds of pounds per second. For example, an inviscid test section of 8 inches x 8 inches operated at Mach 3, with a stagnation pressure of 500 psia and a stagnation temperature of $500^{\circ}R$, would require a mass flow of 180 lb/sec. A 12-inch x 12-inch test section operated under the same conditions would require 405 lb/sec. Providing and controlling such mass flows is not a simple matter, especially for run times on the order of 60 seconds, and the subject is discussed further in connection with the air supply system and the exhaust system.

e. Exhaust System

The purpose of the exhaust system is to accept the air discharging from the wind tunnel diffuser, and to safely discharge it to the atmosphere. This must be done without producing an excessive back pressure on the diffuser, which would cause the tunnel flow to break down due to an insufficient pressure ratio. Exhaust systems are usually of the atmospheric or vacuum types. An atmospheric system employs no pumping devices, and therefore limits the lowest Reynolds numbers attainable with a facility. The primary concern with an atmospheric exhaust system is to diffuse the air to a reasonably low velocity (on the order of 100 ft/sec) and to provide silencing. A vacuum exhaust system usually employs a number of staged vacuum pumps separated from the tunnel by a large vacuum tank, although this can be dispensed with if the pumps are able to accept the entire tunnel mass flow. Ejector systems are sometimes employed in place of mechanical pumps, but for the high mass flows of interest here they are not an economical proposition. Requirements for atmospheric and vacuum exhausts are discussed in more detail below.

(1) Atmospheric Exhaust

For reasons of economy and operational simplicity an atmopsheric exhaust system is desirable. Obviously this becomes more difficult to achieve with increasing test section Mach number but at Mach 3 it is a definite consideration. Referring to Figure A-6, one can see that the probable minimum tunnel pressure ratio required to maintain flow is 2.75, which gives a minimum tunnel stagnation pressure of 40.4 psia at standard atmospheric pressure. With a stagnation temperature of 500^{0}R this would produce a free-stream unit Reynolds number of 7.08 x 10^6 per foot which is higher than the minimum Reynolds number desired for laminar flow testing.

In addition to the question of Reynolds number range, another significant factor associated with a blowdown tunnel which has an atmospheric exhaust is the noise problem. Noise originates both inside the system, due to internal turbulence created by such devices as constrictions, control valves, corners, and shock waves, and outside the system due to the turbulent mixing occurring in the shear layer between the exhaust jet and bounding atmosphere. The former source of noise will cause the containing pipes and ducts to vibrate, producing noise radiation from the entire tunnel, while the latter will radiate from the discharge opening and points downstream. Once the internal flow conditions have been made as aerodynamically smooth as possible, a normal endeavor in wind tunnel design, the only way to handle internal noise is to minimize atmospheric transmission by accoustical treatment of the internal or external surfaces. However, this is not normally done, since the primary source of noise is more likely to be from the exhaust discharge. The intensity of the jet noise is largest at the discharge opening because the shear velocity is highest and gives rise to the most violent eddies which also have the highest frequencies. As the eddies are convected downstream their kinetic energy is converted to potential (pressure) energy, and they propagate as quadrupole noise sources. The eddies formed at the shear layer downstream of the discharge opening become progressively milder, larger, and of lower frequency. To minimize the jet noise it is clear that the first consideration must be to diffuse the flow as much as possible prior to discharge. In this way the energy available to the noise producing mechanism is reduced. This has the obvious advantage of minimizing the required tunnel pressure ratio, but at the same time it increases the size and expense of ducting and components. The addition of a silencer is the second consideration, and presents the necessary compromises between effectiveness and pressure drop and between size and less expense. Another factor which cannot be overlooked is the effect of weather conditions on the design, operation, and life of the system. The result of the silencer considerations is usually determined by pressure drop and cost limitations. This points toward the use of silencers of the absorption type, which employ straight-through acoustically transparent perforated annular tubes, or rectangular sandwich panels, containing noncorrosive material having a high sound absorption coefficient. Figure A-12 illustrates the size of the silencer required for conditions of interest with a silencer inlet velocity of 100 ft/sec. Since the density at the silencer inlet is essentially constant regardless of flow conditions, the size of the silencer required is directly proportional to the tunnel mass flow.

(2) Vacuum Exhaust

The only time a vacuum exhaust system is normally considered is when an atmospheric exhaust system would unacceptably restrict the operating range of the tunnel or when it is important to reduce tunnel starting loads. For the present case it was seen above that the minimum unit Reynolds number attainable with an atmospheric exhaust was 7.08×10^6 per foot, for the stated conditions, whereas numbers on the order of 1.5×10^6 per foot were previously discussed as being desirable for completely laminar conditions on a flat plate model 12 inches long. Figure A-13 shows the vacuum volume required to operate at a Reynolds number low enough to achieve this condition for 60 seconds, assuming the vessel to be completely evacuated prior to the test run. The calculations were made assuming that the pressure in the vessel at the end of 60 seconds would be equal to that necessary to cause flow breakdown at the tunnel pressure ratios indicated. For operation at the highest Reynolds numbers, a 60 second run would pressurize the vessel above atmospheric pressure if an automatic venting system were not incorporated. Clearly the size and expense of a vacuum exhaust system are directly affected by the tunnel mass flow.

The jet noise problem associated with a vacuum exhaust is less than that for an atmospheric exhaust, since the exhaust jet mixing process and shock system are confined to the vacuum vessel, although the vessel itself will transmit noise to the atmoshpere. The internally produced noise originating in the wind tunnel proper will not differ from that of the atmospheric exhaust case, except for effects caused by differences in exhaust ducting configurations.

f. Air Supply

The air supply system, which consists of air storage tanks and associated distribution piping, must be able to deliver the required quantity of air at the proper pressure and temperature for the required length of time. The system characteristics which determine whether this is possible include the air storage volume and related pressure, and the size, length and geometry of the distribution piping. The demands placed upon the system are expressed in terms of the tunnel mass flow rate, stagnation pressure, and run time. The tunnel mass flow is a key parameter, since it affects the minimum storage pressure required at the start of a run, the pressure drop through the piping, the depressurization rate during the run, and therefore the temperature of the air delivered to the tunnel. In addition to the piping pressure losses, the pressure drop across the tunnel pressure control valve and tunnel flow conditioning equipment affects the minimum storage pressure required at the start of a run. It is convenient to express these losses in terms of the tunnel stagnation pressure, since this largely determines the mass flow rate for a cold flow tunnel of given size. Control valves typically have pressure drops ranging from 10 to 100% of the controlled pressure, so that for estimating purposes a pressure drop of 0.75 p_0 would be a realistic allowance, and would probably be sufficient to accomodate the tunnel flow conditioning loss as well. Losses through the air supply piping can be roughly estimated at 0.75 p_0. More nearly exact estimates of piping losses are discussed later, but at this point it is seen that there is a requirement for the storage pressure at the end of a tunnel run to be at least 2.5 p_0. The decrease in storage pressure due to the cooling caused by the expansion of the air in the storage tank will aggravate the problem but the conservatism of the estimates should accommodate this aspect. Figure A-14 shows the storage volume required for three 60 second runs, at the indicated pressures, as a function of tunnel size. The initial storage pressure has been taken as 2200 psia, rather than the maximum system pressure of 3000 psia, since the air supply and recovery systems at ARL serve several major high pressure users. The final storage pressure has been taken as two and one half times the tunnel stagnation pressure for reasons discussed above. The strong effect of tunnel stagnation pressure on air storage requirements is readily apparent from the figure.

3. OUTPUT DESIGN PARAMETERS

The foregoing calculations were made to see how difficult it would be to meet the requirements expressed by the input design parameters. Performing these calculations determines the possible range of design parameters, but the final selection of output design parameters still depends on value judgments and personal philosophies. The output design parameters listed below resulted from numerous discussions between interested parties, and reflect a compromise between technical ideals concerning tunnel size and performance and practical considerations of cost and operability. Supporting arguments for the final choices are given where appropriate.

a. Test Section Mach Number

As indicated previously, the test section Mach number was held constant at $M_\infty = 3.0$ throughout the design process.

b. Test Section Size

It is quite simple to show that for mass flow conservation the maximum Reynolds number based on model length is obtained with the smallest practical model size and the largest practical stagnation pressure. Since the model size is proportional to the test section size, mass flow consideration dictate the use of the smallest practical tunnel. Mass flow has a direct bearing on operating costs, and upon the initial investment required when an adequate air supply does not already exist. Apart from air supply cost considerations, the cost of the tunnel itself is roughly proportional to the test section area, so that there are strong incentives to build a small tunnel. Quite early in the preliminary design process it was established that the smallest acceptable test section size would be 8 x 8 inches, based upon model instrumentation requirements. However, since the attainment of a certain model Reynolds number depends on the available pressure, as well as tunnel size, it is clear that test section size is a parameter which should be varied in the study. In the case of an infinitely large air storage volume, it is obvious that the maximum model Reynolds number would rise in direct proportion to tunnel size, since the maximum supply pressure would be independent of consumption. However, in the case of a finite storage volume there is an optimum size tunnel which will yield maximum model Reynolds numbers. Figure A-15 presents the results of calculating maximum attainable model Reynolds numbers, for a range of test section sizes, based on the maximum stagnation pressures possible with an air supply volume of 8,250 ft^3 (Figure A-14). It is interesting to note that the model Reynolds number is an optimum for a 10 x 10 inch tunnel, although it is only 3.6% higher than that obtainable with an 8 x 8 inch tunnel. Since the mass flow for the 10 x 10 inch tunnel would be 29.6% higher and the test section area would be 56% larger, both significant cost factors, it was decided to design the tunnel on the basis of an 8 x 8 inch inviscid test section size. For comparison purposes Tables A.I and A.II show the testing capabilities of an 8 x 8 inch tunnel and a 10 x 10 inch tunnel. The tabulated information is based upon Figures A-1, A-9, A-10, and A-15. Although the information relates only to zero incidence testing, it does illustrate that an 8 x 8 inch tunnel should be quite capable of testing a wide variety of models under well developed turbulent flow conditions, and to a lesser extent under laminar flow conditions.

c. Stagnation Temperature

Since the tunnel was not to include a heater for the supply air, the stagnation temperature depends upon the ambient temperature and process conditions. Ambient temperature at the facility site (Wright-Patterson AFB, Ohio) ranges from a minimum -20°F to a maximum of 100°F. Process conditions could cause the stagnation temperature of the air to be as much as 100°F below ambient, so that the stagnation temperature range could extend from 340°R to

560^0R. However, practical considerations of air condensation effects, and low temperature limitations associated with ASME coded pressure vessels, require that operation at the lower temperature be subject to certain restrictions. Further details on the ASME code limitations will be given later.

d. Stagnation Pressure

The maximum stagnation pressure for design purposes was chosen to be 570 psia. This corresponds to a design point unit Reynolds number of one hundred million (10^8) per foot at a stagnation temperature of 500^0R, and is consistent with the maximum pressure deduced from air storage volume considerations summarized in Figure A-14. The minimum stagnation pressure possible is basically a function of tunnel pressure ratio requirements and exhaust conditions. For atmospheric exhaust conditions Figure A-6 suggests a minimum running pressure of approximately 40 psia, although pressures on the order of 80 psia may be required for flow initiation. For vacuum operation, with an available volume of 100,000 ft^3, Figure A-13 illustrates that there should be no problem in achieving Reynolds numbers as low as one million (10^6) per foot. The limiting factor for low pressure operation with a vacuum exhaust can be expected to be the stability of the pressure control system.

e. Run Time

The original design goal of maximum run times on the order of 60 seconds is quite feasible. Factors which will influence the actual run times employed will include the time required for flow establishment, the time required for temperature stabilization (if important), instrument response times, model temperature stability (if important), flow visualization requirements (if appropriate), and air consumption.

f. Exhaust System

The decision was made to construct the facility with a vacuum exhaust capability while allowing for atmospheric blowdown operation as well. While a wide Reynolds number range was desired, the principle motivation for having a vacuum exhaust capability was exhaust noise attenuation. Due to the unusually high flow densities and flow rates, there was considerable concern about the effectiveness of low pressure drop silencers. As an interim measure it was therefore agreed to exhaust the tunnel into the 100,000 ft^3 vacuum sphere, and to reconsider this decision after gaining some operational experience of noise and vibration problems. As discussed in Section II of this report this did become necessary.

g. Performance Envelope

The output parameters discussed above are conveniently summarized graphically in Figure A-16. The various zones indicated on the figure are defined as follows:

Zone A - Operation with atmospheric exhaust and tunnel stagnation temperature within normal ambient range. No special restrictions.

Zone B - Operation with vacuum exhaust and tunnel stagnation temperature within normal ambient range. No special restrictions.

Zone C - Operation with atmospheric exhaust and tunnel stagnation temperature below normal ambient range due to air supply polytropic expansion and throttling effects. Special consideration necessary to insure that tunnel wall temperature does not fall below 440^{0}R (-20^{0}F).

Zone C^1 - That portion of Zone C in which air condensation effects are possible. Operation in this zone not desired.

Zone D - Operation with vacuum exhaust and tunnel stagnation temperature below normal ambient range due to air supply polytropic expansion and throttling effects. Special consideration necessary to insure that tunnel wall temperature does not fall below 440^{o}R (-20^{o}F).

TABLE A.I

TURBULENT FLOW TESTING CAPABILITIES

$M_\infty = 3.0$ $\alpha = 0^o$ $T_o = 500^oR$	8" x 8"			10" x 10"		
	$(Re/\ell)_{max} = 9.74 \times 10^7/ft$			$(Re/\ell)_{max} = 8.07 \times 10^7/ft$		
$(Re/\ell)_{max}$ based upon max pressure available based on Fig. A-15	B. L. Transition Length ins.	Max Model Length $\alpha = 0^o$ ins.	Max Turb. B.L. Length ins.	B. L. Transition Length ins.	Max Model Length $\alpha = 0^o$ ins.	Max Turb. B.L. Length ins.
Reference	From Fig. A-2	Figs. A-9 & A-10	---	Fig. A-2	Figs. A-9 & A-10	---
Thin Flat Plate	.25	22.6	22.3	.30	28.3	28.0
5^o Cone	.62	16.4	15.8	.75	20.6	19.8
10^o Cone	.62	12.9	12.3	.75	16.0	15.2
20^o Cone	.62	8.6	8.0	.75	10.7	9.9
30^o Cone	.62	6.0	5.4	.75	7.6	6.8
5^o Wedge	.25	12.9	12.6	.30	16.0	15.7
10^o Wedge	.25	6.4	6.1	.30	8.0	7.7
20^o Wedge	.25	3.2	2.9	.30	3.9	3.6
30^o Wedge	.25	2.1	1.8	.30	2.6	2.3

TABLE A.II

LAMINAR FLOW TESTING CAPABILITIES WITH AN ATMOSPHERIC EXHAUST

$M_\infty = 3.0$ $\alpha = 0^0$ $T_o = 500^0R$ $(Re/\ell)_{min}$ based upon min^n - pressure required to sustain flow with atmospheric exhaust	8" x 8"			10" x 10"		
	$(Re/\ell)_{min} = 7.08 \times 10^6/ft$			$(Re/\ell)_{min} = 7.08 \times 10^6/ft$		
	Length of Laminar B. L. ins.	Max Length of Model $\alpha = 0$ ins.	Max Length of Non-Lam B.L. ins.	Length of Laminar B. L. ins.	Max Length of Model $\alpha = 0$ ins.	Max Length of Non-Lam B.L. ins.
Reference	Fig. A-2	Figs. A-9 & A-10	---	Fig. A-2	Figs. A-9 & A-10	---
Thin Flat Plate	2.6	22.6	20.0	2.6	28.3	25.7
5^0 Cone	6.3	16.4	10.1	6.3	20.6	14.3
10^0 Cone	6.3	12.9	6.6	6.3	16.0	9.7
20^0 Cone	6.3	8.6	2.3	6.3	10.7	4.4
30^0 Cone	6.3	6.0	0	6.3	7.6	1.3
5^0 Wedge	2.6	12.9	10.3	2.6	16.0	13.4
10^0 Wedge	2.6	6.4	3.8	2.6	8.0	5.4
20^0 Wedge	2.6	3.2	0.6	2.6	3.9	1.3
30^0 Wedge	2.6	2.1	0	2.6	2.6	0

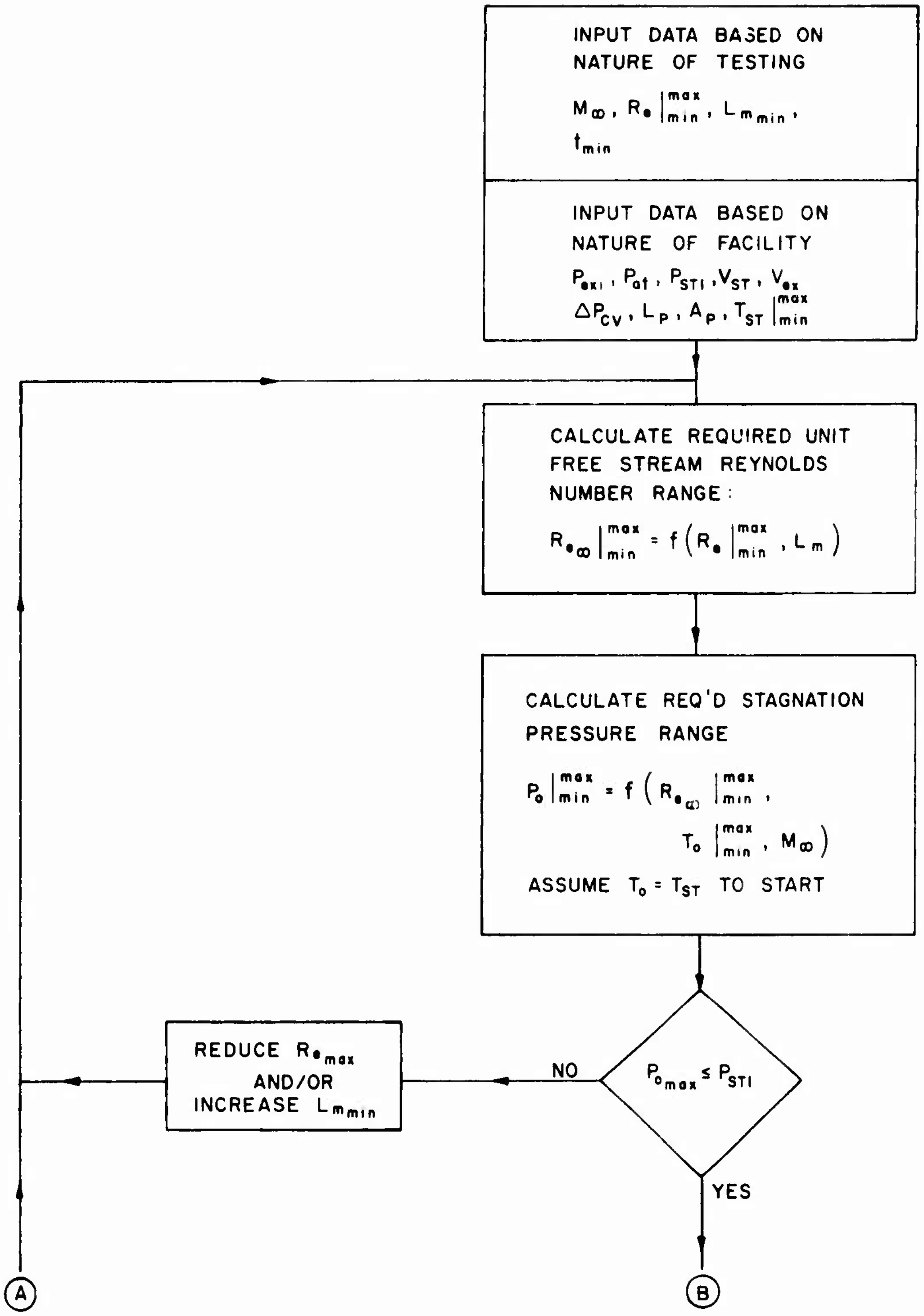

Figure A-1. Design Flow Chart

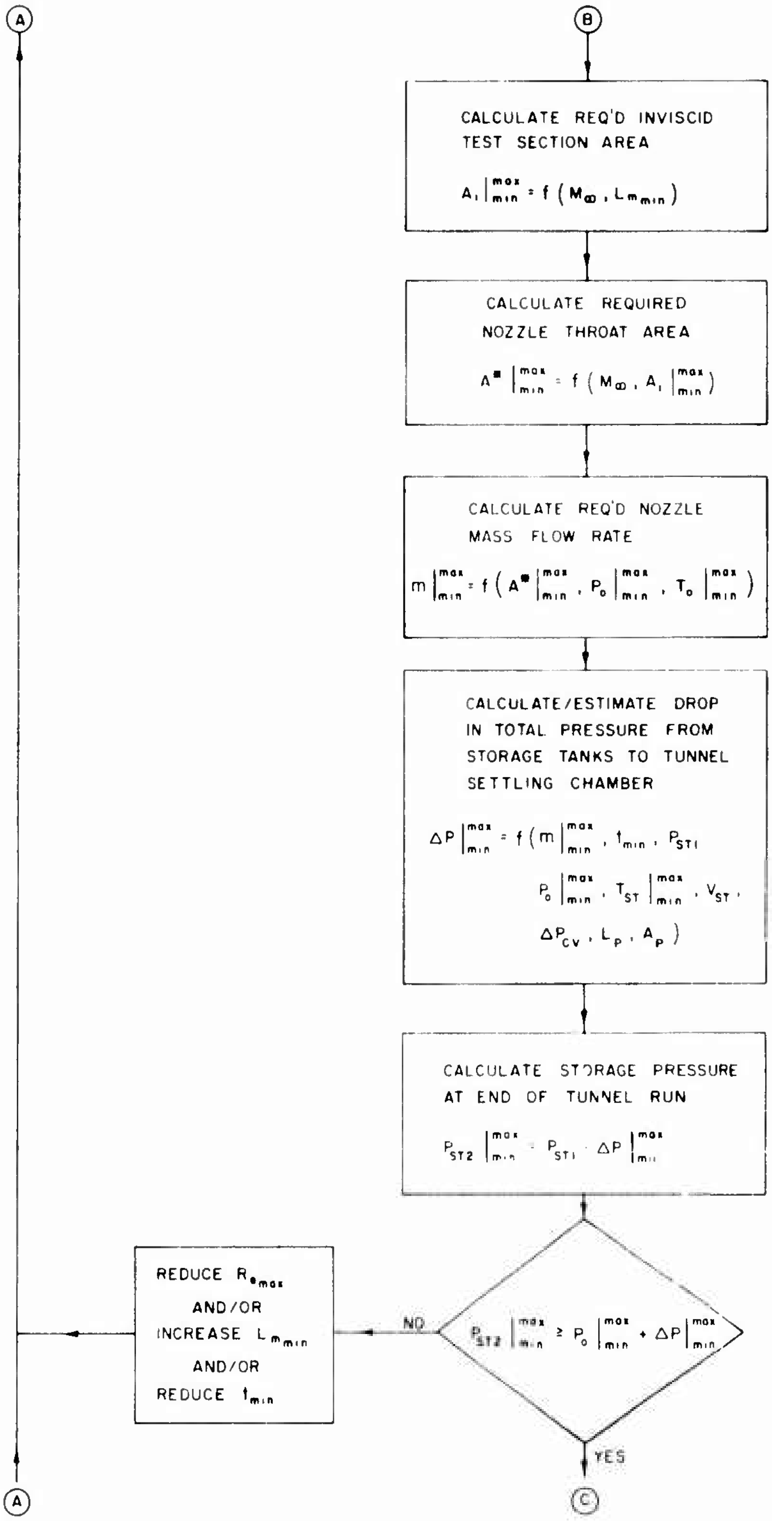

Figure A-1. Continued

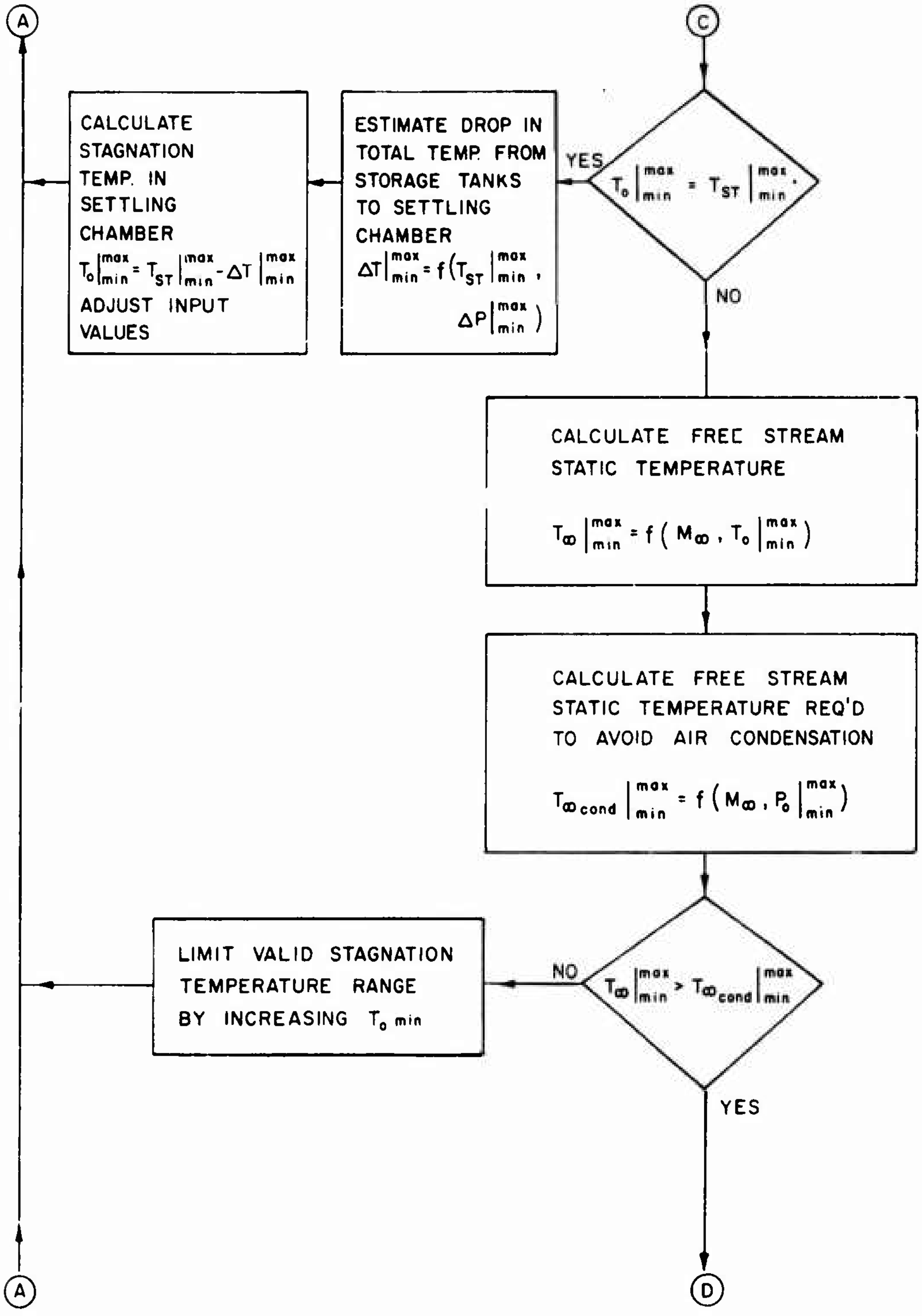

Figure A-1. Continued

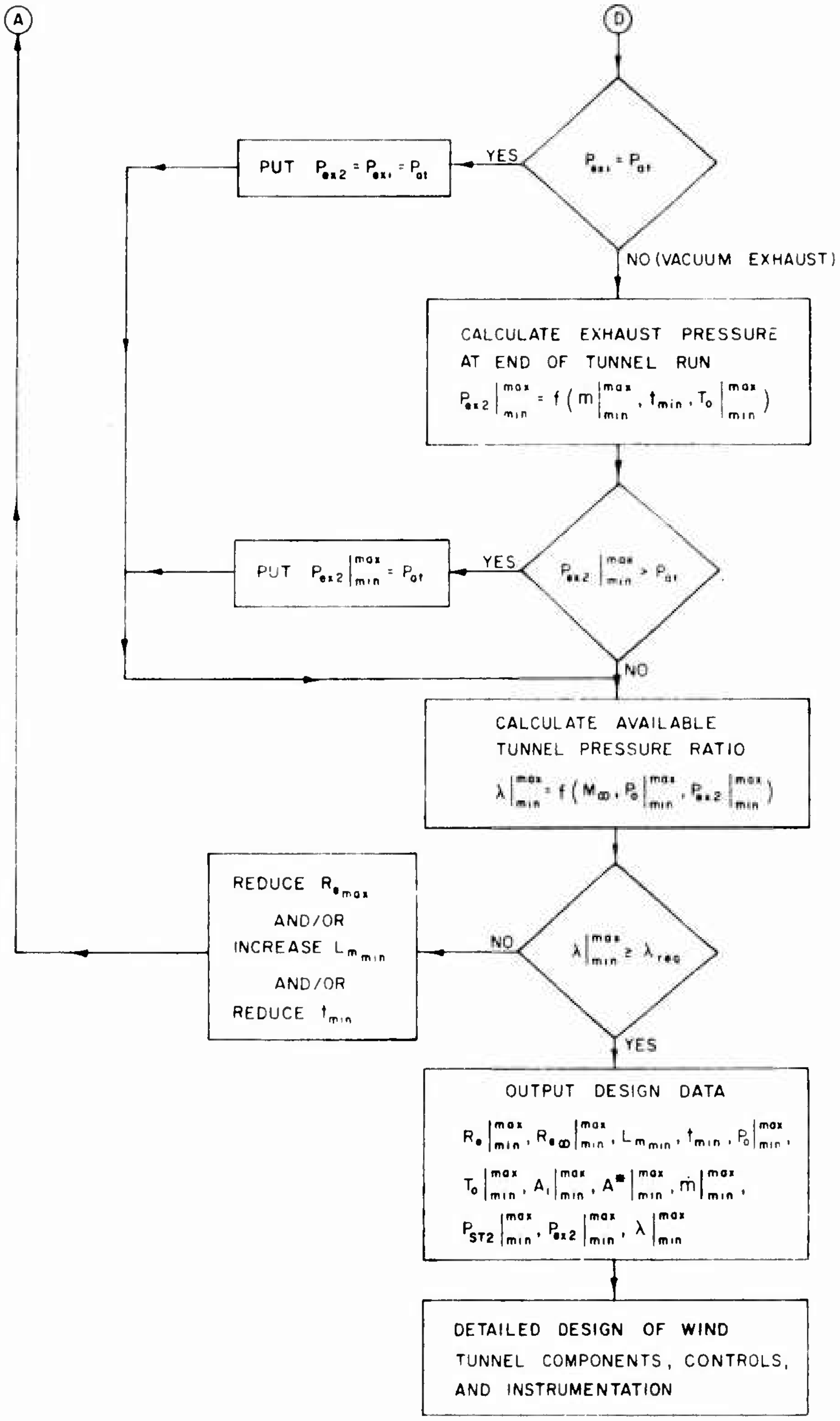

Figure A-1. Concluded

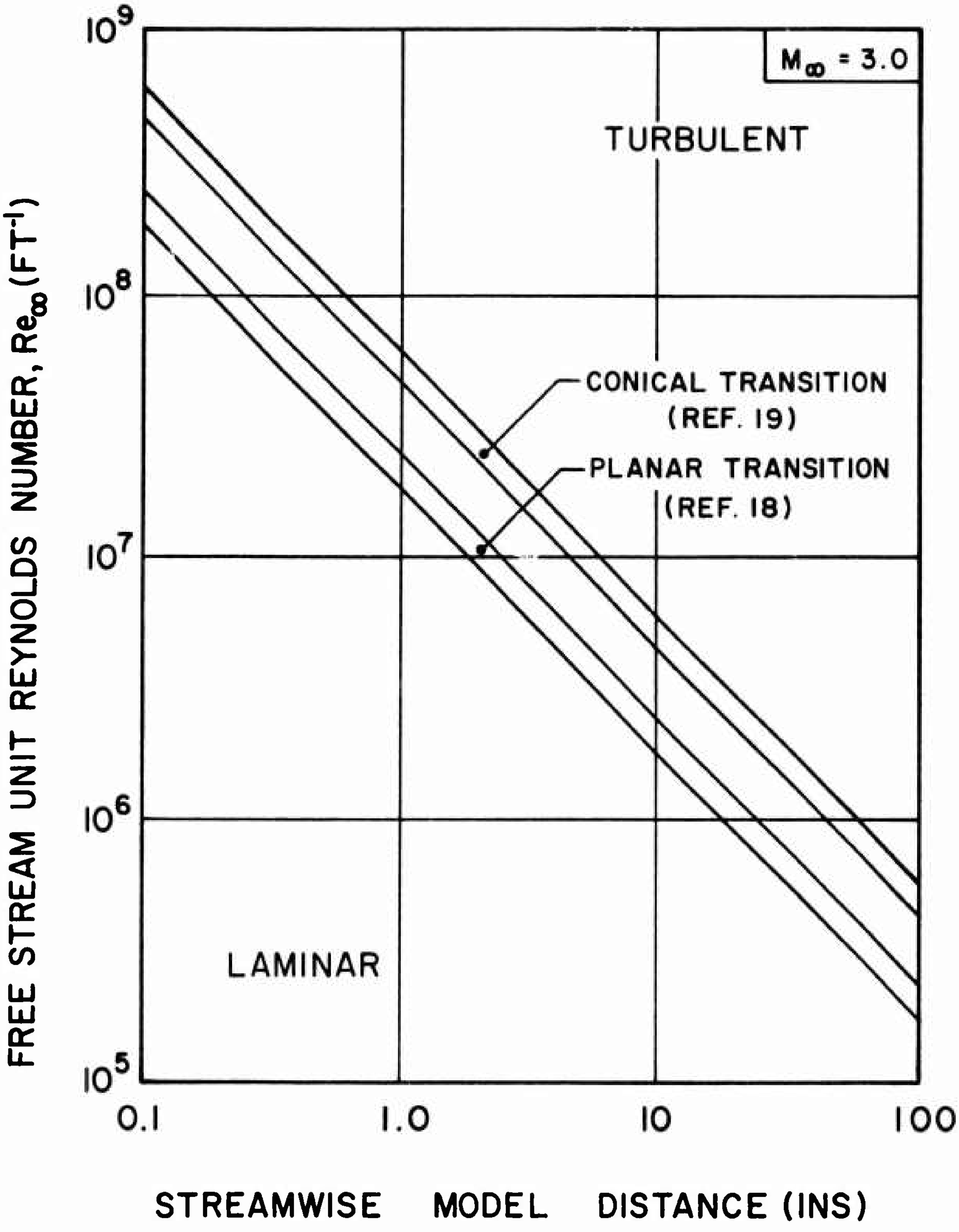

Figure A-2. Streamwise Location of Transition on a Model at Mach 3 as a Function of Free Stream Unit Reynolds Number

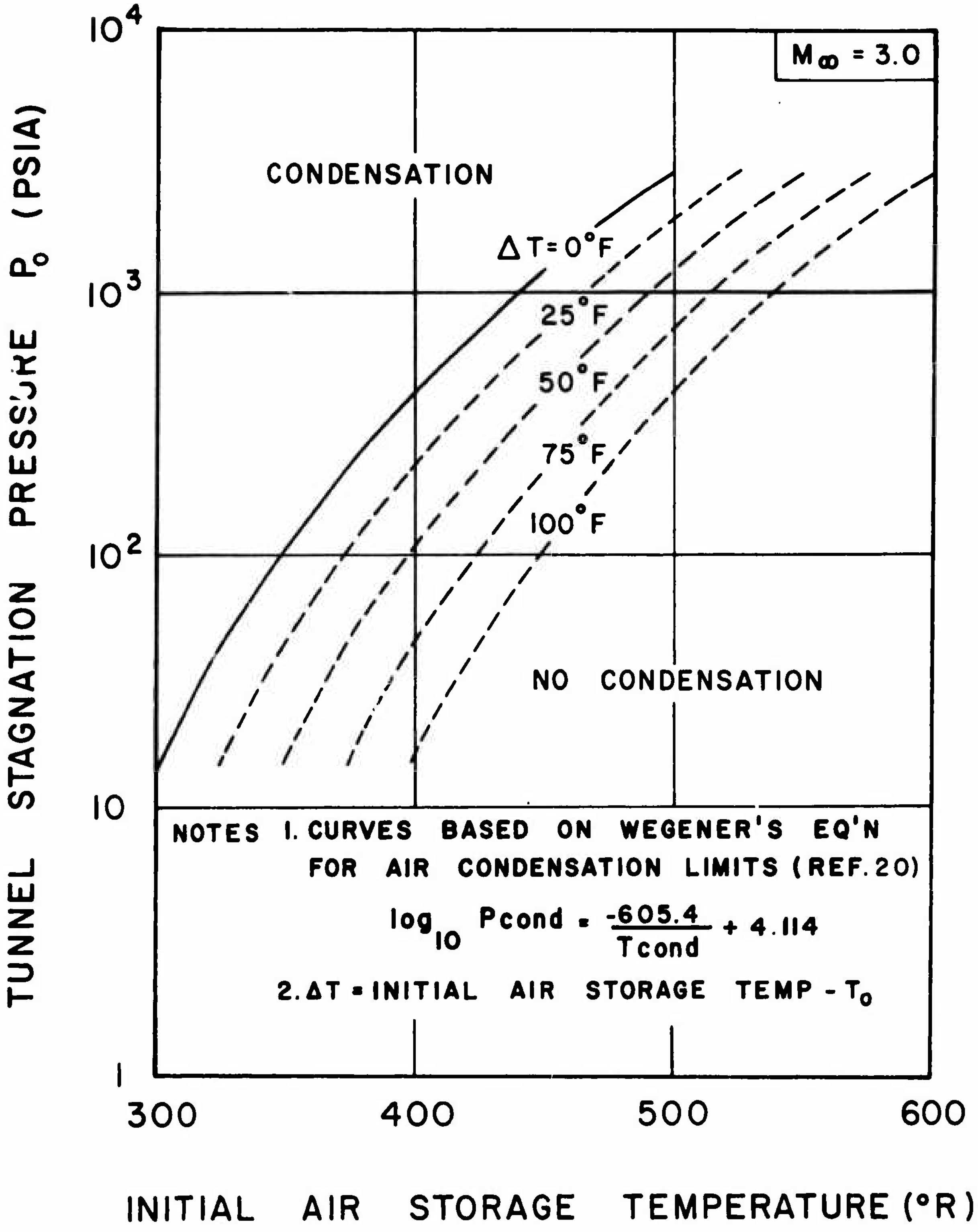

Figure A-3. Effect of Air Condensation on Tunnel Operating Range at a Mach Number of 3

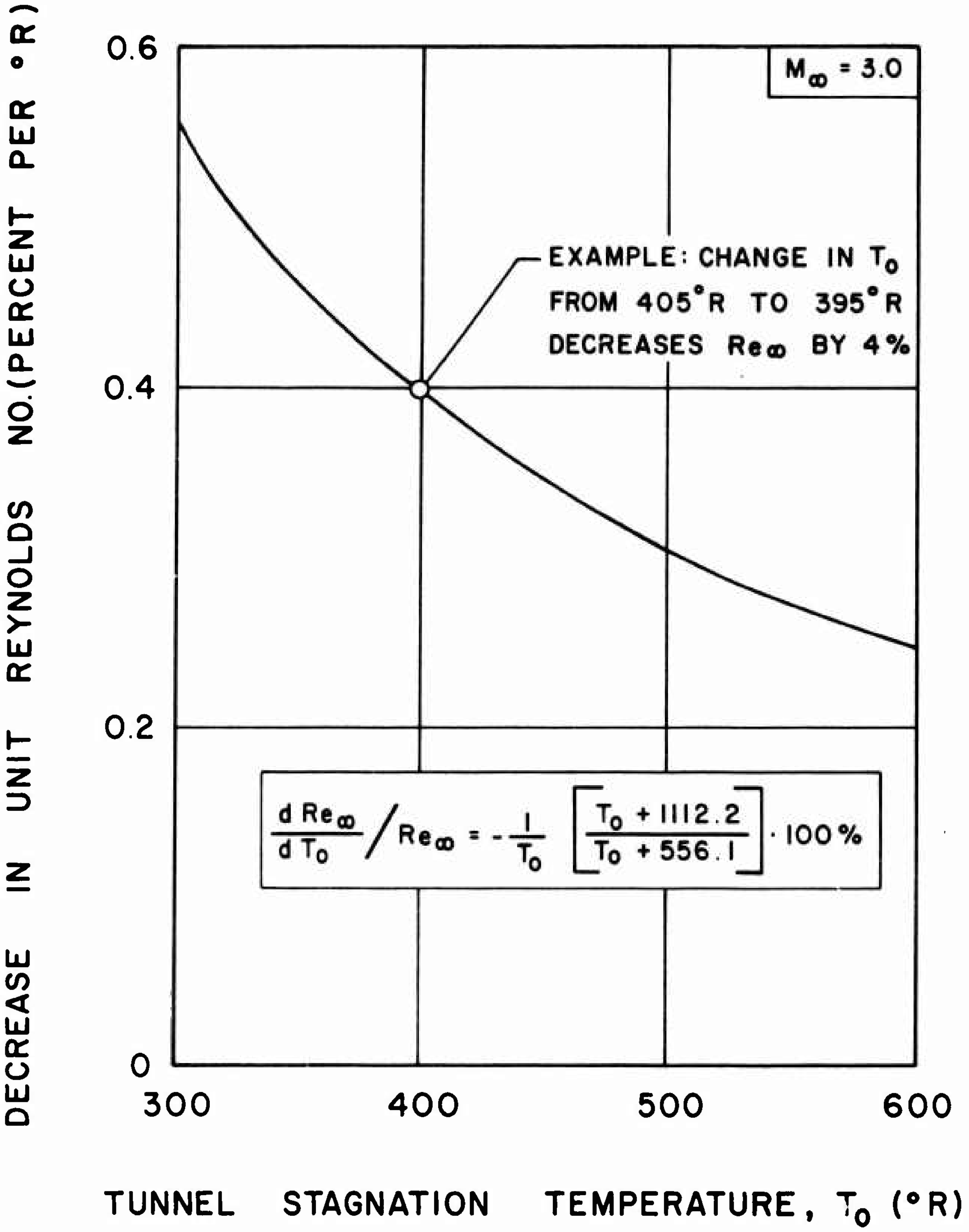

Figure A-4. Rate of Change of Free Stream Unit Reynolds Number with Tunnel Stagnation Temperature at Mach 3

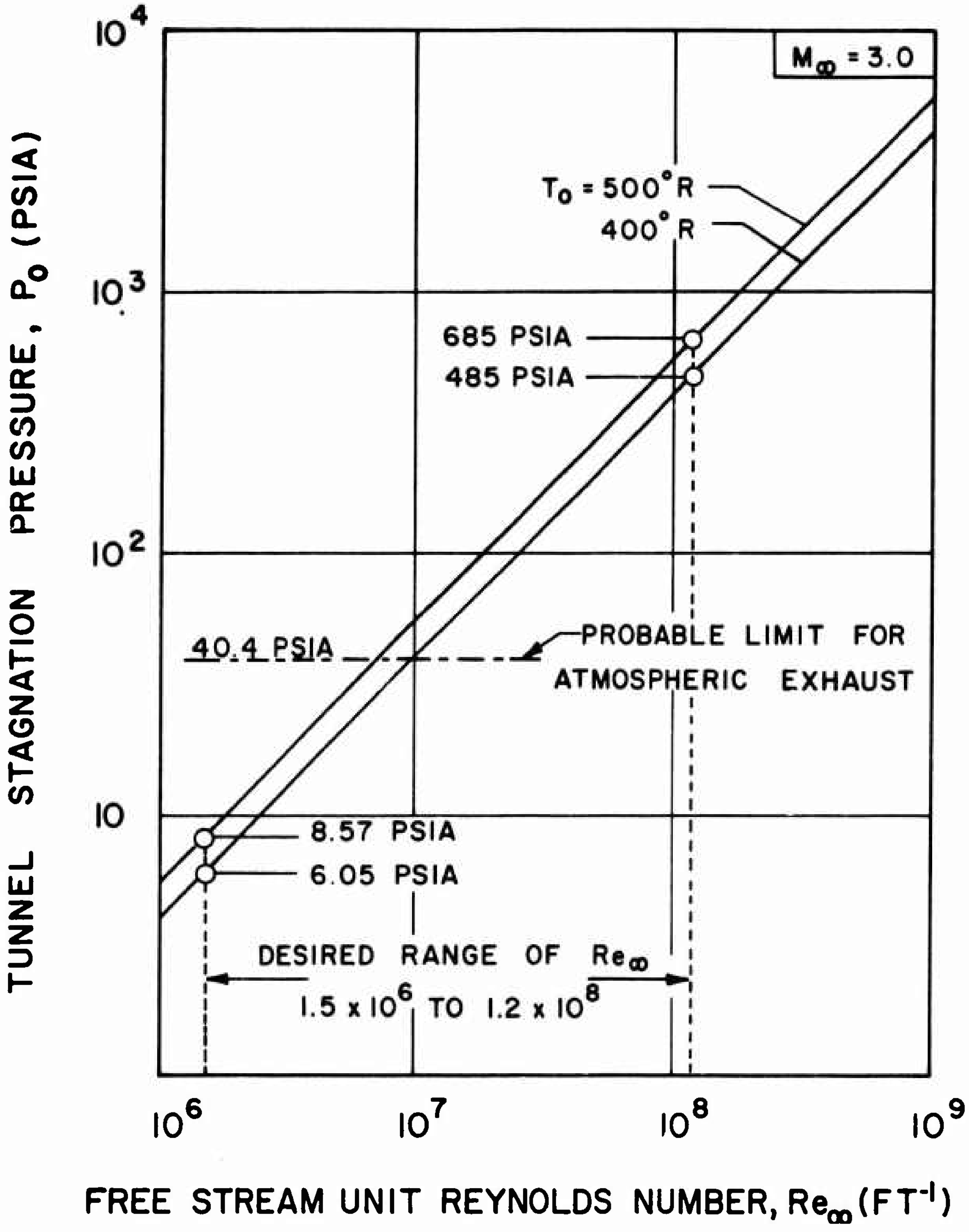

Figure A-5. Variation of Free Stream Unit Reynolds Number with Tunnel Stagnation Pressure and Temperature

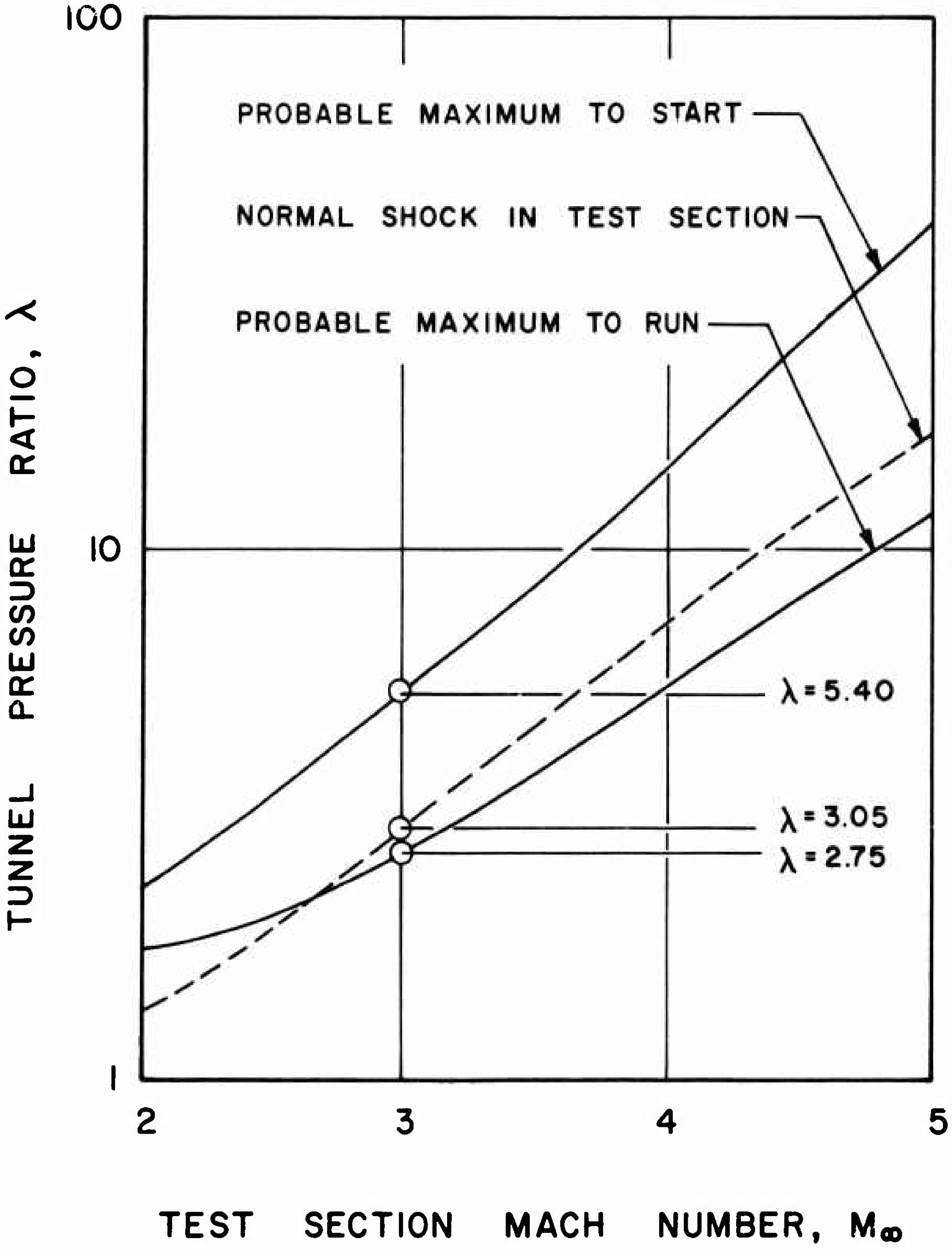

Figure A-6. Tunnel Pressure Ratio Requirements

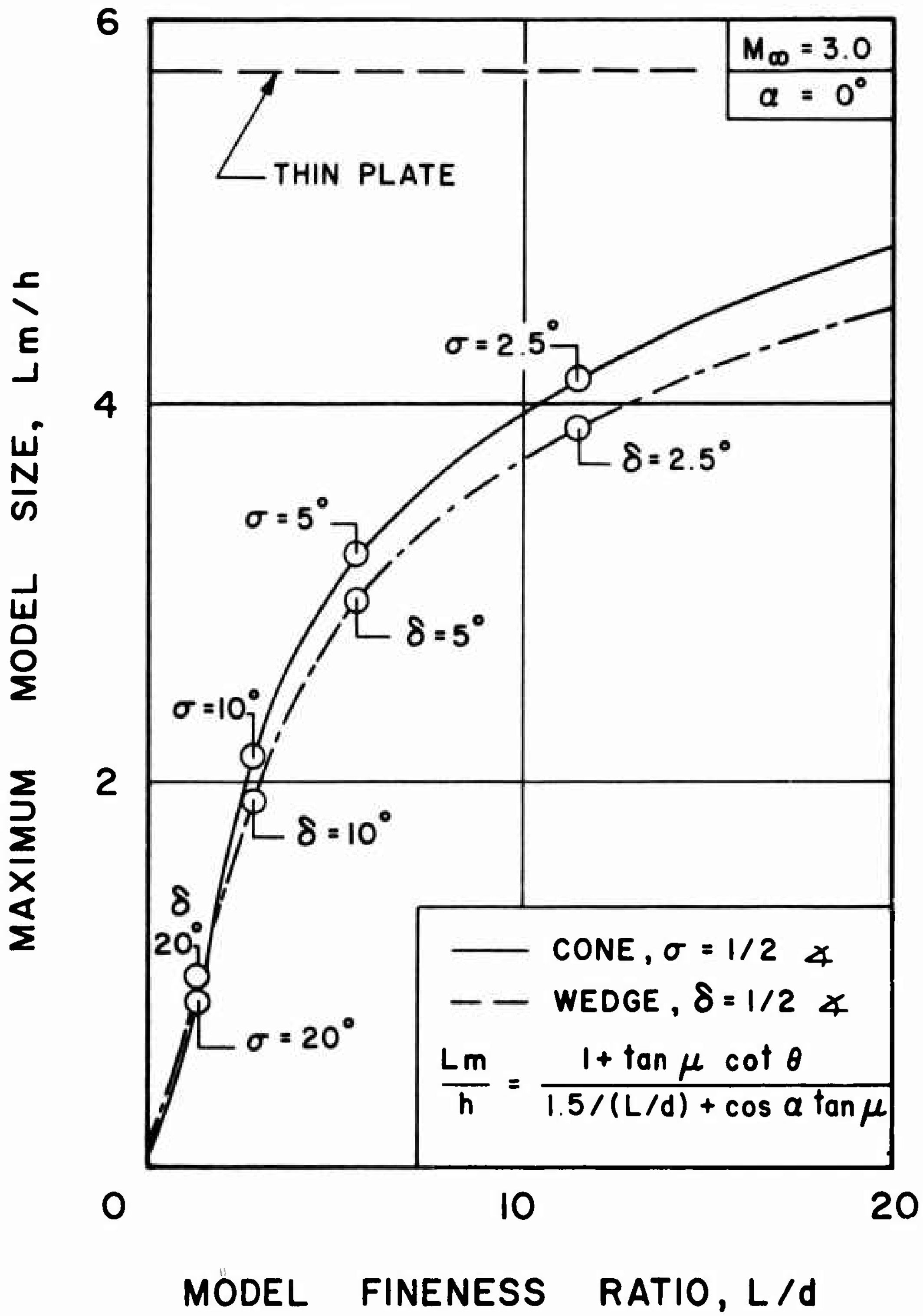

Figure A-7. Variation of Maximum Model Size with Fineness Ratio for Shock Reflection Limited Cases

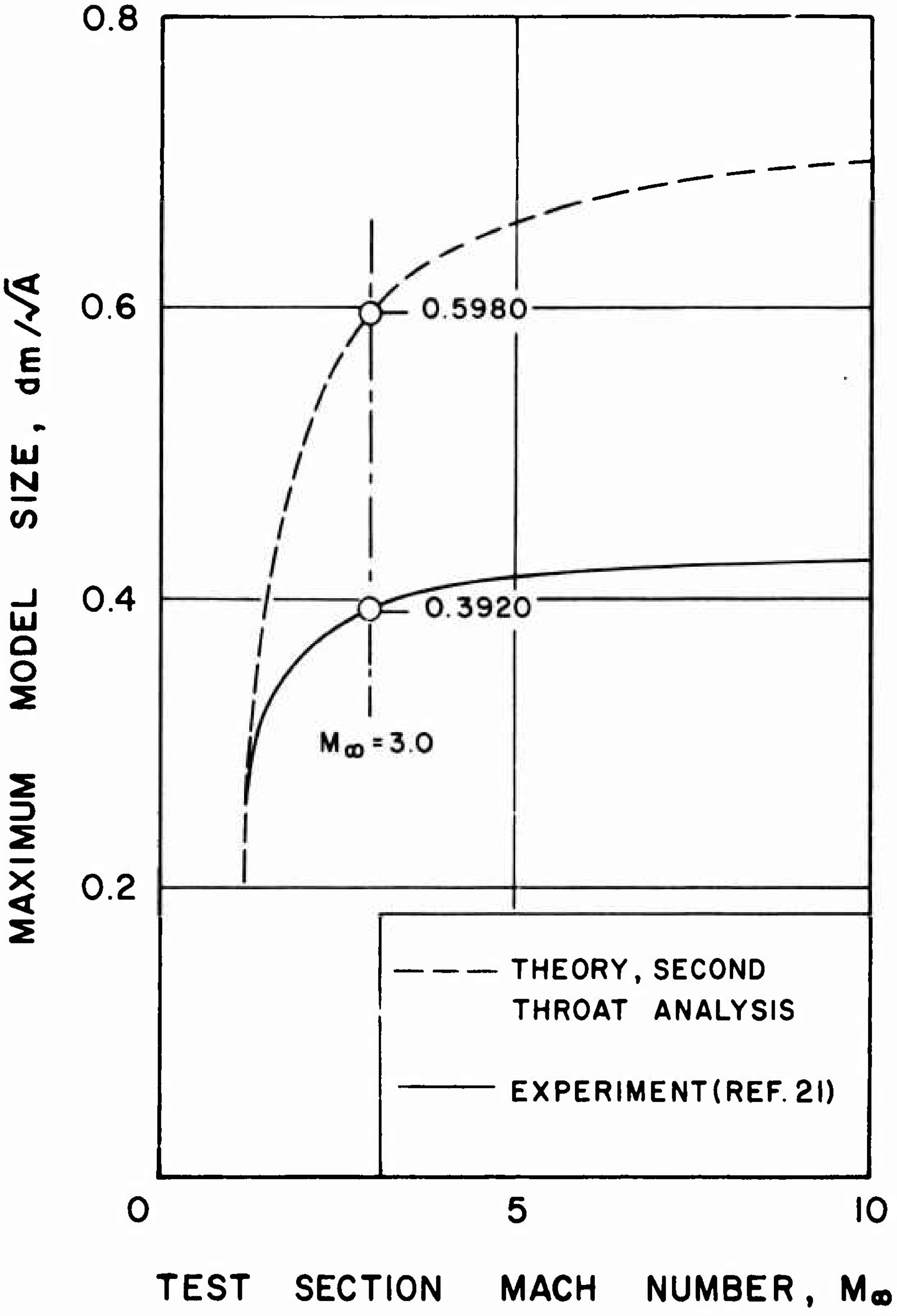

Figure A-8. Variation of Maximum Base Diameter for Starting Tunnel with Blunt Cone Models

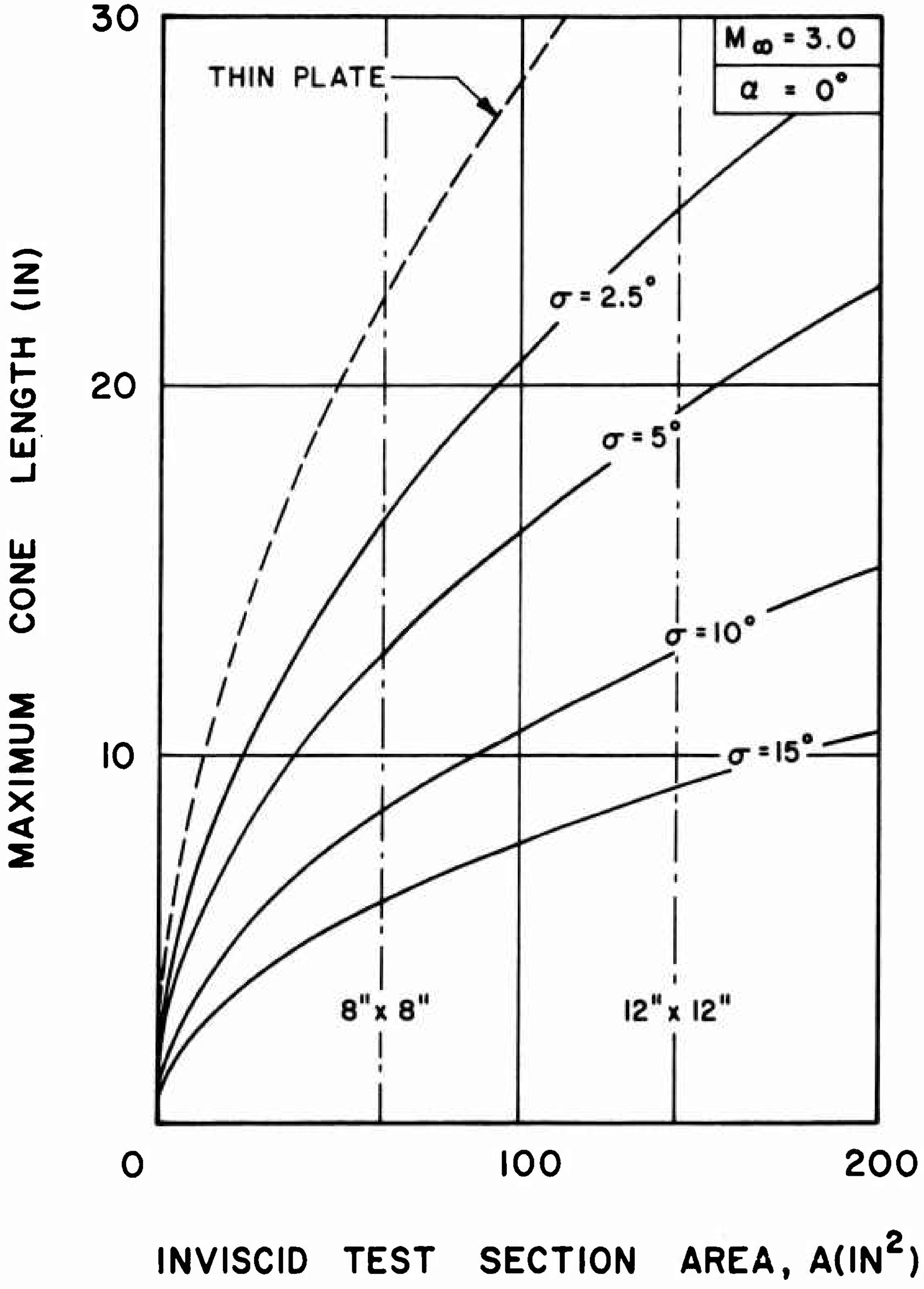

Figure A-9. Variation of Maximum Cone Length with Inviscid Test Section Size for Shock Reflection Limited Cases

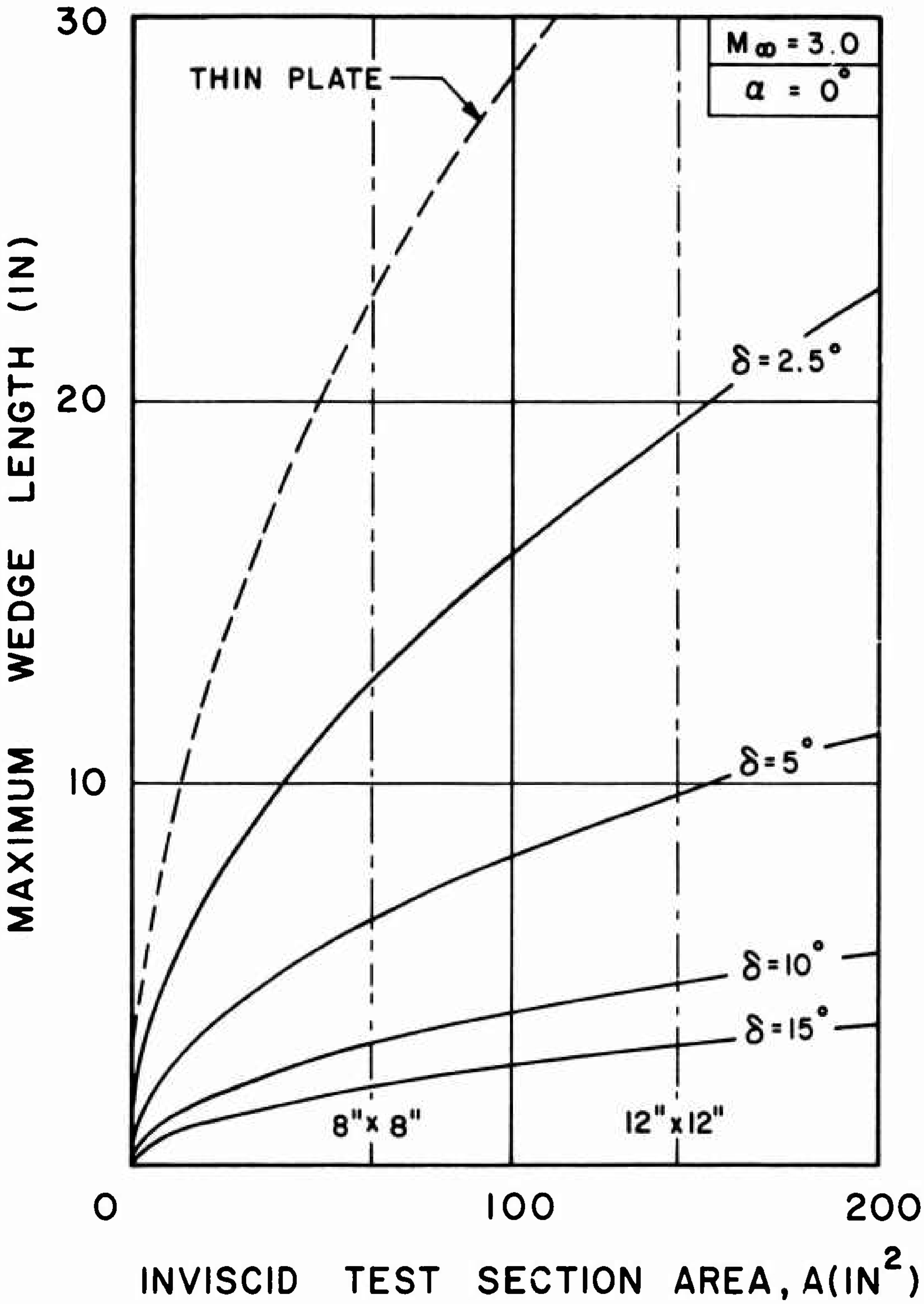

Figure A-10. Variation of Maximum Wedge Length with Inviscid Test Section Size for Blockage Limited Cases

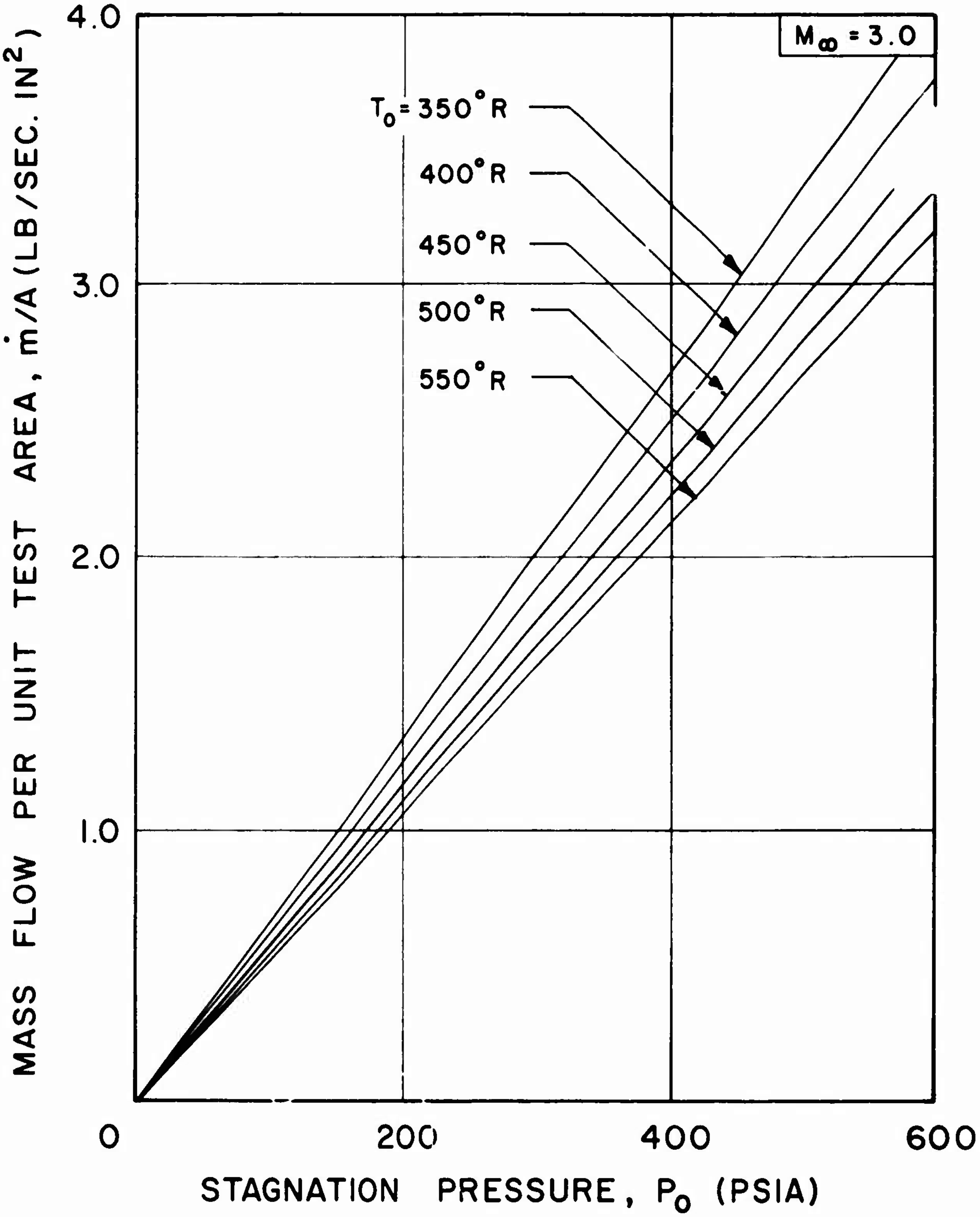

Figure A-11. Mass Flow per Unit Test Section Area as a Function of Tunnel Stagnation Conditions

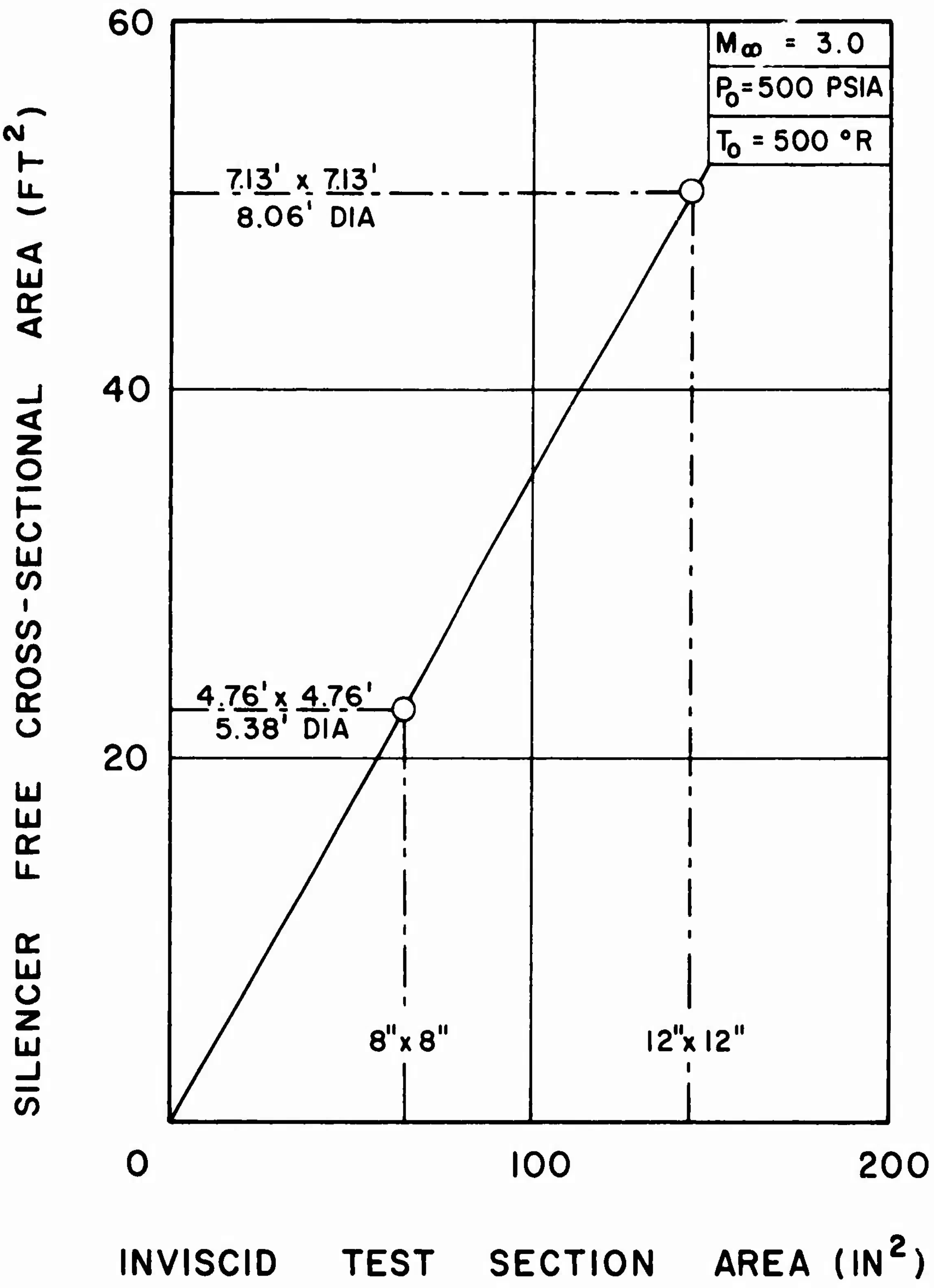

Figure A-12. Variation of Silencer Size with Test Section Size for a Silencer Intake Velocity of 100 ft/sec

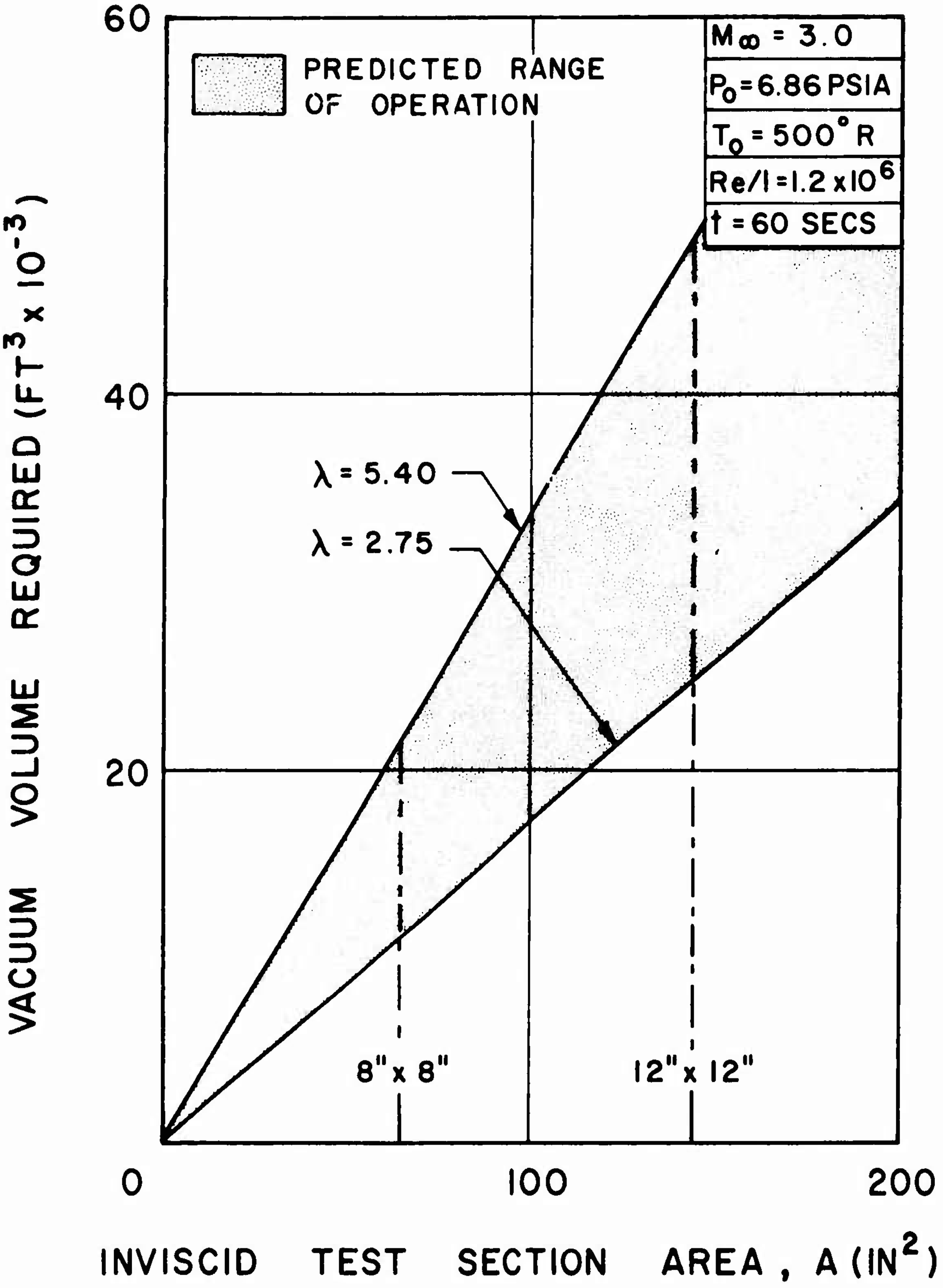

Figure A-13. Variation of Required Vacuum Volume with Test Section Size for a 60-second Run at a Unit Reynolds Number of 1.2×10^6 per Foot

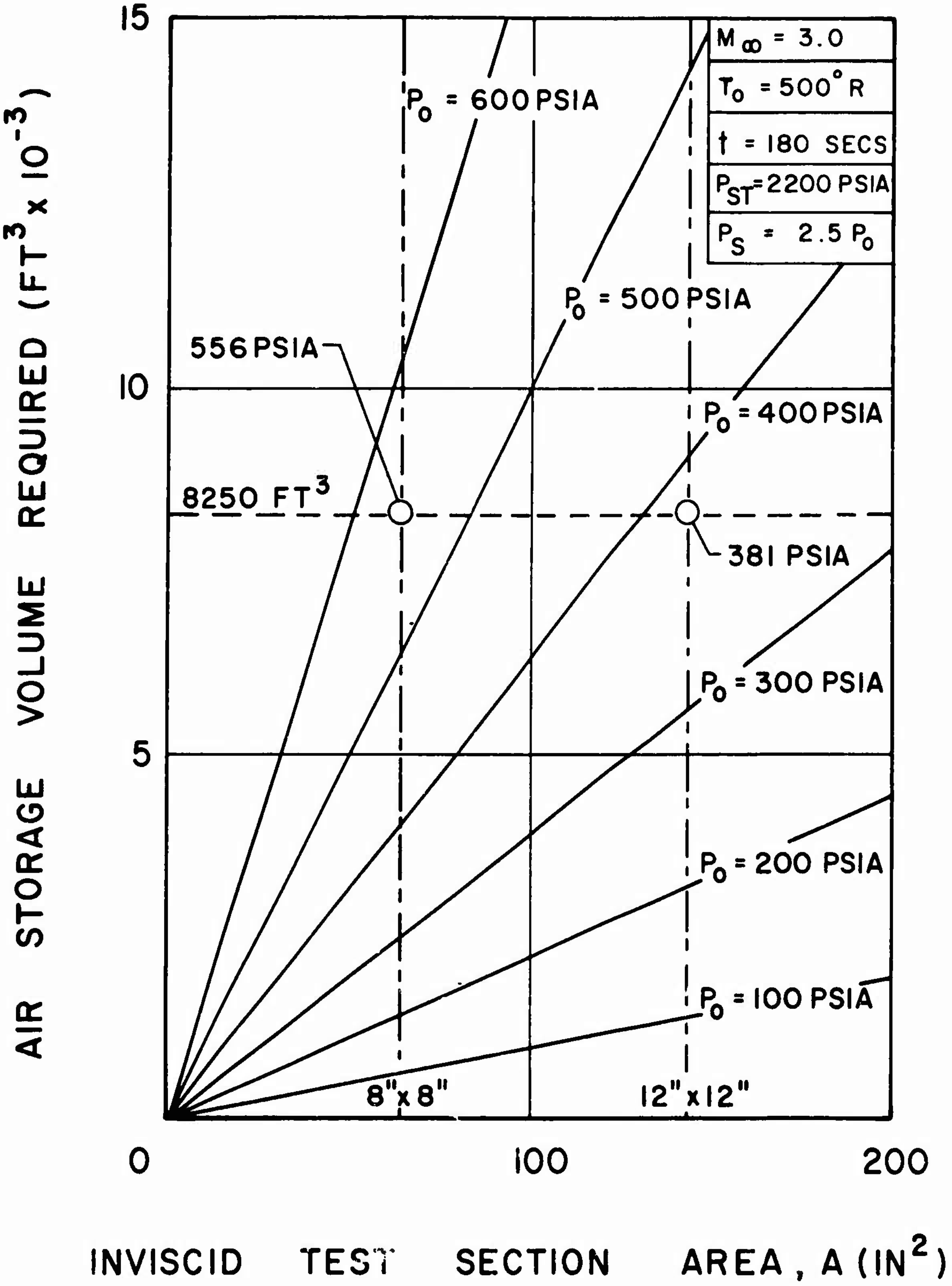

Figure A-14. Variation of Air Storage Volume Requirements with Test Section Size and Operating Pressure

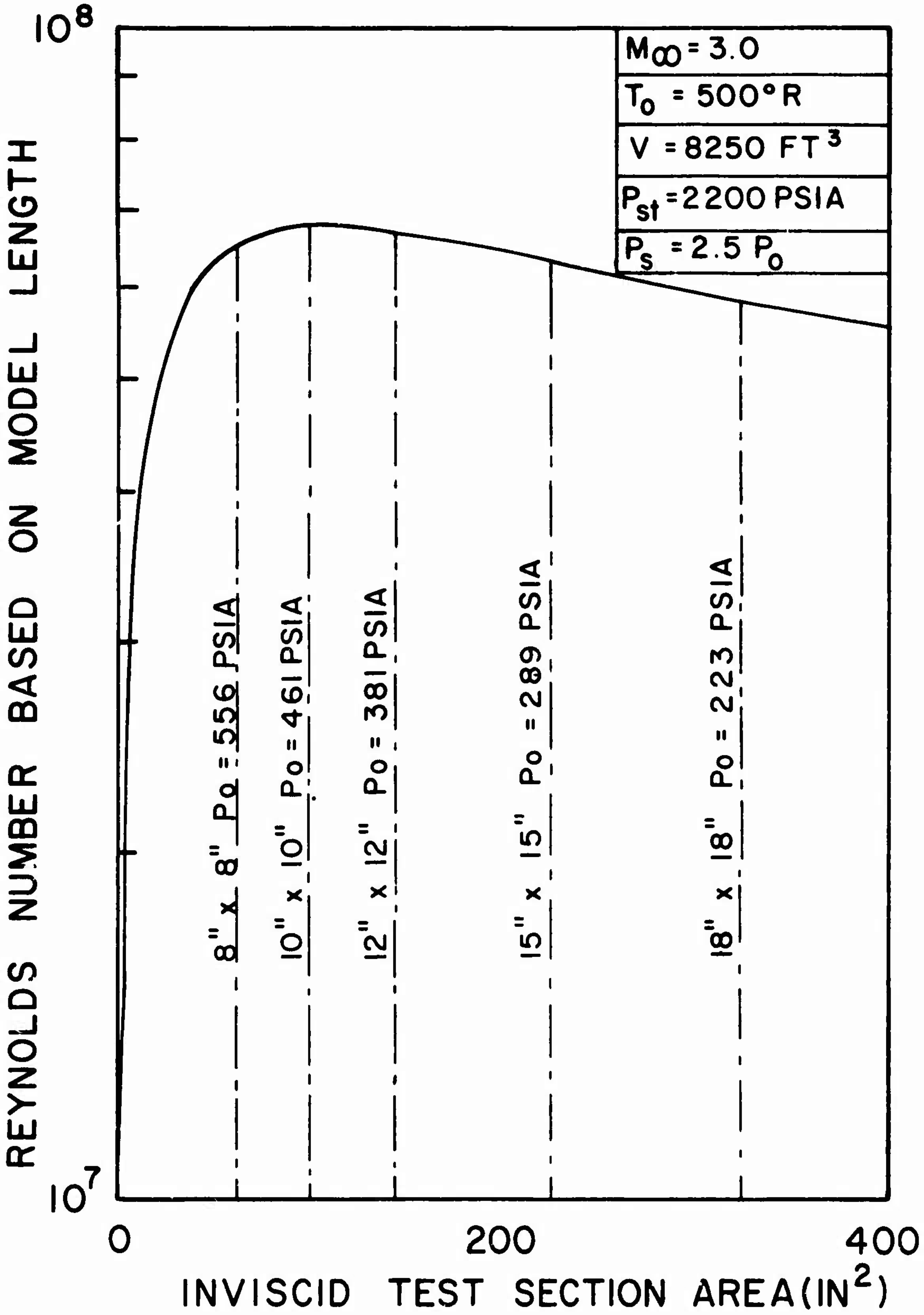

Figure A-15. Maximum Model Reynolds Number Attainable as a Function of Inviscid Test Area

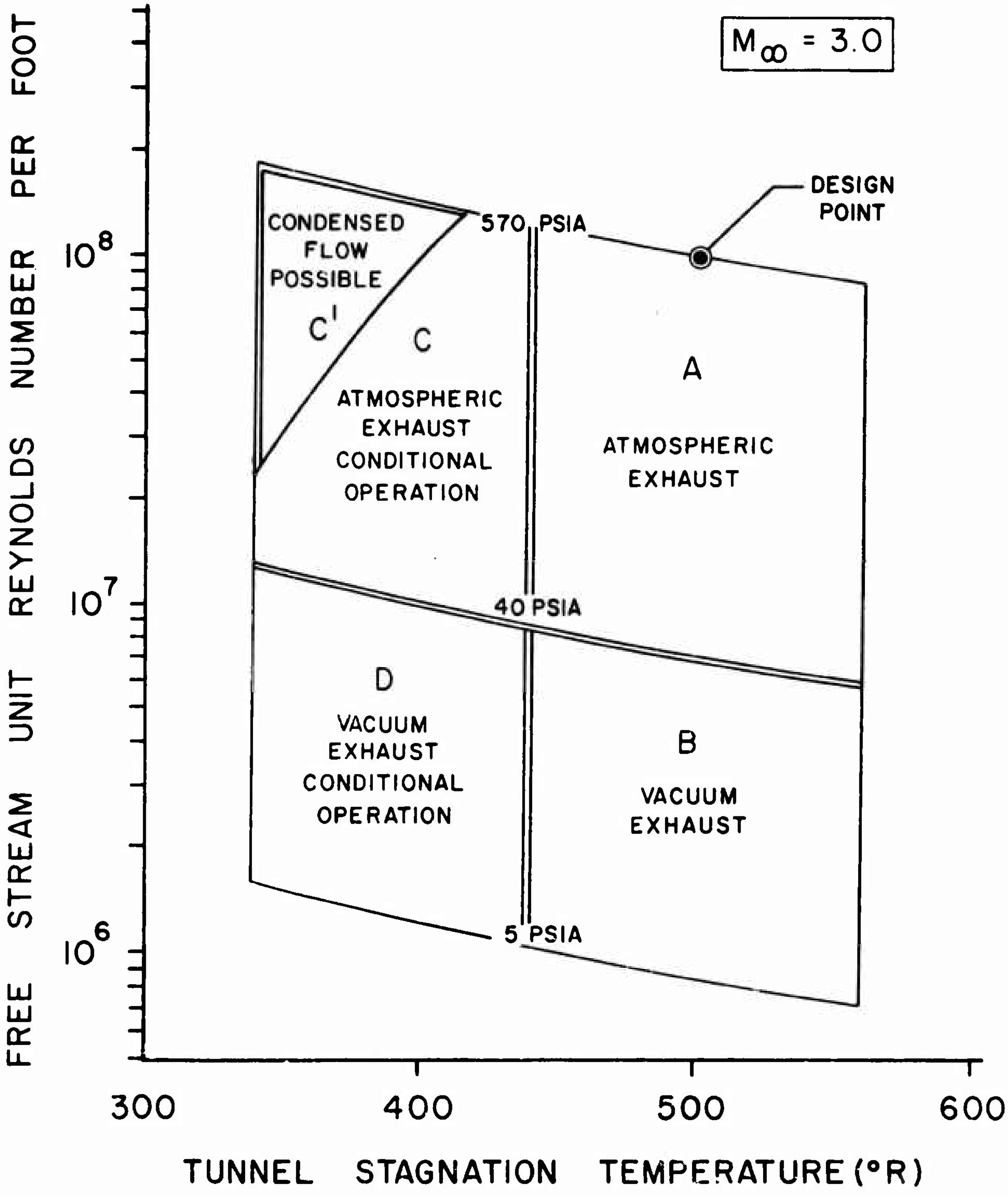

Figure A-16. Predicted Tunnel Performance Envelope

LIST OF SYMBOLS

a	speed of sound of air
A	cross-sectional area of test section
A*	cross-sectional area of nozzle throat
Ai	inviscid test section area
Ap	cross-sectional area of pipe
b	semi-span of test section
Cv	control valve flow coefficient
d	base diameter of blockage cone
d_1	inlet diameter of model settling chamber
d_2	outlet diameter of model settling chamber
dm	maximum model diameter
$\frac{dp}{dy}$	pressure gradient normal to nozzle axis
$\frac{dp}{dz}$	longitudinal pressure gradient
f	frequency of oscillation
g	gravitational constant
G_T	process transfer function
h	base height of blockage wedge
h_{TS}	height of test section
K	process gain
K_1	process gain of controller
K_2	process gain of servo-controller
K_A	process gain of actuator
L	length of model
Lmax	maximum length of model

LIST OF SYMBOLS (CONT'D)

L_n	length of nozzle measured from throat
L_p	length of a section of pipe
$\dot{m}$	mass flow rate
$\bar{m}$	quasi-steady nozzle mass flow rate
M	local Mach number in flow field
M_{rms}	root-mean-square Mach number based upon local Mach number measurements
M_w	Mach number at tunnel wall
M_x	local Mach number at distance x
p_c	static pressure in test section
p_d	static pressure in diffuser
p_e	static pressure in exhaust duct or vacuum sphere
$\bar{p}_o$	quasi-steady settling chamber pressure
P	local static pressure
P_1	supply line static pressure at inlet to isolation valve
P_2	supply line static pressure at inlet to isolation valve
P_{cond}	static pressure at onset of air condensation
P_o	stagnation pressure or settling chamber pressure
P_o'	measured pitot pressure
P_s	supply line static pressure at inlet to control valves
P_{ST}	pressure in storage tanks
P_w	measured nozzle or diffuser wall static pressure
r/R	normalized radial distance in model settling chamber
$r/\Delta s$	normalized radial distance from nozzle axis to impact probe
Re_{Ln}	Reynolds number based on nozzle length

LIST OF SYMBOLS (CONT'D)

Re_m	Reynolds number based on model length
Re_x	local Reynolds number at distance x
$Re/_\ell$, Re_∞	free stream unit Reynolds number
R_n	radius of circular arc section of nozzle contour
s	Laplace operator
t	time period for one oscillation
tm	maximum model thickness
T_c	static (wall) temperature in test section
T_{cond}	static air temperature at onset of air condensation
T_o	stagnation temperature or settling chamber temperature
T_s	static temperature of air at inlet to control valves
T_{ST}	temperature of air in storage tanks
$\overline{u}$	mass-averaged velocity in model settling chamber
U	local velocity in model settling chamber
V	volume of settling chamber
VP	valve position
V_{ST}	volume of air storage tanks
X, x	axial distance from nozzle throat
Xp, xp	axial distance of pitot tube head measured upstream from nozzle exit station
X_R, x_r	axial distance of upstream extremity of test rhombus measured from nozzle exit station
y	nozzle ordinate distance from nozzle axis
$y/\Delta s$	normalized ordinate distance from nozzle axis to impact probe
z	spanwise distance from nozzle axis

LIST OF SYMBOLS (CONT'D)

ΔA_t	total blockage area
Δp	pressure differential or pressure drop
Δs	pitot probe spacing on Mach number survey rake
ΔT	temperature differential due to throttling and expansion = $T_{ST} - T_o$
ΔV	change in fluid velocity in pipe
α	angle of attack
δ	flow angularity
δ^*	local displacement thickness of boundary layer at distance x
δ^*_{Ln}	displacement thickness at nozzle exit
γ	ratio of specific heats for air
λ	tunnel pressure ratio
μ	Mach angle
ϕ	roll angle of survey rake measured clockwise from horizontal plane looking upstream
ρ	density of air
σ	half-angle of wedge or cone model
τ	process time constant
τ_1	process time constant of controller
τ_2	process time constant of servo-controller
τ_A	process time constant of actuator
θ	included angle of flow angularity cone or wedge
θ_s	shock angle

U.S.Government Printing Office: 1975 657-020/483